Studies on Redox Interaction among the Dihydroxybenzene Isomers

by

Afsana Afrin

A thesis submitted in partial fulfillment of the requirements for the degree of Master (M.Sc) in Chemistry

Khulna University of Engineering & Technology
Khulna 9203, Bangladesh.

May 2016

Declaration

This is to certify that the thesis work entitled "Studies on Redox Interaction among the Dihydroxybenzene Isomers" has been carried out by Afsana Afrin in the Department of Chemistry, Khulna University of Engineering & Technology, Khulna, Bangladesh. The above thesis work or any part of this work has not been submitted anywhere for the award of any degree or diploma.

Signature of the Supervisor

Signature of the Candidate

Acknowledgements

First of all I would like to express my grateful thanks to Allah to complete my task.

I would like to express my deepest sense of gratitude and sincere thanks to my respected supervisor **Dr. Md. Abdul Motin**, Professor and Head, Department of Chemistry, Khulna University of Engineering & Technology, Khulna, Bangladesh for providing me the opportunity of working under his kind supervision. For his proper guidance, co-operation, invaluable suggestions and constant encouragement throughout this research work it is easy to find the right way to fulfill the desire research. I will remember his inspiring guidance and cordial behavior forever in my future life.

I am pleased to express my gratitude to **Md. Abdul Hafiz Mia**, Lecturer, Department of Chemistry, Khulna University of Engineering & Technology, Khulna, Bangladesh for helping my research work. I should take this opportunity to express my sincere thanks to **all teachers and stuffs** of this department for their valuable advice and moral support in my research work.

I wish to convey my hearty thanks to all my friends and class fellows specially**, Md. Alim Uddin, Md. Hafizur Rahman** and **Md. Nazim Uddin** for helped me according to their ability.

I wish to thank my **parents** for their grate understanding and support.

Afsana Afrin

Abstract

Redox interaction of catechol, hydroquinone and resorcinol has been investigated in different pH (3-9) media using acetate buffer, phosphate buffer and in only supporting electrolyte containing KCl media at platinum (Pt), glassy carbon (GC) and gold (Au) electrode. The study has been carried out using cyclic voltammetry (CV) and differential pulse voltammetry (DPV) techniques at various scan rates and various concentrations. The results suggest that the all three electrodes exhibited an excellent electrocatalytic effect on the redox behaviors of the dihydroxybenzene isomers. Catechol and hydroquinone show one pair of redox peaks in buffer solution of pH 7 at GC and Pt electrode. But catechol and hydroquinone show two pairs of redox peaks at Au electrode at different pH. In KCl media, catechol and hydroquinone also shows two pairs of peaks at GC and Pt electrode. Resorcinol shows irreversible anodic peak at GC electrode but it shows quasi-reversible voltammogram in Pt and Au electrodes in all electrolytic media. The electrochemical process in all the isomers was controlled by diffusion process.

The electrochemical behavior of catechol, resorcinol and hydroquinone in presence of sulfanilic acid has been studied by cyclic voltammetry and differential pulse voltammetry using glassy carbon (GC), gold (Au) and platinum (Pt) electrodes. Voltammetric appearance reflected that sulfanilic acid has been formed adduct with catechol and hydroquinone. But no reaction has been occurred between sulfanilic acid and resorcinol.

The peak position of the redox couple is also found to be dependent upon pH. Electron transfer is most favorable in neutral media. The slopes of the peak potential, E_p vs pH plot was determined graphically as the anodic peak of dihydroxybenzene isomers or adducts at 0.1V/s at different electrode. The value of slope is close to the theoretical value (60

mV/pH) for one-electron, one-proton transfer process. This indicates that the oxidation reaction of dihydroxybenzene isomers proceeded via the $1e^{-}/1H^{+}$ process. This also suggests that during the reaction not only electron but also proton are released from the oxidation of dihydroxybenzene isomers.

Among the dihydroxybenzene isomers, the electron transfer of hydroquinone is easier than the catechol and catechol is easier than the resorcinol. As -OH sites in resorcinol are connected via *meta* linkage, so the electron transfer at *meta* position is unfavorable (electron deficiency) to that at a *para* (hydroquinone) or *ortho* (catechol) –position. The interaction energy of catechol and hydroquinone in KCl media are 37.63J and 38.60J respectively. So the extent of delocalization of charge through phenyl ring of hydroquinone is higher than the catechol. Resorcinol shows only one anodic peak, -OH sites in resorcinol are connected via *meta* linkage, so the electron transfer at *meta* position is unfavorable due to the deficiency of electron. The redox interactions of the dihydroxybenzene isomers are media dependent.

Contents

LIST OF TABLES

LIST OF FIGURES

CHAPTER I

Introduction

1.1 Overview of redox interactions

The electrochemical behavior of multielectronic functional materials which contain several electroactive sites has been the subject of a number of studies [1-2]. The differences in formal potentials (ΔE^0) of successive one electron systems commonly depend upon the extent of redox interaction between redox sites despite interpretive ambiguities [3, 4]. Sometimes it depends upon other parameters such as solvation changes, ion pairing and structural changes of the molecule [5]. When a compound containing two redox sites has a well defined redox state, the ΔE^0 corresponds to difference in the interaction energy [6]. The electronic communication between the redox sites takes place through a conjugated molecular bridge. The communication is manifested as a mixed-valence (MV) state or an intervalence transfer band [7]. The mixed-valence state has been demonstrated by the appearance of a new energy level in electrochemical current – potential curves or the appearance of a new band in the near –IR spectrum [8, 9]. The properties of MV systems were elaborated by Hush using semiclassical formalism [10]. It can be characterized thermodynamically by comproportionation constant or stability constant [8, 11].

In the absence of significant molecular reorganization or solvation changes, when two redox centers are connected with sigma bonds i.e. the oxidation state of one site is not affected by other sites the potential separation is equal to 35.6 mV for 298 K [12]. The Nernstian voltammetric wave which results from such a situation has the shape of a one-electron transfer reaction, although more than one electron is transferred in the overall reaction. On the electroreduction of poly-2-vinylnapthalene and poly-9-vinylanthracene, evidence was presented for multi electron transfer (up to 1200 electrons per molecule), producing voltammetric waves with the overall shape of one-electron transfer reactions [13]. A theoretical analysis of the expected current-potential characteristics for multiple

electron transfers to a molecule containing any number of non interacting redox centres has been carried out [14]. The statistical factors which governed the behavior of a current-potential response with Nernstian systems have all the characteristics of a one electron transfer reaction except for the large limiting current.

In contrast, when redox centres are connected with π-conjugated linkers, they often take mixed –valence states owing to delocalization of the redox charge, exemplified by dinuclar-metal complexes [15, 16] and arylamine derivatives [17-18]. Generally, an *n*-redox polymer or oligomer connected with π- conjugated linkers, seems to take *n* redox states exhibiting *n* voltammetric waves unless there is any overlap of waves. The statistical mechanical calculation for a linearly conjugated *n*-redox species has demonstrated that the voltammogram has three waves for an odd number of *n* and four for even number of *n* [19]. However, linear complexes with *n* ferocenyl centers show *n* voltmmetric waves for $n \leq 6$ owing to the long –distant interaction [20].

Since intervalence states vary with multi-redox states or various kinds of mixed-valence species, electrochemical study has played a vital role in controlling accurately intervalence states by electrode potential. Geometrically symmetric redox sites have exhibited asymmetric voltammetric behavior in a complicated manner [21, 22]. If detailed potential-dependence of number of electron transfers, *n* is available it is possible to evaluate the cause of asymmetric reactions. Therefore, it is necessary to obtain accurate potential dependence on *n*. Determination of *n* has often carried out with the bulk electrolysis. However, the bulk electrolysis has difficulties in less controllable potential, chemical complications for a long electrolysis, and mixing with solution in a counter electrode cell.
Materials based on dihydroxybenzene have been extensively studied due to their interesting physical, electrochemical and photochemical properties as well as facile synthesis and process, environmental stability and low cost [23-27]. Besides these interesting electronic properties, there has been considerable interest in the redox interactions between the active sites of these dihydroxybenzene with electron transfer number.

1.2 Multi-step charge transfer reaction

Here, we will discuss the theoretical aspects of the multistep charge transfer reversible reactions:

1.2.1 E_rE_r Reactions (Reversible type two electron transfer reactions)

We consider cases in which there are two (or more) heterogeneous electron-transfer reactions.

$$\begin{aligned} A + e &\rightleftharpoons B \cdots E^0_1 \\ B + e &\rightleftharpoons C \cdots E^0_2 \end{aligned} \qquad \Delta E^0 = E^0_2 - E^0_1 \qquad (1\text{-}2\text{-}1)$$

Let us consider the voltammetric behavior for this situation. The appearance of the voltammogram depends upon the location of the standard potentials, E^0_1 and E^0_2, and the spacing between them $\Delta E^0 = E^0_2 - E^0_1$.

The voltammograms behave as independent reversible waves for certain minimum potential separation, ΔE^0. A theoretical polarogram was calculated for a potential separation ΔE^0 of - 180 mV as shown in Figure 1-2-1, Curve A. As the potential separation between the successive reductions becomes less than about 100/ *n* mV the individual waves merge into one broad distorted wave whose peak height and shape are no longer characteristic of a reversible wave (Curve B). The wave is broadened similar to an irreversible wave. For the particular case when both A and B are reduced at the same potential, $\Delta E^0 = 0$ (and assuming that n_1 and n_2 are both unity) the wave observed (Curve C) has a peak height intermediate between a one-electron and a two-electron reversible wave, and $E_p - E_{1/2}$ is about 21 mv. As B becomes easier to reduce than A, the wave height increases and the peak narrows until it reaches the height and shape of a two-electron wave(Curve D). That is, the height of the two electron wave is $2^{3/2}$ times the height of the corresponding single electron reversible

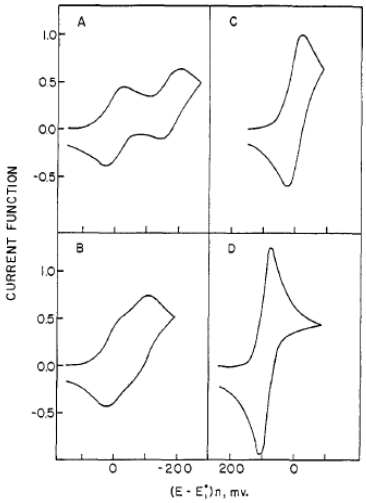

Fig. 1-2-1: Cyclic stationary electrode polarogrrams for case E_rE_r reaction
A. ΔE^0 = -180 mV C. ΔE^0 = 0 mV
B. ΔE^0 = -90 mV D. ΔE^0 = 180 mV

wave, ΔE_p is 29 mV, and the reaction behaves as a direct reduction of A to C. Under these conditions, the working curves in Figure 1-2-2 can be employed to estimate ΔE^0. It's instructive to consider the chemical and structural factors that affect ΔE^0. When the successive electron transfers involve a single molecular orbital, and no large structural changes occur upon electron transfer, then one expects two-well spaced waves ($\Delta E^0 << -125$ mV).

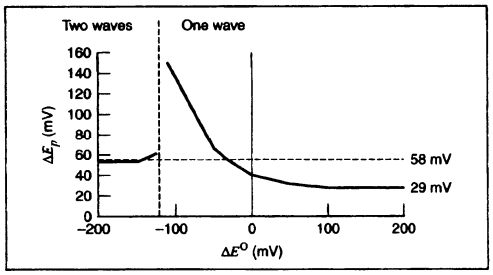

Fig. 1-2-2: ΔEp vs ΔE^0 for the E_rE_r reaction scheme. The discontinuity in the curve at negative value of ΔE^0 occurs when two waves are resolved.

Whenever an E_rE_r reaction takes place, one must consider the possibility of a comproportionation and disproportionation equilibrium also developing in the solution near the electrode,

$$A \underset{}{\overset{E_1^0}{\rightleftharpoons}} B \overset{E_2^0}{\rightleftharpoons} C$$

Where, $\Delta E^0 = E_2^0 - E_1^0$

The electrode potential is expressed as Nernst equation for half reactions for eqn (1-2-1)

$E_1 = E_1^0 + (RT/F) \ln [A]/[B]$

$E_2 = E_2^0 + (RT/F) \ln [B]/[C]$

The relation of the concentrations of A and C to B at equilibrium is expressed by the comproportionation constant, K_c,

Where,

$$A + C \rightleftharpoons 2B \qquad K_c = [B]^2/[A][C] = \exp [(E_2^0 - E_1^0)F/RT] \qquad (1\text{-}2\text{-}2)$$

$$\log K_c = 16.9\, \Delta E^0 \text{ at } 298 \text{ K} \qquad (1\text{-}2\text{-}3)$$

The extent of the reaction, as measured by the equilibrium constant, K_c, is governed by ΔE^0.

If the diffusion coefficients of oxidized species and reduced species are roughly equal, then it is assumed that $E_o = E_{1/2}$ [8].

The equation 1-2-3 becomes,

$$\log K_c = 16.9\, \Delta E_{1/2} \text{ at } 298 \text{ K} \qquad (1\text{-}2\text{-}4)$$

Typically, cyclic voltammetry has been used to obtain $\Delta E_{1/2}$. If the difference in the interaction energy at the para-position, u_p of MPA is estimated only from the difference in the half wave potentials, we have

$$u_p' = F\left[(E_2)_{1/2} - (E_1)_{1/2}\right]/2 \qquad (1\text{-}2\text{-}5)$$

For the case of a molecule with two sites, it is natural to divide the sites into three classes based on the value of *K*c:

$K_c = 4$: This is totally a noninteracting case, i.e., the oxidation state of one site is not affected by the oxidation state of the other. Even though the two sites have the same microscopic redox potentials, notice that $(E_1)_{1/2}$ and $(E_2)_{1/2}$, which are macroscopic properties, are not equal but are separated by 0.0356 V. This separation is due to statistics and has been observed for certain polyferrocenes [14].

$Kc < 4$: This implies that the second electron is easier to add than the first, $\Delta E_{1/2} < 0.0356$ V, and that the mixed valence molecule, Ox-Red, will be unstable with respect to disproportionation. If both sites in the molecule do not change geometrically or chemically, it is unlikely that this case will occur because charge should be sequentially more difficult to add. In the situations where this case occurs, addition of the first electron is usually followed by some process such as bond breaking, rotation about a bond, protonation or structural change [28]. The process causes the second site to be easier to reduce than the first.

$Kc > 4$: In this case the second electron is more difficult to add than the first, $\Delta E_{1/2} > 0.0356$ V, and Ox-Red is stable. This situation is most common and is observed, for example, in many ruthenium complexes certain biferrocenes arylamines [29-34].

Comproportionation constant, K_c can be measured in two ways as spectroscopically by titration method and electrochemically by pulse or cyclic voltammetric method. Sutton et al asserted that spectroscopic method is more reliable than pulse or cyclic voltammetric method because if the value of *Kc* is not more than 2×10^2, it can not be measured by CV method. In contrast Richardson et al [8] determined the comproportionation constant, *Kc* by using the pulse and cyclic voltammetry techniques as a peak separation values, ΔE^0. With this method, values of *Kc* accurate to ± 5% were obtained in the range $4 < Kc <$ ca. 200 (36 mV $< \Delta E^0 <$ 136 mV). For an accurate spectroscopic titration all species involved in equilibrium must be soluble and stable over the time required (~30-60 min), and there must be an isolated absorption band characteristic of a single species. Therefore the

strategy of spectroscopic titration that Sutton et al used for the determination of comproportionation constant, K_c is not always applicable.

1.3 Factors affecting of $\Delta E_{1/2}$

The fundamental importance of multi-step electron-transfer processes is widely recognized and the main factors influencing the $\Delta E_{1/2}$ values for the interaction between the redox sites of successive electron transfer processes (see eq 1-2-1) [35-47] have discussed. Another important factor, namely, the effect of the solvent/ electrolyte medium and structural effect will be discussed in this section. A very large decreases in $\Delta E_{1/2}$ values may occur when the supporting electrolyte cation is changed from weakly to strongly ion pairing and a lower-polarity solvent (dielectric constant, ε, of about 10 or less) is employed.

1.3.1 Role of electrolyte anion

After oxidation of species in electrolyte systems, $\Delta E_{1/2}$ comes about because the first oxidation potential is almost unaffected by the size of the supporting electrolyte anion whereas the second oxidation potential moves to more positive values as the counterion becomes bigger. The dications ion-pairing are much more stronger than monocation because of the dependence of electrostatic attraction on charge. The CVs of bis(fulvalene)dinickel in CH_2Cl_2 (Figure 1-3-1) are good example of $\Delta E_{1/2}$ increasing from 273 mV (A^- = Cl^-) to 480 mV (A^- =[PF6]$^-$) to 753 mV (A^- = TFAB) [31]. Switching A^- from Cl^- to TFAB results in an overall change of 480 mV in $\Delta E_{1/2}$. This is explained by an electrostatic model in which the greater positive charge of the dication accentuates ion-pairing effects, which decrease owing to charge-to-size ratios in the order Cl^- > $[PF_6]^-$ > TFAB. The high degree of charge delocalization in large size anions makes not only weak nucleophiles but also weakly ion pairing.

1.3.2 Role of solvent donor/acceptor properties

The effect of the medium on $\Delta E_{1/2}$ is a complex function of solvent-solute and ion-pairing interactions. The most important solvent parameters are dielectric constant (ε), dipole moment (μ), donor number (DN), and acceptor number (AN). The lower-polarity (ε < 10) solvent facilitates ion pairing, not only through simple tight ion pairs but also through formation of triple ions and even higher aggregates and clusters. A second important aspect of solvent polarity is the relationship of ε to free energies of solvation. On the basis of the Born equation, a lower-polarity solvent is expected to more weakly solvate charged electrode products, leading to an increase in $\Delta E_{1/2}$ for successive one electron couples. Qualitatively this comparison shows the dominance of solvation in high polarity solvents and of ion pairing in low- polarity solvents. There is a significant correlation, however, of $\Delta E_{1/2}$ of bis(fulvalene)dinickel with solvent *acceptor* strength when [NBu$_4$]Cl is the electrolyte, owing to the strong ion-pairing ability of chloride (Figure 1-3-2). The increase of $\Delta E_{1/2}$ is attributed to increased solvation of chloride, thereby decreasing ion-pairing effects.

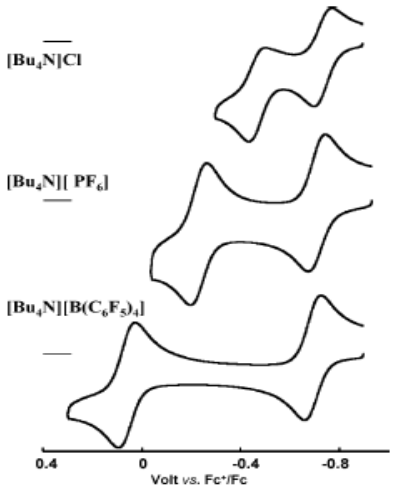

Fig. 1-3-1: CV scans at 0.1 V/s of bis(fulvalene)dinickel in CH_2Cl_2, 0.1 M [Bu$_4$N]Cl, [Bu$_4$N][PF$_6$], or [Bu$_4$N][B(C$_6$F$_5$)$_4$].

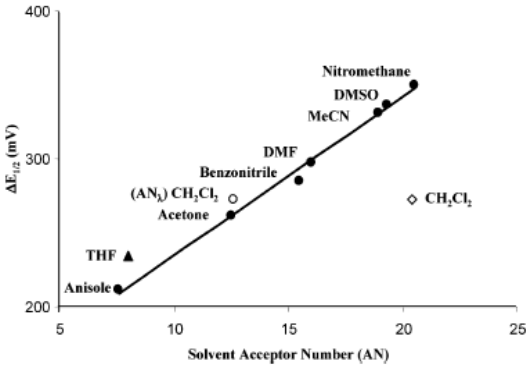

Fig. 1-3-2: Correlation between the measured $\Delta E_{1/2}$ value of bis(fulvalene)dinickel in 0.1 M [NBu$_4$]Cl and the acceptor number (AN) of the solvent.

1.3.3 Ideal medium properties to maximize $\Delta E_{1/2}$ for electrogenerated Cations

Maximizing $\Delta E_{1/2}$ for redox processes that involves positively charged products requires a medium with the following properties: (i) a lower-polarity solvent (preferably of low donor strength) to minimize solvation of analyte cations, (ii) a weakly coordinating electrolyte anion to minimize ion pairing, (iii) a small electrolyte countercation to enhance competitive ion pairing with the supporting salt anions, and (iv) a low concentration of the supporting electrolyte. The nucleophilic properties of the solvent must also be kept in mind, again favoring solvents of low donor number.

Electro active compounds undergo oxidation and/or reduction on the electrode surface within a certain potential range. The electro activity of such compounds depends upon the pH of the medium, nature of the electrode and active moiety (electrophore) present in their structures. Their redox behavior can be influenced by the change in pH, substituents, concentration and scan rate. The variation in redox behavior can be abused for a number of useful purposes like elucidation of electrode reaction mechanism. Cyclic voltammetry (CV) and differential pulse voltammetry (DPV) have used in the present work to achieve the following two main objectives:

- To understand the issue of multi-step ET in dihydroxybenzene isomers.
- To analyses the redox interactions at ortho, meta and para positions.

In recent years the electrochemical techniques have led to the preferment over other techniques in the field of analysis owing to their specificity, high sensitivity, efficient selectivity, greater reliability, extensive versatility and fast detection ability. Direct monitoring, simplicity and low cost facilitated the investigation of the electrode reaction mechanism and interaction studies.

1.4 Biologically Important compounds

The elucidation of reaction mechanism at the electrode surface requires the determination of the electro active moiety (electrophore) of the molecule, number of electrons involved in oxidation and/or reduction processes, number of protons accompanying the transfer of

electrons in different pH media and the reversibility/irreversibility of each step [48]. The redox mechanisms of the following biologically important molecules were proposed on the basis of the results obtained from CV and DPV.

1.4.1 Catechol (Cate)

Catechol (also known as pyrocatechol or 1,2-dihydroxybenzene), is an organic compound with the molecular formula $C_6H_4(OH)_2$ shown in Figure 1.1 . It is the ortho isomer of the three isomeric benzenediols. This colorless compound occurs naturally in trace amounts. About 20M kg are produced annually, mainly as a precursor to pesticides, flavors and fragrances [49]. Catechol occurs as feathery white crystals which are very rapidly soluble in water.

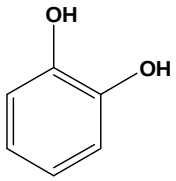

Figure 1.1: Structure of Catechol

1.4.2 Natural Occurrence of Catechol

Small amounts of catechol occur naturally in fruits and vegetables, along with the enzyme polyphenol oxidase (also known as catecholase, or ctechol oxidase). Upon mixing the enzyme with the substrate and exposure to oxygen (as when a potato or apple is cut and left out), the colorless catechol oxidizes to reddish-brown melanoid pigments, derivatives of benzoquinone. The enzyme is inactivated by adding an acid, such as lemon juice, and slowed with cooling. Excluding oxygen also prevents the browning reaction. Benzoquinone is said to be antimicrobial, which slows the spoilage of wounded fruits and other plant parts, Catechol moieties are also found widely within the natural world. Arthropodcutcle consists of chitin linked by a catechol moiety to protein. The cuticle may be strengthened by cross-linking (tanning and sclerotization), particularly in insects, and of course by biomineralozation [50].

1.4.3 Use of Catechol

Approximately 50% of synthetic catechol is consumed in the production of pesticides, the remainder being used as a precursor to fine chemicals such as perfumes and pharmaceuticals [23]. It is a common building block in organic synthesis [24]. Several industrially significant flavors and fragrances are prepared starting from catechol [25]. Guaiacol is prepared by methylation of catechol and is then converted to vanillin on a scale of about 10M kg per year (1990). The related mono ethyl ether of catechol, guethol, is converted to ethylvanillin, a compinent of chocolate confectionaries. 3-trans-Isocamphylcyclohexanol, widely used as a replacement for sandalwood oil, is prepared from catechol via guaiacol and camphor. Piperonal, a flowery scent, is prepared from the methylene diether of catechol followed by condensation with glyoxal and decarboxylation [26]. Catechol is used as a black –and- white photographic developer, but except for some special purpose applications, its use until recently was largely historical. Modern catechol developing was pioneered by noted photographer Sandy King. His “PyroCat” formulation enjoys widespread popularity among modern black and white film photographers.

1.4.4 Resorcinol

Resorcinol (also known as Resorcin or 1,3-dihydroxybenzene), is an organic compound with the molecular formula $C_6H_4(OH)_2$ shown in Figure 1.2. It is the meta isomer of the three isomeric benzenediols. Resorcinol crystallizes from benzene as colorless needles that are readily soluble in water, alcohol, and ether. Resorcinol is most commonly used in skin creams for the treatment of acne, psoriasis, seborrheic dermatitis, eczema, and other skin disorders.

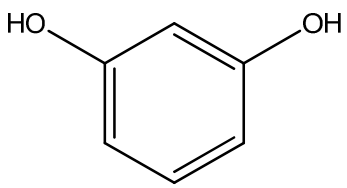

Resorcinol

Figure 1.2: Structure of Resorcinol

It condenses with acids or acid chlorides, in the presence of dehydrating agents, to oxyketones, e.g., with zinc chloride and glacial acetic acid at 145 °C it yields resacetophenone $(HO)_2C_6H_3$~$CO.CH_3$ [51]. In addition to electrophilic aromatic addition, resorcinol undergo nucleophilic substitution via the enone form. With concentrated nitric acid, in the presence of cold concentrated sulfuric acid, it yields trinitro-resorcin (styphnic acid), which forms yellow crystals, exploding violently on rapid heating.

1.4.5 Natural Occurrence of Resorcinol

The resorcinol moiety has been found in a wide variety of natural products. In particular, the plant phenolics, of which resorcinol ring-containing constituents are a part, are ubiquitous in nature and are well documented. Resorcinol itself has been found in the broad bean (*Vicia faba*), detected as a flavour-forming compound in the honey mushroom (*Armillaria mellea*) (Dressler, 1994), and found in exudates of seedlings of the yellow pond lily (*Nuphar lutea*) (Sütfeld et al., 1996). Resorcinol has also been found in extracts of tobacco leaves (Dressler, 1994) and is a component of tobacco smoke (see section 6). In terms of resorcinol derivatives, resorcinol ethers are components of fragrance agents, and there is considerable literature on long-chain alk(en)yl resorcinols in plants and bacteria (Dressler, 1994).

Resorcinol is a monomeric by-product of the reduction, oxidation, and microbial degradation of humic substances. Humic substances are also present in coals, shales, and possibly other carbonaceous sedimentary rocks. Chou & Patrick (1976) found resorcinol in some samples as a decomposition product of corn residues in soil.

1.4.6 Use of Resorcinol

Resorcinol is used as a chemical intermediate for the synthesis of pharmaceuticals and other organic compounds. Resorcinol is an analytical reagent for the qualitative determination of ketoses (Seliwanoff's test). It is also used in the production of diazo dyes and plasticizers and as a UV absorber in resins. Resorcinol is one of the active ingredients in products such as Resinol, Vagisil, and Clearasil. Used externally, it is an antiseptic and disinfectant, and is used 5 to 10% in ointments in the treatment of

chronic skin diseases such as psoriasis, hidradenitis suppurativa, andeczema of a sub-acute character. It can be included as an anti-dandruff agent in shampoo or in sunscreen cosmetics. It has also been employed in the treatment of gastric ulcers in doses of 125 to 250 mg in pills. An emerging use of resorcinol is as a template molecule in supramolecular chemistry.

1.4.7 Hydroquinone

Hydroquinone (also known as Idrochinone or Quinol/1-4 dihydroxy benzene/1-4 hydroxy benzene), is an organic compound with the molecular formula $C_6H_4(OH)_2$ shown in Figure 1.3. It is the para isomer of the three isomeric benzenediols. It is a white granular solid.

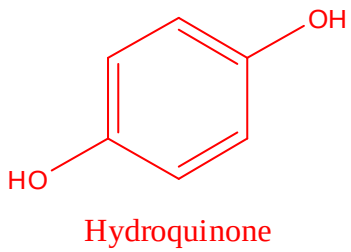

Figure 1.5: Structure of Hydroquinone

Hydroquinone (HQ) is a nonvolatile chemical used in the photographic, rubber, chemical, and cosmetic industries. In human medicine, hydroquinone is used as a topical application in skin whitening to reduce the color of skin.

1.4.8 Natural occurrences of Hydroquinone

Due to its chemical make up, and the reactions it goes through, hydroquinone can be found in the air, as a liquid or a solid. HQ is also known to occur in nature as the beta-D-glucopyranoside conjugate (arbutin), and free HQ is a known component of cigarette smoke. Low concentrations of HQ have been detected in the urine and plasma of humans with no occupational or other known exposure to HQ. Occurring naturally in some insects as well (like millipedes), it is generally part of a defensive chemical secretion.

1.4.9 Uses of Hydroquinone

Hydroquinone is used to lighten the dark patches of skin (also called hyperpigmentation, melasma, "liver spots," "age spots," freckles) caused by pregnancy, birth control pills, hormone medicine, or injury to the skin. It is a major component in most black and white photographic developers for film and paper where, with the compound Metol, it reduces silver halides to elemental silver. It is used in many industrial applications, like photography, manufacturing, and agricultural products as a reducing agent, antioxidant, and polymerization inhibitor [27]. It is also used as a stabilizer for gas and oil, varnishes and paints.

1.4.10 Sulfanilic acid

The Sulfanilic acid (p-aminobenzene sulfonic acid) shown in Figure 1.4, is an important and interesting compound, which finds a number of applications in the syntheses of organic dyes. Sulfanilic acid and certain related substituted derivatives are of considerable medicinal importance as the sulfa drugs. Although they have been supplanted to a wide extent by antibiotics such as penicillin, tetracycline, Chloromycetin, and Aureomycin, the sulfa drugs still have their medical uses, and make up a cons iderable portion of the output of the pharmaceutical sector [52].

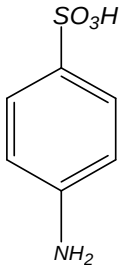

Figure 1.4: Structure of Sulfanilic acid

1.4.11 Uses of Sulfanilic acid

It is used to make dyes and sulpha drugs. It is also used in the manufacture pesticides which can cure wheat rust disease. In addition, it can be used in many organic syntheses.

For example: it reacts with 6-chloro-pyrimidine-2,4-diamine to get 2,4-diamino-6-p-sulphoanilinopyrimidine. This reaction needs reagent HCl and solvent ethanol by heating. The reaction time is 4.0 hours.

1.5 Aim of this thesis

In order to fully understand the issue of multi-step ET (electron transfer) in dihydroxybenzene isomers theoretical and experimental aspect of redox interaction in terms of electrochemical current potential curves analysis is necessary. This research will be devoted to the determination of the electron transfer numbers, analysis of the redox interactions at *ortho*, *meta* and *para* position. Specifically it will cover the area of causes and interpretation of single or multi-step electron reaction in dihydroxybenzene isomers.

The specific aims of this study are:

i) to analyze the redox interaction among different isomers of dihydroxybenzene at different media.
ii) to determine the reaction feasibility among the isomers at different condition.
iii) to study the electron transfer/proton transfer mechanism of reaction by CV and DPV at different pH.
iv) to determine the electro activity of isomers at different pH.

CHAPTER II

Theoretical Background

Electroanalytical chemistry encompasses a group of quantitative analytical methods that are based upon the electrical properties of an analyte solution when it is made part of an electrochemical cell. Voltammetry applies a constant and/or varying potential at an electrode's surface and measures the resulting current with a three electrode system. These electrodes are linked by conducting paths both externally (via electric wires etc.) and internally in solution (via ionic transport) so that charge can be transported.

If the cell configuration permits, the products of the two electrode reactions can be separated. When the sum of the free energy changes at both electrodes is negative, the electrical energy released can be harnessed (batteries). If it is positive, external electrical energy can be supplied to oblige electrode reaction to take place and convert chemical substances (electrolysis) [53].

The electrode can act as a source (for reduction) or a sink (for oxidation) of electrons transferred to or from the species in solution:

$$O + ne \rightarrow R$$

Where, O and R are the oxidized and reduced species. In order for the electron transfer to occur, there must be a correspondence between the energies of the electron orbitals where transfer takes place in the donor and acceptor. In the electrode this level is the highest filled orbital, which in a metal is Fermi energy level. In the soluble species it is the orbital of the valence electron to be given or received. For reduction, there is a minimum energy that the transferable electrons from the electrode must have before the transfer can occur, which corresponds to a sufficiently negative potential. For an oxidation, there is a maximum energy that the lowest unoccupied level in the electrode can have in order to receive electrons from the species in solution, corresponding to a sufficiently positive potential.

In order to study electrode reactions, reproducible experimental conditions must be created which enable minimization of all unwanted factors that can contribute to the measurements and diminish their accuracy. That means to suppress migration effects,

confine the interfacial region as close as possible to the electrode, and minimize solution resistance. These objectives are achieved by the addition of large amount (around 1 mol dm^{-3}) of inert electrolyte, the electroactive species being at a concentration of 5 mM or less [53].

Since an electrode predominantly attracts positively and negatively charged species, which may or may not undergo reaction at the surface, it should be remembered that the species may adsorb at the electrode surface. This makes it clear that in the description of any electrode process we have to consider the transport of species to the electrode surface as well as the electrode reaction itself. This transport can occur by diffusion, convection or migration.

2.1 Mass transfer process in voltammetry

Mass transfer is the movement of material from one location to another in solution. In electrochemical systems, three modes of mass transport are generally considered which a substance may be carried to the electrode surface from bulk solution including diffusion, convection and migration. Any of these or more than one might be operating in a given experiment which is depended on the experimental conditions.

In general, there are three types of mass transfer processes:

- Migration
- Diffusion
- Convection

2.1.1 Migration

Migration is the movement of ions through a solution as a result of electrostatic attraction between the ions and the electrodes. It is the primary cause of mass transfer in the bulk of the solution in a cell. This motion of charged particle through solution, induced by the charges on the electrodes is called migration [54]. This charge movement constitutes a current. This current is called migration current. The larger the number of different kinds of ions in a given solution, the smaller is the fraction of the total charge that is carried by a particular species. Electrolysis is carried out with a large excess of inert electrolyte in the solution so the current of electrons through the external circuit can be balanced by the passage of ions through the solution between the electrodes, and a minimal amount of the

electroactive species will be transported by migration. Migration is the movement of charged species due to a potential gradient. In voltammetric experiments, migration is undesirable but can be eliminated by the addition of a large excess of supporting electrolytes in the electrolysis solution. The effect of migration is applied zero by a factor of fifty to hundred ions excess of an inert supporting electrolyte.

2.1.2 Diffusion

Diffusion refers to the process by which molecules intermingle as a result of their kinetic energy of random motion. Whereas a concentration difference between two regions of a solution, ions or molecules move from the more concentrated region to the dilute and leads to a disappearance of the concentration difference.

The one kind of mode of mass transfer is diffusion to an electrode surface in an electrochemical cell. The rate of diffusion is directly proportional to the concentration difference. When the potential is applied, the cations are reduced at the electrode surface and the concentration is decreased at the surface film. Hence a concentration gradient is produced. Finally, the result is that the rates of diffusion current become larger.

2.1.3 Convection

By mechanical way reactants can also be transferred to or from an electrode. Thus forced convection is the movement of a substance through solution by stirring or agitation. This will tend to decrease the thickness of the diffuse layer at an electrode surface and thus decrease concentration polarization. Natural convection resulting from temperature or density differences also contributes to the transport of species to and from the electrode [55]. At the same time a type of current is produced. This current is called convection current. Removing the stirring and heating can eliminate this current. Convection is a far more efficient means of mass transport than diffusion.

2.2 Cyclic voltammetry (CV)

Cyclic voltammetry is a very versatile electrochemical technique which allows to prove the mechanics of redox and transport properties of a system in solution. This is accomplished with a three electrode arrangement whereby the potential relative to some

reference electrode is scanned at a working electrode while the resulting current flowing through a counter (or auxiliary) electrode is monitored in a quiescent solution. The technique is ideally suited for a quick search of redox couples present in a system; once located, a couple may be characterized by more careful analysis of the cyclic voltammogram. More precisely, the controlling electronic is designed such that the potential between the reference and the working electrodes can be adjusted but the big impedance between these two components effectively forces any resulting current to flow through the auxiliary electrode. Usually the potential is scanned back and forth linearly with time between two extreme values – the switching potentials using triangular potential waveform. When the potential of the working electrode is more positive than that of a redox couple present in the solution, the corresponding species may be oxidized (i.e. electrons going from the solution to the electrode) and produce an anodic current. Similarly, on the return scan, as the working electrode potential becomes more negative than the reduction potential of a redox couple, reduction (i.e. electrons flowing away from the electrode) may occur to cause a cathodic current. For the oxidation reaction involving *n* electrons

$$\mathrm{Red} \rightleftarrows \mathrm{Ox} + ne^-$$

the *Nernst Equation* gives the relationship between the potential and the concentrations of the oxidized and reduced form of the redox couple at equilibrium (at 298 K):

$$E = E^{0'} + \frac{0.059}{n} \log_{10} \frac{[\mathrm{Ox}]_s}{[\mathrm{Red}]}$$

where E is the applied potential and $E^{0'}$ the formal potential; [OX] and [Red] represent surface concentrations at the electrode/solution interface, *not* bulk solution concentrations. Note that the Nernst equation may or may not be obeyed depending on the system or on the experimental conditions.

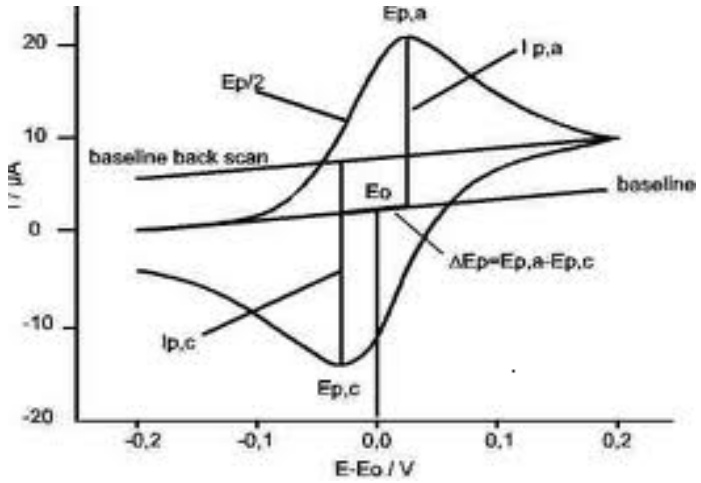

Figure 2.2: The expected response of a reversible redox couple during a single potential cycle

A typical voltammogram is shown in Figure 2.2. The scan shown starts at a slightly negative potential, *(A)* up to some positive switching value, *(D)* at which the scan is reversed back to the starting potential. The current is first observed to peak at E_{pa} (with value i_{pa}) indicating that an oxidation is taking place and then drops due to depletion of the reducing species from the diffusion layer. During the return scan the processes are reversed (reduction is now occurring) and a peak current is observed at E_{pc} (corresponding value, i_{pc}).

Providing that the charge–transfer reaction is reversible, that there is no surface interaction between the electrode and the reagents, and that the redox products are stable (at least in the time frame of the experiment), the ratio of the reverse and the forward current $i_{pr}/i_{pf} = 1.0$ (in Figure 2.2 $i_{pa} = i_{pf}$ and $i_{pc} = i_{pr}$). In addition, for such a system it can be shown that:

- the corresponding peak potentials E_{pa} and E_{pc} are independent of scan rate and concentration
- the formal potential for a reversible couple $E^{0'}$ is centered between E_{pa} and E_{pc}: $E^{0'} = (E_{pa} + E_{pc})/2$
- the separation between peaks is given by $\Delta E_p = E_{pa} - E_{pc} = 59/n$ mV (for a n electron transfer reaction) at all scan rates (however, the measured value for a reversible process is generally higher due to uncompensated solution resistance and non-linear diffusion. Larger values of ΔE_p, which increase with increasing scan rate, are characteristic of slow electron transfer kinetics).

It is possible to relate the half-peak potential ($E_{p/2}$, where the current is half of the peak current) to the polarographic half-wave potential, $E_{1/2}$: $E_{p/2} = E_{1/2} \pm 29mV/n$ (The sign is positive for a reduction process.)

Simply stated, in the forward scan, the reaction is $O + e^- \rightarrow R$, R is electrochemically generated as indicated by the cathodic current. In the reverse scan, $R \rightarrow O + e^-$, R is oxidized back to O as indicated by the anodic current. The CV is capable of rapidly generating a new species during the forward scan and then probing its fate on the reverse scan. This is a very important aspect of the technique [56].

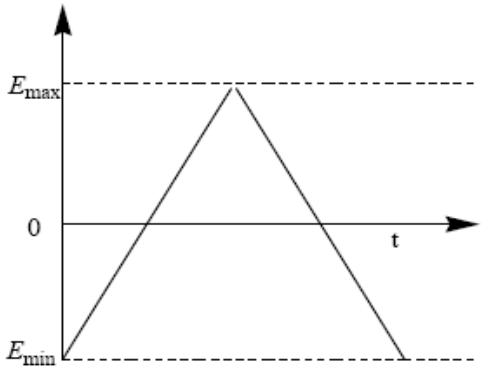

Figure 2.3: Variation of potential with time in cyclic voltammetry

A characteristic feature is the occurrence of peaks, identified by the peak potential E_p, which corresponds to electron transfer reactions. The repetitive triangular potential excitation signal for CV causes the potential of the working electrode to sweep backward and forward between two designate values (the switching potentials).

In cyclic voltammetry of reversible system, the product of the initial oxidation or reduction is then reduced or oxidized, respectively, on reversing the scan direction.

Adsorbed species lead to changes in the shape of the cyclic voltammogram, since they do not have to diffuse from the electrode surface. In particular, if only adsorbed species are oxidized or reduced, in the case of fast kinetics the cyclic voltammogram is symmetrical, with coincident oxidation and reduction peak potentials [57].

Cyclic voltammetry is one of the most versatile techniques for the study of electroactive species, as it has a provision for mathematical analysis of an electron transfer process at the electrode [58-61]. It is an electroanalytical tool for monitoring and recognition of

many electrochemical processes taking place at the surface of electrode and can be used to study redox processes in biochemistry and macromolecular chemistry [53].

2.2.1 Single electron transfer process

Based upon the values of electrochemical parameters, i.e., peak potential E_p, half peak potential ($E_{p/2}$), half wave potential ($E_{1/2}$), peak current (I_p), anodic peak potential E_{pa}, cathodic peak potential E_{pc} etc, it can be ascertained whether a reaction is reversible, irreversible or quasi-reversible. The electrochemical parameters can be graphically obtained from the voltammogram as shown in the Figure 2.3.

Three types of single electron transfer process can be studied.

a. Reversible process. b. Irreversible process and c. Quasi-reversible.

2.2.1(a) Reversible processes

The peak current for a reversible couple (at 25°C), is given by the Randles-Sevcik equation: $\boldsymbol{i}_p = (2.69 \times 10^5)\, n^{3/2} A C D^{1/2} v^{1/2}$

where n is the number of electrons, A the electrode area (in cm^2), C the concentration (in mol/cm^3), D the diffusion coefficient (in cm^2/s), and v the scan rate (in V/s). Accordingly, the current is directly proportional to concentration and increases with the square root of the scan rate. The ratio of the reverse-to-forward peak currents, $\boldsymbol{i}_{pr}/\boldsymbol{i}_{pf}$, is unity for a simple reversible couple. This peak ratio can be strongly affected by chemical reactions coupled to the redox process. The current peaks are commonly measured by extrapolating the preceding baseline current. The position of the peaks on the potential axis (E_p) is related to the formal potential of the redox process. The formal potential for a reversible couple is centered between E_{pa} and E_{pc}:

$$E^\circ = (E_{pa} + E_{pc})/2$$

The separation between the peak potentials (for a reversible couple) is given by:

$$\Delta E_p = E_{pa} - E_{pc} = 59mV/n$$

Thus, the peak separation can be used to determine the number of electrons transferred, and as a criterion for a Nernstian behavior. Accordingly, a fast one-electron process exhibits a ΔE_p of about 59 mV. Both the cathodic and anodic peak potentials are independent of the scan rate. It is possible to relate the half-peak potential ($E_{p/2}$, where the current is half of the peak current) to the polarographic half-wave potential, $E_{1/2}$

$$E_{p/2} = E_{1/2} \pm 29mV/n$$

(The sign is positive for a reduction process.) For multi electron-transfer (reversible) processes, the cyclic voltammogram consists of several distinct peaks, if the E^o values for the individual steps are successively higher and are well separated. An example of such mechanism is the six-step reduction of the fullerenes C_{60} and C_{70} to yield the hexaanion products C_{60}^{6-} and C_{70}^{6-} where six successive reduction peaks can be observed.

The situation is very different when the redox reaction is slow or coupled with a chemical reaction. Indeed, it is these "nonideal" processes that are usually of greatest chemical interest and for which the diagnostic power of cyclic voltammetry is most useful. Such information is usually obtained by comparing the experimental voltammograms with those derived from theoretical (simulated) ones.

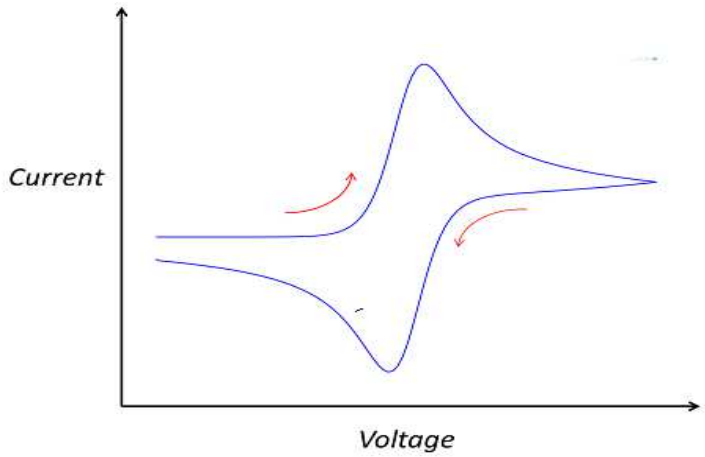

Figure 2.4: Reversible cyclic voltammogram of redox process

2.2.1(b) Irreversible processes

For irreversible processes (those with sluggish electron exchange), the individual peaks are reduced in size and widely separated. Totally irreversible systems are characterized by a shift of the peak potential with the scan rate:

$$E_p = E° - (RT/\alpha n_a F)[0.78 - \ln(k^o/(D)^{1/2}) + \ln (\alpha n_a F\nu/RT)^{1/2}]$$

where α is the transfer coefficient and n_a is the number of electrons involved in the charge-transfer step. Thus, E_p occurs at potentials higher than E°, with the overpotential related to k° and a. Independent of the value k°, such peak displacement can be compensated by an appropriate change of the scan rate. The peak potential and the half-peak potential (at 25°C) will differ by $48/\alpha n$ mV. Hence, the voltammogram becomes more drawn-out as $\alpha\mathbf{n}$ decreases.

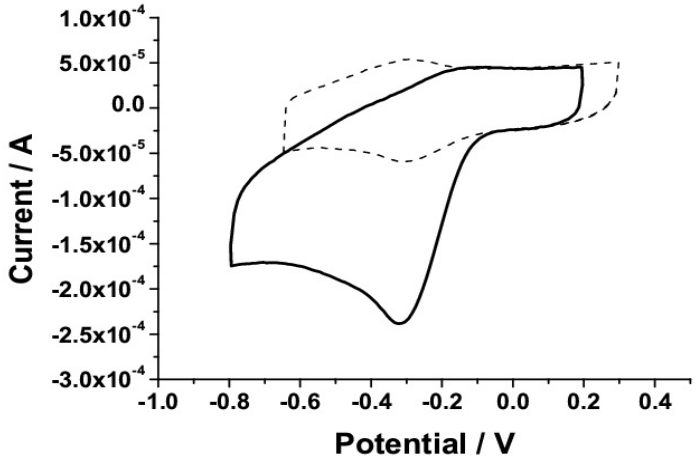

Figure 2.5: Cyclic voltammogram of irreversible redox process

2.2.1(c) Quasi-reversible process

Quasi-reversible process is termed as a process, which shows intermediate behavior between reversible and irreversible processes. In such a process the current is controlled by both the charge transfer and mass transfer.

Cyclic voltammogram for quasi-reversible process is shown in Figure 2.6 [62].

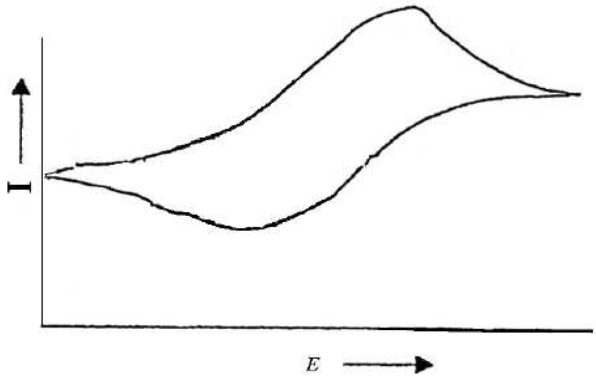

Figure 2.6: Cyclic voltammogram of quasi-reversible redox process

For quasi-reversible process the value of standard heterogeneous electron transfer rate constant, k_{sh}^{o} lies in the range of 10^{-1} to 10^{-5} cm sec^{-1} [63]. An expression relating the current to potential dependent charge transfer rate was first provided by Matsuda and Ayabe [64].

$$I(t) = C_{o(0,t)} k_{sh}^{o} Exp\left[-\frac{\alpha nF}{RT}\{E(t) - E^{o}\}\right] - C_{R(0,t)} k_{sh}^{o} Exp\left[-\frac{\beta nF}{RT}\{E(t) - E^{o}\}\right] \ldots.2.1$$

where k_{sh}^{o} is the heterogeneous electron transfer rate constant at standard potential E^{0} of redox system. α is the transfer coefficient and β = 1- α. In this case, the shape of the peak and the various peak parameters are functions of α and the dimensionless parameter, Λ, defined as [65]

$$\Lambda = \frac{k_{s,h}}{D^{1/2}(nF/RT)^{1/2}\upsilon^{1/2}} \ldots\ldots\ldots\ldots\ldots\ldots\ldots\ldots\ldots\ldots\ldots..2.2$$

when $D_o = D_R = D$

D_o and D_R are the diffusion coefficients of oxidized and reduced species respectively.

2.3 Pulse techniques

The basis of all pulse techniques is the difference in the rate of decay of the charging and the faradaic currents following a potential step (or pulse). The charging current decays considerably faster than the faradaic current. A step in the applied potential or current represents an instantaneous alteration of the electrochemical system. Analysis of the evolution of the system after perturbation permits deductions about electrode reactions and their rates to be made. The potential step is the base of pulse voltammetry. After applying

a pulse of potential, the capacitive current dies away faster than the faradic one and the current is measured at the end of the pulse. This type of sampling has the advantage of increased sensitivity and better characteristics for analytical applications. At solid electrodes there is an additional advantage of discrimination against blocking of the electrode reaction by adsorption [66].

2.3.1 Differential pulse voltammetry (DPV)

The potential wave form for differential pulse voltammetry (DPV) is shown in Figure 2.8. The potential wave form consists of small pulses (of constant amplitude) superimposed upon a staircase wave form. Unlike Normal pulse voltammetry (NPV**)**, the current is sampled twice in each Pulse Period (once before the pulse, and at the end of the pulse), and the difference between these two current values is recorded and displayed.

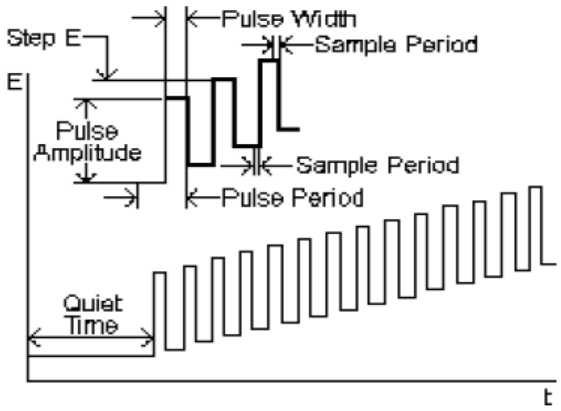

Figure 2.8: Scheme of application of potential

The important parameters for pulse techniques are as follows:

- Pulse amplitude is the height of the potential pulse. This may or may not be constant depending upon the technique.
- Pulse width is the duration of the potential pulse.
- Sample period is the time at the end of the pulse during which the current is measured.

- For some pulse techniques, the pulse period or drop time must also be specified. This parameter defines the time required for one potential cycle, and is particularly significant for polarography (i.e., pulse experiments using a mercury drop electrode), where this time corresponds to the lifetime of each drop (i.e., a new drop is dispensed at the start of the drop time, and is knocked off once the current has been measured at the end of the drop time - note that the end of the drop time coincides with the end of the pulse width).

Quantitative treatments for reversible systems demonstrated that, with only *R* (positive sign) or only *O* (negative sign) initially present, the following equation can be written as

$$E_{max} = E_{1/2} \pm \frac{\Delta E}{2} \quad \text{.....2.11}$$

where ΔE is the pulse amplitude.

CHAPTER III

Experimental

During the course of the present work a number of techniques were involved which were in general standard ones. Constant efforts for attaining the ideal conditions for the experiments were always attempted. The thoroughly cleaned glass pieces were dried in electric oven. The smaller pieces of apparatus were dried in electric oven and stored in a desiccator, while larger pieces of apparatus were used directly from the oven.

The redox interaction among different isomers of dihydroxybenzene and the reaction feasibility among those isomers and electrochemical reactions in aqueous solution and buffer solution at different pH (3, 5, 7 and 9) has been measured using Cyclic Voltammetry (CV) and Differential Pulse Voltammetry (DPV) at glassy carbon (Gc) or platinum electrode (Pt). Details of the instrumentation are given in the following sections. The source of different chemicals, the instruments and brief description of the methods are given below.

3.1 Chemicals

All chemicals and solvents are used in the electrochemical synthesis and analytical work were analytical grade obtained from E. Merck Germany, Merck Specialities private Ltd. Mumbai, India. Loba Chemie Pvt. Ltd. Mumbai of India and Fisher Scientific UK Ltd. The used chemicals were-

Sl. No.	Chemicals	Molecular formula	Molar mass	Reported purity	Producer
1.	Resorcinol	$C_6H_6O_2$	110.11	99.9%	Loba Chemie Pvt. Ltd. Mumbai, India.

Sl. No.	Chemicals	Molecular formula	Molar mass	Reported purity	Producer
2.	Hydroquinone	$C_6H_6O_2$	110.11	99%	Loba Chemie Pvt. Ltd. Mumbai, India.
3.	Catechol	$C_6H_4(OH)_2$	110.11	99%	Fisher Scientific UK Ltd.
4.	Sulfanilic Acid	$C_6H_7NO_3S$	173.19	99%	Merck Specialities private Ltd. Mumbai, India.
5.	Glacial acetic acid	CH_3COOH	60.05	99.5%	Loba Chemie Pvt. Ltd. Mumbai, India.
6.	Sodium acetate	CH_3COONa	136.08	99%	E-Merck, Germany.
7.	Sodium di Hydrogen Ortho Phosphate	$NaH_2PO_4.2H_2O$	156.01	98-100%	Loba Chemie Pvt. Ltd. Mumbai, India.
8.	Di-Sodium Hydrogen Ortho Phosphate	$Na_2HPO_4.2H_2O$	177.99	97-100%	Fisher Scientific UK Ltd.
9.	Sodium Hydroxide	NaOH	40.00	97%	E-Merck, Germany.
10.	Sodium Bicarbonate	$NaHCO_3$	84.00	99%	Loba Chemie Pvt. Ltd. Mumbai, India.
11.	Potassium Chloride	KCl	74.55	99%	Merck Specialities private Ltd. Mumbai, India.

3.2 Equipments

During this research work the following instruments were used.

i) The electrochemical studies (CV, DPV and CA) were performed with a PC controlled µstat 400 Potentiostats/Galvanostats (Drop Sens, Spain) (Figure 3.1),

ii) A Pyrex glass micro cell with Teflon cap,

iii) Glassy carbon(Gc)/ Pt working electrode,

iv) Ag/ AgCl reference electrode,

v) Pt wire counter electrode,

vi) A pH meter (pH Meter, Hanna Instuments, Italy) was employed for maintaining the pH of the solutions. Preparation of the solutions was done by ordinary laboratory glassware, and

vii) A HR 200 electronic balance with an accuracy of ± 0.0001g was used for weighting.

3.3 Cyclic voltammetry (CV)

In several well established electrochemical techniques for the study of electrochemical reactions, we have chosen the CV technique to study and analyze the redox reactions occurring at the polarizable electrode surface. This technique helps us to understand the mechanism of electron transfer reaction of the compounds as well as the nature of adsorption of reactants or products on the electrode surface. CV is often the first experiment performed in an electrochemical study. CV consists of imposing an excitation potential nature on an electrode immersed in an unstirred solution and measuring the current and its potential ranges varies from a few millivolts to hundreds of millivolts per second in a cycle. This variation of anodic and cathodic current with imposed potential is termed as voltammogram [63].

The technique involves under the diffusion controlled mass transfer condition at a stationary electrode utilizing symmetrical triangular scan rate ranging from 1 mVs^{-1} to hundreds millivolts per second.

In CV the current function can be measured as a function of scan rate. The potential of the working electrode is controlled vs a reference electrode such as Ag/AgCl electrode. The electrode potential is ramped linearly to a more negative potential and then ramped is reversed back to the starting voltage. The forward scan produces a current peak for any analyte that can be reduced through the range of potential scan. The current will increase as the current reaches to the reduction potential of the analyte [67].

The current at the working electrode is monitored as a triangular excitation potential is applied to the electrode. The resulting voltammogram can be analyzed for fundamental information regarding the redox reaction. The potential at the working electrode is

controlled vs a reference electrode, Ag/AgCl (standard NaCl) electrode. The excitation signal varies linearly with time. First scan positively and then the potential is scanned in reverse, causing a negative scan back to the original potential to complete the cycle. Signal on multiple cycles can be used on the scan surface. A cyclic voltammogram is plot of response current at working electrode to the applied excitation potential.

3.4 Important features of CV

An electrochemical system containing species 'O' capable of being reversibly reduced to 'R' at the electrode is given by,

$$O + ne^- = R \quad \ldots\ldots\ldots\ldots\ldots\ldots\ldots\ldots 3.1$$

Nernst equation for the system is

$$E = E^0 + \frac{0.059}{n}\log\frac{C_0^s}{C_R^s} \quad \ldots\ldots\ldots\ldots\ldots\ldots\ldots\ldots 3.2$$

Where,

E = Potential applied to the electrode

E^0 = Standard reduction potential of the couple versus reference electrode

n = Number of electrons in Equation (3.1)

C_0^s = Surface concentration of species 'O'

C_R^s = Surface concentration of species 'R'

A redox couple that changes electrons rapidly with the working electrode is termed as electrochemically reverse couple. The relation gives the peak current i_{pc}

$$i_{pc} = 0.4463\ nFA\ (D\alpha)^{1/2}C \quad \ldots\ldots\ldots\ldots\ldots\ldots 3.3$$

$$\alpha = \left(\frac{nFv}{RT}\right) = \left(\frac{nv}{0.026}\right)$$

Where,

i_{pc} = peak current in amperes

F= Faraday`s constant (approximately 96500)

A = Area of the working electrode in cm^2

v= Scan rate in volt/ sec

C= Concentration of the bulk species in mol/L

D= Diffusion coefficient in cm^2 /sec

In terms of adjustable parameters, the peak current is given by the Randless-Sevcik equation,

$$i_{pc}=2.69\times10^{5}\times n^{3/2}AD^{1/2}Cv^{1/2} \quad \ldots\ldots\ldots\ldots\ldots\ldots\ldots 3.4$$

The peak potential E_p for reversible process is related to the half wave potential $E_{1/2}$, by the expression,

$$E_{pc} = E_{1/2} - 1.11\left(\frac{RT}{nF}\right), \quad \text{at } 25^0\text{C} \ldots\ldots\ldots\ldots\ldots\ldots 3.5$$

$$E_{pc} = E_{1/2} - \left(\frac{0.0285RT}{n}\right)\ldots\ldots\ldots\ldots\ldots\ldots\ldots\ldots 3.6$$

The relation relates the half wave potential to the standard electrode potential

$$E_{1/2} = E^0 - \frac{RT}{nF}\ln\frac{f_{red}}{f_{ox}}\left(\frac{D_{ox}}{D_{ox}}\right)^{1/2}$$

$$E_{1/2} = E^0 - \frac{RT}{nF}\ln\left(\frac{D_{ox}}{D_{red}}\right)^{1/2} \ldots\ldots\ldots\ldots\ldots\ldots\ldots 3.7$$

Assuming that the activity coefficient f_{ox} and f_{red} are equal for the oxidized and reduced species involved in the electrochemical reaction.

From Equation (3.6), we have,

$$E_{pa} - E_{pc} = 2.22\left(\frac{RT}{nF}\right) \quad \text{at } 25^0\text{C}\ldots\ldots\ldots\ldots\ldots\ldots 3.8$$

$$\text{or } E_{pa} - E_{pc} = \left(\frac{0.059}{n}\right) \quad \text{at } 25^0\text{C}\ldots\ldots\ldots\ldots\ldots\ldots \quad 3.9$$

This is a good criterion for the reversibility of electrode process. The value of i_{pa} should be close for a simple reversible couple,

$$i_{pa}/i_{pc} = 1\ldots\ldots\ldots\ldots\ldots\ldots\ldots\ldots\ldots 3.10$$

And such a system $E_{1/2}$ can be given by,

$$E_{1/2} = \frac{E_{pa} + E_{pc}}{2}\ldots\ldots\ldots\ldots\ldots\ldots 3.11$$

For irreversible processes (those with sluggish electron exchange), the individual peaks are reduced in size and widely separated, Totally irreversible systems are characterized by a shift of the peak potential with the scan rate [68];

$$E_p=E^0-(RT/\alpha n_aF)[0.78-\ln(k^0/(D)^{1/2})+\ln(\alpha n_aF\alpha/RT)^{1/2}]\ldots\ldots..3.12$$

Where α is the transfer coefficient and n_a is the number of electrons involved in the charge transfer step. Thus E_p occurs at potentials higher than E^0, with the over potential related to k^0 (standard rate constant) and α. Independent of the value k^0, such peak displacement can be compensated by an appropriate change of the scan rate. The peak potential and the half-peak potential (at 25^0 C) will differ by 48/ αn mV. Hence, the voltammogram becomes more drawn-out as αn decreases.

3.5 Differential pulse voltammetry (DPV)

Differential pulse voltammetry (DPV) is a technique that is designed to minimize background charging currents. The waveform in DPV is a sequence of pulses, where a baseline potential is held for a specified period of time prior to the application of a potential pulse. Current is sampled just prior to the application of the potential pulse. The potential is then stepped by a small amount (typically < 100 mV) and current is sampled again at the end of the pulse. The potential of the working electrode is then stepped back by a lesser value than during the forward pulse such that baseline potential of each pulse is incremented throughout the sequence.

By contrast, in normal pulse voltammetry the current resulting from a series of ever larger potential pulse is compared with the current at a constant 'baseline' voltage. Another type of pulse voltammetry is square wave voltammetry, which can be considered a special type of differential pulse voltammetry in which equal time is spent at the potential of the ramped baseline and potential of the superimposed pulse. The potential wave form consists of small pulses (of constant amplitude) superimposed upon a staircase wave form [69]. Unlike NPV, the current is sampled twice in each pulse Period (once before the pulse, and at the end of the pulse), and the difference between these two current values is recorded and displayed.

3.6 Important features of DPV

Differential pulse voltammetry has these prominence:

i) Current is sampled just prior to the application of the potential pulse.

ii) Reversible reactions show symmetrical peaks and irreversible reaction show asymmetrical peaks.

iii) The peak potential is equal to $E_{1/2}^{r}$-ΔE in reversible reactions, and the peak current is proportional to the concentration.

3.7 Computer controlled potentiostats

The main instrument for voltammetry is the Potentiostats/ Galvanostats (μStat 400, DropSens, Spain), which will be applied to the desired potential to the electrochemical cell (i.e. between a working electrode and a reference electrode), and a current-to-voltage converter, which measures the resulting current, and the data acquisition system produces the resulting voltammogram.

3.8 Electrochemical cell

This research work was performed by a three electrode electrochemical cell. The voltammetric cell also contains a Teflon cap. The electrochemical reaction of interest takes place at the working electrode and the electrical current at this electrode due to electron transfer is termed as faradic current. The counter electrode is driven by the potentiostatic circuit to balance the faradic process at the working electrode with an electron transfer of opposite direction.

3.9 Electrodes

Three types of electrodes are used in this research:

i) Working electrodes are Glassy carbon (GC) electrode with 3.0 mm diameter disc, Gold (Au) & Platinum (Pt) electrode with 1.6 mm diameter disc

ii) Ag/ AgCl (standard NaCl) electrode used as reference electrode from BASi, USA

iii) Counter electrode is a Pt wire

The working electrode is an electrode on which the reaction of interest is occurring. The reference electrode is a half-cell having a known electrode potential and it keeps the potential between itself and the working electrode. The counter electrode is employed to allow for accurate measurements to be made between the working and reference electrodes.

3.10 Preparation of electrodes

In this study, Glassy carbon (GC), Gold (Au) and Platinum (Pt) electrodes purchase from the BASi, USA are used as working electrode. Electrode preparation includes polishing and conditioning of the electrode. The electrode was polished with 0.05µm alumina powder on a wet polishing cloth. For doing so a part of the cloth was made wet with deionized water and alumina powder was sprinkled over it. Then the electrode was polished by softly pressing the electrode against the polishing surface at least 10 minutes. The electrode surface would look like a shiny mirror after thoroughly washed with deionized water.

3.11 Removing dissolved Oxygen from solution

Dissolved oxygen can interfere with observed current response so it is needed to remove it. Experimental solution was indolented by purging for at least 5-10 minutes with 99.99% pure and dry nitrogen gas (BOC, Bangladesh). By this way, traces of dissolved oxygen were removed from the solution.

3.12 Electrode polishing

Materials may be adsorbed to the surface of a working electrode after each experiment. Then the current response will degrade and the electrode surface needs to clean. In this case, the cleaning required is light polishing with 0.05µm alumina powder. A few drops of polish are placed on a polishing pad and the electrode is held vertically and the polish rubbed on in a figure-eight pattern for a period of 30 seconds to a few minutes depending upon the condition of the electrode surface. After polishing the electrode surface is rinsed thoroughly with deionized water.

3.13 Experimental procedure

The electrochemical cell filled with solution 50mL of the experimental solution and the Teflon cap was placed on the cell. The working electrode together with reference electrode and counter electrode was inserted through the holes. The electrodes were sufficiently

immersed. The solution system is deoxygenated by purging the nitrogen gas for about 10 minutes. The solution has been kept quiet for 10 seconds. After determinating the potential window the voltammogram is taken at various scan rates, pH and concentrations from the Drop View Software.

3.14 Preparation of buffer solutions

Acetate Buffer Solution: To prepare acetate buffer (pH 3.0-5.0) solution definite amount of sodium acetate was dissolved in 0.1M acetic acid in a volumetric flask and the pH was measured. The pH of the buffer solution was adjusted by further addition of acetic acid and / or sodium acetate.

Phosphate Buffer Solution: Phosphate buffer solution (pH 6.0-8.0) was prepared by mixing a solution of 0.1M sodium dihydrogen ortho-phosphate ($NaH_2PO_4.2H_2O$) with a solution of 0.1M disodium hydrogen ortho-phosphate ($Na_2HPO_4.2H_2O$). The pH of the prepared solution was measured with pH meter. Hydroxide Buffer Solution: To prepare hydroxide buffer (pH 9.0-11.0) solution definite amount of sodium hydroxide was dissolved in 0.1M sodium bicarbonate in a volumetric flask. The pH of the prepared solution was measured with pH meter.

Figure 3.1: Experimental setup (Software controlled Potentiostats (µstat 400))

CHAPTER IV

Results and Discussion

The redox interaction of` the isomers of dihydroxybenzene for example catechol, hydroquinone and resorcinol have been studied using cyclic voltammetry (CV) and differential pulse voltammetry (DPV). The study was carried out at glassy carbon electrode (GC), Gold electrode (Au) and Platinum electrode (Pt) in buffer solution of different pH (3, 5, 7 and 9) at various scan rates and various concentrations.

4.1 Electrochemical behavior of Catechol, Resorcinol and Hydroquinone

Figure 4.1 shows the cyclic voltammogram of 2mM catechol (brown line), 2mM resorcinol (blue line) and 2mM hydroquinone (green line) in buffer solution of pH 7 of GC electrode at scan rate 0.1V/s in the first scan of potential. Catechol shows an anodic peak at 0.39V and corresponding cathodic peak at 0.01V. The corresponding peak potential difference is 0.38V which is higher than theoretical value. The peak current ratio is 1.4. The voltammogram is quasi-reversible. Resorcinol shows an anodic peak at 0.77V and corresponding cathodic peak is absent. The voltammogram of resorcinol is irreversible. Hydroquinone shows an anodic peak at 0.22V and corresponding cathodic peak at -0.11V. The corresponding peak potential difference is 0.33V which is higher than theoretical value. The peak current ratio is 1.1. The voltammogram is almost reversible. The current potential data, peak potential difference, peak current and peak current ratio data for first scan are presented in Table 4.1-4.3. The anodic peak current of catechol, resorcinol and hydroquinone are almost equal at the same condition.

Catechol showed one anodic peak related to its transformation to *o*-quinone and corresponding cathodic peak related to its transformation to catechol from *o*-quinone (Scheme 1) within a quasi-reversible two-electron transfer process. Resorcinol showed one anodic peak related to its transformation to *m*-quinone (Scheme 1) within a irreversible two-electron transfer process. Hydroquinone showed one anodic peak related to its

transformation to *p*-quinone and corresponding cathodic peak related to its transformation to hydroquinone from *p*-quinone (Scheme 1) within a reversible two-electron transfer process. The anodic peak potential of resorcinol (0.77V) is higher than the catechol (0.39V) and catechol is higher than the hydroquinone (0.22V). Among the isomers, the electron transfer of hydroquinone is easier than the catechol and catechol is easier than the resorcinol. As-OH sites in resorcinol are connected via *meta* linkage, so the electron transfer at *meta* position is unfavorable (electron deficiency) to that at a *para* (hydroquinone) or *ortho* (catechol) –position.

During the repetitive cycling of potential of catechol and hydroquinone, the anodic and cathodic peak current ratio is nearly unity that can be considered as criteria for the stability of *o*-quinone or *p*-quinone produced at the surface of electrode. After repetitive cycling of potential of resorcinol the anodic peak current decreases abruptly may be due to the formation of electro-inactive species on the electrode surface through polymerization or chemical complications.

Figure 4.2 shows the cyclic voltammogram of 2mM catechol (brown line), 2mM resorcinol (blue line) and 2mM hydroquinone (green line) in buffer solution of pH 7 of Au electrode at scan rate 0.1V/s in the first scan of potential. For catechol, two anodic peaks appeared at 0.23V and 1.01V and corresponding cathodic peaks appeared at -0.04V and 0.41V.The corresponding peak potential differences are 0.27V and 0.60V which are higher than theoretical value. The corresponding first and second peak current ratio are ~1.0 and 1.9 respectively. The first corresponding peak is reversible whereas second one is quasi-reversible. The first and second anodic peak potential difference, ΔE is 0.78V. Resorcinol shows a broad anodic peak at 1.02V and corresponding cathodic peak at 0.37V. The corresponding peak potential difference is 0.65V which is higher than theoretical value. The peak current ratio is ~2. The voltammogram is quasi-reversible. For hydroquinone, two anodic peaks appeared at 0.21V and 1.01V and corresponding cathodic peaks appeared at -0.01V and 0.48 V. The corresponding peak potential differences are 0.22V and 0.53V which are higher than theoretical value. The corresponding first and second peak current ratio are ~1.0 and 1.8 respectively. The first corresponding peak is reversible whereas second one is quasi-reversible. The first and second anodic peak potential difference, ΔE is

0.80V. The current potential data, peak potential difference, peak current and peak current ratio data for first scan are presented in Table 4.4 - 4.6.

Catechol and hydroquinone at Au electrode showed two anodic peaks related to its transformation to *o*-quinone at two steps and corresponding cathodic peak related to its transformation to catechol from *o*-quinone at two steps (Scheme 2) within a quasi-reversible two step two-electron transfer process. Resorcinol showed one anodic peak related to its transformation to *m*-quinone and corresponding cathodic peak related to its transformation to resorcinol from *m*-quinone (Scheme 2) within a quasi-reversible two electron transfer process.

The anodic peak potential of resorcinol is higher to that of catechol and catechol is higher to that of hydroquinone which is similar to GC electrode.

When a compound containing two redox sites has a well-defined redox state, the ΔE corresponds to difference in the interaction energy [6]. For catechol and hydroquinone, the ΔE is 0.78V and 0.80V respectively. If the difference in the interaction energy is estimated only from the difference in the half wave potentials, we have

$$u_e' = F\left[(E_2) - (E_1)\right]/2$$

The interaction energy of catechol and hydroquinone are 37.63J and 38.60J respectively.

So the extent of delocalization of charge through phenyl ring of hydroquinone will be higher than the catechol. Resorcinol shows only one anodic and cathodic peak, -OH sites in resorcinol are connected via *meta* linkage, so the electron transfer at *meta* position is unfavorable due to the deficiency of electron.

The electronic communication between the redox sites takes place through a conjugated molecular bridge. The communication is manifested as a mixed-valence (MV) state or an intervalence transfer band. When redox centers are connected with π-conjugated linkers, they often take mixed valence states owing to delocalization of the redox charge, exemplified by dinuclear-metal complexes [7, 10, 16, 35] and aryl amine derivatives [17, 23-32, 70]. Among the isomers, the electron transfer of hydroquinone is easier than the catechol and catechol is easier than the resorcinol. As -OH sites in resorcinol are connected via *meta* linkage, so the electron transfer at *meta* position is unfavorable (electron deficiency) to that at a *para* (hydroquinone) or *ortho* (catechol) –position.

Figure 4.3 shows the cyclic voltammogram of 2mM catechol (brown line), 2mM resorcinol (blue line) and 2mM hydroquinone (green line) in buffer solution of pH 7 of Pt electrode at scan rate 0.1V/s in the first scan of potential. Catechol shows an anodic peak at 0.39V and corresponding cathodic peak at -0.07V. The corresponding peak potential difference is 0.46V which is higher than theoretical value. The peak current ratio is nearly 0.75. The voltammogram is quasi-reversible. Resorcinol shows an anodic peak at 0.92V and corresponding cathodic peak at -0.11V. The corresponding peak potential difference is higher than theoretical value. The peak current ratio is nearly 5. The voltammogram of resorcinol is quasi-reversible. Hydroquinone shows anodic peaks at 0.35V and 0.87V and corresponding cathodic peaks at -0.09V and 0.39V. The corresponding peak potential differences are 0.44V and 0.48V which are higher than theoretical value. The corresponding first peak current ratio is 1.2. The first corresponding peak is reversible whereas second one is quasi reversible. The first and second anodic peak potential difference, ΔE is 0.47V. The corresponding interaction energy of hydroquinone is 22.67J. So the extent of delocalization of charge through phenyl ring of hydroquinone is higher than the catechol and resorcinol. Resorcinol shows only one anodic and cathodic peak, -OH sites in resorcinol are connected via *meta* linkage, so the electron transfer at *meta* position is unfavorable due to the deficiency of electron. For catechol, the second anodic and cathodic peak is too weak to determine the peak potential and peak current.

The current potential data, peak potential difference, peak current and peak current ratio data are presented in Table 4.7- 4.9.

Figure 4.4 shows the cyclic voltammogram of 2mM catechol (brown line), 2mM resorcinol (blue line) and 2mM hydroquinone (green line) in buffer solution of pH 3 of GC electrode at scan rate 0.1V/s in the first scan of potential. In Figure 4.4 catechol shows an anodic peak at 0.85V and corresponding cathodic peak at 0.06V. The corresponding peak potential difference is 0.79V. The peak current ratio is 1.15. The voltammogram is quasi-reversible. Resorcinol shows an anodic peak at 1.08V and corresponding cathodic peak is absent. The voltammogram of resorcinol is irreversible. Hydroquinone shows an anodic peak at 0.71V and corresponding cathodic peak at -0.07 V. The corresponding peak potential difference is 0.78V. The peak current ratio is 1.5. The voltammogram is almost reversible. The anodic peak current of catechol is higher than resorcinol and hydroquinone but both resorcinol and

hydroquinone are almost equal at the same condition. Among the isomers, the electron transfer of hydroquinone is easier than the catechol and catechol is easier than the resorcinol.

Figure 4.5 shows the cyclic voltammogram of 2mM catechol (brown line), 2mM resorcinol (blue line) and 2mM hydroquinone (green line) in buffer solution of pH 3 of Au electrode at scan rate 0.1V/s in the first scan of potential. In Figure 4.5, catechol shows two anodic peaks at 0.57V and 1.35V and corresponding cathodic peaks at 0.18V and 0.59V. The corresponding peak potential difference are 0.39V and 0.76V which is higher than theoretical value. The peak current ratio are 1.0 and 0.41. The voltammogram is quasi-reversible. Resorcinol shows two anodic peaks at 1.0V and 1.38V and corresponding two cathodic peaks at -0.22V and 0.58V. Hydroquinone shows two anodic peaks at 0.21V and 0.99V and corresponding cathodic peaks at 0.02V and 0.45V. The corresponding peak potential difference are 0.19V and 0.45V. The peak current ratio is 0.79 and 0.30. The voltammogram is almost reversible. The current potential data, peak potential difference, peak current and peak current ratio data for first scan are presented in Table 4.10- 4.12. The anodic peak current of all isomers, catechol, resorcinol and hydroquinone are almost equal at the same condition.

Catechol showed two anodic peaks related to its transformation to *o*-quinone and corresponding cathodic peaks related to its transformation to catechol from *o*-quinone (Scheme 2) within a quasi-reversible two-electron transfer process. Resorcinol showed one anodic peak related to its transformation to *m*-quinone (Scheme 2) within a irreversible two-electron transfer process. Hydroquinone showed one anodic peak related to its transformation to *p*-quinone and corresponding cathodic peak related to its transformation to hydroquinone from *p*-quinone (Scheme 1) within a reversible two-electron transfer process. Among the isomers, the electron transfer of hydroquinone is easier than the catechol and catechol is easier than the resorcinol.

Figure 4.6 shows the cyclic voltammogram of 2mM catechol (brown line), 2mM resorcinol (blue line) and 2mM hydroquinone (green line) in buffer solution of pH 3 of Pt electrode at scan rate 0.1V/s in the first scan of potential. In Figure 4.6, catechol shows an anodic peak at 0.68V and corresponding cathodic peak at -0.05V. The peak current ratio is 1.0. The voltammogram is quasi-reversible. Resorcinol shows an anodic peak at 1.05V and

corresponding cathodic peak at -0.02V. The peak current ratio is 2.67. The voltammogram of resorcinol is quasireversible. Hydroquinone shows an anodic peak at 0.66V and corresponding cathodic peak at -0.04V. The corresponding peak potential difference is 0.70V which is higher than theoretical value. The voltammogram is almost reversible. The current potential data, peak potential difference, peak current and peak current ratio data for first scan are presented in Tables 4.13- 4.15.

Figures 4.7-4.9 shows the cyclic voltammogram of 2mM catechol (brown line), 2mM resorcinol (blue line) and 2mM hydroquinone (green line) in buffer solution of pH 5 of GC, Au and Pt electrodes at scan rate 0.1V/s in the first scan of potential respectively. From these Figure it is seen that the peak current and peak position of catechol and hydroquinone are closer but the behavior of resorcinol is different. The anodic peak is shifted positively. In GC electrode resorcinol shows no cathodic peak and electro-inactive behavior. But, at Au and Pt electrodes resorcinol shows anodic and corresponding cathodic peak in first cycle and second cycle also.

Figure 4.10 shows the cyclic voltammogram of 2mM catechol (red line), 2mM resorcinol (blue line) and 2mM hydroquinone (green line) in buffer solution of pH 9 of GC electrode at scan rate 0.1V/s in the first scan of potential. Figure 4.10, catechol shows an anodic peak at 0.18V and corresponding cathodic peak at -0.05V. The peak current ratio is 1.77. The voltammogram is quasi-reversible. Resorcinol shows an anodic peak at 0.47V and corresponding cathodic peak is absent. The voltammogram of resorcinol is irreversible. Hydroquinone shows an anodic peak at 0.06V and corresponding cathodic peak at -0.12V. The corresponding peak potential difference is 0.18V which is higher than theoretical value. The peak current ratio is 0.91. The voltammogram is reversible. The current potential data, peak potential difference, peak current and peak current ratio data are presented in Table 4.16- 4.18.

Figures 4.11-4.12 shows the cyclic voltammogram of 2mM catechol (red line), 2mM resorcinol (blue line) and 2mM hydroquinone (green line) in buffer solution of pH 9 of Au and Pt electrodes at scan rate 0.1V/s in the first and second scan of potential respectively. From these Figure it is seen that the anodic peak current and peak position of catechol and hydroquinone are quite similar but the behavior of resorcinol is different. The anodic peak

resorcinol and hydroquinone is shifted positively compared with catechol. At Au and Pt electrodes resorcinol shows corresponding anodic and cathodic peaks. But, at GC electrode resorcinol shows only anodic peak in the first cycle.

Figures 4.13, 4.14 and 4.15 shows CV graph of 2mM catechol, 2mM resorcinol and 2mM hydroquinone in supporting electrolyte (1M KCl) at GC, Au and Pt electrode respectively. In Figure 4.13 catechol and hydroquinone shows two anodic and corresponding two cathodic peaks but resorcinol shows irreversible anodic peak. In Figure 4.14 and 4.15 both catechol and hydroquinone shows two pairs of redox peaks at Au and Pt electrode but resorcinol shows irreversible anodic peak in Pt whereas electroinactive at Au electrode.

4.2 Effect of pH of Isomers

The influence of pH on the cyclic voltammogram of 2mM catechol at GC (3 mm) electrode in the first scan of potential was studied at pH from 3 to 9 in Figure 4.16. The voltammetric behavior of 2mM catechol at different pH are completely different whether shows one anodic and one cathodic peak. At pH 3, the anodic peak potential shows at 0.68V and corresponding cathodic peak at 0.06V, whereas at pH 5 it found 0.5V & 0.06V, pH 7 it found 0.39V & 0.0V, and pH 9 it found at 0.18V & -0.02V. It is shown that the anodic and cathodic peak position shifted negatively from pH 3 to pH 9. The corresponding peak current ratios of pH 3-7 are nearly unity which is close to the theoretical value of reversible process. But at pH 9 the ratio is close to the theoretical value of quasi-reversible process. Also, it is seen that in pH 7 the peaks are sharp and the peak current is higher than acidic and basic medium. The peak position of the redox couple is found to be dependent upon pH.

Figure 4.17 shows the plot of oxidation peak (A_1) current, I_p against pH of solution. It is seen that the maximum peak current is obtained at pH 7 suggested that electron transfer is most favorable in neutral media. Figure 4.18 shows the plot of peak potential, E_p values against pH. As shown, the peak potential for A_1 peak shifted to the negative potentials by increasing pH. This is expected because of participation of proton in the transformation of catechol to *o*-quinone. From the Figure 4.18, the slope of the plot was determined graphically as the anodic peak (69mV/pH for oxidation peak A_1) at 0.1V/s, which is close to the theoretical value (60 mV/pH) for one-electron, one-proton transfer process. This indicates that the oxidation of the catechol proceeded via the $1e^-/1H^+$ processes. This also

suggests that during the transformation not only electron but also proton are released from the catechol.

The peak current ratio (I_{pc1}/I_{pa1}) increases with increasing pH. This suggests that the rate of reaction is pH dependent and enhanced by decreasing pH. At pH 9, the difference between the peak current ratio (I_{pc1}/ I_{pa1}) is maximum. Consequently, in this study buffer solution of pH 7 has been selected as suitable medium for electrochemical study of catechol. This ascribed that the electrochemical oxidation of catechol is facilitated in neutral media and hence the rate of electron transfer is faster. Figure 4.19 shows the differential pulse voltammogram (DPV) of 2mM catechol in different buffer solution of GC electrode at scan rate 0.1V/s. The peak positions are shifted in the negative potential which is consistent with CV graph.

The effect of pH on the cyclic voltammogram of 2mM catechol at Au (1.6 mm) electrode in the first scan of potential was studied at pH from 3 to 9 in Figure 4.20. The influence of pH for Au electrode in the same systems, the voltammetric properties are some different from GC electrode. However, the peak position of the redox species is found to be dependent upon pH. Figure 4.21 shows the plots of oxidation peak current, I_p against pH of solution. It is seen that the maximum peak current is obtained at pH 7 attributed that reaction is most favorable in neutral media. Figure 4.22 shows the plot of the peak potential, E_p against pH at first cycle in the same condition. The slope of the plot was (45 mV/pH for anodic peak A_1) which is close to theoretical value for one electron, one proton transfer process. Figure 4.23 shows the differential pulse voltammogram (DPV) of 2mM catechol in different buffer solution of Au electrode at scan rate 0.1V/s. The peak positions are shifted in the negative potential which is consistent with CV graph.

CV of catechol at Platinum (Pt) (1.6 mm) electrode in the first scan of potential was also studied in pH 3 to 9 in Figure 4.24. The peak position and peak current of the redox element is found to be dependent upon pH. Figure 4.25 shows the plot of oxidation peak current, I_p against pH of solution. It is seen that the maximum peak current is obtained at pH 7. Figure 4.26 shows the plot of peak potential, E_p vs pH. The slope of the plot was 55 mV/pH which close to the value of one electron, one proton transfer process. Figure 4.27 shows the differential pulse voltammogram (DPV) of 2mM catechol in different buffer solution of Pt electrode at scan rate 0.1V/s.

The influence of pH on the cyclic voltammogram of 2mM resorcinol at GC (3 mm) electrode in the first scan of potential was studied at pH from 3 to 9 in Figure 4.28. The voltammetric behavior of 2mM resorcinol at different pH are completely different whether shows one anodic peak and being irreversible. At pH 3, the anodic peak potential shows at 1.08V whereas at pH 5 it found 0.85V, pH 7 it found 0.77V, and pH 9 it found at 0.48V(Figure 4.28). It is seen that the anodic position shifted negatively from pH 3 to pH 9. In pH 7 the peaks are sharp and the peak current is higher than acidic and basic medium. The peak position of the redox couple is found to be dependent upon pH.

Figure 4.29 shows the plot of oxidation peak (A_1) current, I_p against pH of solution. It is seen that the maximum peak current is obtained at pH 7 suggested that electron transfer is most favorable in neutral media. Figure 4.30 shows the plot of peak potential, E_p values against pH. As shown, the peak potential for A_1 peak shifted to the negative potentials by increasing pH. This is expected because of participation of proton in the transformation of resorcinol to *m*-quinone. From the Figure 4.30, the slope of the plot was determined graphically as the anodic peak (73mV/pH for oxidation peak A_1) at 0.1V/s, which is close to the theoretical value (60mV/pH) for one-electron, one-proton transfer process. This indicates that the oxidation of the resorcinol proceeded via the $1e^-/1H^+$ processes. This also suggests that during the transformation not only electron but also proton are released from the resorcinol.

In this study buffer solution of pH 7 has been selected as suitable medium for electrochemical study of resorcinol. This ascribed that the electrochemical oxidation of resorcinol is facilitated in neutral media and hence the rate of electron transfer is faster. Figure 4.31 shows the differential pulse voltammogram (DPV) of 2mM resorcinol in different buffer solution of GC electrode at scan rate 0.1V/s. The peak positions are shifted in the negative potential which is consistent with CV graph.

The effect of pH on the cyclic voltammogram of 2mM resorcinol at Au (1.6 mm) electrode in the first scan of potential was studied at pH from 3 to 9 in Figure 4.32. The influence of pH for Au electrode in the same systems, the voltammetric properties are some different from GC electrode. However, the peak position of the redox species is found to be dependent upon pH. Figure 4.33 shows the plots of oxidation peak current, I_p against pH of solution. It

is seen that the maximum peak current is obtained at pH 7 attributed that reaction is most favorable in neutral media. Figure 4.34 shows the plot of the peak potential, E_p against pH at first cycle in the same condition. The slope of the plot was (65mV/pH for anodic peak A_1) which is close to theoretical value for one electron, one proton transfer process.

CV of resorcinol at Platinum (Pt) (1.6 mm) electrode in the first and second scan of potential was also studied in pH 3 to 9 in Figure 4.36. The peak position and peak current of the redox element is found to be dependent upon pH. Figure 4.37 shows the plot of oxidation peak current, I_p against pH of solution. It is seen that the maximum peak current is obtained at pH 7. Figure 4.38 shows the plot of peak potential, E_p vs pH. The slope of the plot was 49mV/pH which close to the value of one electron, one proton transfer process.

The influence of pH on the cyclic voltammogram of 2mM hydroquinone at GC (3 mm) electrode in the first scan of potential was studied at pH from 3 to 9 in Figure 4.40. The voltammetric behavior of 2mM hydroquinone at different pH are completely different whether shows one anodic and one cathodic peak. At pH 3, the anodic peak potential shows at 0.58V and corresponding cathodic peak at 0.01V, whereas at pH 5 it found 0.43V & -0.05V, pH 7 it found 0.24V & -0.10V, and pH 9 it found at 0.06V & -0.13V. It is shown that the anodic and cathodic peak position shifted negatively from pH 3 to pH 9. The corresponding peak current ratios of pH 3-9 are nearly unity which is close to the theoretical value of reversible process. Also, it is seen that in pH 7 the peaks are sharp and the peak current is higher than acidic and basic medium. The peak position of the redox couple is found to be dependent upon pH.

Figure 4.41 shows the plot of oxidation peak (A_1) current, I_p against pH of solution. It is seen that the maximum peak current is obtained at pH 7 suggested that electron transfer is most favorable in neutral media. Figure 4.42 shows the plot of peak potential, E_p values against pH. As shown, the peak potential for A_1 peak shifted to the negative potentials by increasing pH. This is expected because of participation of proton in the transformation of hydroquinone to *p*-quinone. From the Figure 4.42, the slope of the plot was determined graphically as the anodic peak (75mV/pH for oxidation peak A_1) at 0.1V/s, which is close to the theoretical value (60 mV/pH) for one-electron, one-proton transfer process. This indicates that the oxidation of the hydroquinone proceeded via the $1e^-/1H^+$ processes. This

also suggests that during the transformation not only electron but also proton are released from the hydroquinone.

The peak current ratio (I_{pc1}/I_{pa1}) increases with increasing pH. This suggests that the rate of reaction is pH dependent and enhanced by decreasing pH. In this study buffer solution of pH 7 has been selected as suitable medium for electrochemical study of hydroquinone. This ascribed that the electrochemical oxidation of hydroquinone is facilitated in neutral media and hence the rate of electron transfer is faster. Figure 4.43 shows the differential pulse voltammogram (DPV) of 2mM hydroquinone in different buffer solution of GC electrode at scan rate 0.1V/s. The peak positions are shifted in the negative potential which is consistent with CV graph.

The effect of pH on the cyclic voltammogram of 2mM hydroquinone at Au (1.6 mm) electrode in the first scan of potential was studied at pH from 3 to 9 in Figure 4.44. The influence of pH for Au electrode in the same systems, the voltammetric properties are some different from GC electrode. However, the peak position of the redox species is found to be dependent upon pH. Figure 4.45 shows the plots of oxidation peak current, I_p against pH of solution. It is seen that the maximum peak current is obtained at pH 7 attributed that reaction is most favorable in neutral media. Figure 4.46 shows the plot of the peak potential, E_p against pH at first cycle in the same condition. The slope of the plot was (73mV/pH for anodic peak A_1) which is close to theoretical value for one electron, one proton transfer process. Figure 4.47 shows the differential pulse voltammogram (DPV) of 2mM hydroquinone in different buffer solution of Au electrode at scan rate 0.1V/s. The peak positions are shifted in the negative potential which is consistent with CV graph.

CV of hydroquinone at Pt (1.6 mm) electrode in the first scan of potential was also studied in pH 3 to 9 in Figure 4.48. The peak position and peak current of the redox element is found to be dependent upon pH. Figure 4.49 shows the plot of oxidation peak current, I_p against pH of solution. It is seen that the maximum peak current is obtained at pH 7. Figure 4.50 shows the plot of peak potential, E_p vs pH. The slope of the plot was 51mV/pH which close to the value of one electron, one proton transfer process.

4.3 Effect of scan rate

Figure 4.52 shows the CV of first cycle of 2mM catechol of GC (3 mm) electrode in buffer solution (pH 3) at different scan rates. The peak current of both the anodic and the corresponding cathodic peaks increases with the increasing of scan rate. The cathodic peaks are shifted towards left and the anodic peaks are to the right direction with increase in scan rate. As can be seen in Figure 4.52 the cathodic peak for reduction of *o*-benzoquinone is very small in the scan rate of 0.05V/s. By increasing the scan rate, the cathodic peak for reduction of *o*-benzoquinone begins to appear and increase. The anodic and cathodic peak current, peak current ratio and peak potential difference are tabulated in Tables 4.19. Figure 4.53-4.55 shows the CV at different scan rate for first cycle of 2mM catechol at different pH (5-9). Figure 4.56-4.59 shows the plots of the anodic and cathodic net peak currents against the square-root of the scan rates at the same condition. The nearly proportionality of the anodic and the cathodic peaks for the studied all pH suggests that the peak current of the reactant at each redox reaction is controlled by diffusion process. Although most of the lines have non zero intercept.

Figure 4.59 shows the plots of the anodic and cathodic net peak currents of 2mM catechol for first cycle against the square-root of scan rates where the net current means the second peak subtracted from the first one by the scan-stopped method [18, 33-34]. The nearly proportionality of the anodic and corresponding cathodic peaks suggests that the peak current of the reactant at each redox reaction is controlled by diffusion process [71]. The reactivity of catechol is pH dependent. So the voltammetric behavior of the above isomer verified at different pH and scan rate.

Figure 4.60-4.63 shows the CV of first scan at Au electrode of 2mM catechol in different buffer solution (pH 3 to 9). The peak current of both the anodic and cathodic peaks increases with the increase of scan rate. Figure 4.64-4.67 shows the plots of the anodic and cathodic peak currents for the first scan of potential against square-root of the scan rates. Figure 4.68-4.71 shows the CV of first scan of potential of 2mM catechol of Pt electrode at scan rate from 0.05V/s to 0.50V/s. The peak current of both the anodic and cathodic peaks increases with the increase of scan rate. Figure 4.72 -4.75 shows the plots of the anodic and cathodic peak currents for the first scan of potential against square-root of the scan rates of 2mM catechol. A typical observation was found for the species of the redox isomer was linearly

increased with the square root of scan rate for Au and Pt electrodes, suggesting diffusion controlled process.

The reactivity of resorcinol is pH dependent. So the voltammetric behavior of the isomer verified at different pH and scan rate. Figure 4.76-4.79 show the CV at different scan rate for first cycle of 2mM resorcinol at different pH (3 to 9). From the Figures it is seen that the voltammograms at all pH is irreversible. At different scan rate the cathodic peak is almost absent, with the increasing of scan rate anodic peak is increased. Figure 4.80-4.83 shows the plots of the anodic net peak currents against the square-root of the scan rates at the same condition. The anodic peak for the studied all pH found to be linear. Although all of the lines have non zero intercept. Figures 4.84-4.87 and 4.92-4.95 shows the CV and Figures 4.88-4.91 and 4.96-4.99 shows net peak current vs square root of scan rates in different buffer solution for first cycle at Au and Pt electrode respectively. At the Au electrode it is seen that the voltammograms at all pH is reversible but at Pt electrode it shows quasi reversible which are dissimilar from GC electrode for resorcinol.
Figures 4.100-4.103, 4.108-4.111 and 4.116-4.119 shows the CV and Figures 4.104-4.107, 4.112-4.115 and 4.120-4.123 shows the plots of the anodic and cathodic net peak currents against the square-root of the scan rates at GC, Au and Pt electrodes respectively for first cycle of 2mM hydroquinone in different pH (3 to 9). The peak current of both the anodic and cathodic peaks increases with the increase of scan rate. The nearly proportionality of the anodic and the cathodic peaks for the studied all pH suggests that the peak current of the reactant at each redox reaction is controlled by diffusion process.

4.4 Effect of electrode materials

Electrochemical properties of pure catechol was examined by different electrodes for example Glassy carbon (GC), Gold (Au) and Platinum (Pt) in the buffer solution pH 7 at scan rate 0.1 V/s. The Cyclic voltammograms of 2mM catechol at GC, Au and Pt electrodes in the first scan of potential are shown in Figure 4.124.

The nature of voltammograms, the peak position and current intensity for the studied systems are different for different electrodes although the diameter of GC electrode (3 mm) is higher than Au and Pt (1.6 mm) electrodes. The CV of Au electrode is significantly

different from those of the GC and Pt electrodes. At the Au electrode it shows two anodic and two cathodic peaks for the first scan of potential (Figure 4.124). In case of GC electrode it shows one anodic and one cathodic peak for the first scan of potential whereas at Pt electrode it shows one anodic and corresponding cathodic peak. Voltammetric measurements performed at Au electrode in only buffer solution of without catechol at pH 7, showed a peak at 1.1 V to the formation of Au(III) hydroxide. Consequently, the third peak (1.08 V) of Au electrode in presence of catechol at pH 7 is due to the oxidation of Au in buffer solution. Electrochemical properties of catechol for example change of pH, scan rate etc. were studied in detail using Pt and Au electrodes. But among the electrodes, the voltammetric response of GC electrode was better than Pt and Au electrodes in the studied systems.

The Cyclic voltammograms of 2mM resorcinol at GC, Au and Pt electrodes in the first scan of potential are shown in Figure 4.125. The nature of voltammograms, the peak position and current intensity for the studied systems are different for different electrodes although the diameter of GC electrode (3 mm) is higher than Au and Pt (1.6 mm) electrodes. The CV of GC electrode is significantly different from those of the Au and Pt electrodes. At the Au and Pt electrodes shows one anodic and one cathodic peak for the first scan of potential (Figure 4.125). In case of GC electrode it shows one anodic peak and no cathodic peak for the first scan of potential. Electrochemical properties of resorcinol for example change of pH, scan rate etc. were studied in detail using GC, Pt and Au electrodes. But among the electrodes, the voltammetric response of GC electrode was different than Pt and Au electrodes in the studied systems.

The Cyclic voltammograms of 2mM hydroquinone at GC, Au and Pt electrodes in the first scan of potential are shown in Figure 4.126. At the Au electrode it shows two anodic and two cathodic peaks for the first scan of potential (Figure 4.126). In case of GC and Pt electrode shows one anodic and one cathodic peak for the first scan of potential. Among the electrodes, the voltammetric response of GC electrode was better than Pt and Au electrodes in the studied systems. At GC electrode the anodic peak and cathodic peak are sharp than another electrodes. So, the reaction easily occurred at the surface of GC electrode.

4.5 Electrochemical behavior of dihydroxybenzene isomers + sulfanilic acid

Figures 4.127-4.128 show the comparison of pure catechol, pure sulfanilic acid and catechol with sulfanilic acid in the first and second scan of potential respectively of GC electrode in pH 7 at scan rate 0.1V/s. In the second cycle (Figure 4.128), the cyclic voltammogram of catechol (red line) displays one anodic peak at 0.5V and corresponding cathodic peak at -0.04V connected to its transformation to *o*-quinone and vice versa. Pure sulfanilic acid is electrochemically active having anodic peak 0.96V and corresponding cathodic peak at 0.06V in the potential range studied (Figure 4.128, green line). Figure 4.128 (blue line) shows the CV of catechol (2mM) in the presence of sulfanilic acid (2mM) in the second scan of potential in the same condition. In the second cycle of potential catechol with sulfanilic acid shows three anodic peaks at 0.12V, 0.44V and 0.96V and the corresponding three cathodic peaks at - 0.26V, 0.21V and 0.82V respectively. The nature of voltammogram of catechol in presence of sulfanilic acid is quasi-reversible. Upon addition of sulfanilic acid to catechol solution, the cathodic peak C_1 shifted negatively. Also, in the second cycle of potential a new anodic peak A_o appears and anodic peaks A_1 and A_2 shifted. In the first scan of potential, the anodic peak of catechol in presence of sulfanilic acid is very similar to pure catechol and pure sulfanilic acid (Figure 4.127). But in the second scan of potential appearance of new peak A_o and shifting of A_1, A_2 and C_1 peaks positions, which is indicative of a chemical reaction of sulfanilic acid (**2**) with the *o*-quinone (**1a**) produced at the surface of electrode (Scheme 2)[72]. In the case of catechol in presence of sulfanilic acid, the oxidation of sulfanilic acid substituted *o*-benzoquinone is easier than the oxidation of parent catechol. This behavior is in agreement with that reported by other research groups for similar electrochemically generated compounds such as catechol and different nucleophiles [58, 60, 73-75]. In the absence of other nucleophiles, water or hydroxide ion often adds to the *o*-benzoquinone.

The corresponding peak potential differences (ΔE) in the first scan of potential of 2mM catechol + 2mM sulfanilic acid at GC electrode are tabulated in Table 4.20. The peak potential differences are usually independent of scan rate. The peak separation potential increases with the increasing of scan rate that indicates there is a limitation according to ohomic potential drop or charge transfer kinetics [62].

Figures 4.129-4.130 show the comparison of pure resorcinol, pure sulfanilic acid and resorcinol with sulfanilic acid in the first and second scan of potential respectively of GC electrode in pH 7 at scan rate 0.1V/s. In the second cycle (Figure 4.130), the cyclic voltammogram of resorcinol (red line) displays a weak anodic peak at (0.77V) and having no corresponding cathodic peak. Pure sulfanilic acid is electrochemically active having anodic peak 0.96V and corresponding cathodic peak at 0.06V in the potential range studied. Figure 4.130 (blue line) shows the CV of resorcinol (2mM) in the presence of sulfanilic acid (2mM) in the second scan of potential in the same condition. In the second cycle of potential catechol with sulfanilic acid shows one small anodic peaks at 0.78V and corresponding cathodic peak absent. The nature of voltammograms of resorcinol in presence of sulfanilic acid is irreversible. In the first scan of potential, the anodic peak of resorcinol in presence of sulfanilic acid is similar to pure resorcinol and pure sulfanilic acid (Figure 4.129). But in the second scan of potential appearance of peak shifting of A_1 peak position, which is indicative of a chemical reaction of sulfanilic acid (**2**) with the *m*-quinone (**1a**) produced at the surface of electrode (Scheme 2).

Figures 4.131-4.132 show the CV of 2mM hydroquinone with 2mM sulfanilic acid in the first and second scan of potential at GC (3 mm) electrode in pH 7. In Figure 4.131, the first scan of potential hydroquinone shows one anodic peak at 0.23Vand the corresponding cathodic peak at -0.08V. In the second scan of potential (Figure 4.132) hydroquinone with sulfanilic acid shows two anodic peaks at 0.4V, 1.07V and the corresponding two cathodic peaks at -0.18V, 0.87V. Upon addition of sulfanilic acid to hydroquinone solution, the cathodic peak C_1 increases. Also, in the second scan of potential anodic peaks A_1 and A_2 shifted. This observation can be stated by considering nucleophilic attack of sulfanilic acid to *p*-benzoquinone. The peak potential, corresponding peak potential differences, peak current in the first scan of potential of 2mM hydroquinone + 2mM sulfanilic acid at GC electrode are tabulated in Table 4.21.

Figure 4.133 show the CV of 2mM catechol + 2mM sulfanilic acid, 2mM resorcinol + 2mM sulfanilic acid and 2mM hydroquinone + 2mM sulfanilic acid in the second scan of potential at GC (3 mm) electrode in pH 7. Catechol + sulfanilic acid shows electro-activity having a new anodic peak in the negative potential compared with catechol peak (A_1) in the second scan of potential. Resorcinol + sulfanilic acid shows electro-inactivity in the second cycle.

Hydroquinone + sulfanilic acid shows electro-activity having a very weak new anodic peak (A_0) in the second scan of potential.

Among the isomers, the electron transfer of catechol is easier than the hydroquinone and hydroquinone is easier than the resorcinol. As -OH sites in resorcinol are connected via *meta* linkage, so the electron transfer at *meta* position is unfavorable (electron deficiency) to that at a *para* (hydroquinone) or *ortho* (catechol) –position.

Figure 4.134 show the differential pulse voltammogram (DPV) of 2mM catechol + 2mM sulfanilic acid, 2mM resorcinol + 2mM sulfanilic acid and 2mM hydroquinone + 2mM sulfanilic acid in the second scan of potential at GC (3 mm) electrode in pH 7. In Figure 4.134, the second scan of potential catechol + sulfanilic acid shows four anodic peaks at -0.09V, 0.05V, 0.34V and 0.91V. Resorcinol + sulfanilic acid shows two anodic peaks at 0.08V, 0.68V. Hydroquinone + sulfanilic acid shows three anodic peaks at -0.04 V, 0.28 V, 1.0 V. In the second scan of potential two new anodic peaks appears for catechol + sulfanilic acid, one for hydroquinone + sulfanilic acid and no new peak for resorcinol + sulfanilic acid. This observation can be stated by considering nucleophilic attack of sulfanilic acid to *o*-quinone is much easier than other isomers.

Figures 4.135-4.136 show the comparison of pure catechol, pure sulfanilic acid and catechol with sulfanilic acid in the first and second scan of potential respectively of Au electrode in pH 7 at scan rate 0.1V/s. In the second cycle (Figure 4.136), the cyclic voltammogram of catechol (red line) displays two anodic peaks at (0.23V and 0.96V) and corresponding cathodic peak at (0.09V and 0.4V) connected to its transformation to *o*-quinone and vice versa. Pure sulfanilic acid is electrochemically active having anodic peak 1.03V and corresponding cathodic peak at 0.41V in the potential range studied (Figure 4.136, green line). Figure 4.136 (blue line) shows the CV of catechol (2mM) in the presence of sulfanilic acid (2mM) in the second scan of potential in the same condition. In the second cycle of potential catechol with sulfanilic acid shows three anodic peaks at -0.05V, 0.16V and 0.89V and the corresponding three cathodic peaks at -0.13V, 0.09V and 0.4V respectively. The nature of voltammograms of catechol in presence of sulfanilic acid is quasi-reversible. Upon addition of sulfanilic acid to catechol solution, the cathodic peak C_1 shifted negatively. Also, in the second cycle of potential a new anodic peak A_o appears and anodic peaks A_1 and A_2 shifted. In the first scan of potential, the anodic peak of catechol in presence of sulfanilic acid is very similar to pure catechol and pure sulfanilic acid (Figure 4.135). But in the second

scan of potential appearance of new peak A_o and shifting of A_1, A_2 and C_1 peaks positions, which is indicative of a chemical reaction of sulfanilic acid (**2**) with the *o*-quinone (**1a**) produced at the surface of electrode (Scheme 2).

Figures 4.137-4.138 show the CV of first and second scan of potential of 2mM resorcinol + 2mM sulfanilic acid at Gold (Au) (1.6mm) electrode in pH 7 and at scan rate 0.1V/s. Figure 4.137 shows the cyclic voltammogram of only 2mM resorcinol (red line), pure sulfanilic acid (green line) and resorcinol (2mM) with sulfanilic acid (2mM) (blue line) in the first scan of potential at the same condition. A new reduction peak (C_0) appears at 0.28V after the addition of 2mM sulfanilic acid to the solution at second scan of potential (Figure 4.138). The peak current decreases significantly with respect to the only resorcinol. In Figure 4.138, the second scan of potential resorcinol with sulfanilic acid shows one anodic peaks at 1.05V and the corresponding cathodic peak at 0.37V. Upon addition of sulfanilic acid to resorcinol solution, the cathodic peak C_1 decreases. Also, in the second scan of potential anodic peak A_1 decreases with respect of pure resorcinol and pure sulfanilic acid similar to GC electrode. This observation can be stated by considering nucleophilic attack of sulfanilic acid to *o*-benzoquinone which is not observed in the CV graph.

The comparison of CV of pure hydroquinone (red line), pure sulfanilic acid (green line) and hydroquinone with sulfanilic acid (blue line) of Au electrode in the first and second scan of potential at the same condition are shown in Figures 4.139-4.140. The CV of hydroquinone in presence of sulfanilic acid shows two anodic peaks at 0.37 V, 1.03V and two cathodic peaks at -0.1 V, 0.6V, respectively in the second scan of potential (Figure 4.140). In the second scan of potential no new oxidation peak appears. The peak position of the CV of hydroquinone with sulfanilic acid in the second cycle was shifted positively and the anodic and cathodic peak current increases. The peak current, peak potential, corresponding peak potential differences (ΔE) in the first scan of potential of 2mM hydroquinone + 2mM sulfanilic acid at Au electrode are tabulated in Table 4.24.

Figure 4.142 shows the differential pulse voltammogram (DPV) of 2mM catechol + 2mM sulfanilic acid, 2mM resorcinol + 2mM sulfanilic acid and 2mM hydroquinone + 2mM sulfanilic acid in the second scan of potential at Au (1.6 mm) electrode in pH 7. In Figure 4.142, the second scan of potential of catechol + sulfanilic acid shows three anodic peaks at

-0.04V, 0.16V, 0.88V and Resorcinol + sulfanilic acid shows two anodic peaks at 0.88V, 0.68V and Hydroquinone + sulfanilic acid shows two anodic peaks at 0.23V, 0.37V respectively. In the second scan of potential one new anodic peaks appears for catechol + sulfanilic acid, no new peak for hydroquinone + sulfanilic acid and resorcinol + sulfanilic acid. This observation can be stated by considering nucleophilic attack of sulfanilic acid to *o*-quinone is much easier than other isomers.

Figure 4.143-4.144 show the CV of 2mM catechol with 2mM sulfanilic acid in the first and second scan of potential at Pt (1.6 mm) electrode in pH 7. In Figure 4.144, the second scan of potential catechol with sulfanilic acid shows three anodic peaks at 0.09V, 0.44V and 0.98V and the corresponding three cathodic peaks at -0.25V, -0.05V and 0.79V, respectively. Upon addition of sulfanilic acid to catechol solution, the cathodic peak C_1 decreases. Also, in the second scan of potential a new anodic peak A_o appears and anodic peak A_1 and A_2 shifted. This observation can be stated by considering nucleophilic attack of sulfanilic acid to *o*-benzoquinone. The peak potential, corresponding peak potential differences, peak current in the first scan of potential of 2mM catechol + 2mM sulfanilic acid at Pt electrode are tabulated in Table 4.23. When we considered the second cycle Figure 4.146 (blue line) shows the CV of resorcinol (2mM) in the presence of sulfanilic acid (2mM) in the same condition shows no new anodic peak and corresponding cathodic peak. The nature of voltammograms of resorcinol in presence of sulfanilic acid is quasireversible. In the first scan of potential (Figure 4.147) hydroquinone with sulfanilic acid shows two anodic peaks at 0.42V, 1.06V and the corresponding two cathodic peaks at -0.14V, 0.87V. Also, in the second scan of potential a very small new anodic peak appeared at 0.02V and anodic peaks A_1 and A_2 shifted. This observation can be stated by considering nucleophilic attack of sulfanilic acid to *p*-benzoquinone. The peak potential, corresponding peak potential differences, peak current in the first scan of potential of 2mM hydroquinone + 2mM sulfanilic acid at Pt electrode are tabulated in Table 4.25.

Figure 4.149 shows the CV of 2mM catechol + 2mM sulfanilic acid, 2mM resorcinol + 2mM sulfanilic acid and 2mM hydroquinone + 2mM sulfanilic acid in the second scan of potential at Pt (1.6 mm) electrode in pH 7. Figure 4.150 show the differential pulse voltammogram (DPV) of 2mM catechol + 2mM sulfanilic acid, 2mM resorcinol + 2mM sulfanilic acid and 2mM hydroquinone + 2mM sulfanilic acid in the second scan of potential

at Pt (1.6mm) electrode in the same condition. In Figure 4.150, the second scan of potential catechol + sulfanilic acid shows a new anodic peak appeared at -0.06V. But, resorcinol + sulfanilic acid and hydroquinone + sulfanilic acid shows no appeared anodic peak. This observation can be stated by considering nucleophilic attack of sulfanilic acid to *o*-quinone is much easier than other isomers.

4.6 Effect of scan rate of different isomer + sulfanilic acid

Figures 4.151-4.153 show the CV of second scan of potential at GC electrode of 2mM catechol + 2mM Sulfanilic, 2mM resorcinol + 2mM Sulfanilic acid and 2mM hydroquinone + 2mM Sulfanilic acid respectively in pH 7. The voltammograms of resorcinol at GC electrode is seen that irreversible behavior, here redox couple shows no cathodic peak. The peak current of both the anodic and cathodic peaks increases with the increase of scan rate. The anodic peaks are shifted towards right and the cathodic peaks are to the left direction except resorcinol. It is seen that in Figures 4.151-4.153, the anodic and cathodic peaks are very small in the scan rate of 0.05V/s. By increasing the scan rate, the anodic peaks begin to appear and increase. Figures 4.154- 4.156 shows the plots of peak currents against square-root of the scan rates of second scan of potential at GC electrode of 2mM catechol + 2mM Sulfanilic acid , 2mM resorcinol + 2mM Sulfanilic acid and 2mM hydroquinone + 2mM Sulfanilic acid respectively in pH 7. Where the net peaks current means the second peak subtracted from the first one by the scan stopped method. The nearly proportionality of the anodic and cathodic peaks suggest that the peak the current of the reactant at each redox reaction is controlled by diffusion process. Figures 4.157-4.159 show the CV of 2mM catechol + 2mM Sulfanilic, 2mM resorcinol + 2mM Sulfanilic acid and 2mM hydroquinone + 2mM Sulfanilic acid of second scan of potential at Au electrode respectively. The voltammograms at Au electrode, the peak current of both the anodic and cathodic peaks increases with the increase of scan rate. Figures 4.160-4.162 show plots of peak current versus square-root of the scan rates in the same condition at Au electrode. A typical observation was found for the species of the redox system was linearly increased with the square root of scan rate for Au electrode, suggesting diffusion controlled process.

Figures 4.163-4.165 show the cyclic voltammograms and Figures 4.166-4.168 shows the plots of peak currents versus square-root of the scan rates of second scan of potential at Pt

electrode of 2mM catechol, 2mM resorcinol and 2mM hydroquinone in the presence of 2mM Sulfanilic in pH 7 respectively. The voltammetric behavior of the above system are similar to the GC and Au electrode.

4.7 Effect of Electrode materials on isomers + sulfanilic acid

Electrochemical properties of 2mM catechol in presence of 2mM Sulfanilic acid was examined by different electrodes for example Glassy carbon (GC), Gold (Au) and Platinum (Pt) in the buffer solution pH 7 at scan rate 0.1 V/s. The Cyclic voltammograms of 2mM catechol in presence of 2mM Sulfanilic acid at GC, Au and Pt electrodes in the second scan of potential are shown in Figure 4.169.

The nature of voltammograms, the peak position and current intensity for the studied systems are different for different electrodes although the diameter of GC electrode (3 mm) is higher than Au and Pt (1.6 mm) electrodes. The CV of Au electrode is significantly different from those of the GC and Pt electrodes. At Au and Pt electrode it shows two anodic and two corresponding cathodic peaks for the second of potential in Figure 4.169. In case of GC electrode it shows three anodic (0.11V, 0.41V and 0.96V) and three corresponding cathodic peaks for the second scan of potential. At second scan it shows one new anodic peak at 0.11V which indicate that reaction happened in the surface of GC electrode.
Voltammetric measurements performed at Au electrode in only buffer solution of without catechol at pH 7, showed a peak at 1.1V to the formation of Au (III) hydroxide. Consequently, the third peak (1.08V) of Au electrode in presence of catechol at pH 7 is due to the oxidation of Au in buffer solution [76]. Electrochemical properties of catechol for example change of pH, scan rate etc. were studied in detail using Pt and Au electrodes. But among the electrodes, the voltammetric response of GC electrode was better than Pt and Au electrodes in the studied systems.

The Cyclic voltammograms of 2mM resorcinol in presence of 2mM Sulfanilic acid at GC, Au and Pt electrodes in the second scan of potential are shown in Figure 4.170. The nature of voltammograms, the peak position and current intensity for the studied systems are different for different electrodes although the diameter of GC electrode (3 mm) is higher than Au and Pt (1.6 mm) electrodes. The CV of GC electrode is significantly different from

those of the Au and Pt electrodes. At Au and Pt electrodes both show two anodic and two cathodic peaks for the seconf scan of potential (Figure 4.170). In case of GC electrode it shows two anodic peaks and no cathodic peak for the second scan of potential. In second scan there is on appeared anodic and cathodic peak. Electrochemical properties of resorcinol for example change of pH, scan rate etc. were studied in detail using GC, Pt and Au electrodes. But among the electrodes, the voltammetric response of GC electrode was different than Pt and Au electrodes in the studied systems.

The Cyclic voltammograms of 2mM hydroquinone at GC, Au and Pt electrodes in the second scan of potential are shown in Figure 4.171. At Au and Pt electrode it shows two anodic and two cathodic peaks for the second scan of potential Figure 4.171. In case of GC electrode it shows two anodic and two cathodic peaks for the first scan of potential but it shows a weak appeared anodic (0.01V) and cathodic peak in second scan. Among the electrodes, the voltammetric response of GC electrode was better than Pt and Au electrodes in the studied systems. At GC electrode the anodic peak and cathodic peak are sharp than another electrodes. So, the reaction easily occurred at the surface of GC electrode.

4.8 Subsequent cycles of CV of isomers + sulfanilic acid

Figures 4.172-4.174 shows the cyclic voltammograms of the first 5 cycles of 2mM catechol with 2mM Sulfanilic acid of GC, Au and Pt electrodes respectively in buffer solution of pH 7. The voltammogram at the scan rate 0.1 Vs^{-1} has two anodic peaks at 0.37V and 0.95V and three cathodic peaks at -0.15V, 0.11V and 0.85V when considered the first scan of potential (dot line) at GC electrode. In the subsequent potential cycles a new anodic peak appeared at ~ - 0.08V and intensity of the first and the second anodic peak current decreased progressively and shifted positively on cycling. This can be attributed to produce of the catechol-sulfanilic acid adduct through nucleophilic substitution reaction in the surface of electrode (Scheme 1) [72]. The successive decrease in the height of the catechol oxidation and reduction peaks with cycling can be ascribed to the fact that the concentrations of catechol-sulfanilic adduct formation increased by cycling leading to the decrease of concentration of catechol or quinone at the electrode surface. The positive shift of the second anodic peak in the presence of sulfanilic acid is probably due to the formation of a thin film

of product at the surface of the electrode, inhibiting to a certain extent the performance of electrode process.

The effect of the cyclic voltammograms of the first 5 cycles of 2mM Catechol with 2mM sulfanilic acid of Au electrode and Pt electrode in buffer solution of pH 7 were also studied in the same condition. In Figure 4.173 at Au electrode there were two anodic peaks at 0.27V and 1.01V and three cathodic peaks at - 0.11V, 0.15V and 0.49V respectively in the first scan of potential (dot line). In the subsequent scan of potential Au electrode shows a new anodic peak at 0.02V with another three anodic peaks (black line). But at Pt electrode there was two anodic peaks at 0.45V and 0.99V and corresponding two cathodic peaks at - 0.01V and - 0.19V in the first scan of potential (dot line) (Figure 4.174). In the subsequent potential cycles a new anodic peak appeared at 0.07V and the first and the second anodic peak current decreased progressively on cycling and shifted positively on cycling. This can be suggested to produce the catechol-sulfanilic acid adduct through nucleophilic substitution reaction in the surface of electrode (Scheme 1).

Figures 4.175-4.177 shows the cyclic voltammograms of the first 5 cycles of 2mM resorcinol with 2mM Sulfanilic acid of GC, Au and Pt electrodes respectively in buffer solution of pH 7. The voltammogram at the scan rate 0.1 Vs^{-1} has two anodic peaks at 0.74V and 1.04V and no corresponding cathodic peaks when considered the first scan of potential (dot line). In the subsequent potential cycles intensity of the anodic peak current decreased progressively.

The effect of the cyclic voltammogram of the first 5 cycles of 2mM resorcinol with 2mM sulfanilic acid of Au electrode and Pt electrode in buffer solution of pH 7 were also studied in the same condition. In Figure 4.176 at Au electrode there were two anodic peaks at 0.75V and 1.14V and two cathodic peaks at - 0.28V, 0.4V respectively in the first scan of potential (dot line). In the subsequent scan of potential Au electrode shows only one anodic peak at 0.99V (black line). But at Pt electrode there was two anodic peaks at 0.76V and 1.02V and corresponding one cathodic peak at - 0.12V in the first scan of potential (dot line) (Figure 4.177). In the subsequent potential cycles no new anodic peak appeared and the anodic peak current decreased progressively on cycling.

Figures 4.178-4.180 show the cyclic voltammograms of the first 5 cycles of 2mM hydroquinone with 2mM Sulfanilic acid of GC, Au and Pt electrodes respectively in buffer solution of pH 7. The voltammogram at the scan rate 0.1 Vs^{-1} has two anodic peaks at 0.36V and 1.04V and three cathodic peaks at -0.14V, 0.19V and 0.89V when considered the first scan of potential (dot line) at GC electrode. In the subsequent potential cycles no new anodic peak appeared and intensity of the first and the second anodic peak current decreased progressively and shifted positively on cycling. The successive decrease in the height of the hydroquinone oxidation and reduction peaks with cycling can be ascribed to the fact that the concentrations of hydroquinone-sulfanilic adduct formation increased by cycling leading to the decrease of concentration of hydroquinone or *p*-quinone at the electrode surface. The positive shift of the second anodic peak in the presence of sulfanilic acid is probably due to the formation of a thin film of product at the surface of the electrode, inhibiting to a certain extent the performance of electrode process.

The effect of the cyclic voltammograms of the first 5 cycles of 2mM hydroquinone with 2mM sulfanilic acid of Au electrode and Pt electrode in buffer solution of pH 7 were also studied in the same condition. In Figure 4.179 at Au electrode there were two anodic peaks at 0.31V and 1.05V and three cathodic peaks at - 0.05V, 0.63V and 1.05V respectively in the first scan of potential (dot line). In the subsequent scan of potential Au electrode shows no new anodic peaks (black line). But at Pt electrode there was two anodic peaks at 0.41V and 1.05V and corresponding two cathodic peaks at - 0.09V and 0.89V in the first scan of potential (dot line) (Figure 4.180). In the subsequent potential cycles no new anodic peak appeared and the first and second anodic peak current decreased progressively on cycling and shifted positively on cycling. This can be suggested to produce the hydroquinone-sulfanilic acid adduct through nucleophilic substitution reaction in the surface of electrode (Scheme 1).

Table 4.1: Peak potential (E_{pa}), corresponding peak potential difference (ΔE), peak separation ($\Delta E_{1/2}$), peak current (I_p) and corresponding peak current ratio (I_{pa}/I_{pc}) of 2mM Catechol at GC electrode at different scan rate in pH 7 (1st cycle)

v/Vs^{-1}	E_{pa} /V	E_{pc} /V	$\Delta E = E_{pc} \sim E_{pa}$	$\Delta E_{1/2}$/V	I_{pa} /μA	I_{pc} /μA	I_{pa}/ I_{pc}
0.05	0.43	-0.03	0.46	0.20	32.60	-15.00	2.17
0.1	0.39	0	0.38	0.20	51.13	-31.46	1.62
0.2	0.50	-0.06	0.56	0.22	58.76	-39.73	1.47
0.3	0.51	-0.07	0.58	0.22	75.67	-43.62	1.73
0.4	0.56	-0.10	0.66	0.23	70.52	-52.24	1.34
0.5	0.53	-0.09	0.62	0.22	77.02	-53.86	1.43

Table 4.2: Peak potential (E_{pa}) and peak current (I_p) of 2mM Resorcinol at Gc electrode at different scan rate in pH 7 (1st cycle)

v/Vs^{-1}	E_{pa} /V	I_{pa} /μA
0.05	0.82	24.28
0.1	0.77	42.13
0.2	0.91	41.33
0.3	0.97	57.19
0.4	1.02	61.89
0.5	0.81	75.58

Table 4.3: Peak potential (E_{pa}), corresponding peak potential difference (ΔE), peak separation ($\Delta E_{1/2}$), peak current (I_p) and corresponding peak current ratio (I_{pa}/I_{pc}) of 2mM Hydroquinone at GC electrode at different scan rate in pH 7 (1st cycle)

v/Vs^{-1}	E_{pa} /V	E_{pc} /V	$\Delta E = E_{pc} \sim E_{pa}$	$\Delta E_{1/2}$/V	I_{pa} /μA	I_{pc}/μA	I_{pa}/ I_{pc}
0.05	0.25	-0.08	0.33	0.08	30.60	-27.85	1.09
0.1	0.22	-0.11	0.33	0.05	45.86	-37.05	1.23
0.2	0.27	-0.09	0.36	0.09	46.04	-37.60	1.22
0.3	0.28	-0.12	0.40	0.08	62.48	-55.30	1.12
0.4	0.31	-0.11	0.42	0.10	69.05	-62.82	1.09
0.5	0.28	-0.12	0.40	0.08	81.12	-62.17	1.30

Table 4.4: Peak potential (E_{pa}), corresponding peak potential difference (ΔE), peak separation ($\Delta E_{1/2}$), peak current Ip (μA) and corresponding peak current ratio (I_{pa}/I_{pc}) of 2mM Catechol at Au electrode at different scan rate in pH 7 (1st cycle)

v/Vs^{-1}	E_{pa1} /V	E_{pa2} /V	E_{pc1} /V	E_{pc2} /V	$\Delta E = E_{pc2} \sim E_{pa1}$	$\Delta E = E_{pc1} \sim E_{pa2}$	$\Delta E_{1/2}$/V	I_{pa1} /μA	I_{pa2} /μA	I_{pc1} /μA	I_{pc2} /μA	I_{pa1}/ I_{pc1}	I_{pa2}/ I_{pc2}
0.05	0.28		0.45	0.09	0.19	0.45	0.18	9.45	0	-2.92	-7.77	1.21	0
0.1	0.23	1.01	0.42	0.07	0.16	0.59	0.15	14.71	5.42	-12.94	-13.06	0.97	1.13
0.2	0.31	1.14	0.41	0.05	0.26	0.73	0.18	18.07	3.69	-15.92	-16.10	1.12	0.62
0.3	0.32	1.17	0.39	0.03	0.29	0.78	0.17	20.16	5.48	-10.98	-19.46	1.03	0.49
0.4	0.33	1.22	0.38	0.02	0.31	0.84	0.17	21.59	7.26	-12.83	-23.22	0.92	0.56

Table 4.5: Peak potential (E_{pa}), corresponding peak potential difference (ΔE), peak separation ($\Delta E_{1/2}$), peak current (I_p) and corresponding peak current ratio (I_{pa}/I_{pc}) of 2mM Resorcinol at Au electrode at different scan rate in pH 7 (1st cycle)

v/Vs^{-1}	E_{pa} /V	E_{pc} /V	$\Delta E = E_{pc} \sim E_{pa}$	$\Delta E_{1/2}$/V	I_{pa} /μA	I_{pc} /μA	I_{pa}/ I_{pc}
0.05	0.79	0.43	0.36	0.61	7.30	-2.44	2.99
0.1	1.02	0.37	0.65	0.69	13.12	-6.96	2.07
0.2	0.89	0.42	0.47	0.65	14.52	-4.64	3.12
0.3	0.93	0.41	0.52	0.67	16.29	-5.53	2.94
0.4	0.97	0.40	0.57	0.68	19.48	-5.50	3.54
0.5	1.20	0.31	0.89	0.75	29.96	-13.58	2.20

Table 4.6: Peak potential (E_{pa}), corresponding peak potential difference (ΔE), peak separation ($\Delta E_{1/2}$), peak current (I_p) and corresponding peak current ratio (I_{pa}/I_{pc}) of 2mM Hydroquinone at Au electrode at different scan rate in pH 7 (1st cycle)

v/Vs^{-1}	E_{pa} /V	E_{pc1} /V	E_{pc2} /V	$\Delta E = E_{pc2} \sim E_{pa}$	$\Delta E_{1/2}$/V	I_{pa} /μA	I_{pc1}/μA	I_{pc2}/μA	I_{pa}/ I_{pc2}
0.05	0.15	0.48	0	0.15	0.07	8.85	-0.49	-10.34	0.85
0.1	0.22	0.45	0.01	0.21	0.11	12.11	-3.75	-16.75	0.72
0.2	0.15	0.46	0.02	0.17	0.06	17.54	-0.40	-25.04	0.70
0.3	0.15	0.46	0.02	0.17	0.06	26.51	-0.49	-33.51	0.79

Table 4.7: Peak potential (E_{pa}), corresponding peak potential difference (ΔE), peak separation ($\Delta E_{1/2}$), peak current (I_p) and corresponding peak current ratio (I_{pa}/I_{pc}) of 2mM Catechol at Pt electrode at different scan rate in pH 7 (1st cycle)

v/Vs^{-1}	E_{pa} /V	E_{pc} /V	$\Delta E = E_{pc} \sim E_{pa}$	$\Delta E_{1/2}$/V	I_{pa} /μA	I_{pc} /μA	I_{pa}/ I_{pc}
0.05	0.05	-0.09	0.14	23.80	6.24	-9.19	0.67
0.1	0.41	-0.11	0.52	38.32	6.20	-8.09	0.76
0.2	0.20	-0.17	0.37	41.73	15.34	-16.10	0.95
0.3	0.30	-0.26	0.56	59.64	15.18	-20.17	0.75
0.4	0.40	-0.27	0.67	61.33	18.16	-23.38	0.77

Table 4.8 : Peak potential (E_{pa}), corresponding peak potential difference (ΔE), peak separation ($\Delta E_{1/2}$), peak current (I_p) and corresponding peak current ratio (I_{pa}/I_{pc}) of 2mM Resorcinol at Pt electrode at different scan rate in pH 7 (1st cycle)

v/Vs^{-1}	E_{pa} /V	E_{pc} /V	$\Delta E = E_{pc} \sim E_{pa}$	$\Delta E_{1/2}$/V	I_{pa} /μA	I_{pc} /μA	I_{pa}/ I_{pc}
0.05	0.86	-0.13	0.99	0.36	7.15	-1.62	4.41
0.1	0.89	-0.14	1.03	0.37	15.42	-3.34	4.61
0.2	1.02	-0.14	1.16	0.44	14.72	-1.67	8.81
0.3	1.01	-0.16	1.17	0.42	16.32	-2.58	6.32
0.4	1.19	-0.17	1.36	0.51	21.45	-2.54	8.44
0.5	1.20	0.31	0.89	0.50	29.96	-13.58	2.20

Table 4.9: Peak potential (E_{pa}), corresponding peak potential difference (ΔE), peak separation ($\Delta E_{1/2}$), peak current (I_p) and corresponding peak current ratio (I_{pa}/I_{pc}) of 2mM Hydroquinone at Pt electrode at different scan rate in pH 7 (1st cycle)

v/Vs^{-1}	E_{pa} /V	E_{pc} /V	$\Delta E = E_{pc} \sim E_{pa}$	$\Delta E_{1/2}$/V	I_{pa} /μA	I_{pc}/μA	I_{pa}/ I_{pc}
0.05	0.30	-0.06	0.36	0.12	8.38	-6.74	1.24
0.1	0.35	-0.11	0.44	0.13	15.17	-20.50	0.74
0.2	0.35	-0.10	0.45	0.12	18.42	-14.76	1.24
0.3	0.37	-0.12	0.46	0.12	20.12	-16.40	1.21
0.4	0.37	-0.12	0.49	0.12	22.17	-18.18	1.03
0.5	0.39	-0.15	0.54	0.12	21.66	-20.84	1.03

Table 4.10: Peak potential (E_{pa}), corresponding peak potential difference (ΔE), peak separation ($\Delta E_{1/2}$), peak current (I_p) and corresponding peak current ratio (I_{pa}/I_{pc}) of 2mM Catechol at Au electrode at different scan rate in pH 3 (1st cycle)

v/Vs^{-1}	E_{pa1} /V	E_{pc1} /V	E_{pc2} /V	$\Delta E = E_{pc2} \sim E_{pa1}$	$\Delta E_{1/2}$/V	I_{pa1} /μA	I_{pc1}/μA	I_{pc2}/μA	I_{pa1}/ I_{pc2}
0.05	0.49	0.68	0.26	0.46	0.37	12.29	-5.80	-4.73	1.26
0.1	0.57	0.57	0.16	0.41	0.36	10.72	-6.14	-9.72	1.10
0.2	0.59	0.63	0.21	0.63	0.40	19.11	-11.58	-12.39	1.09
0.3	0.59	0.59	0.17	0.69	0.38	24.69	-12.76	-12.85	1.23
0.4	0.59	0.53	0.16	0.75	0.37	22.58	-11.90	-18.18	1.24
0.5	0.64	0.52	0.11	0.78	0.37	23.95	-16.47	-10.80	1.49

Table 4.11: Peak potential (E_{pa}), corresponding peak potential difference (ΔE), peak separation ($\Delta E_{1/2}$), peak current (I_p) and corresponding peak current ratio (I_{pa}/I_{pc}) of 2mM Resorcinol at Au electrode at different scan rate in pH 3 (1st cycle)

v/Vs^{-1}	E_{pa1} /V	E_{pa2} /V	E_{pc} /V	$\Delta E = E_{pc1}$~E_{pa2}	$\Delta E_{1/2}$/V	I_{pa1} /μA	I_{pa2} /μA	I_{pc}/μA	I_{pa2}/ I_{pc1}
0.05	0.94	1.30	0.59	0.71	0.94	4.68	1.98	-7.99	0.24
0.1	1.01	1.37	0.56	0.81	0.96	4.30	2.65	-8.92	0.29
0.2	1.08	1.47	0.51	0.96	0.99	8.15	3.82	-12.38	0.30
0.3	1.13	1.59	0.44	1.15	1.01	9.86	5.55	-15.86	0.34
0.4	1.24	1.70	0.3	1.40	1.00	7.18	8.00	-23.77	0.33
0.5	1.10	1.80	0.28	1.52	1.04	6.34	8.17	-21.23	0.38

Table 4.12: Peak potential (E_{pa}), corresponding peak potential difference (ΔE), peak separation ($\Delta E_{1/2}$), peak current (I_p) and corresponding peak current ratio (I_{pa}/I_{pc}) of 2mM Hydroquinone at Au electrode at different scan rate in pH 3 (1st cycle)

v/Vs^{-1}	$E_{pa\ 1}$/V	$E_{pa\ 2}$/V	E_{pc1} /V	ΔE= E_{pc1}~E_{pa1}	$\Delta E_{1/2}$/V	I_{pa1} /μA	I_{pa2} /μA	I_{pc1}/μA	I_{pa1}/ I_{pc1}
0.05	0.48	0.68	0.08	0.4	0.28	7.48	0.06	-6.07	1.23
0.1	0.21	0.98	0.04	0.20	0.33	16.80	0.72	-9.11	1.88
0.2	0.56	0.81	-0.03	0.59	0.26	10.75	1.38	-7.20	1.49
0.3	0.62	0.86	-0.06	0.68	0.28	14.53	1.08	-8.23	1.76
0.4	0.64	0.9	-0.08	0.72	0.28	14.30	0.98	-8.89	1.60
0.5	0.69	0.95	-0.03	0.72	0.33	19.84	0.76	-11.96	1.65

Table 4.13: Peak potential (E_{pa}), corresponding peak potential difference (ΔE), peak separation ($\Delta E_{1/2}$), peak current (I_p) and corresponding peak current ratio (I_{pa}/I_{pc}) of 2mM Catechol at Pt electrode at different scan rate in pH 3 (1st cycle)

v/Vs^{-1}	E_{pa} /V	E_{pc} /V	$\Delta E = E_{pc} \sim E_{pa}$	$\Delta E_{1/2}$/V	I_{pa} /μA	I_{pc}/μA	I_{pa}/ I_{pc}
0.05	0.63	0.17	0.46	0.40	7.03	-5.80	1.21
0.1	0.67	0.14	0.53	0.40	10.73	-7.85	1.36
0.2	0.73	0.10	0.63	0.41	13.04	-11.58	1.12
0.3	0.76	0.07	0.69	0.41	14.91	-12.76	1.16
0.4	0.80	0.05	0.75	0.42	16.27	-11.90	1.36
0.5	0.81	0.03	0.78	0.42	16.53	-16.47	1.00

Table 4.14: Peak potential (E_{pa}), corresponding peak potential difference (ΔE), peak separation ($\Delta E_{1/2}$), peak current (I_p) and corresponding peak current ratio (I_{pa}/I_{pc}) of 2mM Resorcinol at Pt electrode at different scan rate in pH 3 (1st cycle)

v/Vs^{-1}	E_{pa} /V	E_{pc} /V	$\Delta E = E_{pc} \sim E_{pa}$	$\Delta E_{1/2}$/V	I_{pa} /μA	I_{pc}/μA	I_{pa}/ I_{pc}
0.05	0.97	0.09	0.88	0.53	6.53	-4.12	1.58
0.1	1.04	0.05	0.99	0.54	11.17	-6.59	1.69
0.2	1.08	0	1.08	0.54	13.34	-7.08	1.88
0.3	1.14	-0.02	1.16	0.56	16.31	-12.41	1.31
0.4	1.16	-0.07	1.23	0.54	16.08	-11.32	1.42
0.5	1.21	-0.15	1.36	0.53	19.31	-9.95	1.94

Table 4.15: Peak potential (E_{pa}), corresponding peak potential difference (ΔE), peak separation ($\Delta E_{1/2}$), peak current (I_p) and corresponding peak current ratio (I_{pa}/I_{pc}) of 2mM Hydroquinone at Pt electrode at different scan rate in pH 3 (1st cycle)

v/Vs^{-1}	E_{pa} /V	E_{pc} /V	$\Delta E = E_{pc} \sim E_{pa}$	$\Delta E_{1/2}$/V	I_{pa} /μA	I_{pc}/μA	I_{pa}/ I_{pc}
0.05	0.67	-0.02	0.69	0.32	8.31	-3.05	2.72
0.1	0.66	0.02	0.64	0.34	13.20	-3.15	4.19
0.2	0.78	-0.14	0.92	0.32	13.90	-4.19	3.31
0.3	0.85	-0.17	1.02	0.34	15.81	-5.56	2.84
0.4	0.86	-0.21	1.07	0.32	15.47	-4.73	3.27
0.5	0.73	-0.01	0.74	0.36	21.11	-9.74	2.16

Table 4.16: Peak potential (E_{pa}), corresponding peak potential difference (ΔE), peak separation ($\Delta E_{1/2}$), peak current (I_p) and corresponding peak current ratio (I_{pa}/I_{pc}) of 2mM Catechol at GC electrode at different scan rate in pH 9 (1st cycle)

v/Vs^{-1}	E_{pa} /V	E_{pc}/V	$\Delta E = E_{pc} \sim E_{pa}$	$\Delta E_{1/2}$/V	I_{pa}/μA	I_{pc}/μA	I_{pa}/ I_{pc}
0.05	0.15	-0.03	0.18	0.06	30.52	-2.72	11.22
0.1	0.17	-0.03	0.20	0.07	42.34	-2.29	18.48
0.2	0.21	-0.04	0.25	0.08	65.42	-6.59	9.92
0.3	0.20	-0.04	0.24	0.08	60.95	-8.65	7.04
0.4	0.22	-0.05	0.27	0.08	73.31	-12.12	6.04
0.5	0.22	-0.05	0.27	0.08	84.27	-16.85	5.00

Table 4.17: Peak potential (E_{pa}) and peak current (I_p) of 2mM Resorcinol at GC electrode at different scan rate in pH 9 (1st cycle)

v/Vs^{-1}	E_{pa1} /V	I_{pa} /μA
0.05	0.45	21.41
0.1	0.46	27.26
0.2	0.48	33.16
0.3	0.48	42.61
0.4	0.49	46.56
0.5	0.48	46.71

Table 4.18: Peak potential (E_{pa}), corresponding peak potential difference (ΔE), peak separation ($\Delta E_{1/2}$), peak current (I_p) and corresponding peak current ratio (I_{pa}/I_{pc}) of 2mM Hydroquinone at GC electrode at different scan rate in pH 9 (1st cycle)

v/Vs^{-1}	E_{pa} /V	E_{pc} /V	$\Delta E = E_{pc} \sim E_{pa}$	$\Delta E_{1/2}$/V	I_{pa} /μA	I_{pc} /μA	I_{pa}/ I_{pc}
0.05	0.62	-0.33	0.70	0.14	15.25	-8.73	1.74
0.1	0.70	-0.40	0.79	0.15	18.68	-12.00	1.55
0.2	0.76	-0.46	0.77	0.15	26.31	-15.41	1.70
0.3	0.84	-0.47	0.78	0.18	29.49	-18.67	1.57
0.4	0.90	-0.53	0.86	0.18	34.17	-19.19	1.78
0.5	0.96	-0.56	0.79	0.20	35.87	-21.85	1.64

Table 4.19: Peak potential (E_{pa}), corresponding peak potential difference (ΔE), peak separation ($\Delta E_{1/2}$), peak current (I_p) and corresponding peak current ratio (I_{pa}/I_{pc}) of 2mM Catechol at GC electrode at different scan rate in pH 3 (1st cycle)

v/Vs^{-1}	E_{pa} /V	E_{pc} /V	$\Delta E = E_{pc} \sim E_{pa}$	$\Delta E_{1/2}$/V	I_{pa} /μA	I_{pc}/μA	I_{pa}/ I_{pc}
0.05	0.61	0.11	0.50	0.36	34.98	-24.44	1.43
0.1	0.84	0.06	0.78	0.45	36.69	-28.08	1.30
0.2	0.80	-0.03	0.83	0.38	55.76	-36.71	1.51
0.3	0.86	-0.07	0.93	0.39	60.54	-40.69	1.48
0.4	0.79	-0.03	0.82	0.38	80.05	-56.59	1.41
0.5	0.81	-0.03	0.84	0.39	90.18	-60.59	1.48

Table 4.20: Peak potential (E_{pa}), corresponding peak potential difference (ΔE), peak separation ($\Delta E_{1/2}$), peak current (I_p) and corresponding peak current ratio (I_{pa}/I_{pc}) of 2mM Catechol with 2mM Sulfanilic acid at GC electrode at different scan rate in pH 7 (1st cycle)

v/Vs^{-1}	E_{pa1} /V	E_{pa2} /V	E_{pc1} /V	E_{pc2} /V	$\Delta E = E_{pc2} \sim E_{pa1}$	$\Delta E = E_{pc1} \sim E_{pa2}$	$\Delta E_{1/2}$/V	I_{pa1} /μA	I_{pa2} /μA	I_{pc1} /μA	I_{pc2} /μA	I_{pa1}/ I_{pc2}	I_{pa2}/ I_{pc1}
0.05	0.40	0.95	0.78	-0.22	0.62	0.17	0.09	58.72	23.74	-3.78	-5.22	11.24	6.28
0.1	0.42	0.97	0.79	-0.27	0.69	0.18	0.07	74.92	32.55	-4.18	-8.65	8.66	7.78
0.2	0.41	0.98	0.76	-0.29	0.70	0.22	0.06	90.32	51.85	-7.72	-11.80	7.65	6.71
0.3	0.41	0.98	0.78	-0.27	0.68	0.20	0.07	106.02	68.78	-9.85	-11.63	9.11	6.98
0.4	0.42	0.99	0.80	-0.26	0.68	0.19	0.08	122.19	86.61	-11.04	-9.50	12.86	7.84
0.5	0.42	1.00	0.77	-0.23	0.65	0.23	0.09	134.22	95.63	-9.44	10.32	-13.00	10.13

Table 4.21: Peak potential (E_{pa}), corresponding peak potential difference (ΔE), peak separation ($\Delta E_{1/2}$), peak current (I_p) and corresponding peak current ratio (I_{pa}/I_{pc}) of 2mM Hydroquinone with 2mM Sulfanilic acid at GC electrode at different scan rate in pH 7 (1st cycle)

v/Vs^{-1}	E_{pa1} /V	E_{pa2} /V	E_{pc} /V	$\Delta E = E_{pc}$~E_{pa1}	$\Delta E_{1/2}$/V	I_{pa1} /µA	I_{pa2}/µA	I_{pc}/µA	I_{pa1}/ I_{pc}
0.05	0.32	1.02	-0.10	0.42	0.41	33.19	12.22	-27.61	1.20
0.1	0.37	1.08	-0.17	0.54	0.43	55.02	40.85	-33.47	1.64
0.2	0.41	1.08	-0.16	0.57	0.46	60.83	52.37	-45.72	1.33
0.3	0.45	1.13	-0.20	0.65	0.46	79.44	56.76	-50.14	1.58
0.4	0.47	1.16	-0.22	0.69	0.44	92.38	72.13	-53.19	1.73
0.5	0.50	1.17	-0.23	0.73	0.46	83.09	62.60	-63.00	1.31

Table 4.22: Peak potential (E_{pa}), corresponding peak potential difference (ΔE), peak separation ($\Delta E_{1/2}$), peak current Ip (µA) and corresponding peak current ratio (I_{pa}/I_{pc}), of 2mM Catechol with 2mM Sulfanilic acid at Au electrode at different scan rate in pH 7 (1st cycle).

v/Vs^{-1}	E_{pa1} /V	E_{pa2} /V	E_{pc1} /V	E_{pc2} /V	E_{pc3} /V	$\Delta E = E_{pc3}$~E_{pa1}	$\Delta E = E_{pc1}$~E_{pa2}	$\Delta E_{1/2}$/V	I_{pa1} /µA	I_{pa2} /µA	I_{pc1} /µA	I_{pc2} /µA	I_{pc3} /µA	I_{pa1}/ I_{pc3}	I_{pa2}/ I_{pc1}
0.05	0.26	0.97	0.48	0.14	-0.13	0.39	0.49	0.06	14.57	9.04	-4.29	-4.14	-2.51	5.80	2.10
0.1	0.27	1.02	0.46	0.10	-0.13	0.40	0.56	0.07	22.54	12.40	-8.38	-6.31	-3.63	6.20	1.47
0.2	0.28	1.01	0.46	0.14	-0.17	0.45	0.55	0.05	25.64	18.96	-20.16	-9.68	-4.24	6.04	0.94
0.3	0.29	1.07	0.44	0.14	-0.16	0.45	0.63	0.06	27.51	27.28	-29.31	-8.84	-3.59	7.66	0.93
0.4	0.29	1.11	0.44	0.12	-0.20	0.49	0.67	0.04	31.50	32.74	-37.60	-9.91	-3.50	9.00	0.87
0.5	0.30	1.10	0.43	0.11	-0.29	0.59	0.67	0.005	30.04	33.19	-38.65	-6.99	-2.59	11.59	0.85

Table 4.23: Peak potential (E_{pa}), corresponding peak potential difference (ΔE), peak separation ($\Delta E_{1/2}$), peak current (I_p) and corresponding peak current ratio (I_{pa}/I_{pc}) of 2mM Catechol with 2mM Sulfanilic acid at Pt electrode at different scan rate in pH 7 (1st cycle)

v/Vs^{-1}	E_{pa} /V	E_{pc} /V	$\Delta E = E_{pc} \sim E_{pa}$	$\Delta E_{1/2}$/V	I_{pa} /μA	I_{pc} /μA	I_{pa}/ I_{pc}
0.05	0.54	-0.05	0.59	0.24	12.83	-2.92	4.39
0.1	0.54	-0.05	0.59	0.24	16.09	-5.38	2.99
0.2	0.56	-0.07	0.63	0.24	21.72	-7.65	2.83
0.3	0.55	-0.07	0.62	0.24	26.19	-7.85	3.33
0.4	0.55	-0.09	0.64	0.23	26.66	-12.41	2.14
0.5	0.55	-0.10	0.65	0.22	28.56	-12.87	2.21

Table 4.24: Peak potential (E_{pa}), corresponding peak potential difference (ΔE), peak separation ($\Delta E_{1/2}$), peak current (I_p) and corresponding peak current ratio (I_{pa}/I_{pc}) of 2mM Hydroquinone with 2mM Sulfanilic acid at Au electrode at different scan rate in pH 7 (1st cycle)

v/Vs^{-1}	E_{pa1} /V	E_{pa2} /V	E_{pc1} /V	E_{pc2} /V	$\Delta E = E_{pc2} \sim E_{pa1}$	$\Delta E = E_{pc1} \sim E_{pa2}$	$\Delta E_{1/2}$/V	I_{pa1} /μA	I_{pa2}/μA	I_{pc1}/μA	I_{pc2}/μA	I_{pa1}/ I_{pc2}	I_{pa2}/ I_{pc1}
0.05	0.29	1.01	0.57	-0.07	0.36	0.44	0.11	9.84	11.20	-0.99	-8.12	1.21	11.31
0.1	0.31	1.03	0.55	-0.10	0.41	0.48	0.10	11.6	14.24	-1.91	-10.92	1.06	7.45
0.2	0.33	1.05	0.50	-0.12	0.45	0.55	0.10	15.71	16.44	-2.75	-12.25	1.28	5.97
0.3	0.40	1.06	0.51	-0.14	0.54	0.55	0.13	18.1	20.74	-4.59	-18.92	0.95	4.51
0.4	0.43	1.09	0.50	-0.15	0.58	0.59	0.14	18.55	22.98	-4.18	-18.86	0.98	5.49
0.5	0.43	1.12	0.47	-0.17	0.6	0.65	0.13	20.85	22.83	-3.26	-18.21	1.14	7.00

Table 4.25: Peak potential (E_{pa}), corresponding peak potential difference (ΔE), peak separation ($\Delta E_{1/2}$), peak current (I_p) and corresponding peak current ratio (I_{pa}/I_{pc}) of 2mM Hydroquinone with 2mM Sulfanilic acid at Pt electrode at different scan rate in pH 7 (1st cycle)

v/Vs^{-1}	E_{pa1} /V	E_{pa2} /V	E_{pc} /V	$\Delta E = E_{pc} \sim E_{pa1}$	$\Delta E_{1/2}$/V	I_{pa1} /μA	I_{pa2}/μA	I_{pc}/μA	I_{pa1}/ I_{pc}
0.05	0.40	1.02	-0.10	0.50	0.15	0.02	7.67	-6.32	0.003
0.1	0.42	1.04	-0.14	0.56	0.14	0.05	10.10	-8.51	0.005
0.2	0.47	1.09	-0.17	0.64	0.15	0.10	13.64	-11.66	0.008
0.3	0.49	1.12	-0.21	0.70	0.14	0.15	15.26	-13.33	0.011
0.4	0.52	1.14	-0.23	0.75	0.14	0.20	18.21	-14.40	0.013
0.5	0.53	1.15	-0.22	0.75	0.15	0.25	22.09	-16.23	0.015

Table 4.26: Peak potential (E_{pa}) and peak current (I_p) of 2mM Resorcinol at GC electrode at different scan rate in pH 3 (1st cycle)

v/Vs^{-1}	E_{pa} /V	I_{pa} /μA
0.05	0.99	22.17
0.1	1.08	33.03
0.2	1.16	52.78
0.3	1.29	60.26
0.4	1.36	75.83
0.5	1.34	86.20

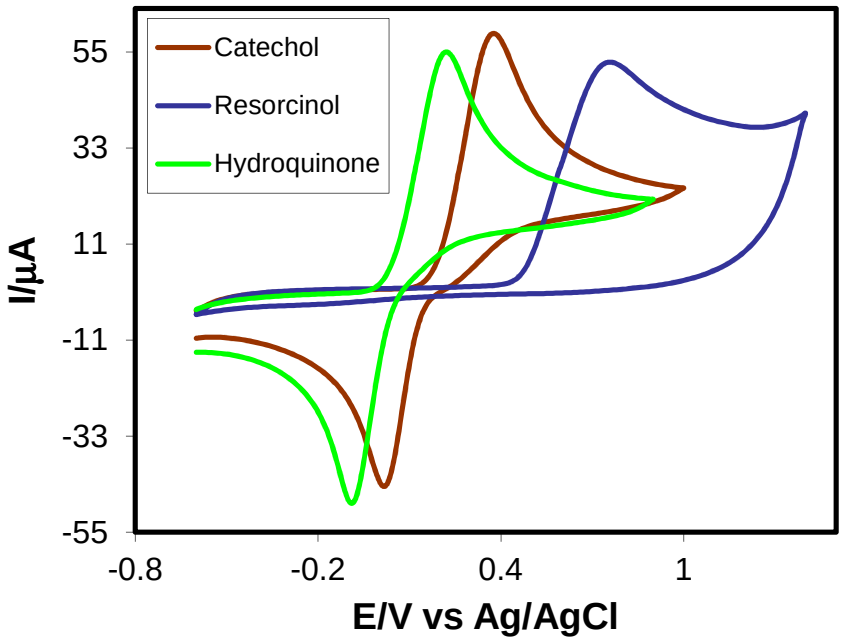

Fig. 4.1: Comparison of cyclic voltammogram of 2mM Resorcinol, 2mM Catechol and 2mM Hydroquinone in buffer solution (pH 7) of GC electrode at scan rate 0.1 V/s (1st cycle)

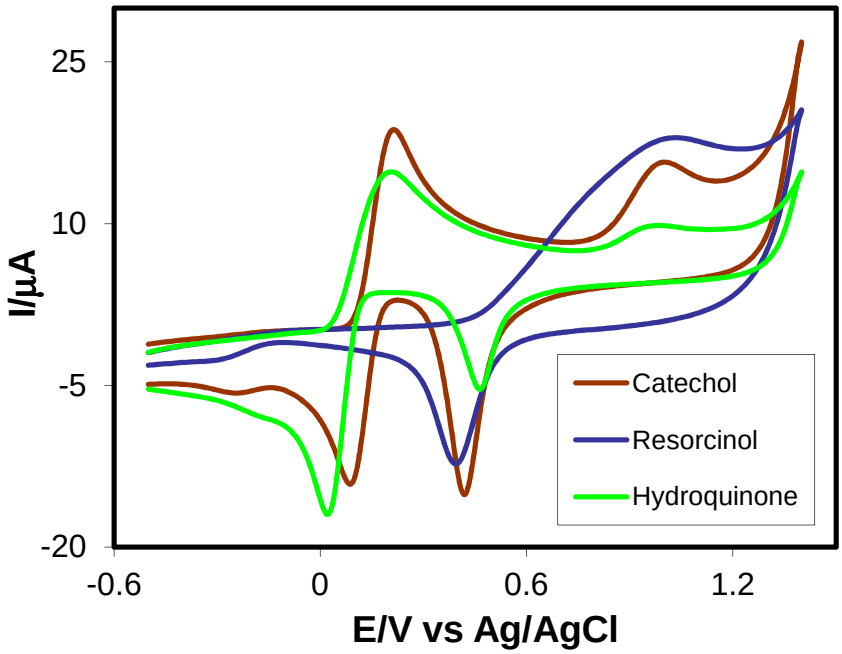

Fig. 4.2: Comparison of cyclic voltammogram of 2mM Resorcinol, 2mM Catechol and 2mM Hydroquinone in buffer solution (pH 7) of Au electrode at scan rate 0.1 V/s (1st cycle)

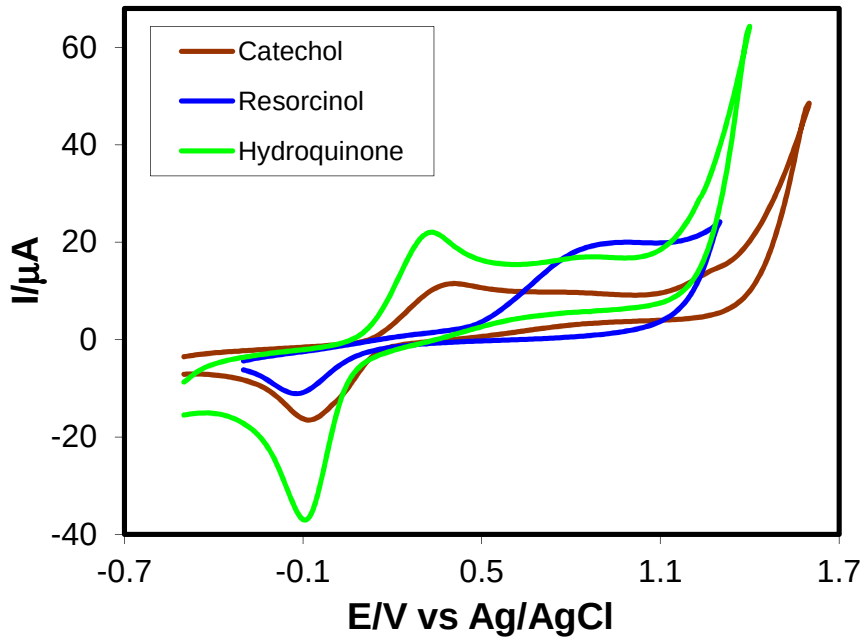

Fig. 4.3: Comparison of cyclic voltammogram of 2mM Resorcinol, 2mM Catechol and 2mM Hydroquinone in buffer solution (pH 7) of Pt electrode at scan rate 0.1 V/s (1st cycle)

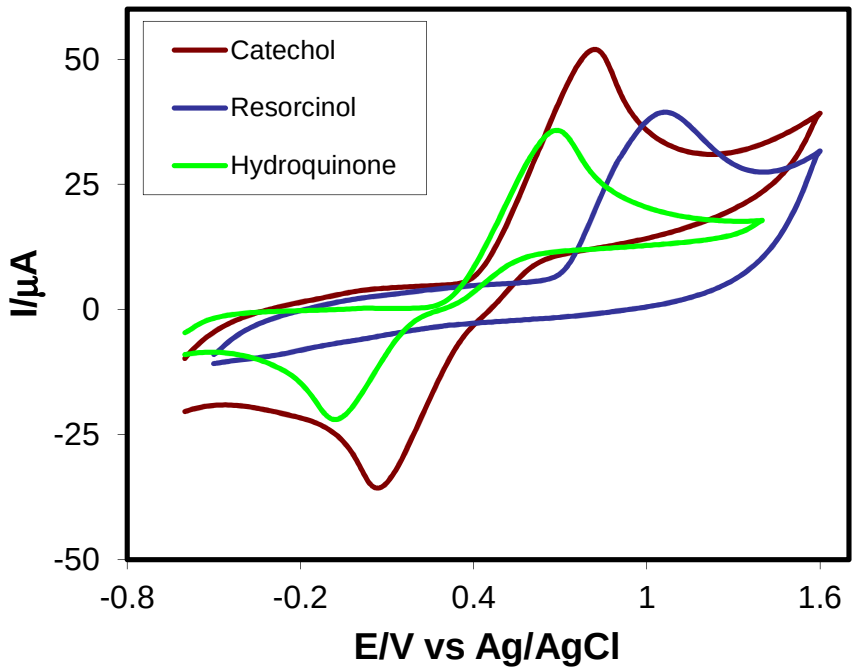

Fig. 4.4: Comparison of cyclic voltammogram of 2mM Resorcinol, 2mM Catechol and 2mM Hydroquinone in buffer solution (pH 3) of GC electrode at scan rate 0.1V/s (1st cycle)

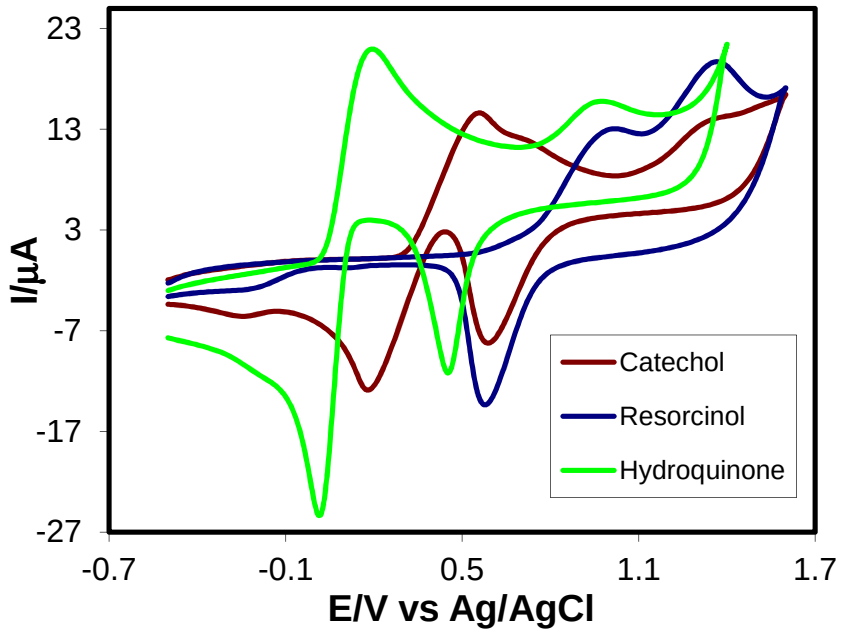

Fig. 4.5: Comparison of cyclic voltammogram of 2mM Resorcinol, 2mM Catechol and 2mM Hydroquinone in buffer solution (pH 3) of Au electrode at scan rate 0.1V/s (1st cycle)

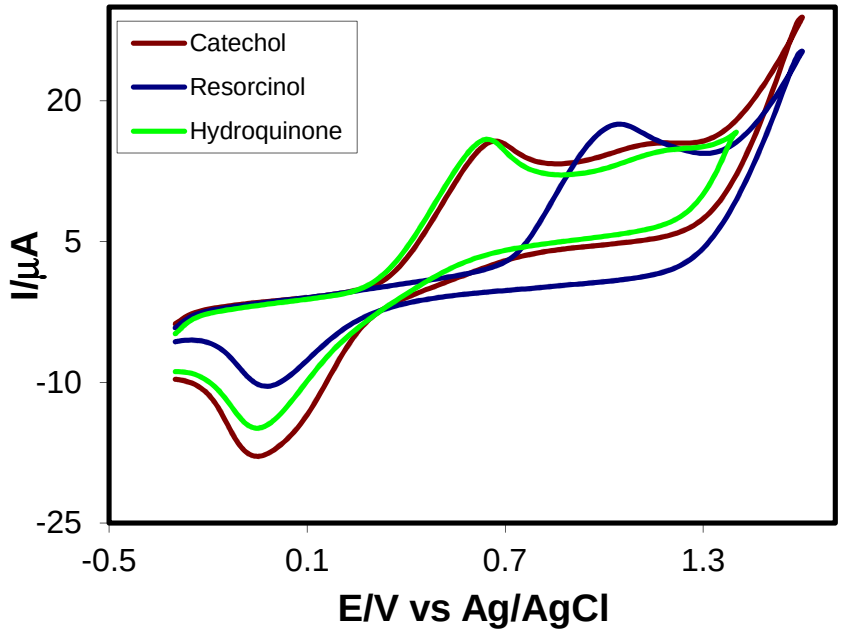

Fig. 4.6: Comparison of cyclic voltammogram of 2mM Resorcinol, 2mM Catechol and 2mM Hydroquinone in buffer solution (pH 3) of Pt electrode at scan rate 0.1 V/s (1st cycle)

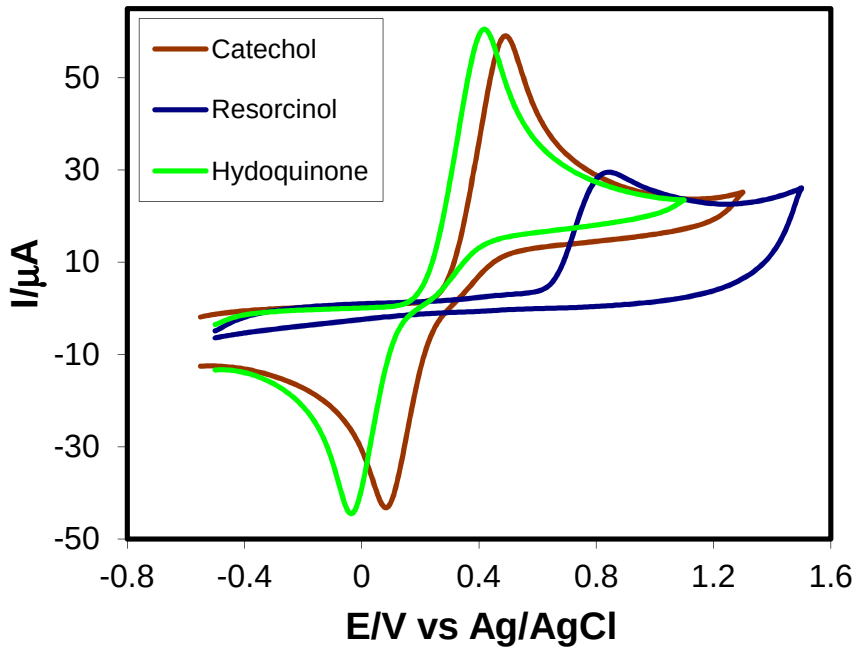

Fig. 4.7: Comparison of cyclic voltammogram of 2mM Resorcinol, 2mM Catechol and 2mM Hydroquinone in buffer solution (pH 5) of GC electrode at scan rate 0.1V/s (1st cycle)

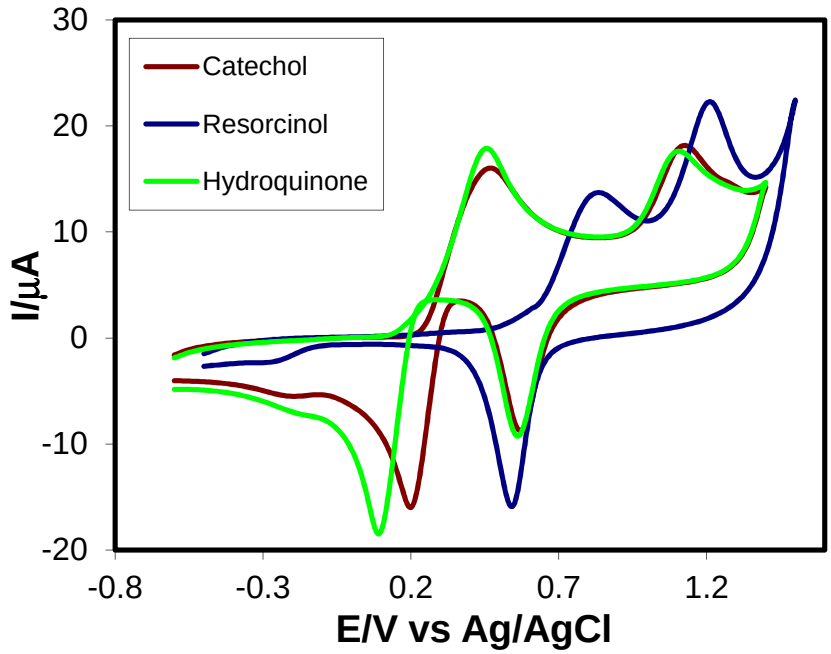

Fig. 4.8: Comparison of cyclic voltammogram of 2mM Resorcinol, 2mM Catechol and 2mM Hydroquinone in buffer solution (pH 5) of Au electrode at scan rate 0.1V/s (1st cycle)

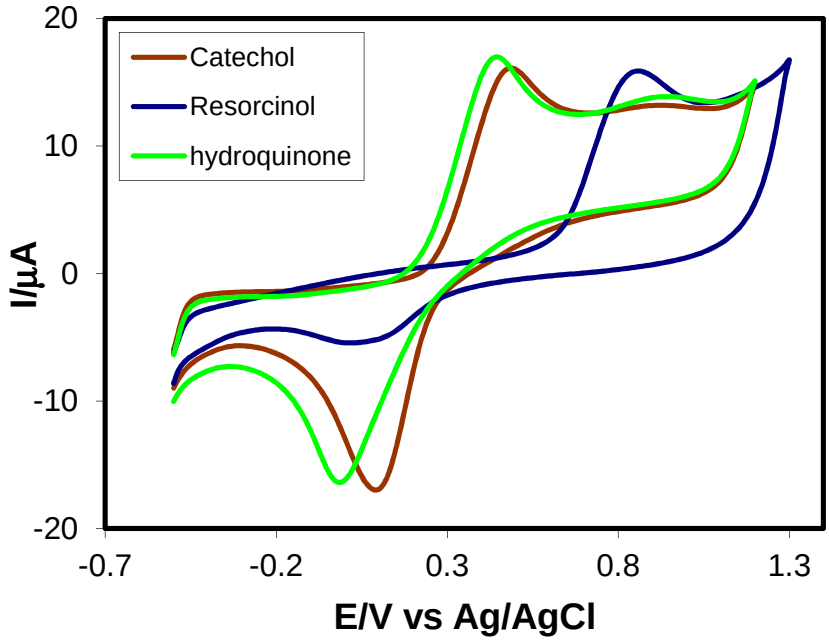

Fig. 4.9: Comparison of cyclic voltammogram of 2mM Resorcinol, 2mM Catechol and 2mM Hydroquinone in buffer solution (pH 5) of Pt electrode at scan rate 0.1V/s (1st cycle)

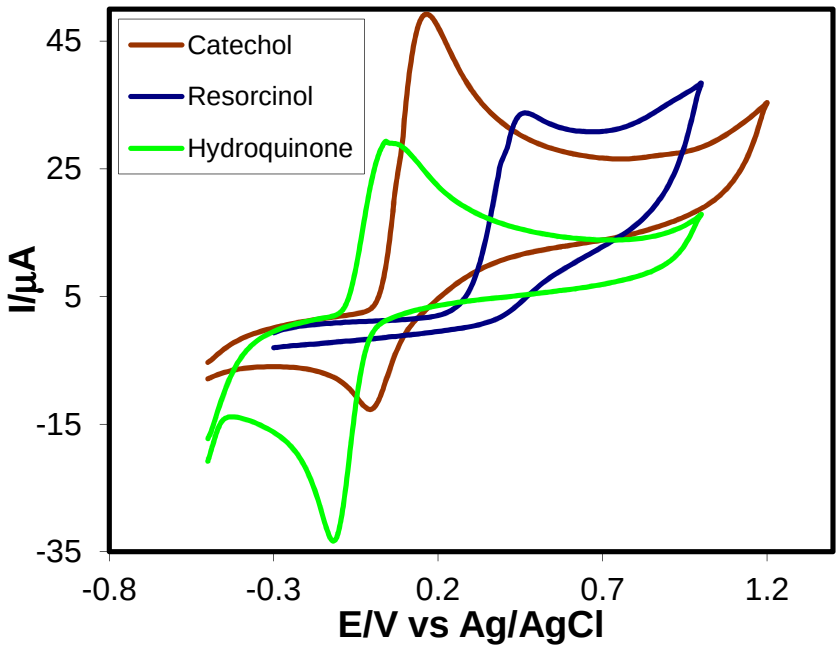

Fig. 4.10: Comparison of cyclic voltammogram of 2mM Catechol, 2mM Resorcinol and 2mM Hydroquinone in buffer solution (pH 9) of at GC electrode at scan rate 0.1 V/s (1st cycle)

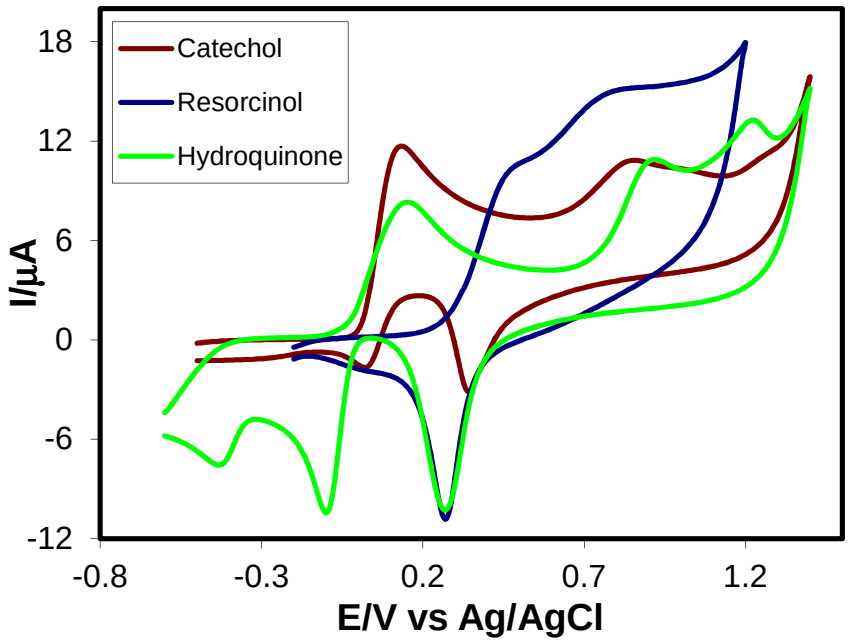

Fig. 4.11: Comparison of cyclic voltammogram of 2mM Catechol, 2mM Resorcinol and 2mM Hydroquinone in buffer solution (pH 9) of at Au electrode at scan rate 0.1 V/s (1st cycle)

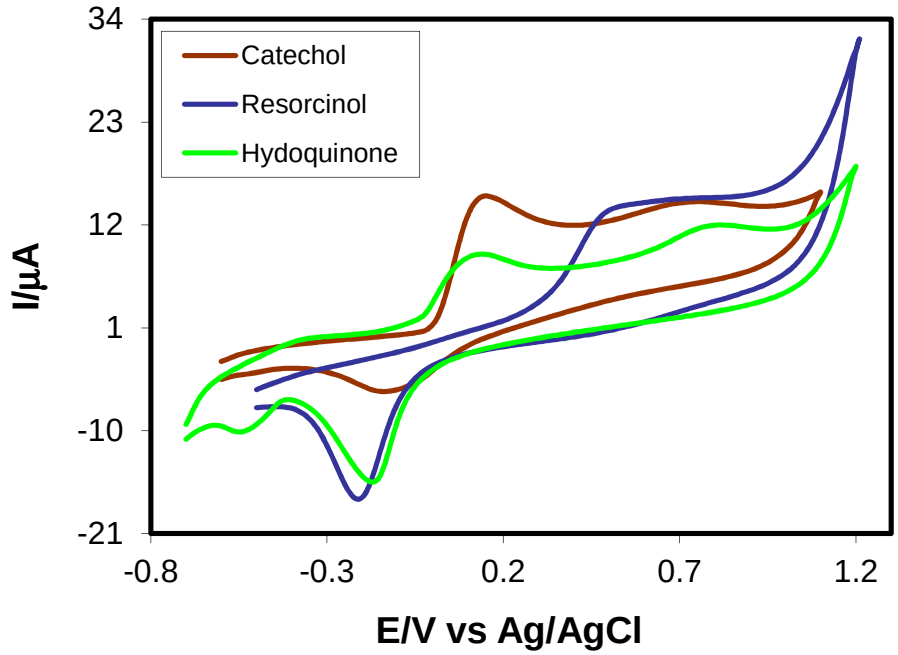

Fig. 4.12: Comparison of cyclic voltammogram of 2mM Catechol, 2mM Resorcinol and 2mM Hydroquinone in buffer solution (pH 9) of Pt electrode at scan rate 0.1 V/s (1st cycle)

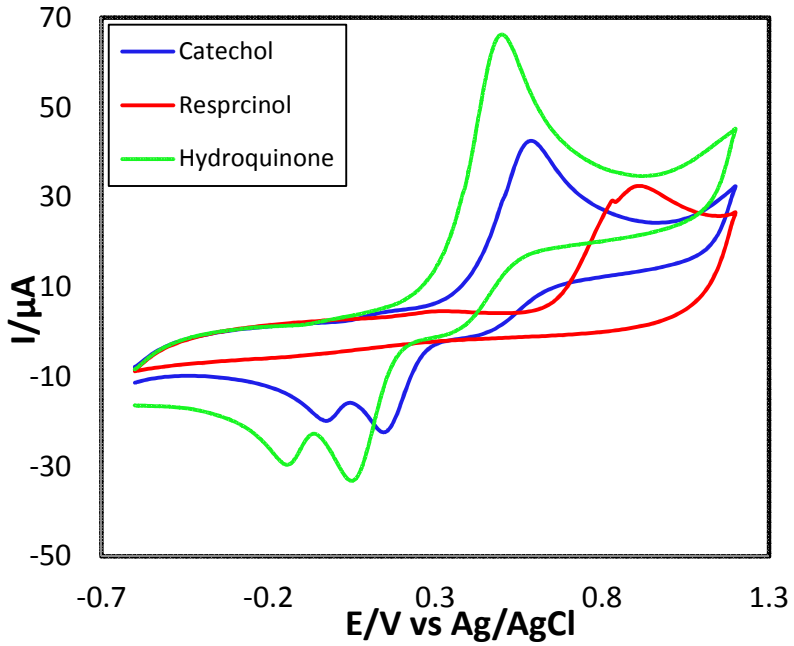

Fig. 4.13: Comparison of cyclic voltammogram of 2mM Catechol, 2mM Resorcinol and 2mM Hydroquinone in supporting electrolyte (1M KCl) of GC electrode at scan rate 0.1 V/s (1st cycle)

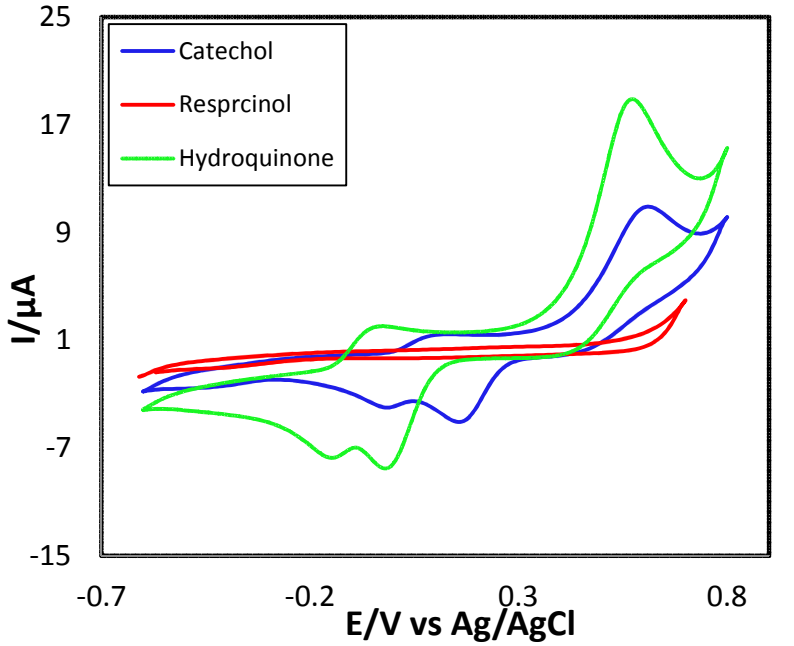

Fig. 4.14: Comparison of cyclic voltammogram of 2mM Catechol, 2mM Resorcinol and 2mM Hydroquinone in supporting electrolyte (1M KCl) of Au electrode at scan rate 0.1 V/s (1st cycle)

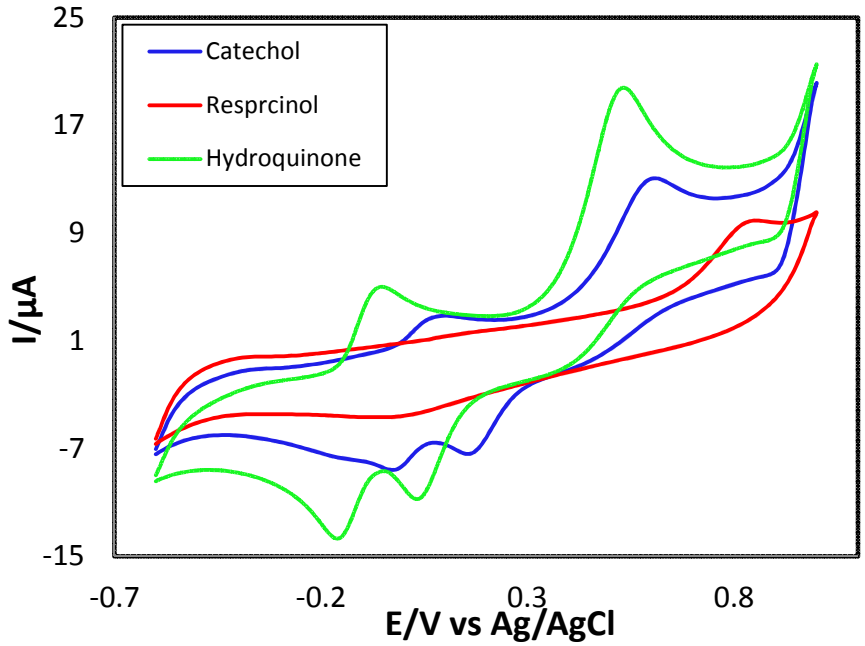

Fig. 4.15: Comparison of cyclic voltammogram of 2mM Catechol, 2mM Resorcinol and 2mM Hydroquinone in supporting electrolyte (1M KCl) of Pt electrode at scan rate 0.1 V/s (1st cycle)

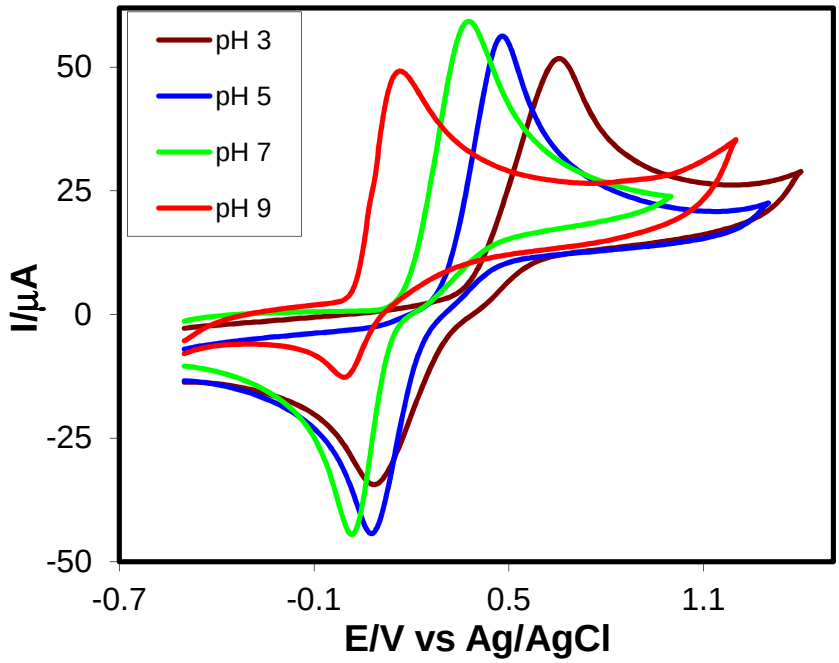

Fig. 4.16: Comparison of Cyclic voltammogram of different pH (3, 5, 7 & 9) of 2mM Catechol of GC electrode at scan rate 0.1V/s (1st cycle)

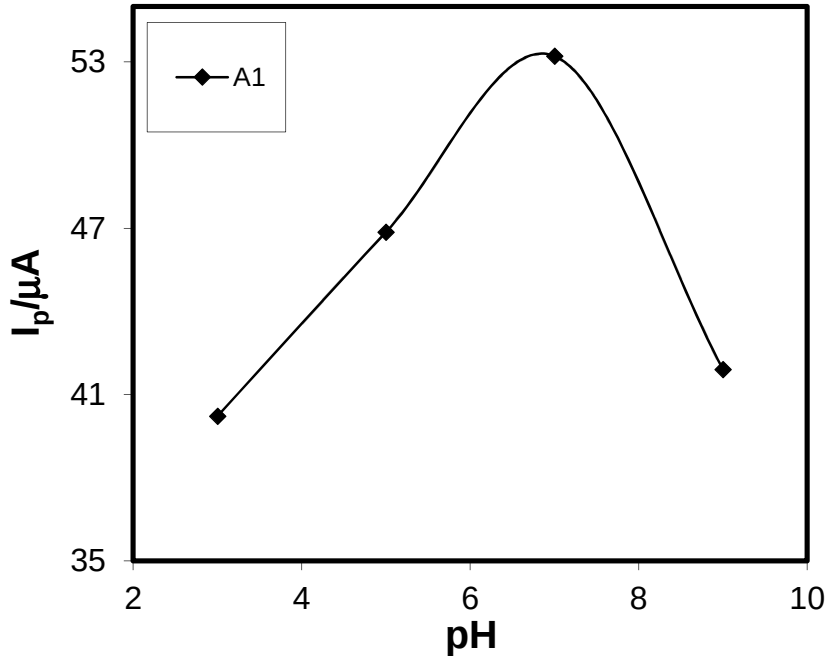

Fig. 4.17: Plots of peak current (I_p) versus pH of 2mM Catechol of GC electrode at scan rate 0.1V/s (1st cycle)

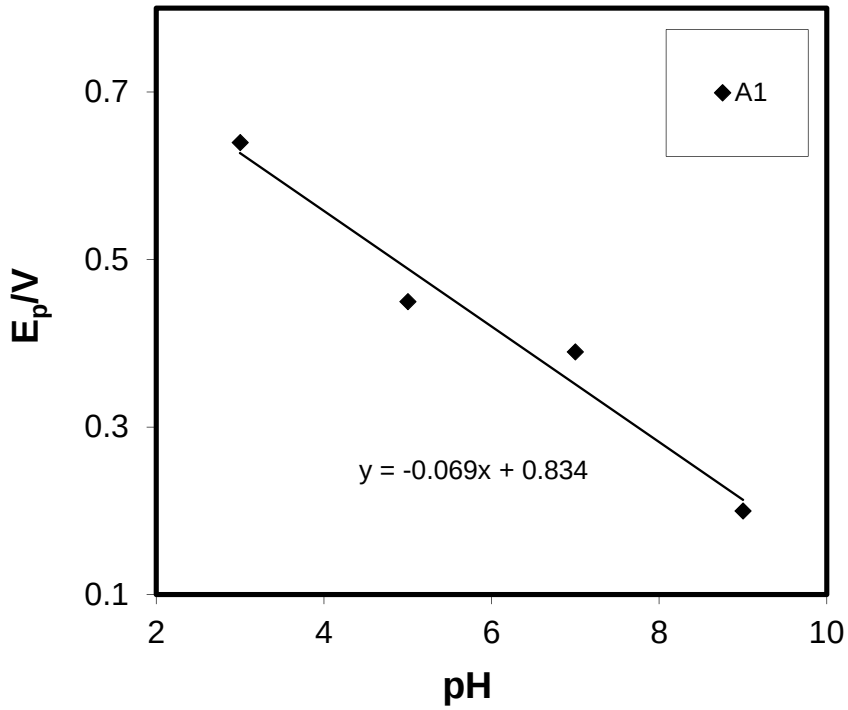

Fig. 4.18: Plots of peak potential (E_p) versus pH of 2mM Catechol of GC electrode at scan rate 0.1V/s (1st cycle)

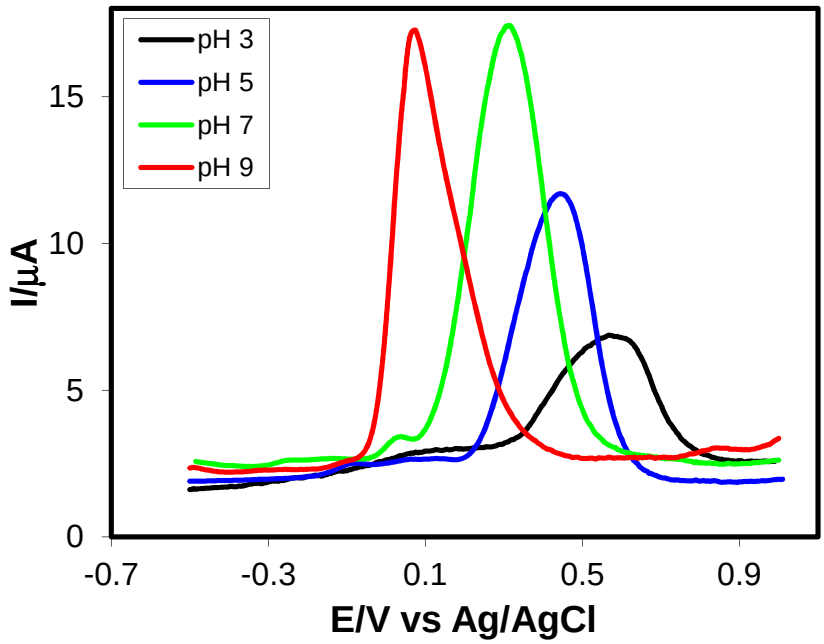

Fig. 4.19: Comparison of Differential pulse voltammogram of different pH (3, 5, 7 & 9) of 2mM Catechol of GC electrode at scan rate 0.1V/s (1st cycle)

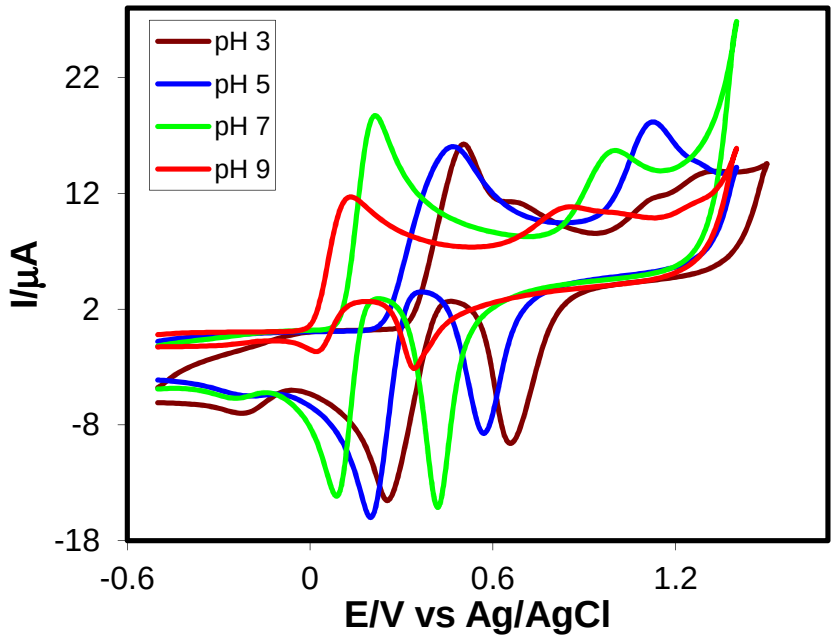

Fig. 4.20: Comparison of Cyclic voltammogram of different pH (3, 5, 7 & 9) of 2mM Catechol of Au electrode at scan rate 0.1V/s (1st cycle)

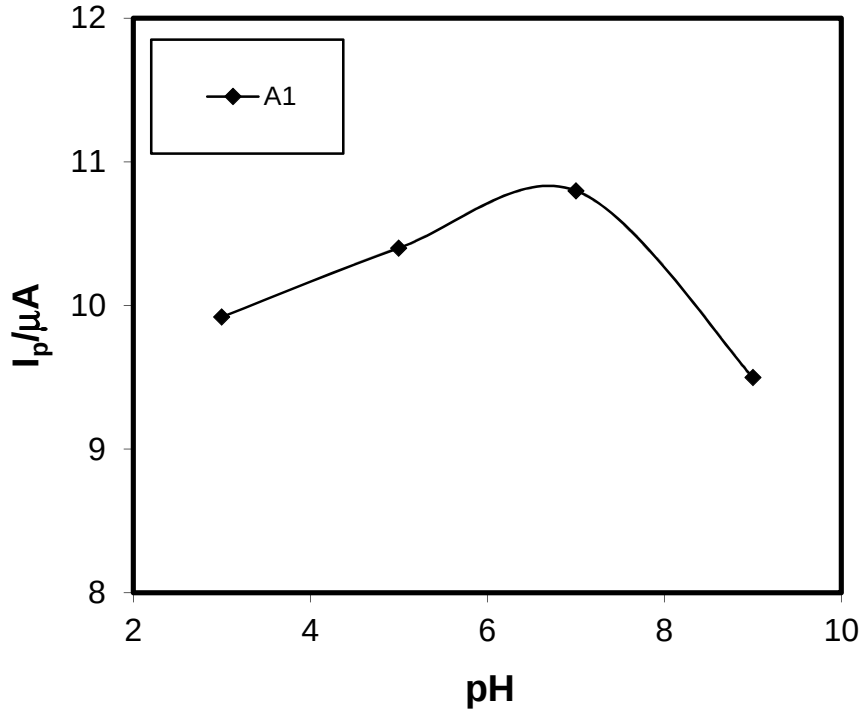

Fig. 4.21: Plots of peak current (I_p) versus pH of 2mM Catechol of Au electrode at scan rate 0.1V/s

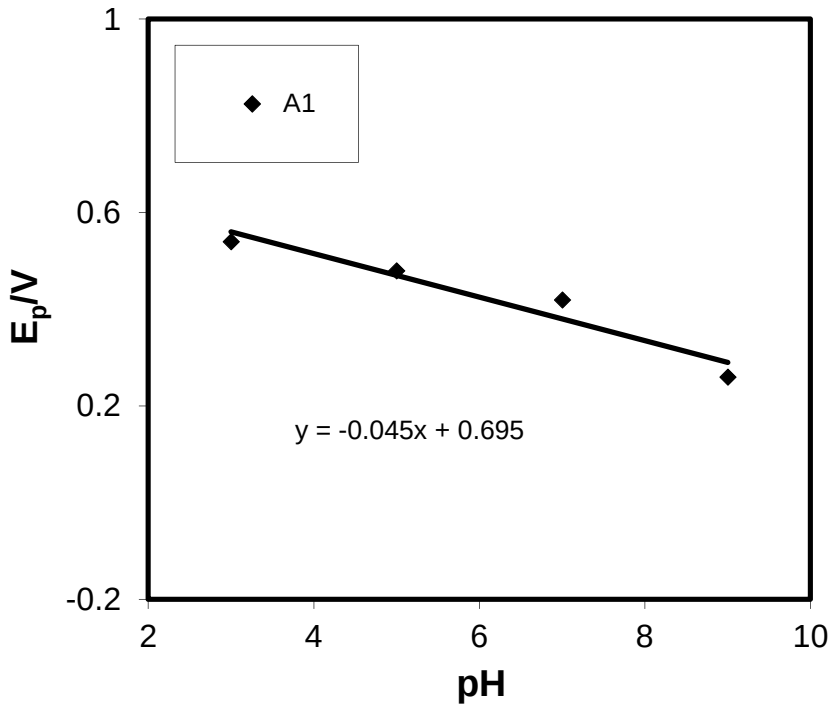

Fig. 4.22: Plots of peak potential (E_p) versus pH of 2mM Catechol of Au electrode at scan rate 0.1V/s

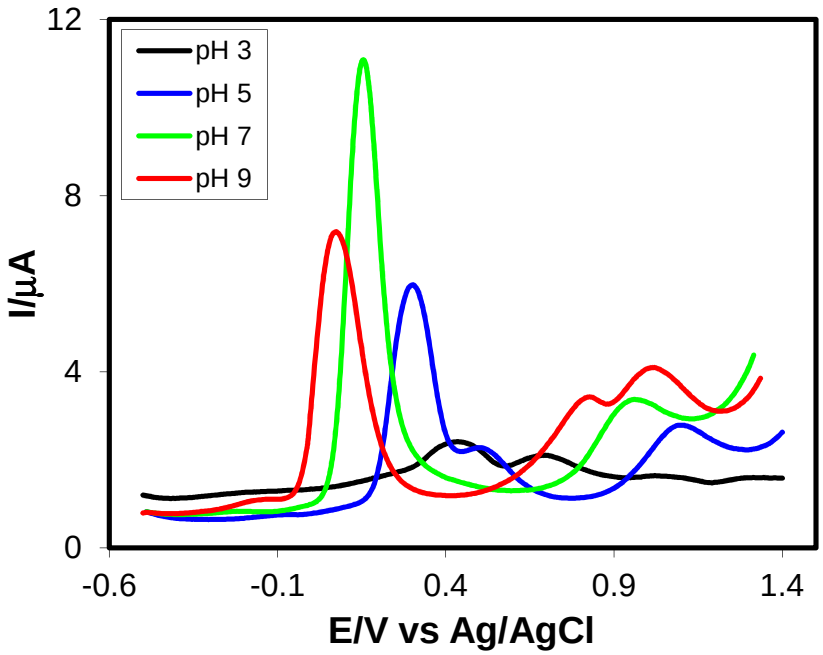

Fig. 4.23: Comparison of Differential pulse voltammogram of different pH (3, 5, 7 & 9) of 2mM Catechol of Au electrode at scan rate 0.1V/s (1st cycle)

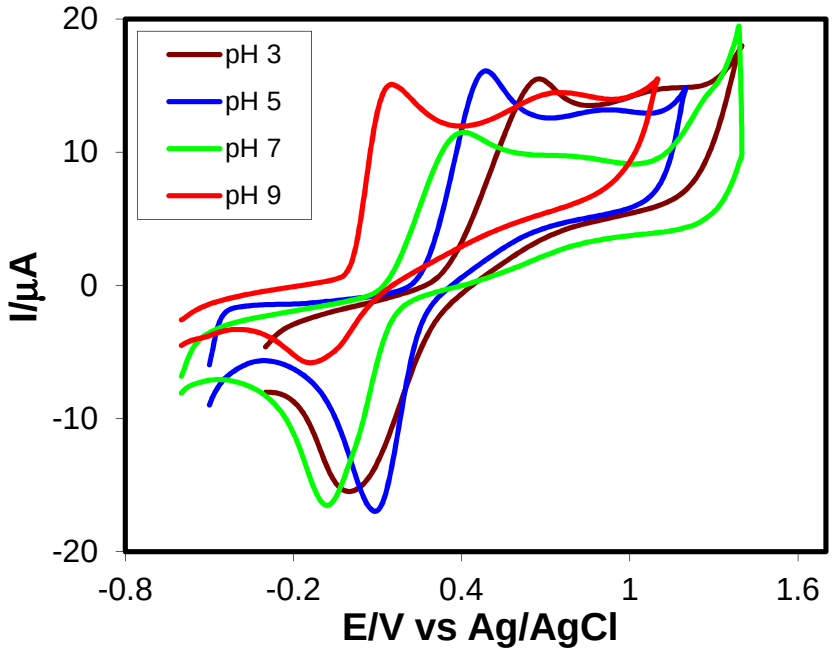

Fig. 4.24: Comparison of Cyclic voltammogram of different pH (3, 5, 7 & 9) of 2mM Catechol of Pt electrode at scan rate 0.1V/s (1st cycle)

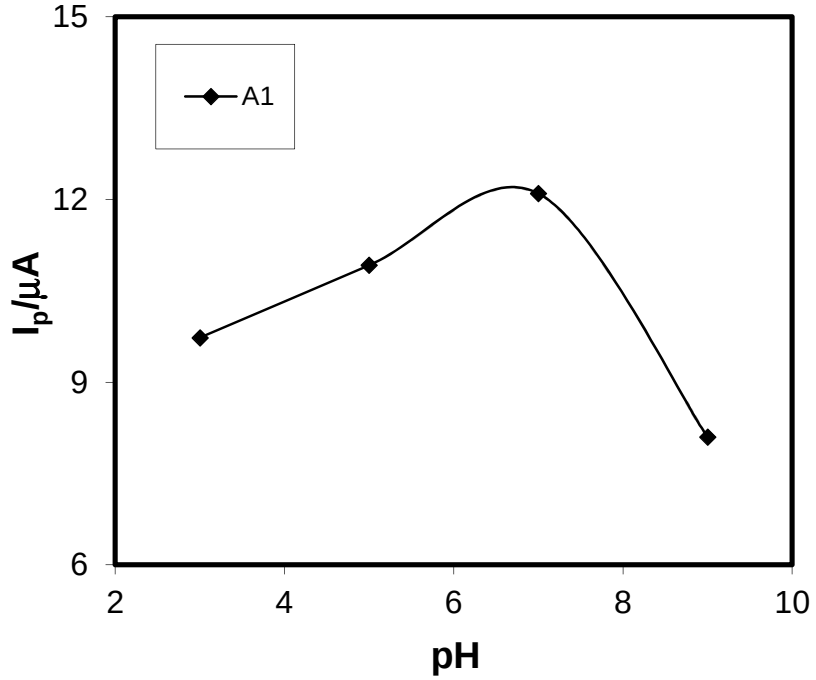

Fig. 4.25: Plots of peak current (I_p) versus pH of 2mM Catechol of Pt electrode at scan rate 0.1V/s

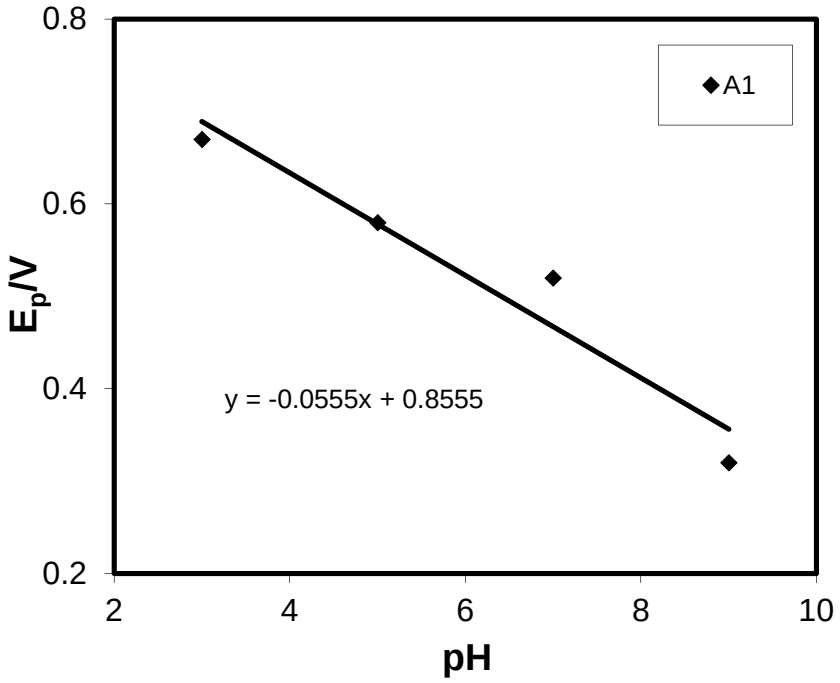

Fig. 4.26: Plots of peak potential (E_p) versus pH of 2mM Catechol of Pt electrode at scan rate 0.1V/s

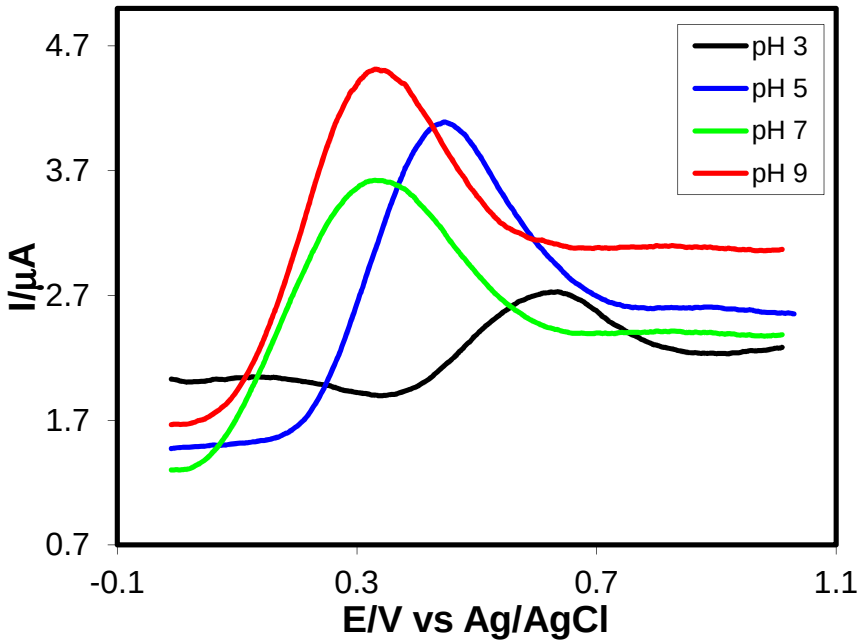

Fig. 4.27: Comparison of Differential pulse voltammogram of different pH (3, 5, 7 & 9) of 2mM Catechol of Pt electrode at scan rate 0.1V/s (1st cycle)

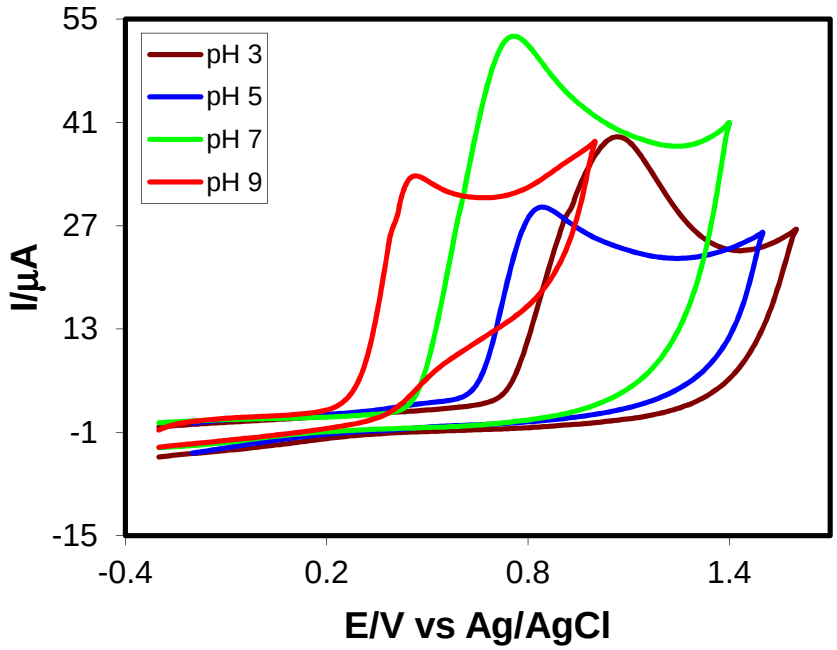

Fig. 4.28: Comparison of Cyclic voltammogram of different pH (3, 5, 7 & 9) of 2mM Resorcinol of GC electrode at scan rate 0.1V/s (1st cycle)

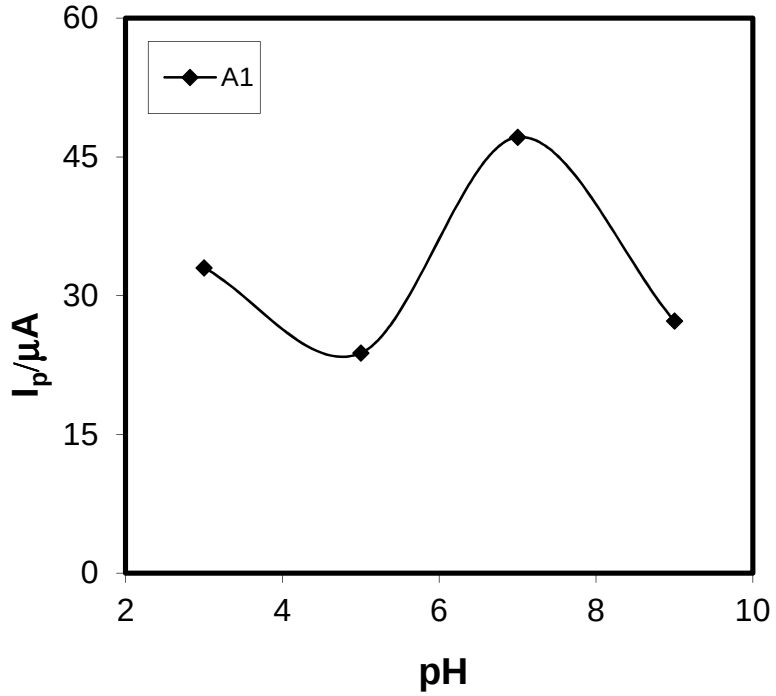

Fig. 4.29: Plots of peak current (I_p) versus pH of 2mM Resorcinol of GC electrode at scan rate 0.1V/s (1st cycle)

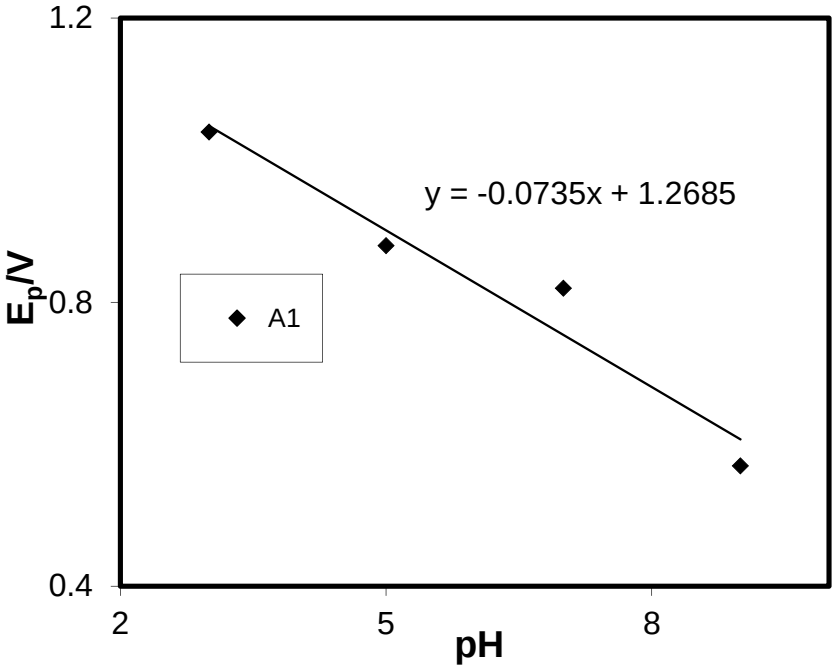

Fig. 4.30: Plots of peak potential (E_p) versus pH of 2mM Resorcinol of GC electrode at scan rate 0.1V/s

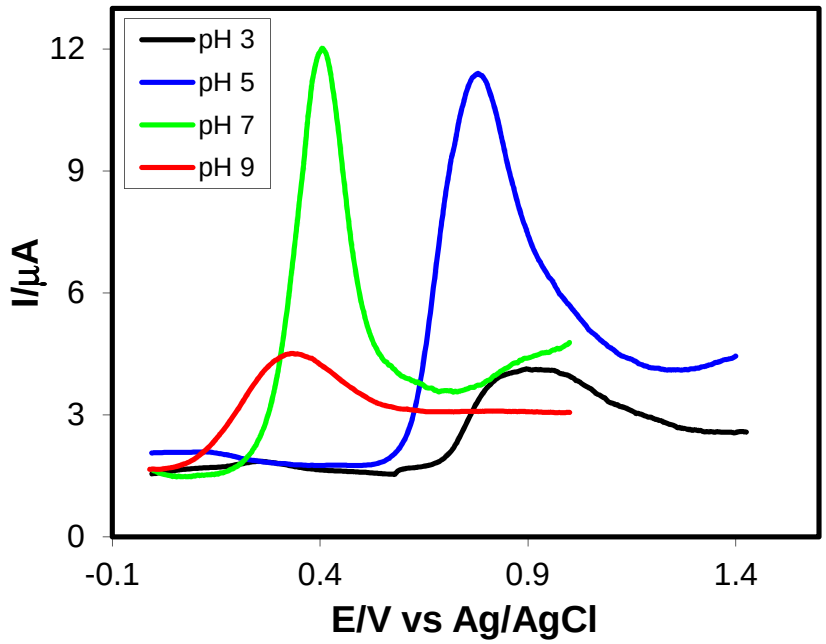

Fig. 4.31: Comparison of Differential pulse voltammogram of different pH (3, 5, 7 & 9) of 2mM Resorcinol of GC electrode at scan rate 0.1V/s (1st cycle)

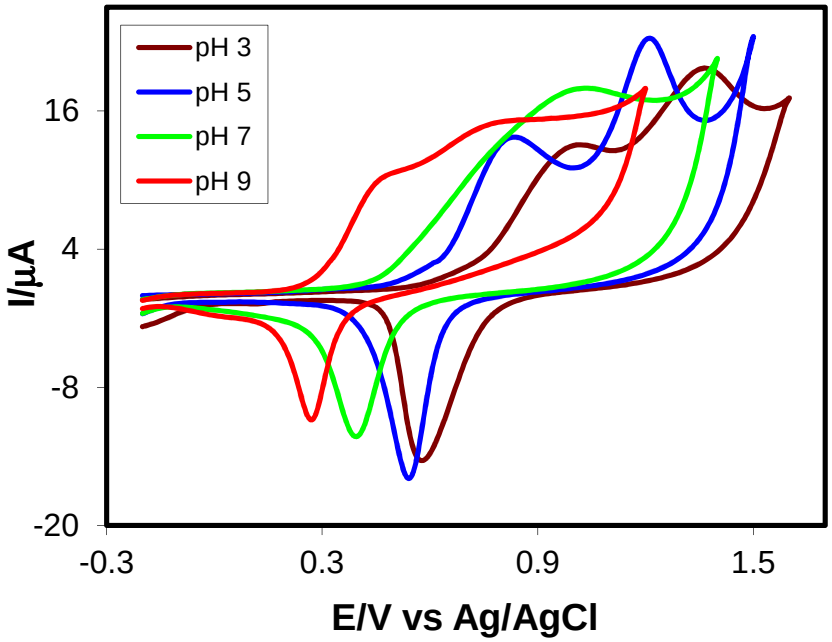

Fig. 4.32: Comparison of Cyclic voltammogram of different pH (3, 5, 7 & 9) of 2mM Resorcinol of Au electrode at scan rate 0.1V/s (1st cycle)

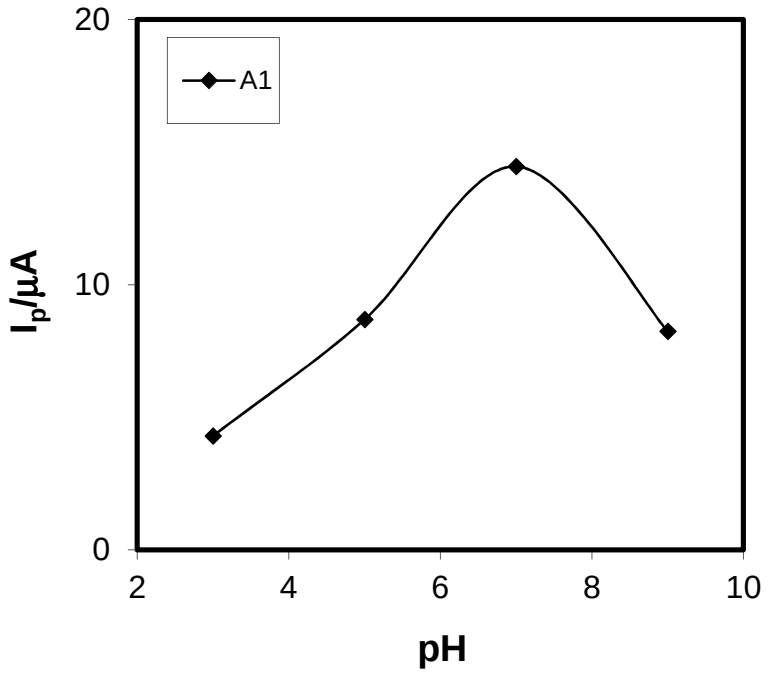

Fig. 4.33: Plots of peak current (I_p) versus pH of 2mM Resorcinol of Au electrode at scan rate 0.1V/s (1st cycle)

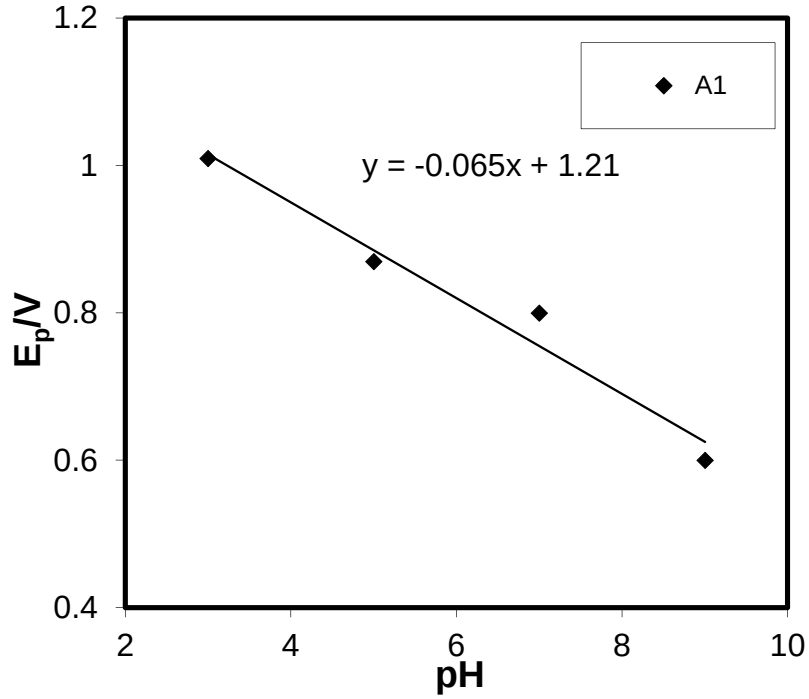

Fig. 4.34: Plots of peak potential (E_p) versus pH of 2mM Resorcinol of Au electrode and scan rate 0.1V/s (1st cycle)

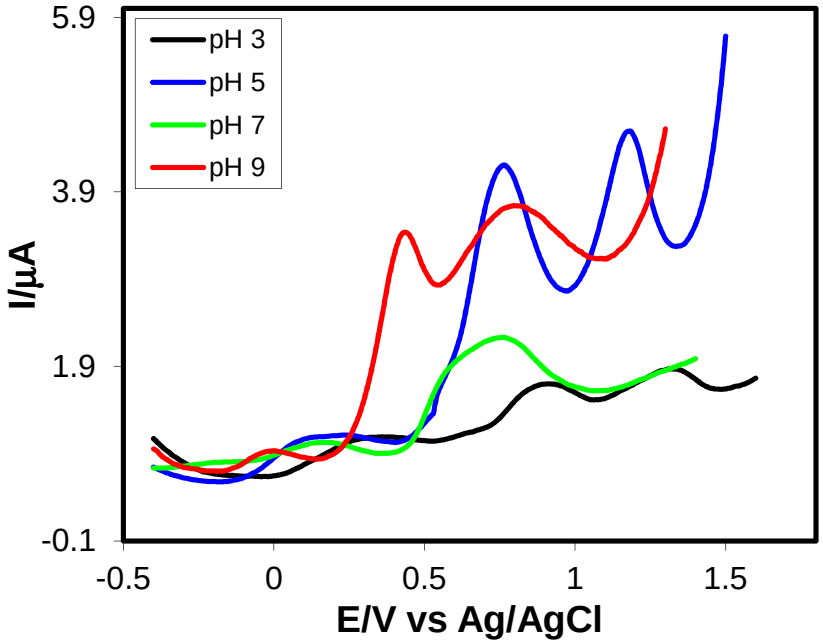

Fig. 4.35: Comparison of Differential pulse voltammogram of different pH (3, 5, 7 & 9) of 2mM Resorcinol of Au electrode at scan rate 0.1V/s (1st cycle)

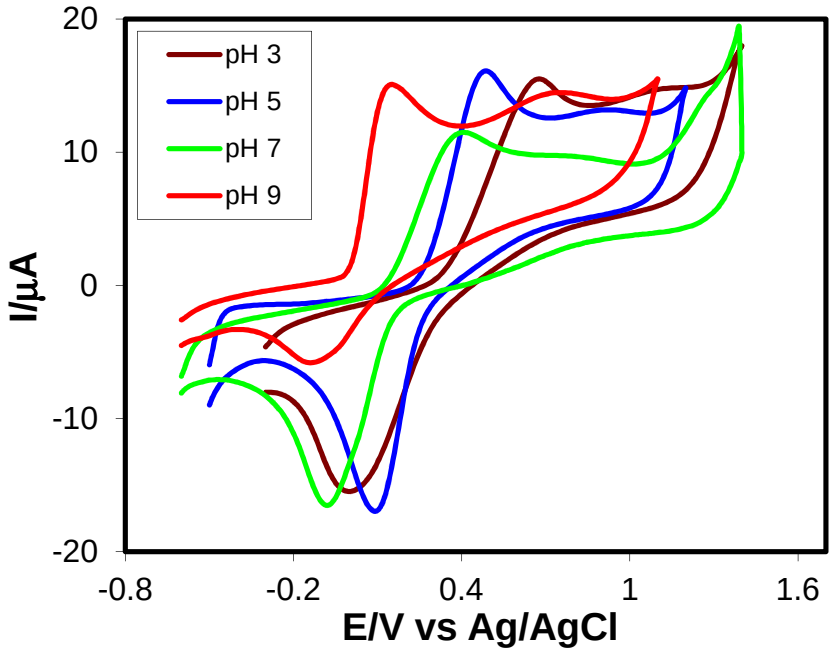

Fig. 4.36: Comparison of Cyclic voltammogram of different pH (3, 5, 7 & 9) of 2mM Resorcinol of Pt electrode at scan rate 0.1V/s (1st cycle)

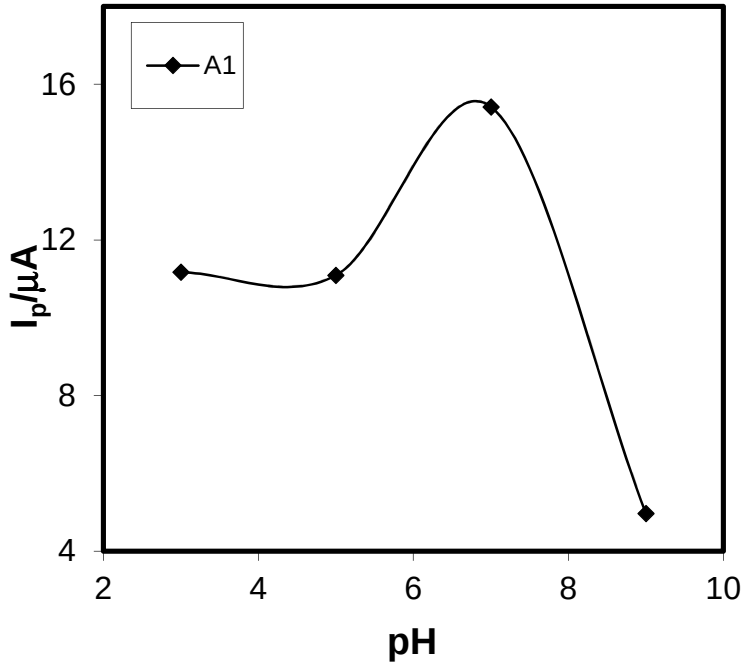

Fig. 4.37: Plots of peak current (I_p) versus pH of 2mM Resorcinol of Pt electrode at scan rate 0.1V/s (1st cycle)

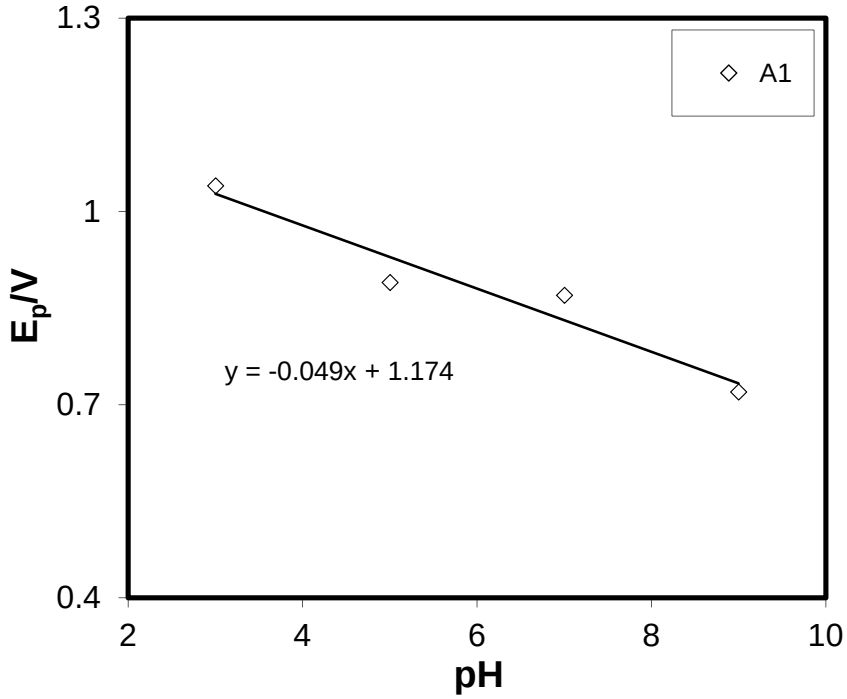

Fig. 4.38: Plots of peak potential (E_p) versus pH of 2mM Resorcinol of Pt electrode at scan rate 0.1V/s (1st cycle)

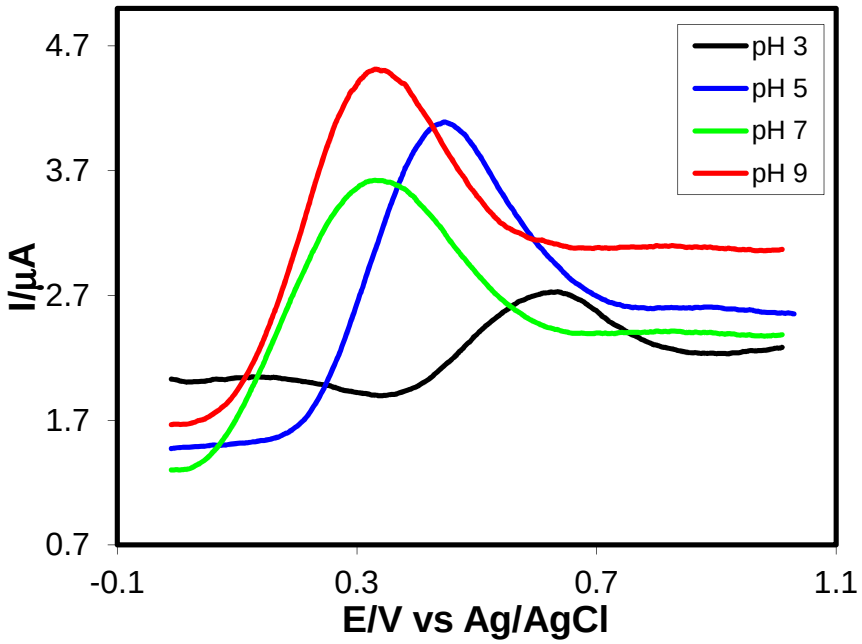

Fig. 4.39: Comparison of Differential pulse voltammogram of different pH (3, 5, 7 & 9) of 2mM Resorcinol of Pt electrode at scan rate 0.1V/s (1st cycle)

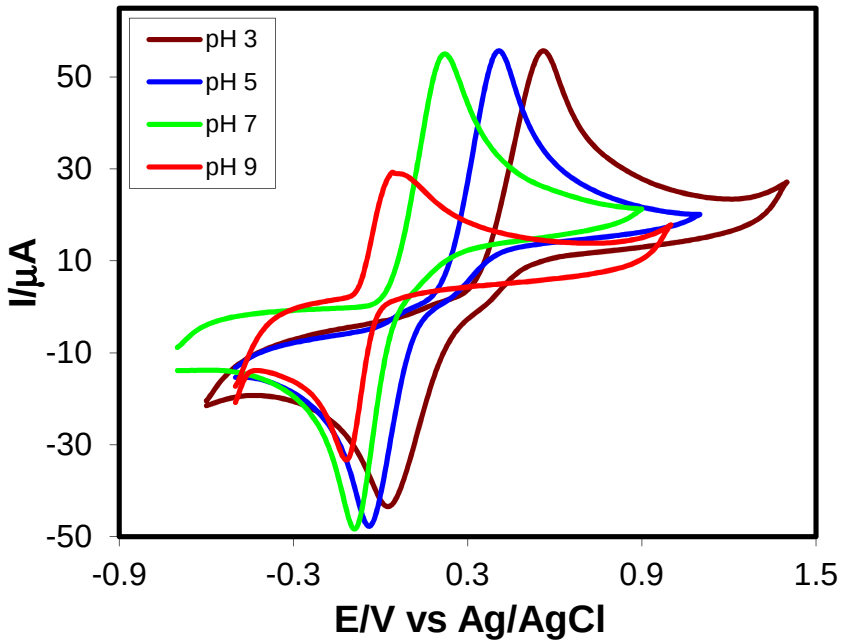

Fig. 4.40: Comparison of Cyclic voltammogram of different pH (3, 5, 7 & 9) of 2mM Hydroquinone of GC electrode at scan rate 0.1V/s (1st cycle)

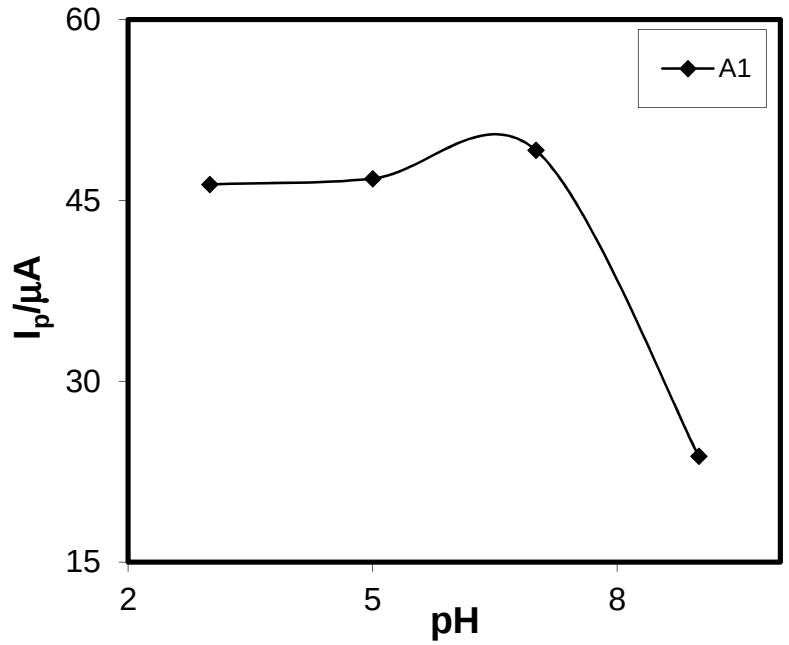

Fig 4.41: Plots of peak current (I_p) versus pH of 2mM Hydroquinone of GC electrode at scan rate 0.1V/s (1st cycle)

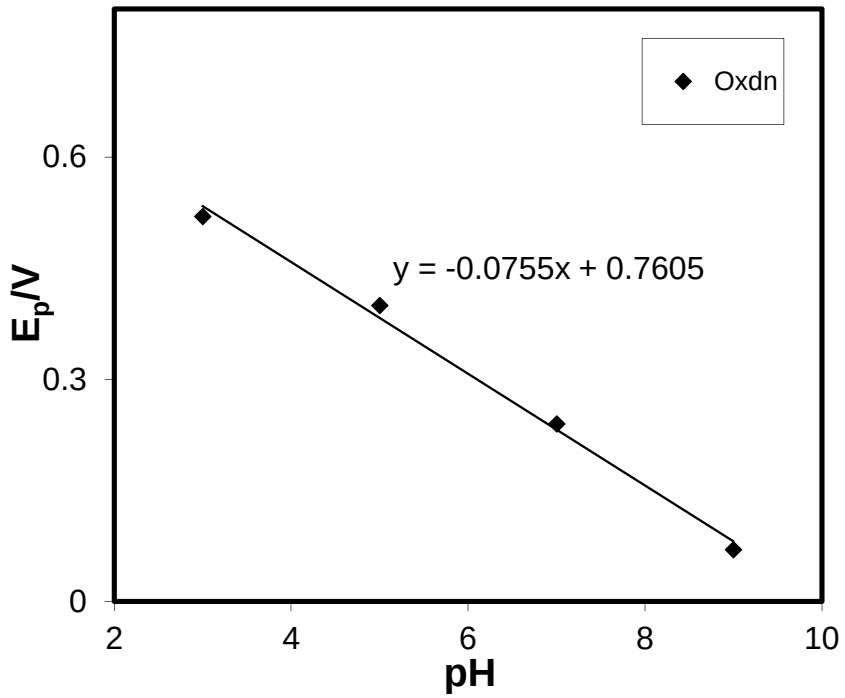

Fig. 4.42: Plots of peak potential (E_p) versus pH of 2mM Hydroquinone of GC electrode and scan rate 0.1V/s (1st cycle)

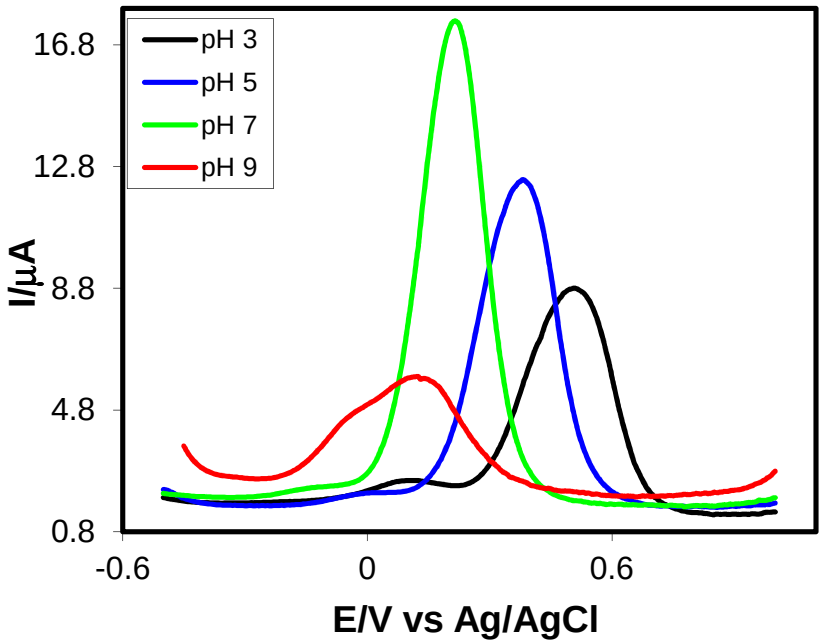

Fig. 4.43: Comparison of Differential pulse voltammogram of different pH (3, 5, 7 & 9) of 2mM Hydroquinone of GC electrode at scan rate 0.1V/s (1st cycle)

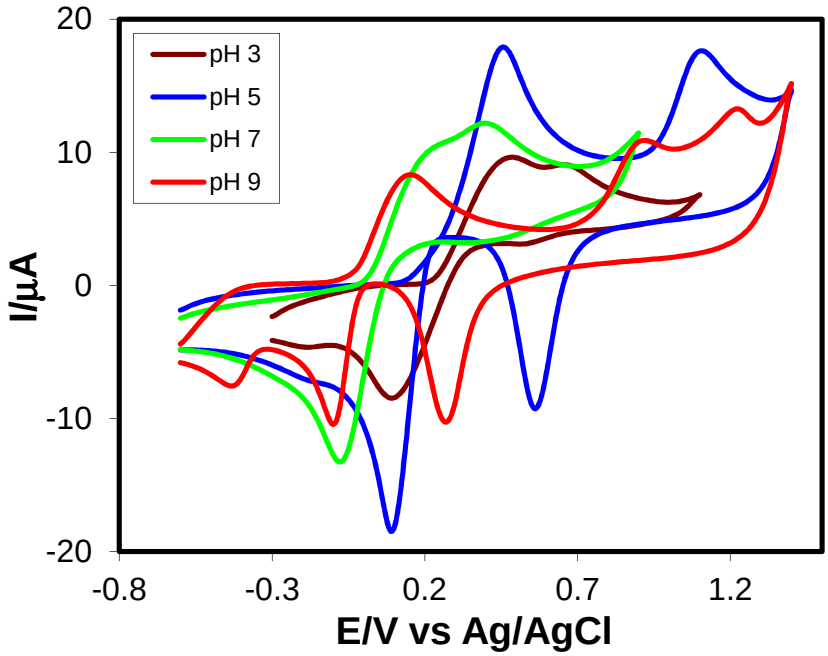

Fig. 4.44: Comparison of Cyclic voltammogram of different pH (3, 5, 7 & 9) of 2mM Hydroquinone of Au electrode at scan rate 0.1V/s (1st cycle)

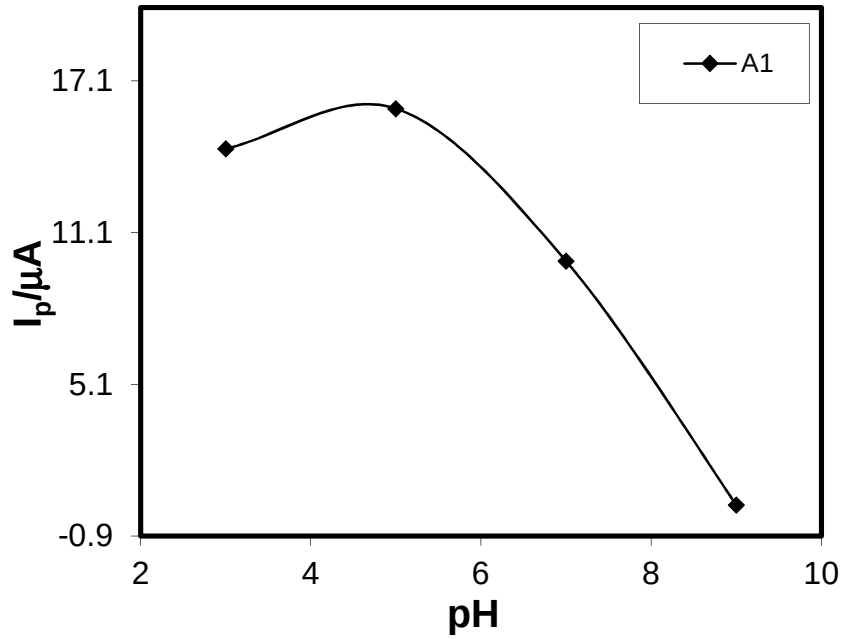

Fig. 4.45: Plots of peak current (I_p) versus pH of 2mM Hydroquinone of Au electrode at scan rate 0.1V/s (1st cycle)

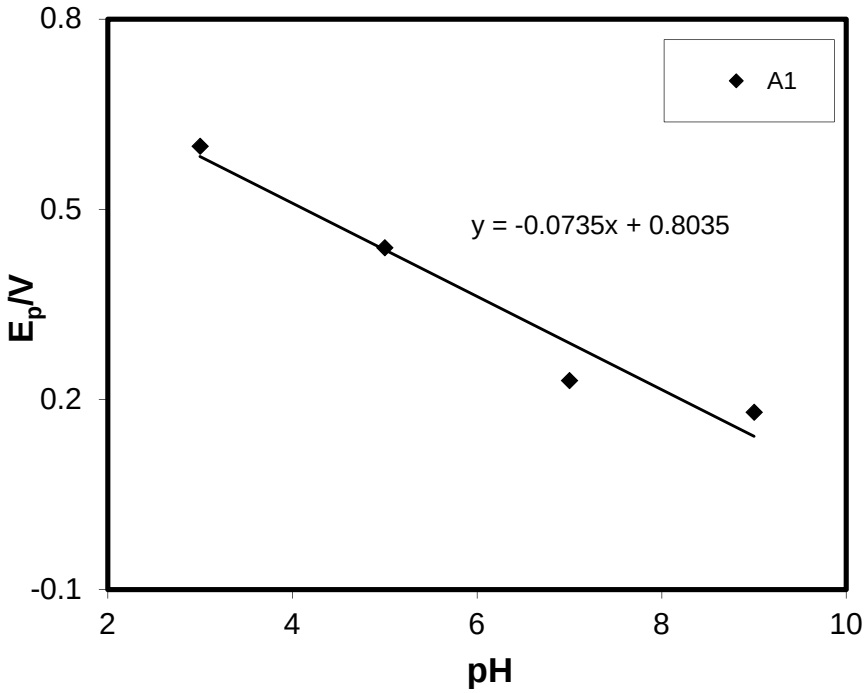

Fig. 4.46: Plots of peak potential (E_p) versus pH of 2mM Hydroquinone of Au electrode at scan rate 0.1V/s (1st cycle)

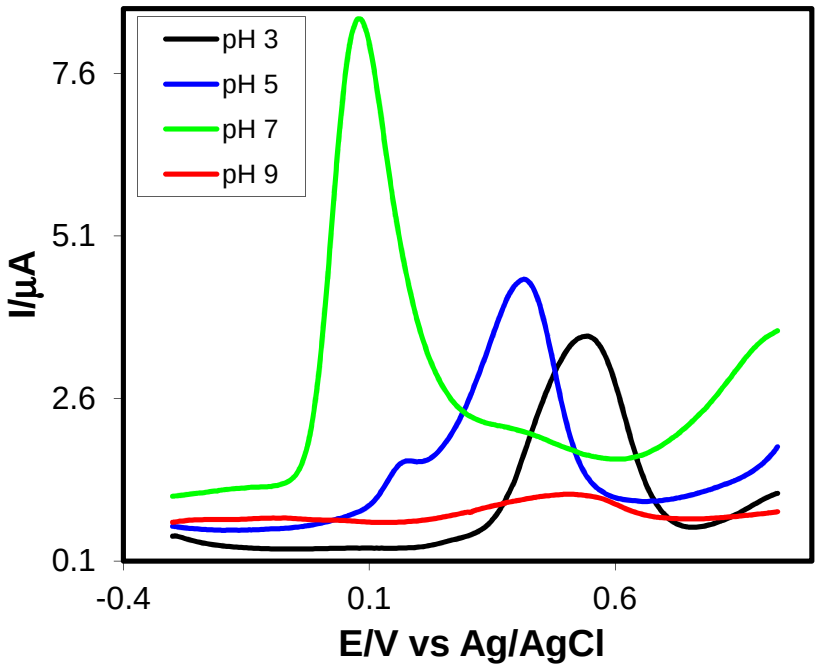

Fig. 4.47: Comparison of Differential pulse voltammogram of different pH (3, 5, 7 & 9) of 2mM Hydroquinone of Au electrode at scan rate 0.1V/s (1st cycle)

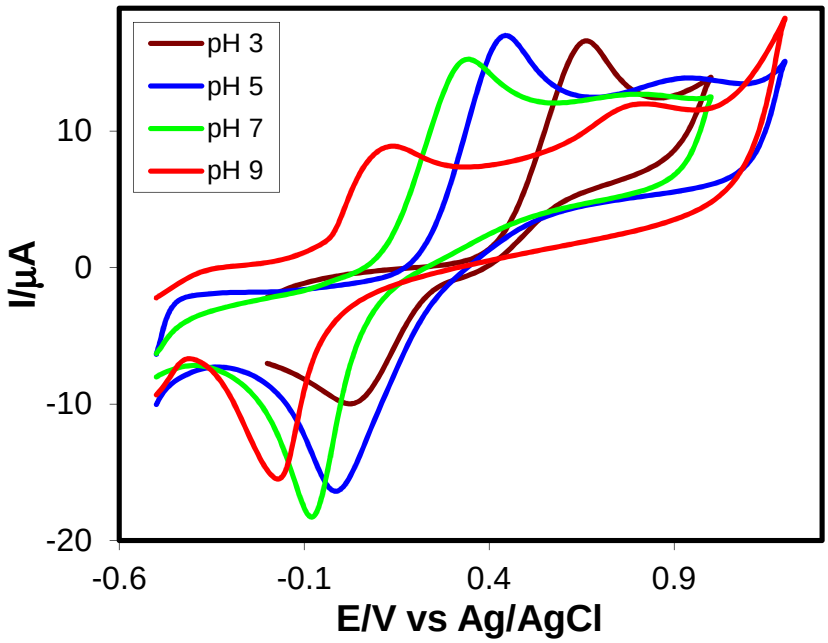

Fig. 4.48: Comparison of Cyclic voltammogram of different pH (3, 5, 7 & 9) of 2mM Hydroquinone of Pt electrode at scan rate 0.1V/s (1st cycle)

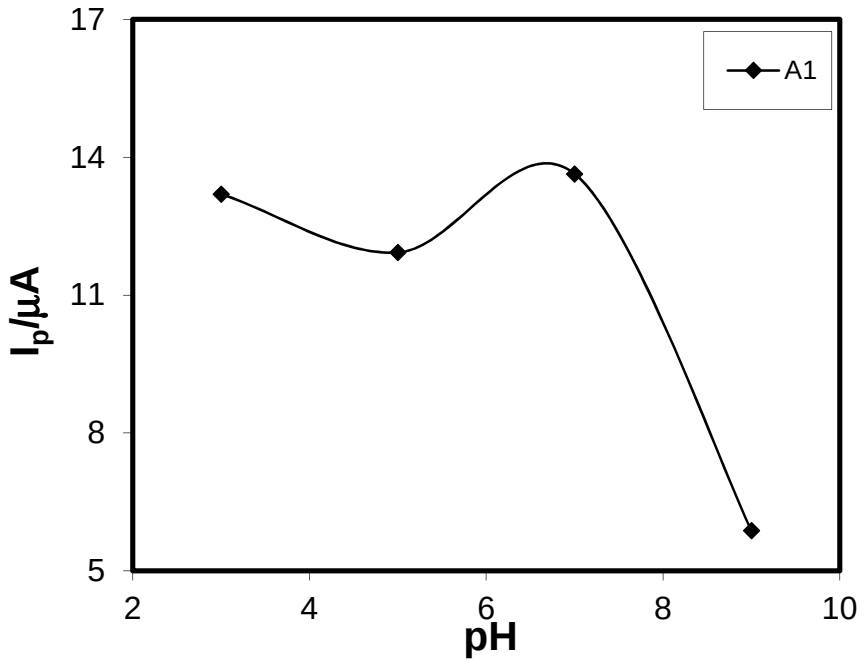

Fig. 4.49: Plots of peak current (I_p) versus pH of 2mM Hydroquinone of Pt electrode at scan rate 0.1V/s (1st cycle)

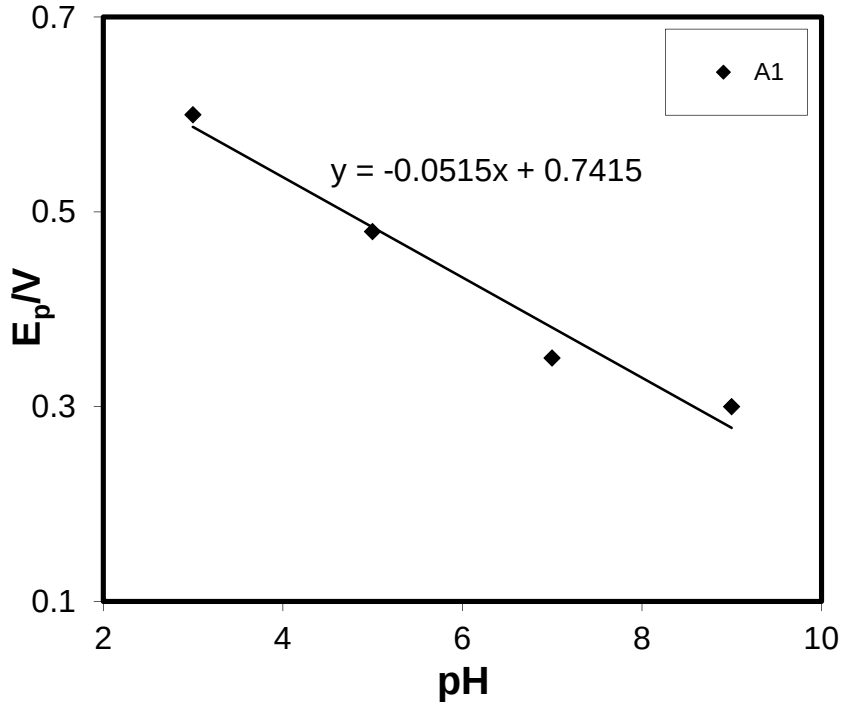

Fig. 4.50: Plots of peak potential (E_p) versus pH of 2mM Hydroquinone of Pt electrode at scan rate 0.1V/s

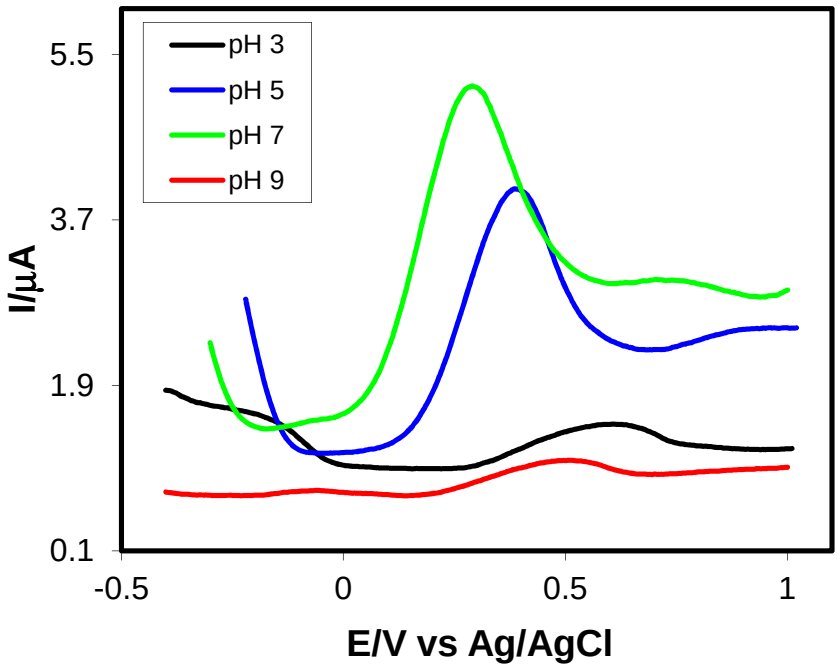

Fig. 4.51: Comparison of Differential pulse voltammogram of different pH (3, 5, 7 & 9) of 2mM Hydroquinone of Pt electrode at scan rate 0.1V/s (1st cycle)

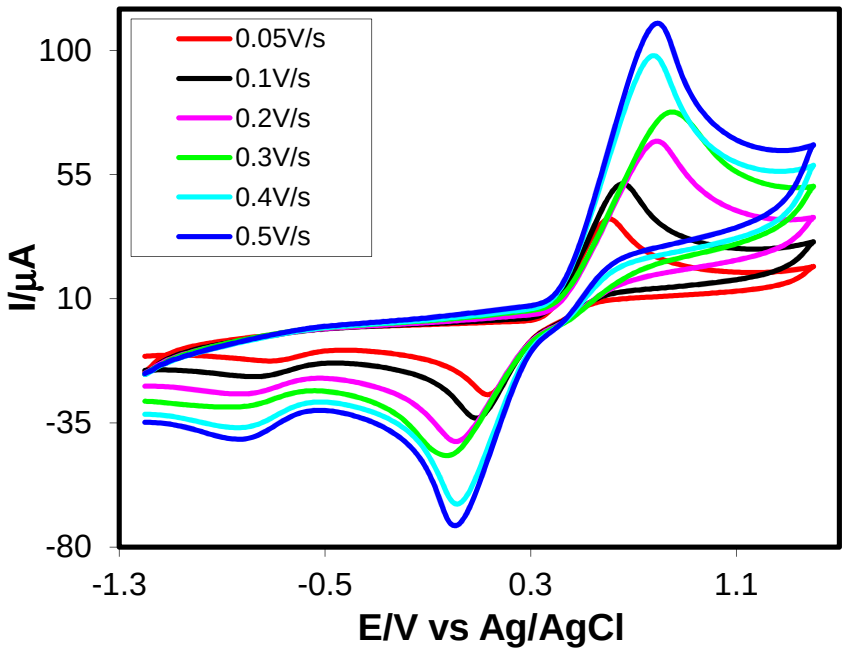

Fig. 4.52: Cyclic voltammogram of 2mM Catechol in buffer solution (pH 3) of GC electrode at different scan rate (1st cycle)

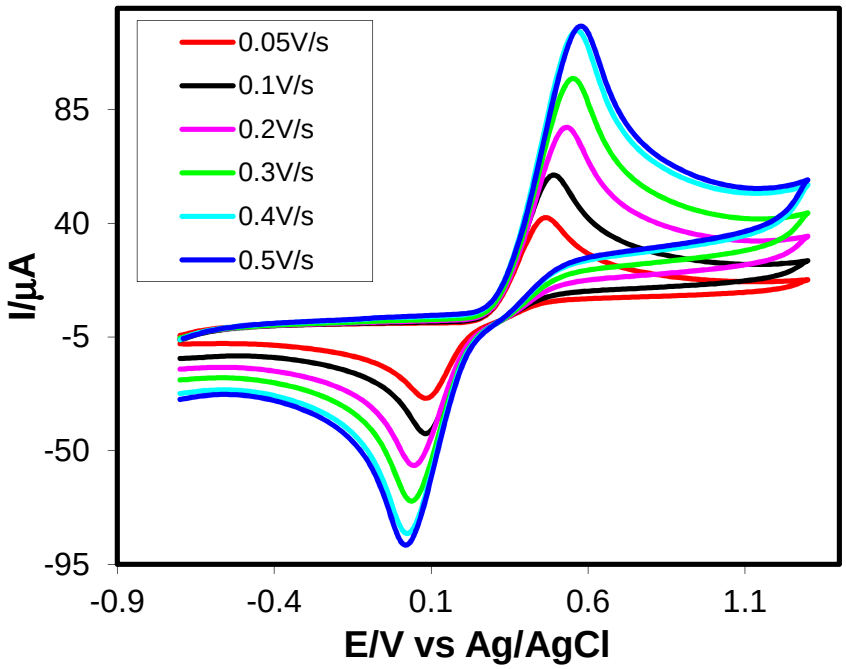

Fig. 4.53: Cyclic voltammogram of 2mM Catechol in buffer solution (pH 5) of GC electrode at different scan rate (1st cycle)

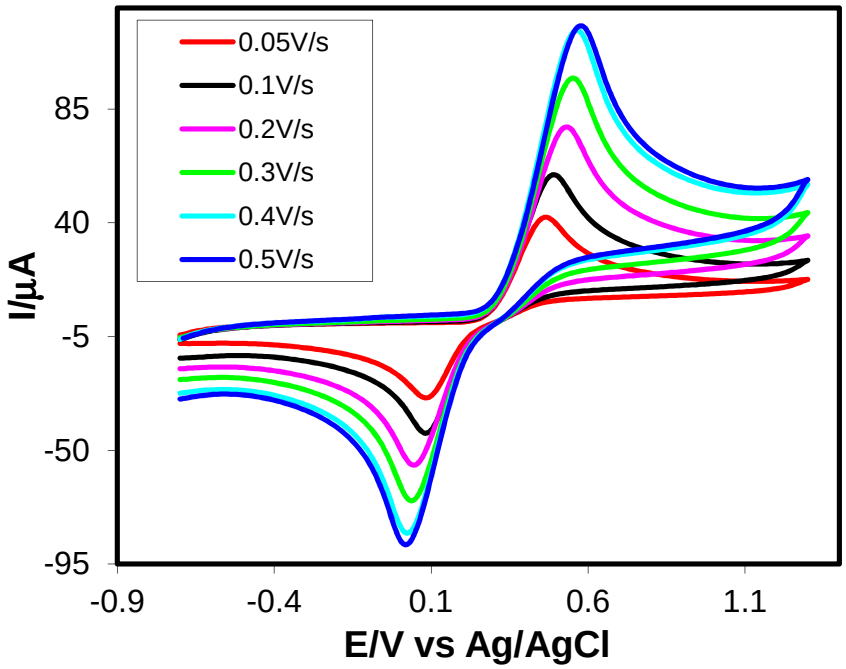

Fig. 4.54: Cyclic voltammogram of 2mM Catechol in buffer solution (pH 7) of GC electrode at different scan rate (1st cycle)

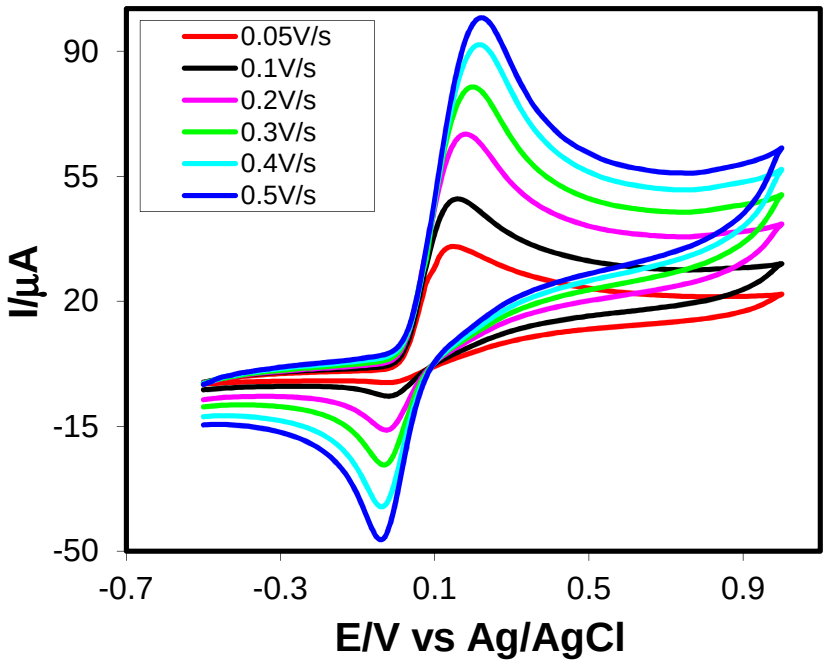

Fig. 4.55: Cyclic voltammogram of 2mM Catechol in buffer solution (pH 9) of Gc electrode at different scan rate (1st cycle)

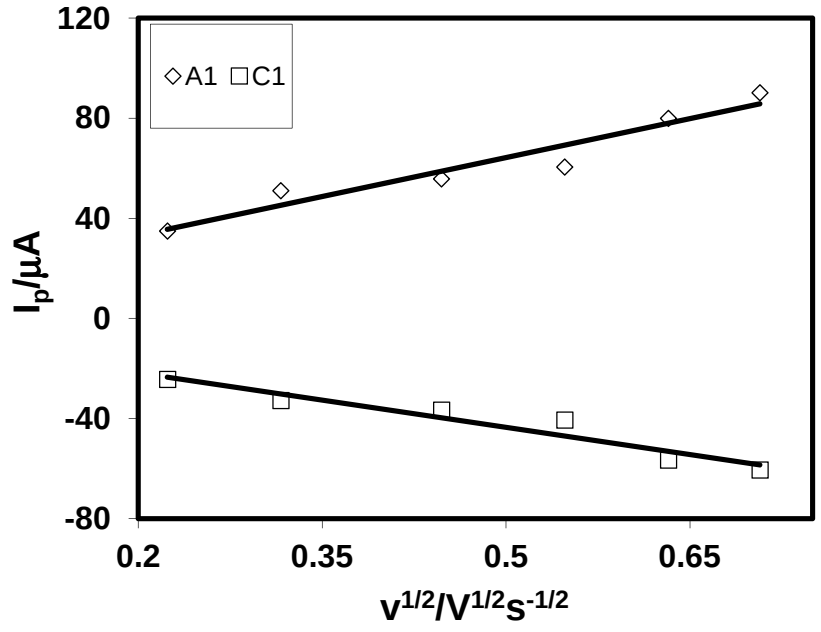

Fig. 4.56: Plots of peak current (I_p) versus square root of scan rate ($v^{1/2}$) of 2mM Catechol in buffer solution (pH 3) of GC electrode (1st cycle)

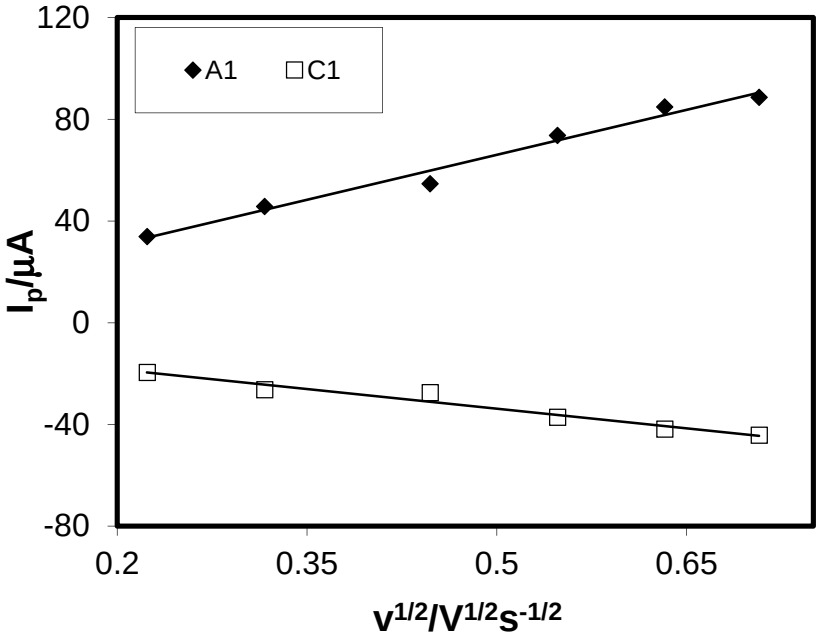

Fig. 4.57: Plots of peak current (I_p) versus square root of scan rate ($v^{1/2}$) of 2mM Catechol in buffer solution (pH 5) of GC electrode (1st cycle)

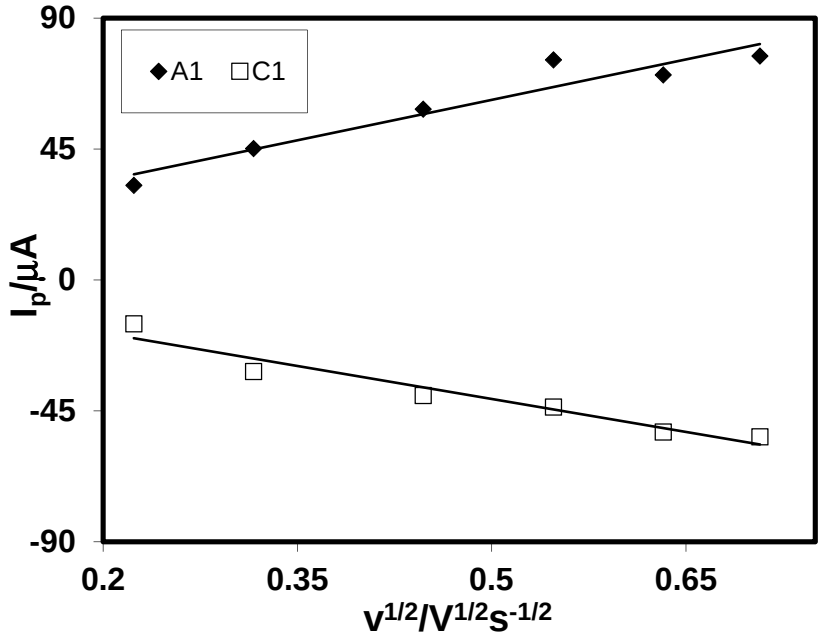

Fig. 4.58: Plots of peak current (I_p) versus square root of scan rate of 2mM Catechol in buffer solution (pH 7) of GC electrode (1st cycle)

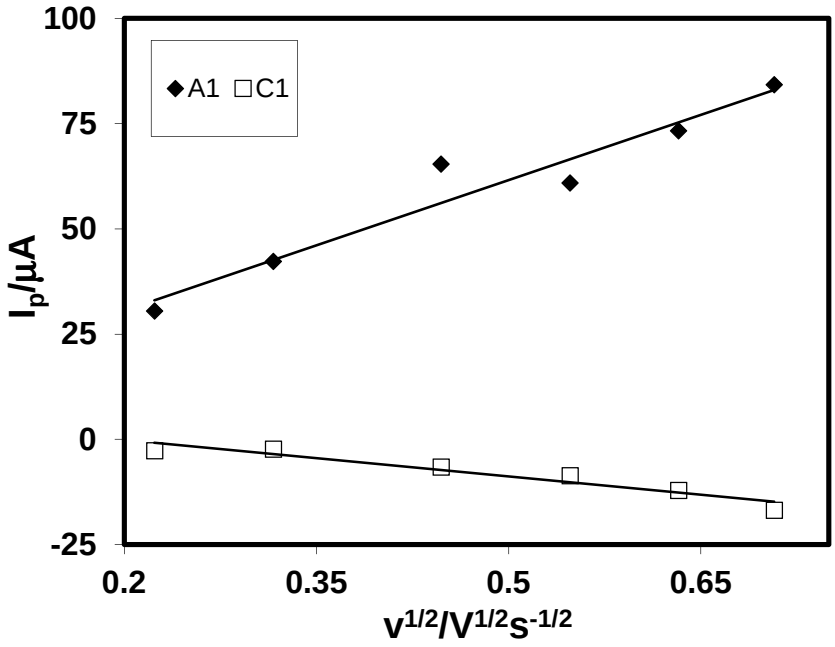

Fig. 4.59: Plots of peak current (I_p) versus Square root of scan rate of 2mM Catechol in buffer solution (pH 9) of GC electrode (1st cycle)

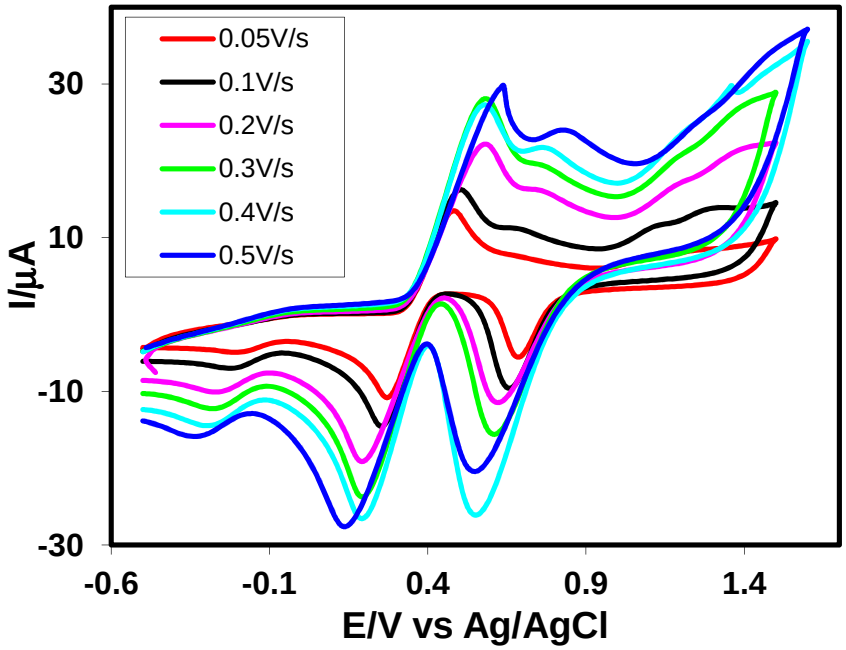

Fig. 4.60: Cyclic voltammogram of 2mM Catechol in buffer solution (pH 3) of Au electrode at different scan rate (1st cycle)

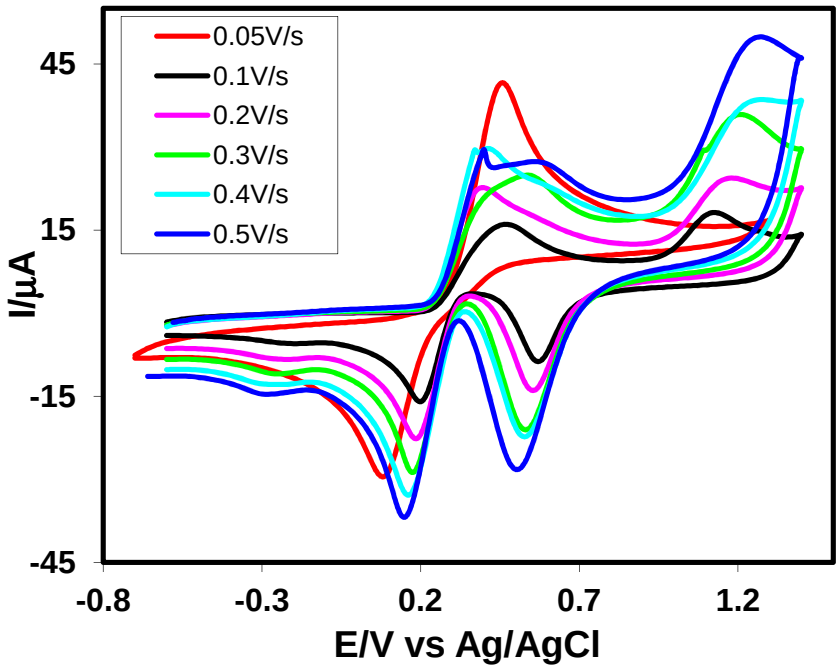

Fig. 4.61: Cyclic voltammogram of 2mM Catechol in buffer solution (pH 5) of Au electrode at different scan rate (1st cycle)

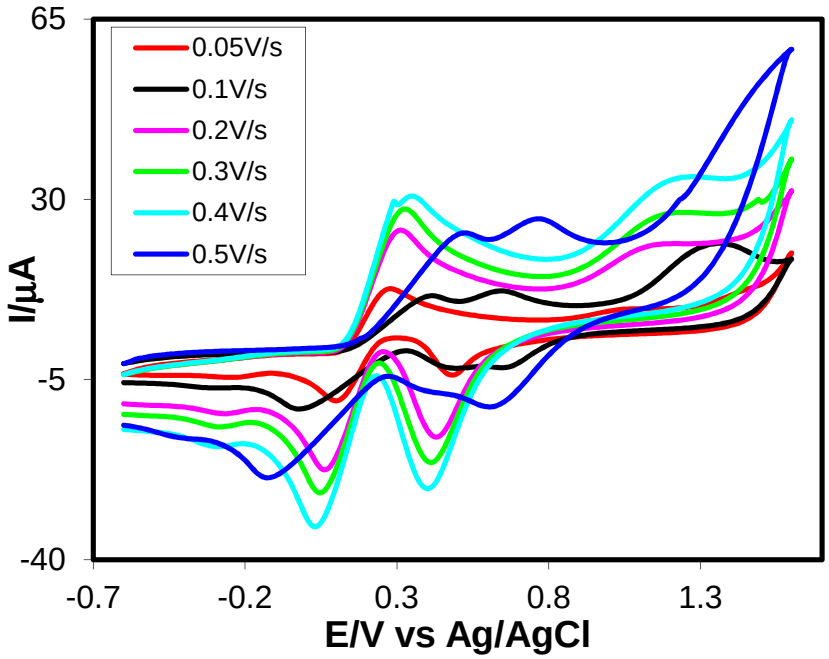

Fig. 4.62: Cyclic voltammogram of 2mM Catechol in buffer solution (pH 7) of Au electrode at different scan rate (1st cycle)

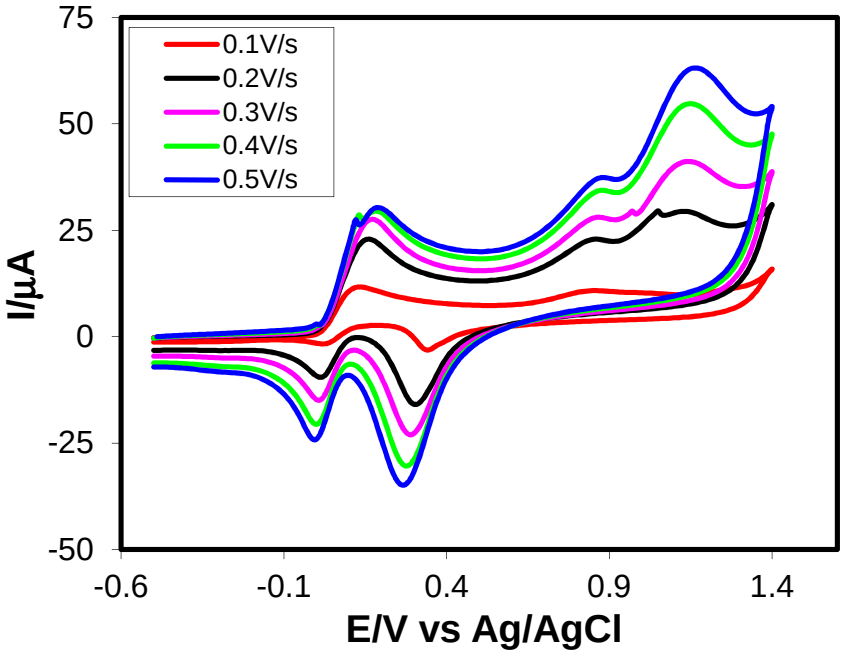

Fig. 4.63: Cyclic voltammogram of 2mM Catechol in buffer solution (pH 9) of Au electrode at different scan rate (1st cycle)

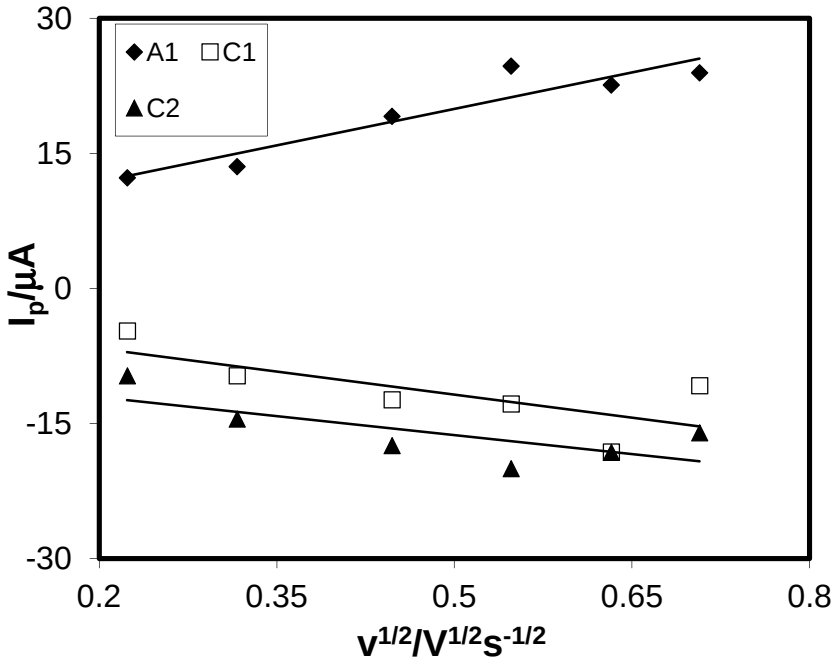

Fig. 4.64: Plots of peak current (I_p) versus square root of scan rate ($v^{1/2}$) of 2mM Catechol in buffer solution (pH 3) of Au electrode (1st cycle)

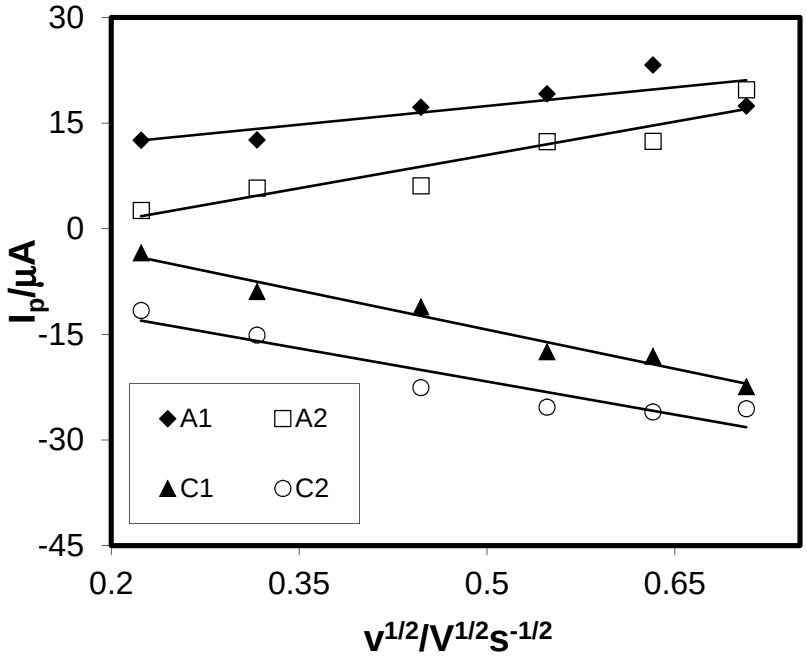

Fig. 4.65: Plots of peak current (I_p) versus square root of scan rate ($v^{1/2}$) of 2mM Catechol in buffer solution (pH 5) of Au electrode (1st cycle)

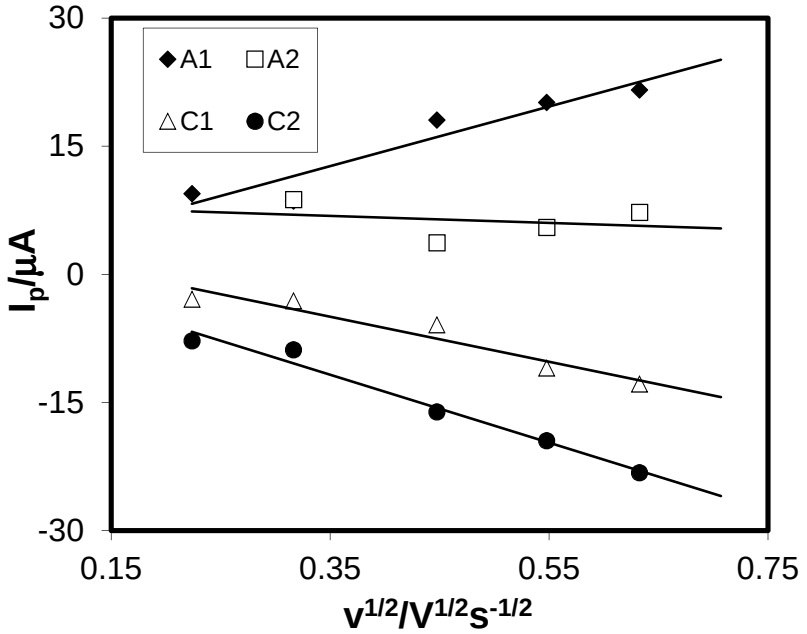

Fig. 4.66: Plots of peak current (I_p) versus square root of scan rate ($v^{1/2}$) of 2mM Catechol in buffer solution (pH 7) of Au electrode (1st cycle)

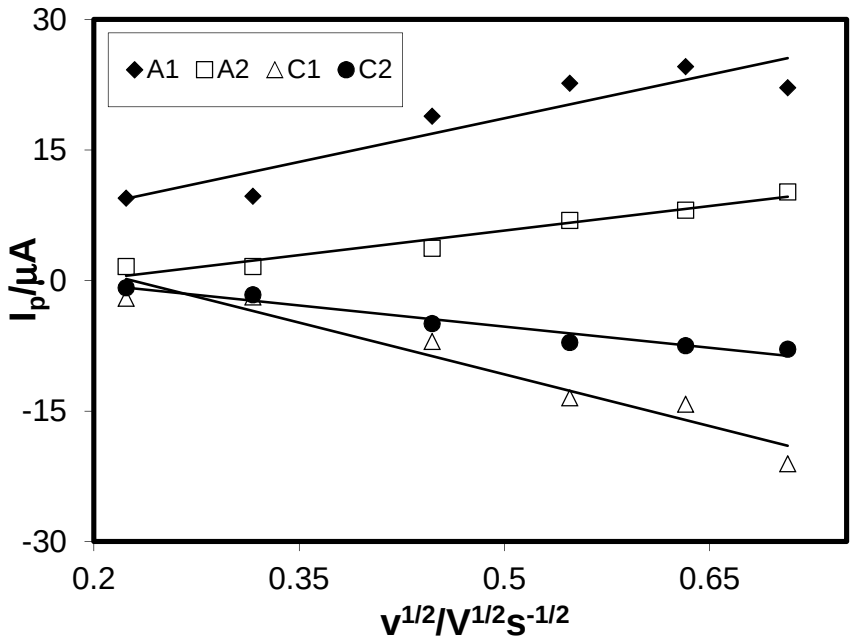

Fig. 4.67: Plots of peak current (I_p) versus square root of scan rate ($v^{1/2}$) of 2mM Catechol in buffer solution (pH 9) of Au electrode (1st cycle)

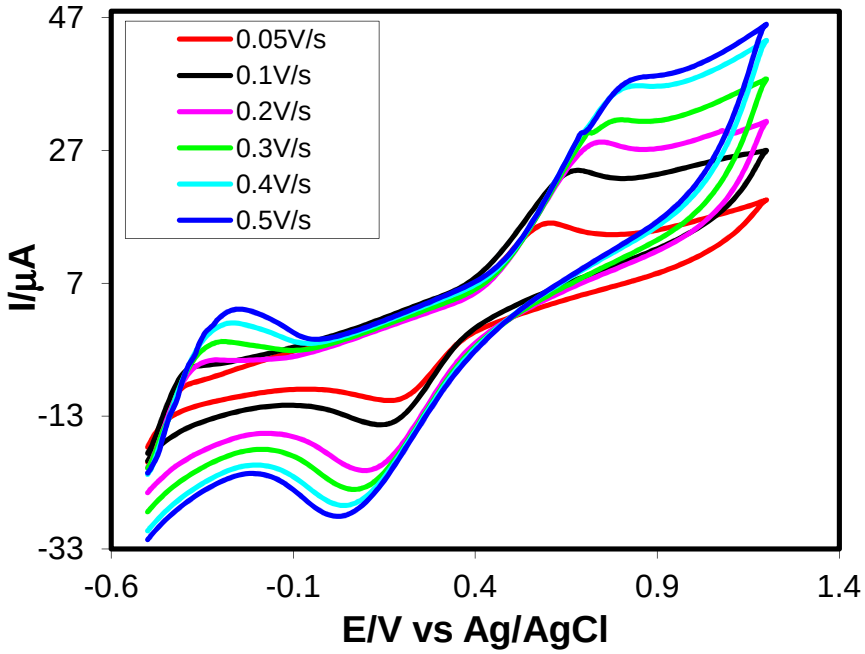

Fig. 4.68: Cyclic voltammogram of 2mM Catechol in buffer solution (pH 3) of Pt electrode at different scan rate (1st cycle)

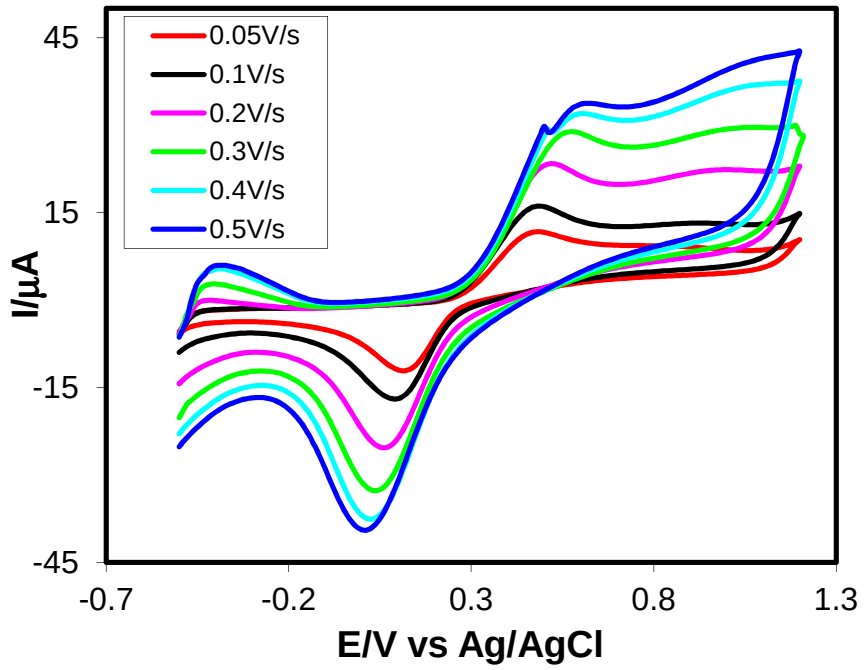

Fig. 4.69: Cyclic voltammogram of 2mM Catechol in buffer solution (pH 5) of Pt electrode at different scan rate (1st cycle)

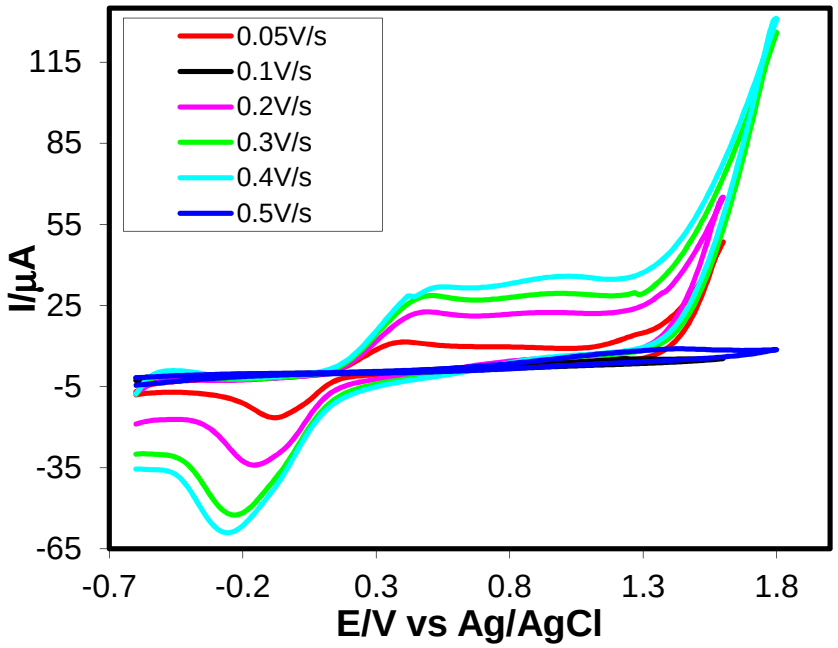

Fig. 4.70: Cyclic voltammogram of 2mM Catechol in buffer solution (pH 7) of Pt electrode at different scan rate (1st cycle)

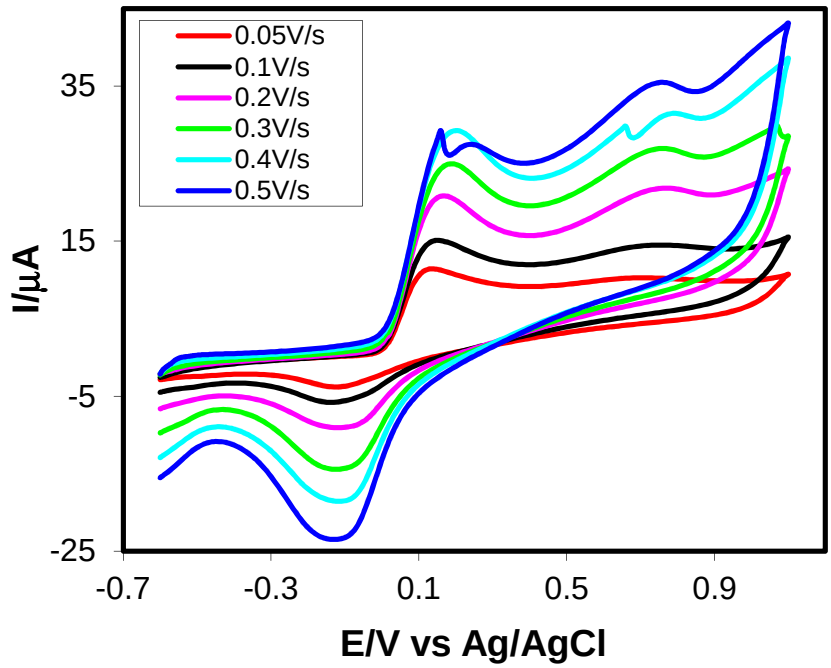

Fig. 4.71: Cyclic voltammogram of 2mM Catechol in buffer solution (pH 9) of Pt electrode at different scan rate (1st cycle)

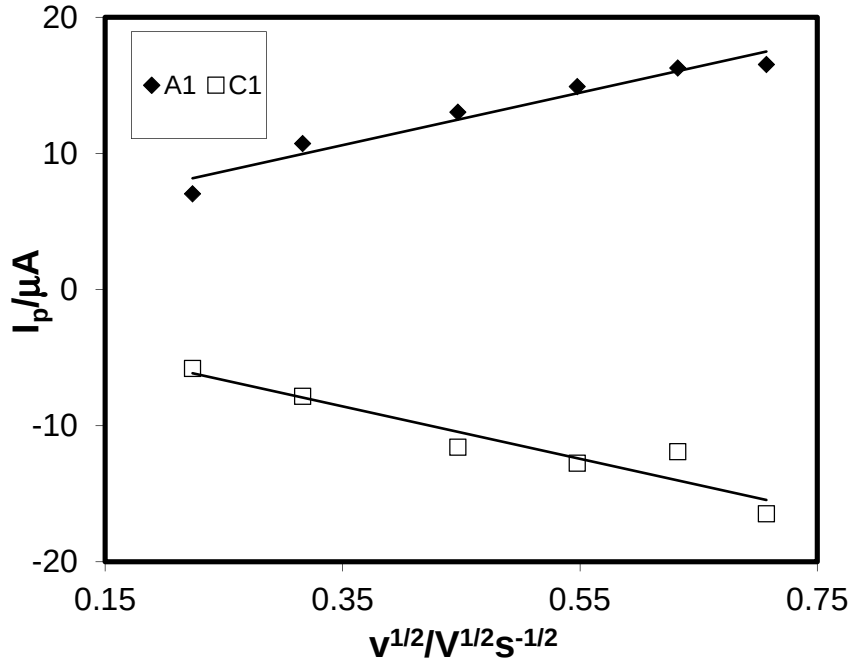

Fig. 4.72: Plots of peak current (I_p) versus square root of scan rate ($v^{1/2}$) of 2mM Catechol in buffer solution (pH 3) of Pt electrode (1st cycle)

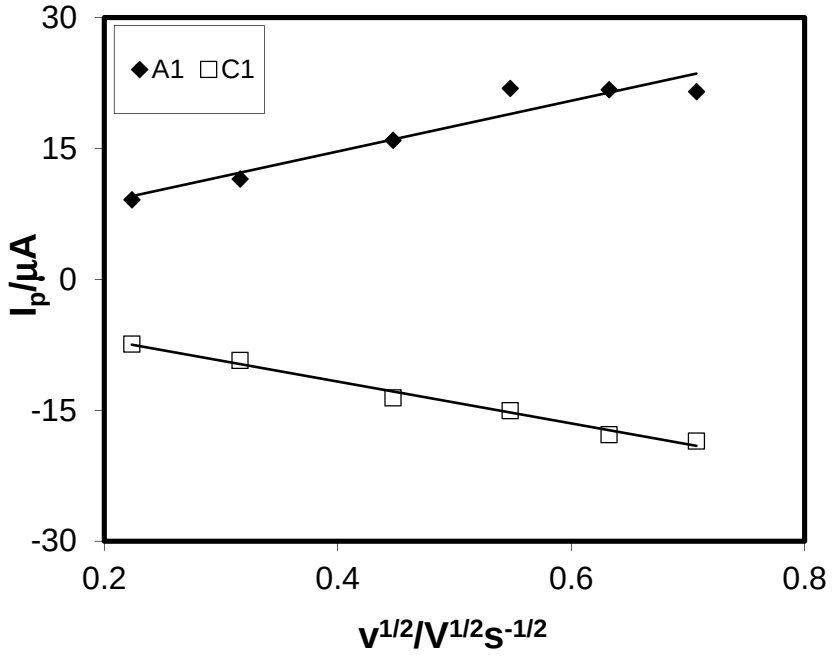

Fig. 4.73: Plots of peak current (I_p) versus square root of scan rate ($v^{1/2}$) of 2mM Catechol in buffer solution (pH 5) of Pt electrode (1st cycle)

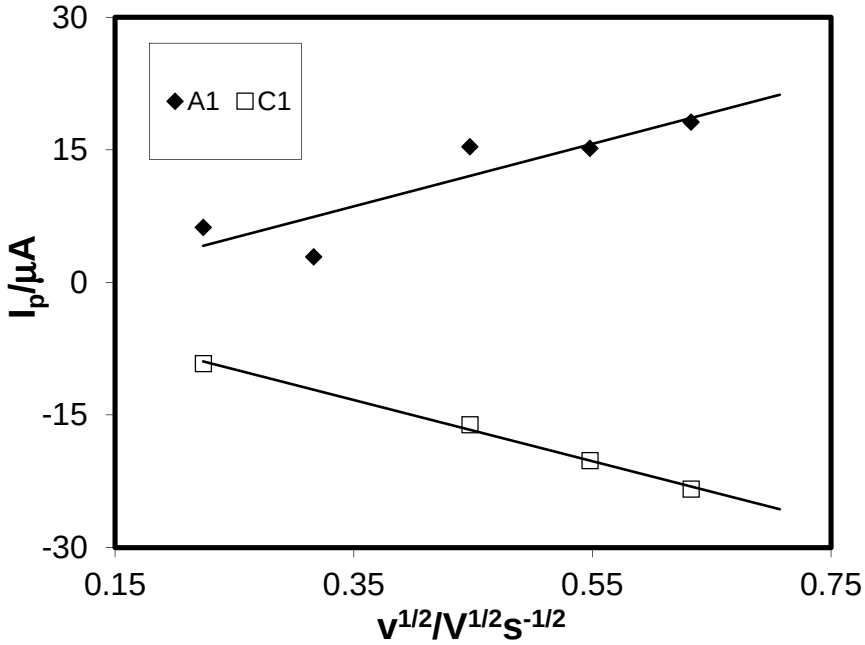

Fig. 4.74: Plots of peak current (I_p) versus square root of scan rate ($v^{1/2}$) of 2mM Catechol in buffer solution (pH 7) of Pt electrode (1st cycle)

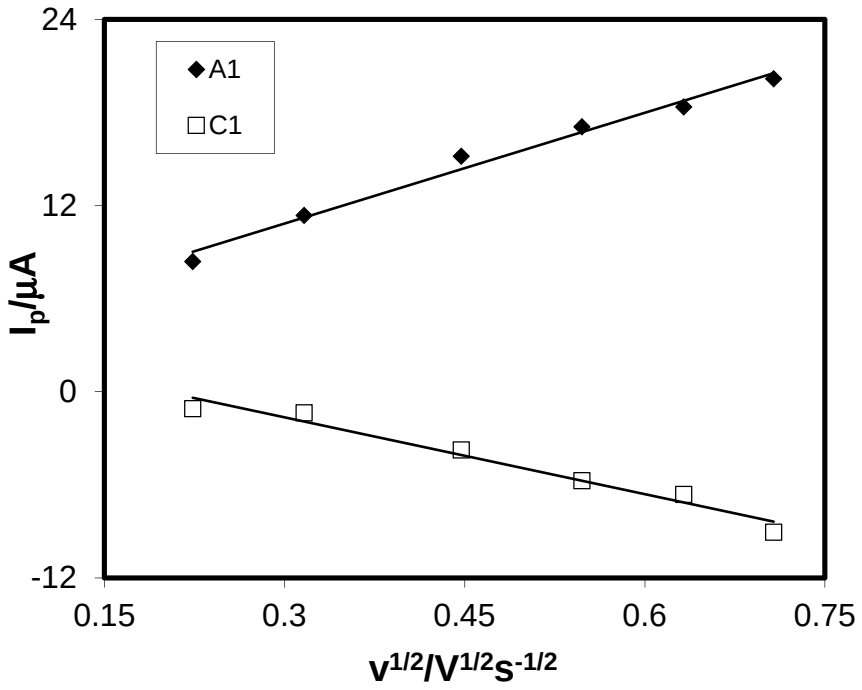

Fig. 4.75: Plots of peak current (I_p) versus square root of scan rate ($v^{1/2}$) of 2mM Catechol in buffer solution (pH 9) of Pt electrode (1st cycle)

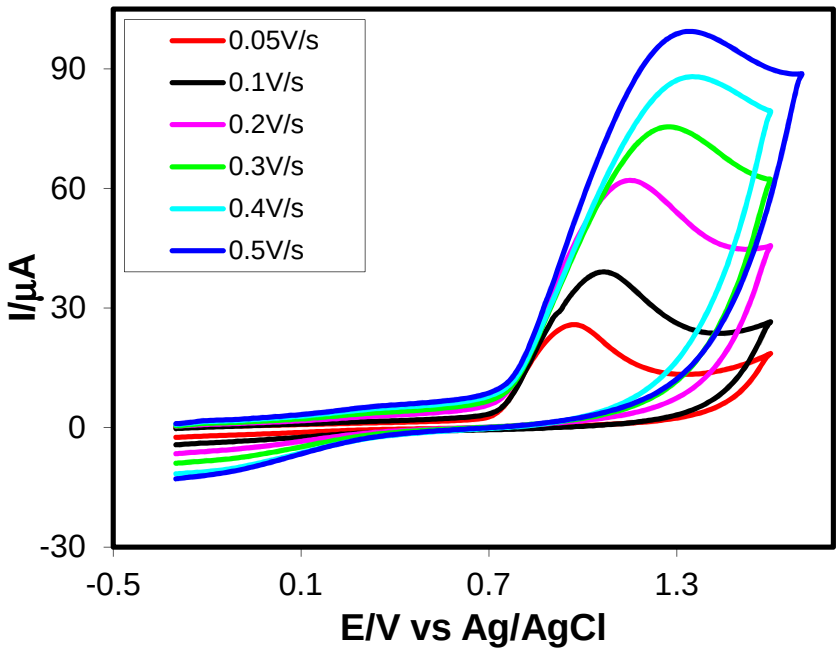

Fig. 4.76: Cyclic voltammogram of 2mM Resorcinol in buffer solution (pH 3) of GC electrode at different scan rate (1st cycle)

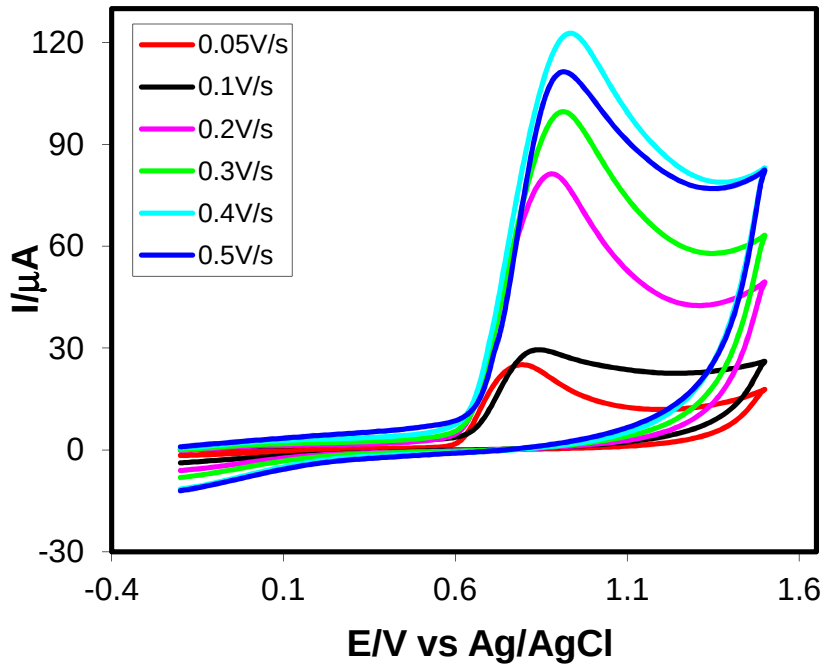

Fig. 4.77: Cyclic voltammogram of 2mM Resorcinol in buffer solution (pH 5) of GC electrode at different scan rate (1st cycle)

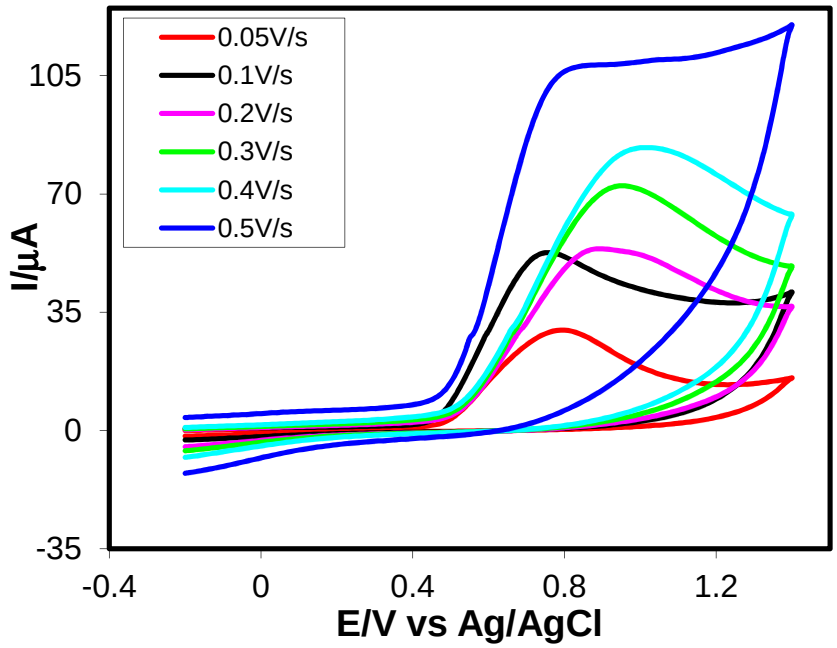

Fig. 4.78: Cyclic voltammogram of 2mM Resorcinol in buffer solution (pH 7) of GC electrode at different scan rate (1st cycle)

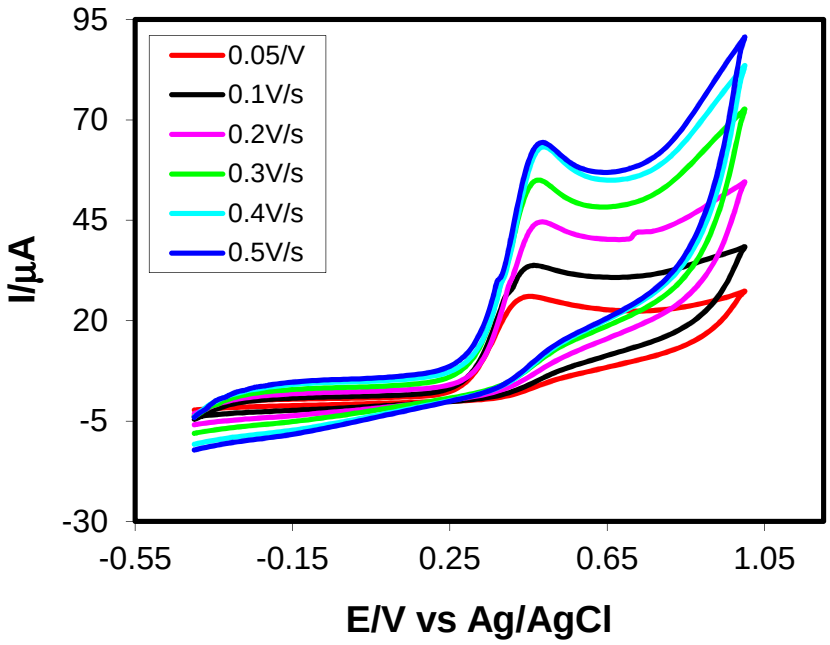

Fig. 4.79: Cyclic voltammogram of 2mM Resorcinol in buffer solution (pH 9) of GC electrode at different scan rate (1st cycle)

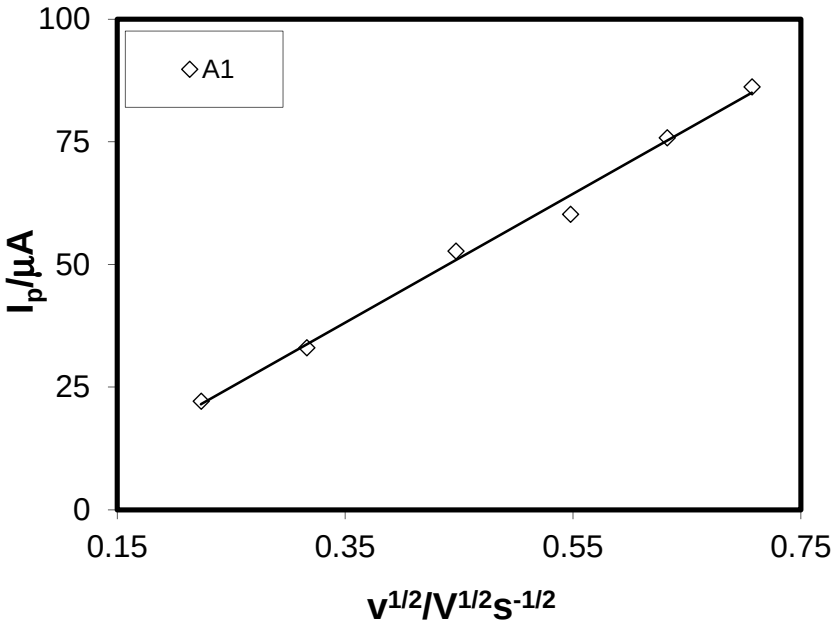

Fig. 4.80: Plots of peak current (I_p) versus square root of scan rate ($v^{1/2}$) of 2mM Resorcinol in buffer solution (pH 3) of GC electrode (1st cycle)

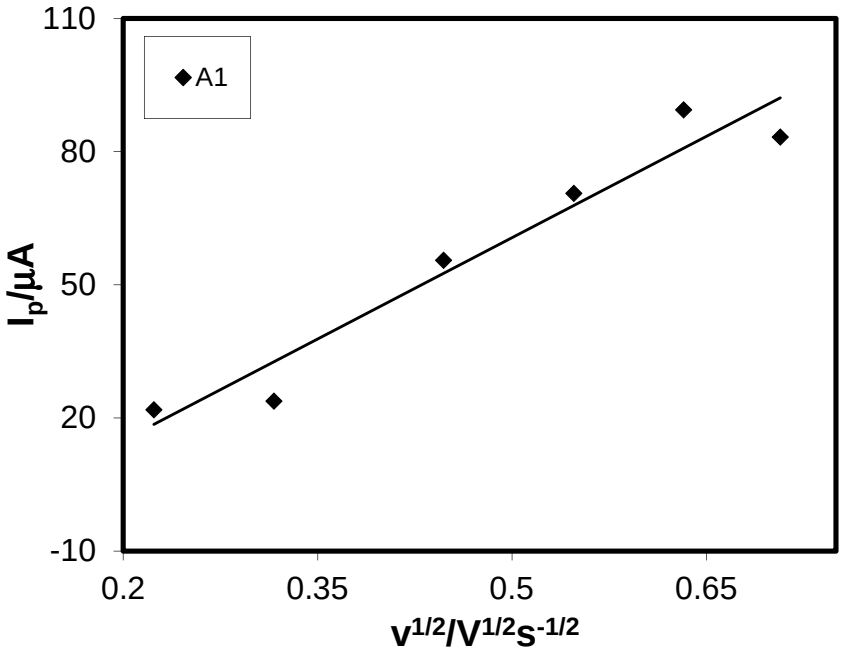

Fig. 4.81: Plots of peak current (I_p) versus square root of scan rate ($v^{1/2}$) of 2mM Resorcinol in buffer solution (pH 5) of GC electrode (1st cycle)

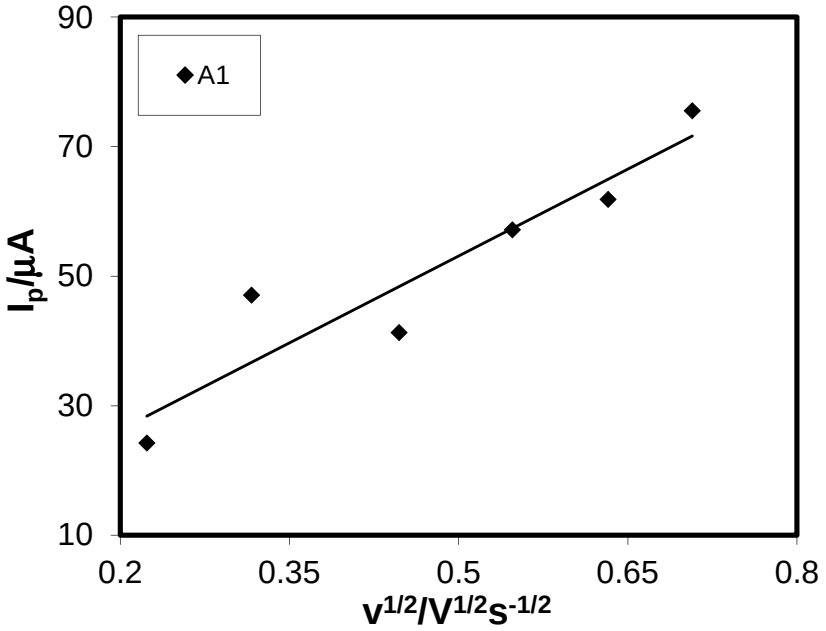

Fig. 4.82: Plots of peak current (I_p) versus square root of scan rate ($v^{1/2}$) of 2mM Resorcinol in buffer solution (pH 7) of GC electrode (1st cycle)

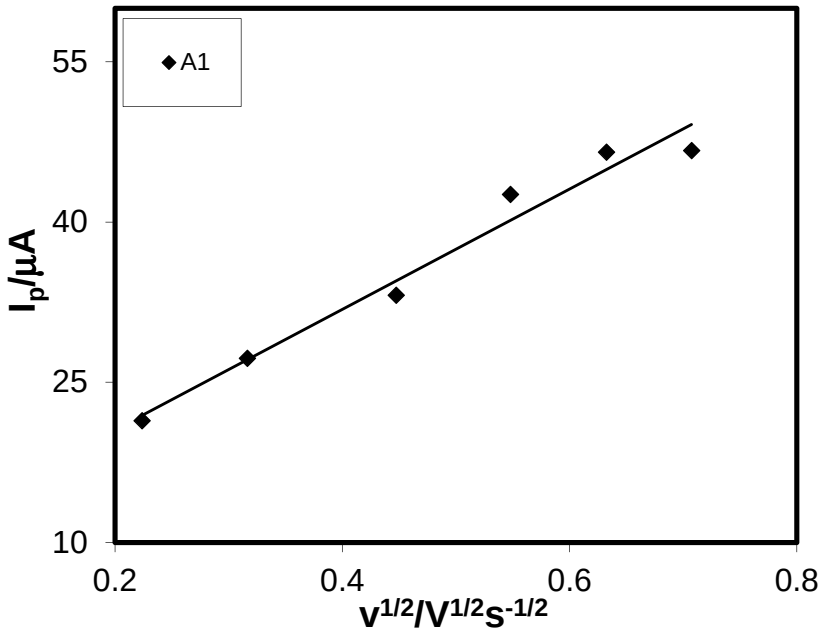

Fig. 4.83: Plots of peak current (I_p) versus square root of scan rate ($v^{1/2}$) of 2mM Resorcinol in buffer solution (pH 9) of GC electrode (1st cycle)

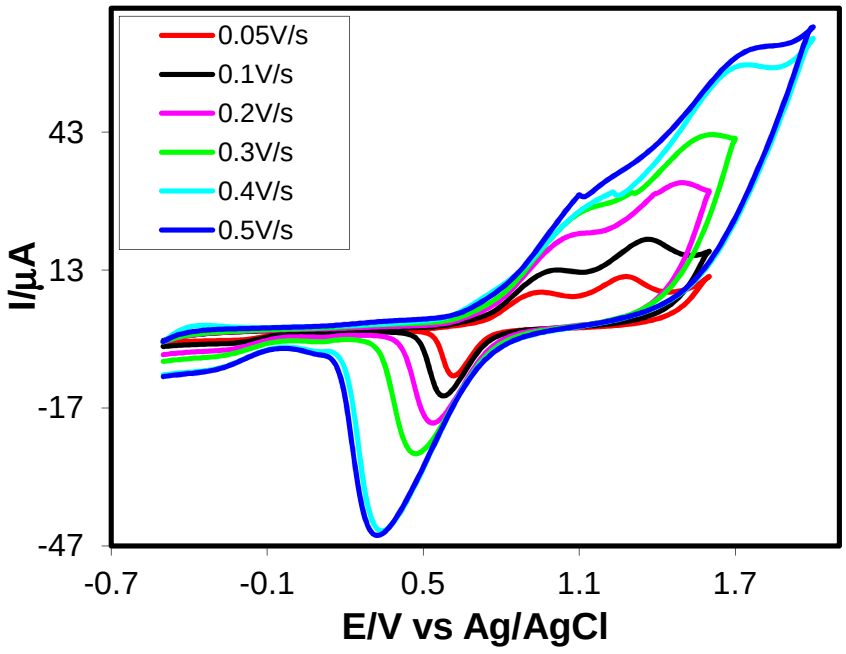

Fig. 4.84: Cyclic voltammogram of 2mM Resorcinol in buffer solution (pH 3) of Au electrode at different scan rate (1st cycle)

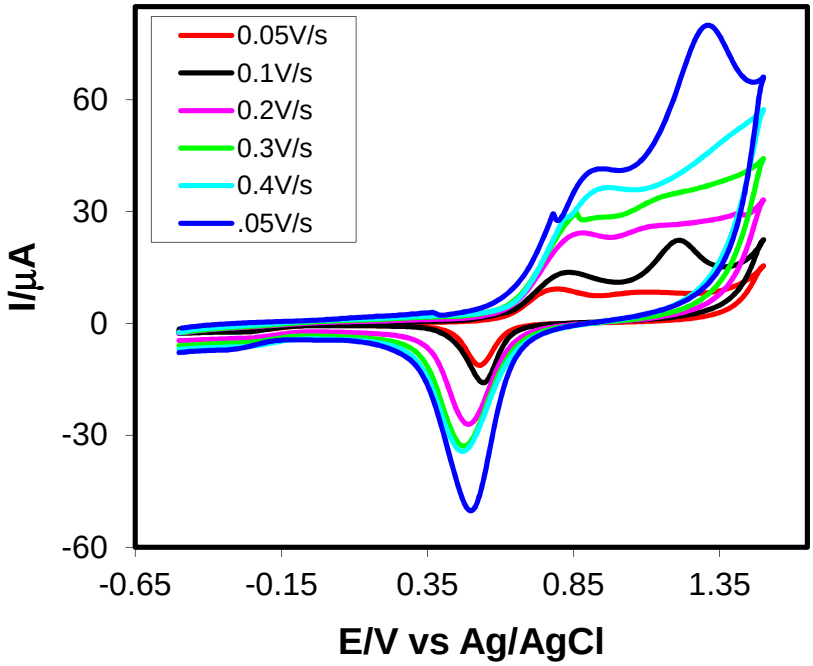

Fig. 4.85: Cyclic voltammogram of 2mM Resorcinol in buffer solution (pH 5) of Au electrode at different scan rate (1st cycle)

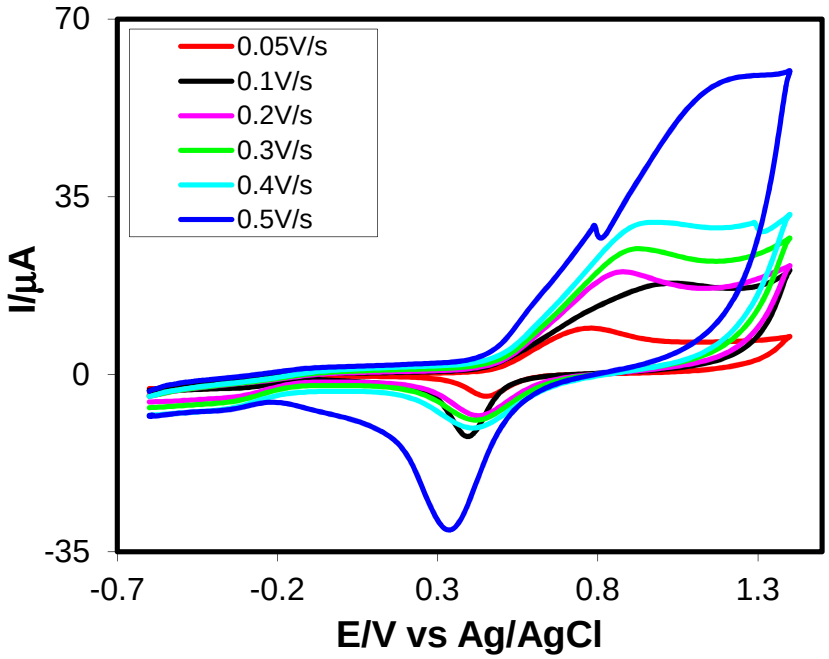

Fig. 4.86: Cyclic voltammogram of 2mM Resorcinol in buffer solution (pH 7) of Au electrode at different scan rate (1st cycle)

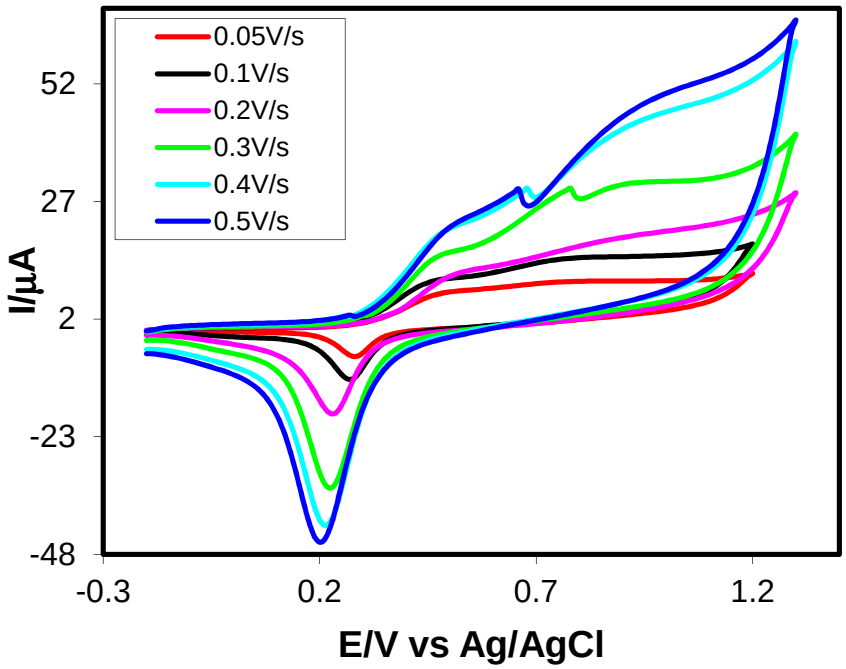

Fig. 4.87: Cyclic voltammogram of 2mM Resorcinol in buffer solution (pH 9) of Au electrode at different scan rate (1st cycle)

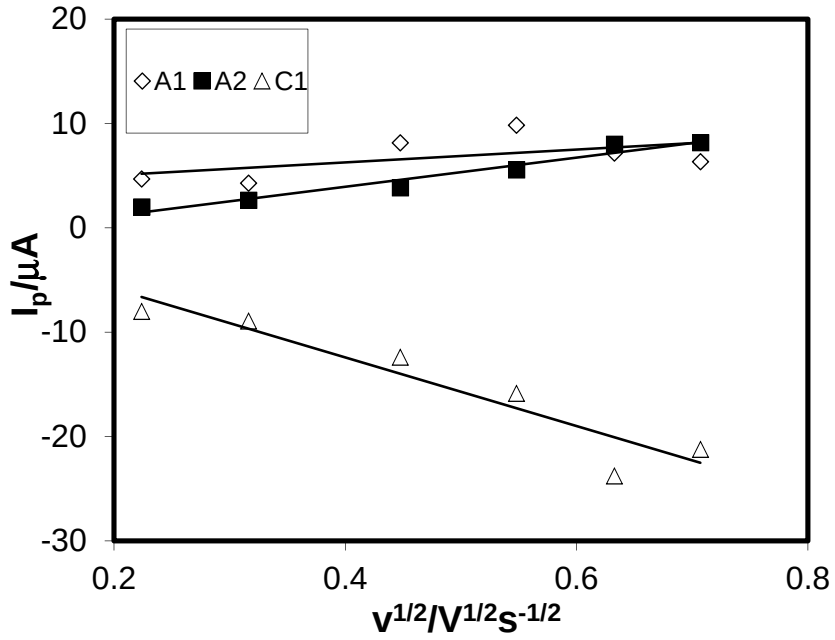

Fig. 4.88: Plots of peak current (I_p) versus square root of scan rate ($v^{1/2}$) of 2mM Resorcinol in buffer solution (pH 3) of Au electrode (1st cycle)

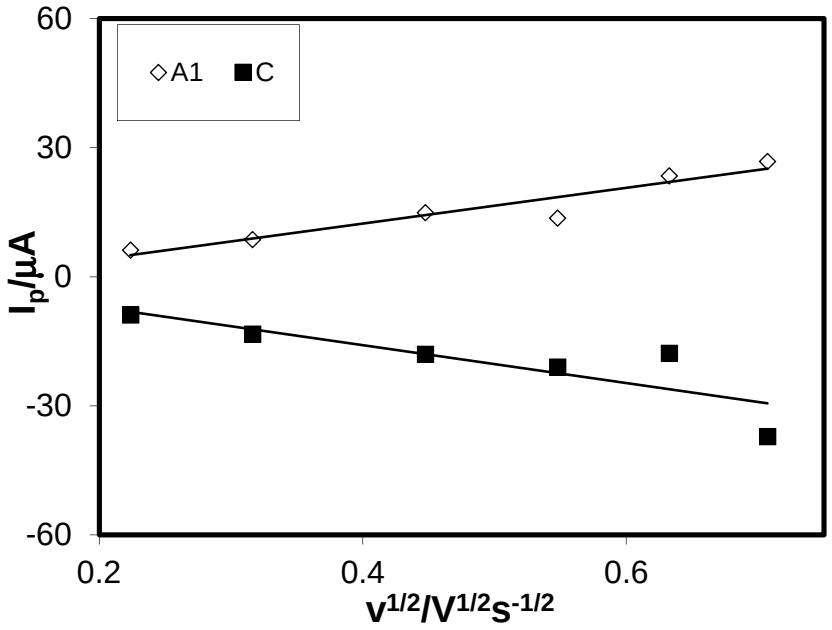

Fig. 4.89: Plots of peak current (I_p) versus square root of scan rate ($v^{1/2}$) of 2mM Resorcinol in buffer solution (pH 5) of Au electrode (1st cycle)

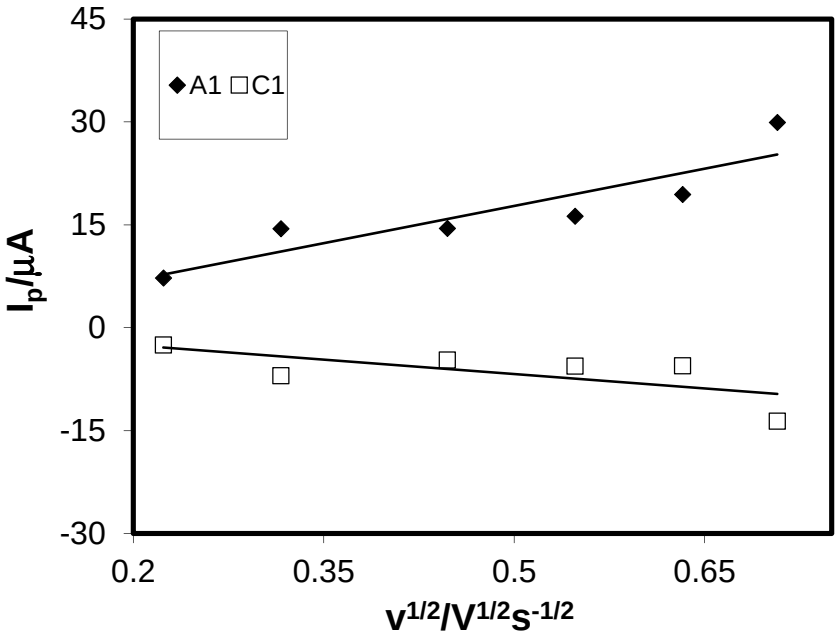

Fig. 4.90: Plots of peak current (I_p) versus square root of scan rate ($v^{1/2}$) of 2mM Resorcinol in buffer solution (pH 7) of Au electrode (1st cycle)

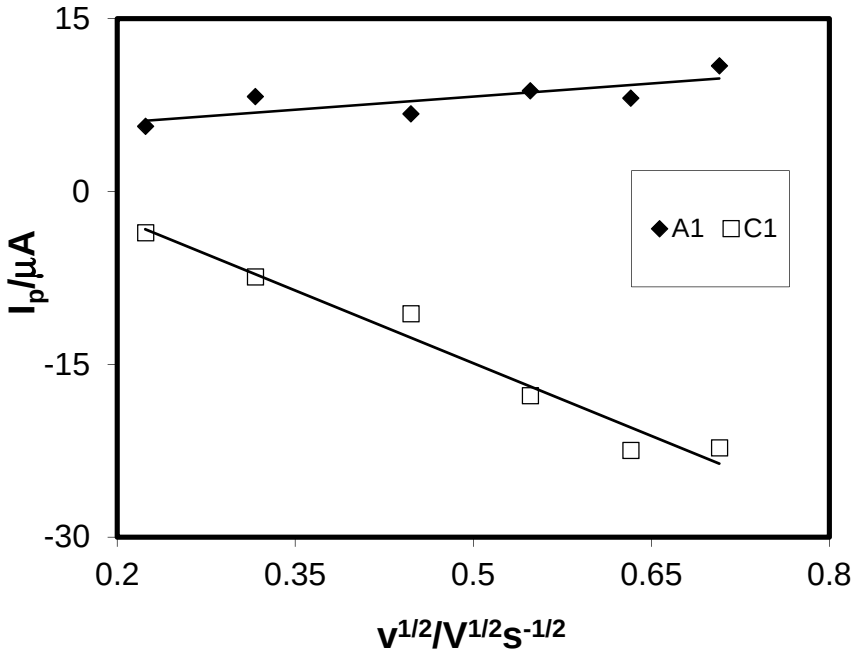

Fig. 4.91: Plots of peak current (I_p) versus square root of scan rate ($v^{1/2}$) of 2mM Resorcinol in buffer solution (pH 9) of Au electrode (1st cycle)

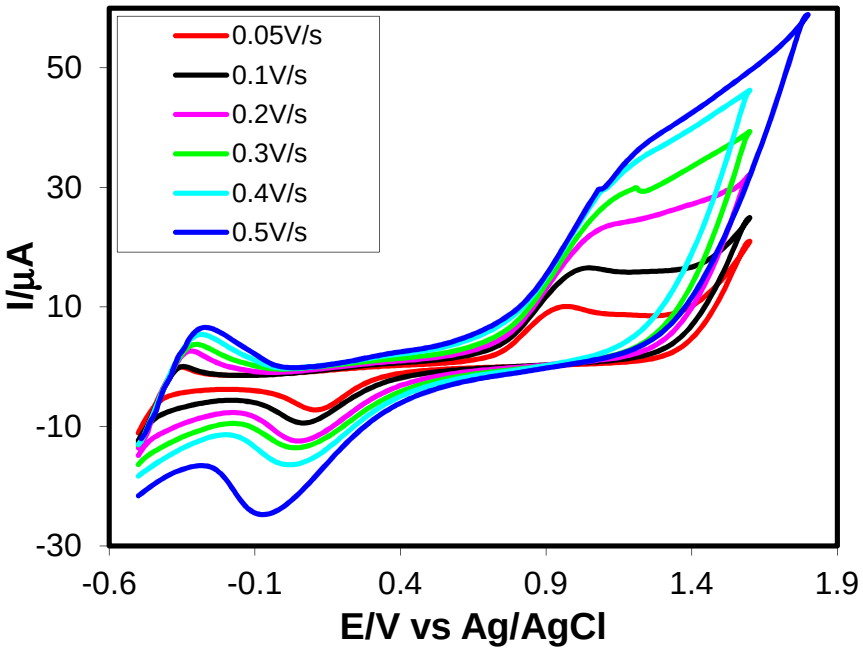

Fig. 4.92: Cyclic voltammogram of 2mM Resorcinol in buffer solution (pH 3) of Pt electrode at different scan rate (1st cycle)

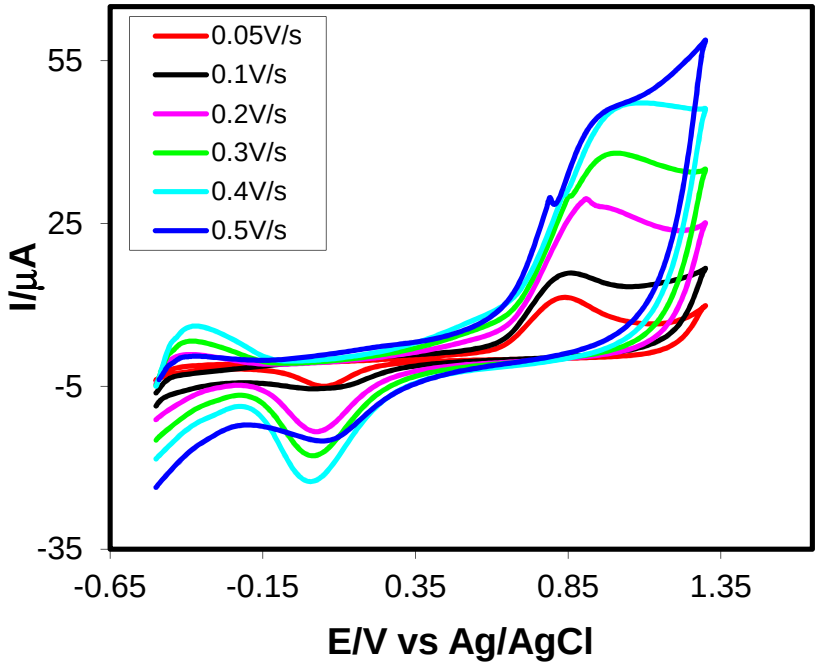

Fig. 4.93: Cyclic voltammogram of 2mM Resorcinol in buffer solution (pH 5) of Pt electrode at different scan rate (1st cycle)

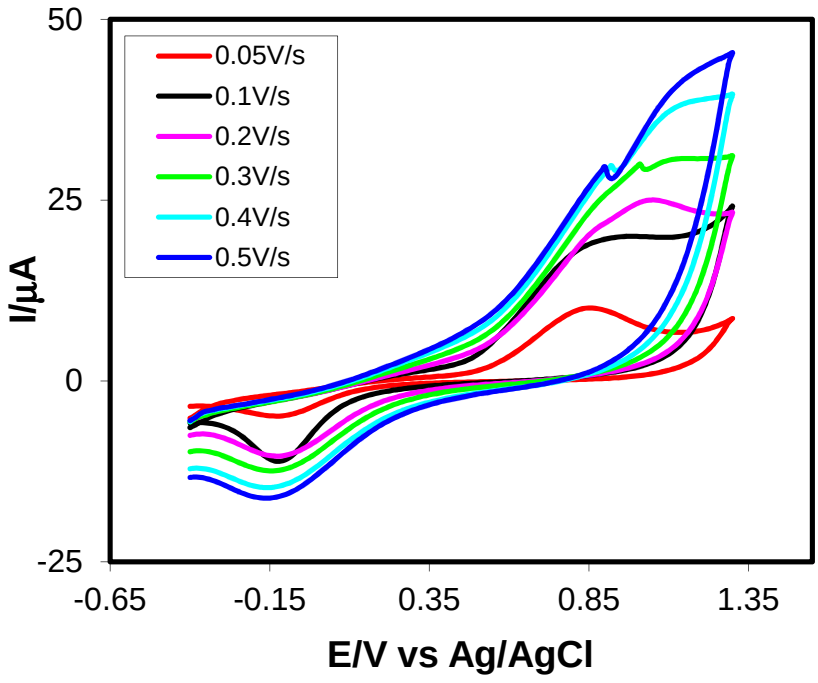

Fig. 4.94: Cyclic voltammogram of 2mM Resorcinol in buffer solution (pH 7) of Pt electrode at different scan rate (1st cycle)

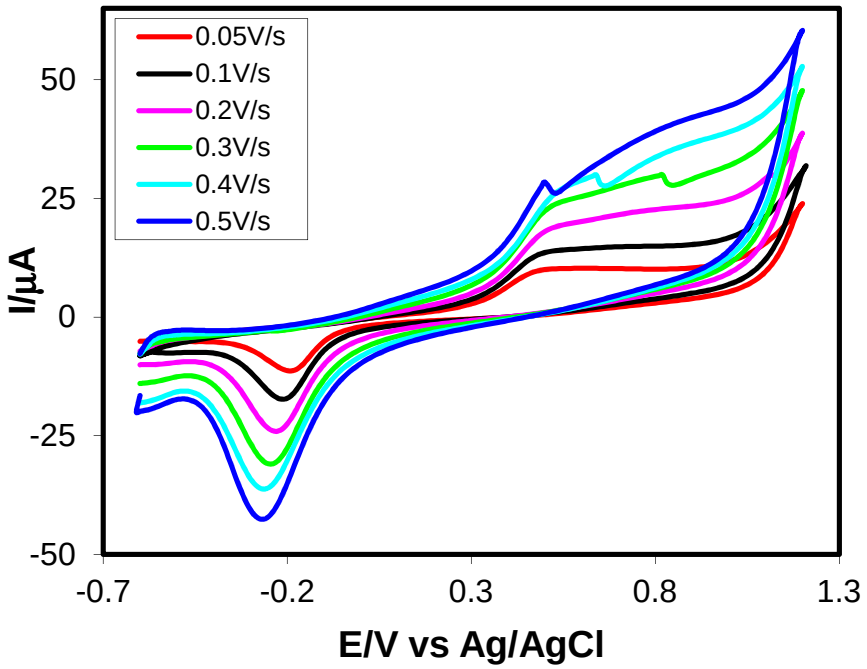

Fig. 4.95: Cyclic voltammogram of 2mM Resorcinol in buffer solution (pH 9) of Pt electrode at different scan rate (1st cycle)

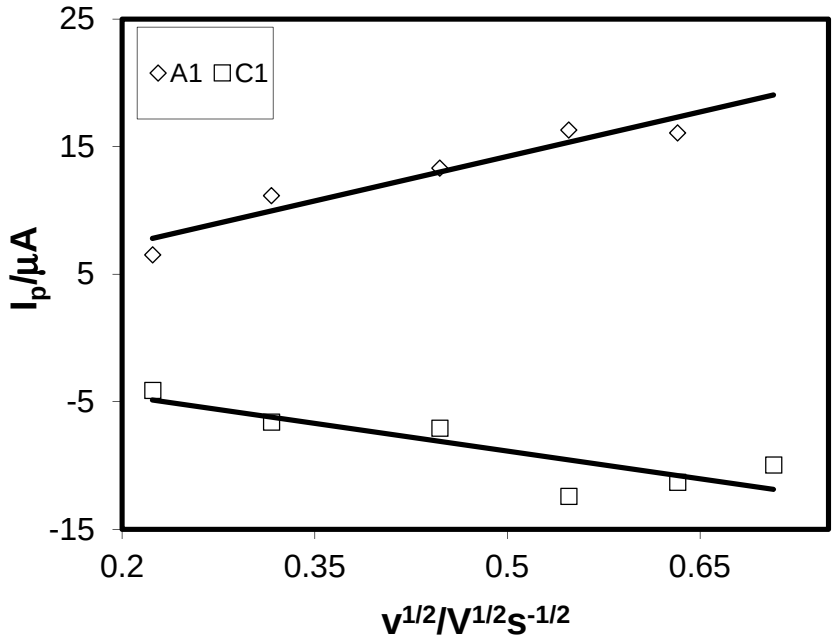

Fig. 4.96: Plots of peak current (I_p) versus square root of scan rate ($v^{1/2}$) of 2mM Resorcinol in buffer solution (pH 3) of Pt electrode (1st cycle)

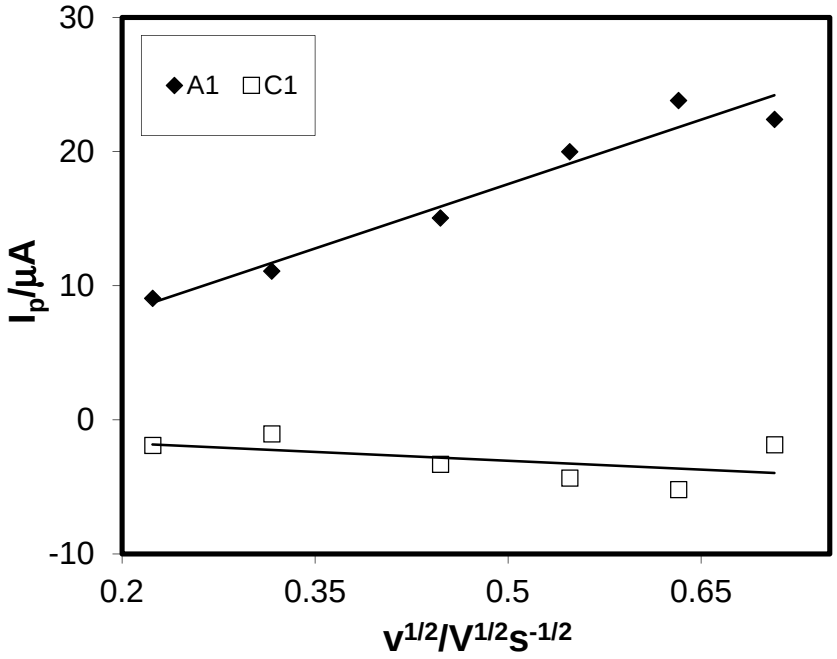

Fig. 4.97: Plots of peak current (I_p) versus square root of scan rate ($v^{1/2}$) of 2mM Resorcinol in buffer solution (pH 5) of Pt electrode (1st cycle)

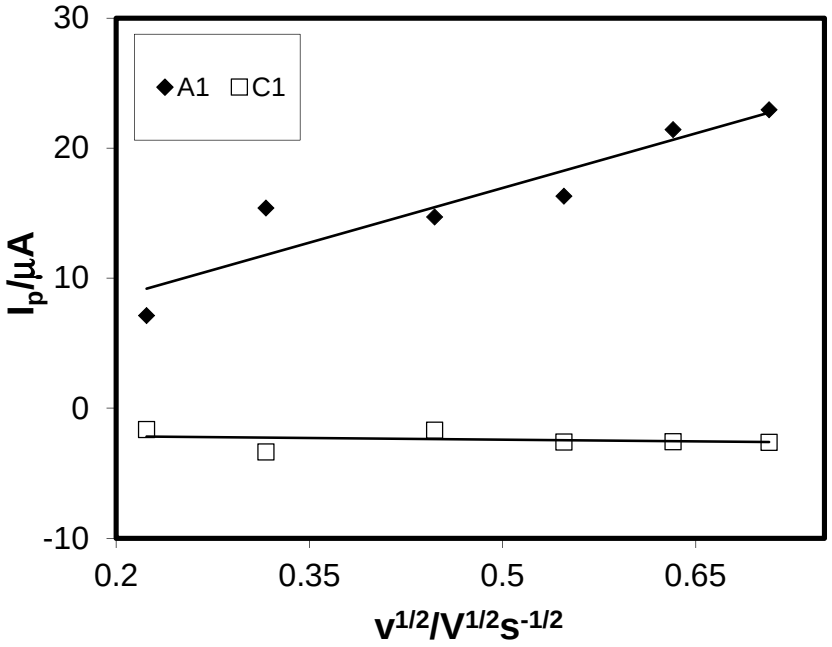

Fig. 4.98: Plots of peak current (I_p) versus square root of scan rate ($v^{1/2}$) of 2mM Resorcinol in buffer solution (pH 7) of Pt electrode (1st cycle)

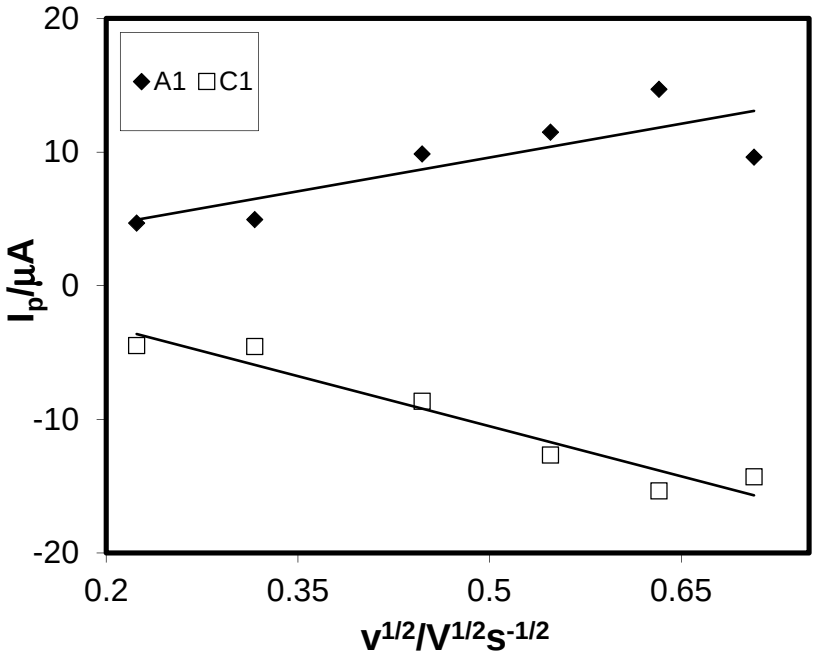

Fig. 4.99: Plots of peak current (I_p) versus square root of scan rate ($v^{1/2}$) of 2mM Resorcinol in buffer solution (pH 9) of Pt electrode (1st cycle)

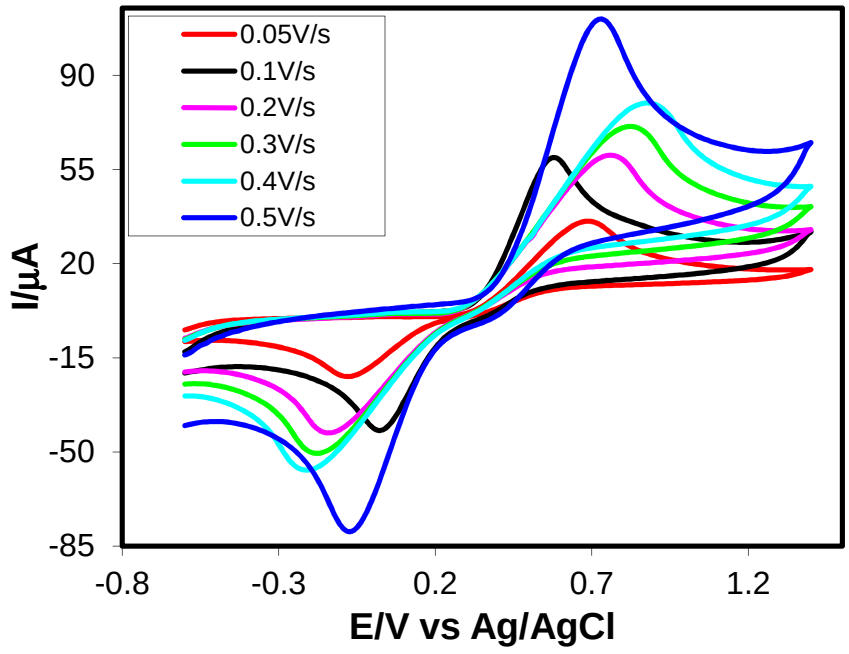

Fig. 4.100: Cyclic voltammogram of 2mM Hydroquinone in buffer solution (pH 3) of GC electrode at different scan rate (1st cycle)

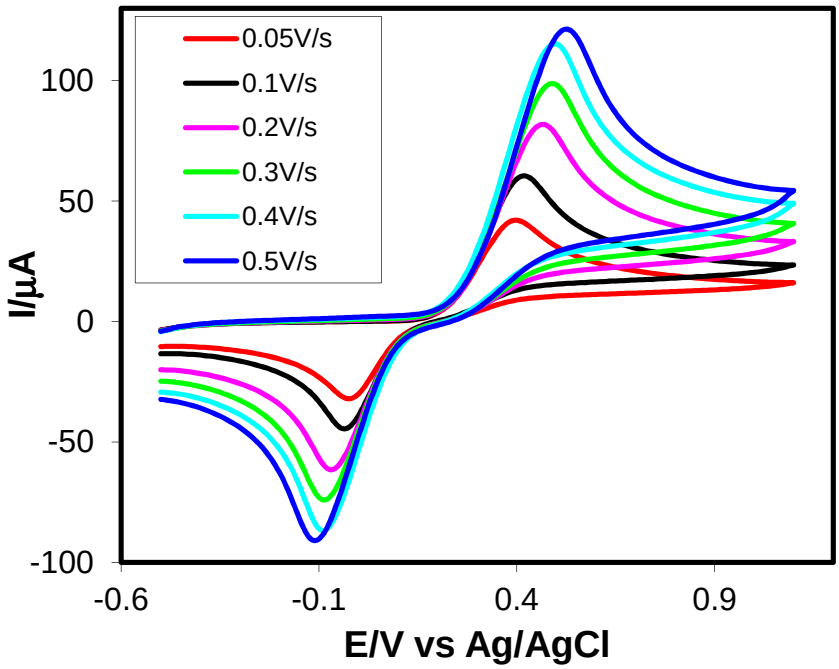

Fig. 4.101: Cyclic voltammogram of 2mM Hydroquinone in buffer solution (pH 5) of GC electrode at different scan rate (1st cycle)

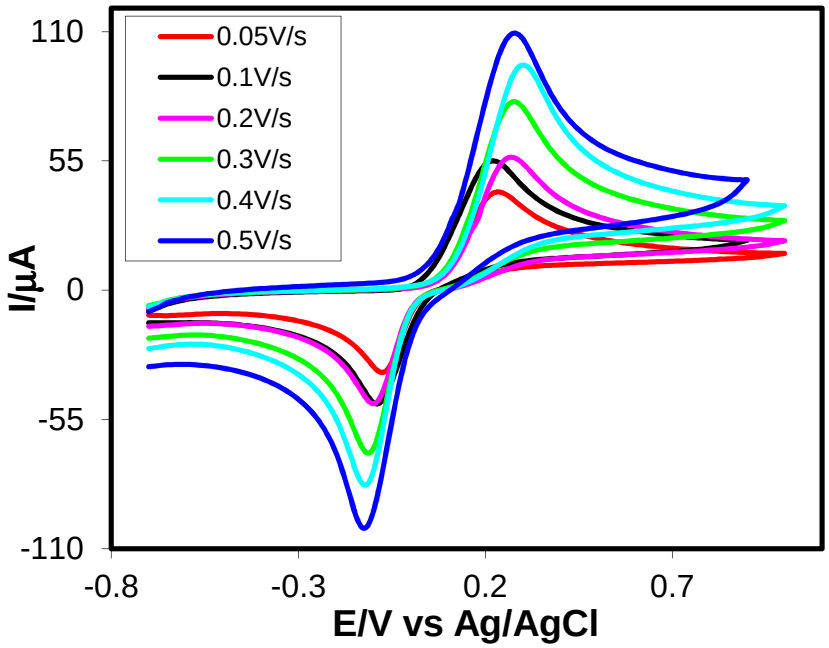

Fig. 4.102: Cyclic voltammogram of 2mM Hydroquinone in buffer solution (pH 7) of GC electrode at different scan rate (1st cycle)

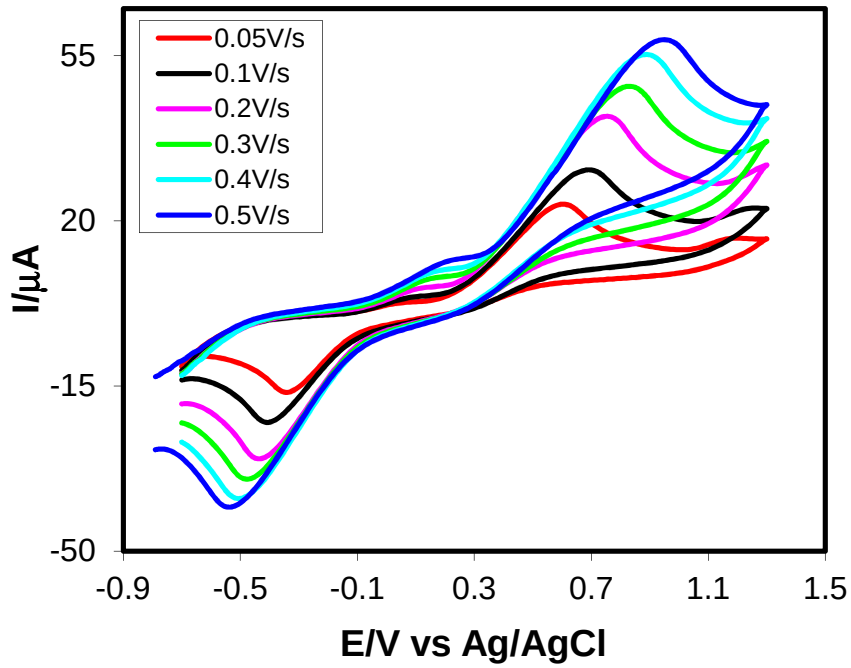

Fig. 4.103: Cyclic voltammogram of 2mM Hydroquinone in buffer solution (pH 9) of GC electrode at different scan rate (1st cycle)

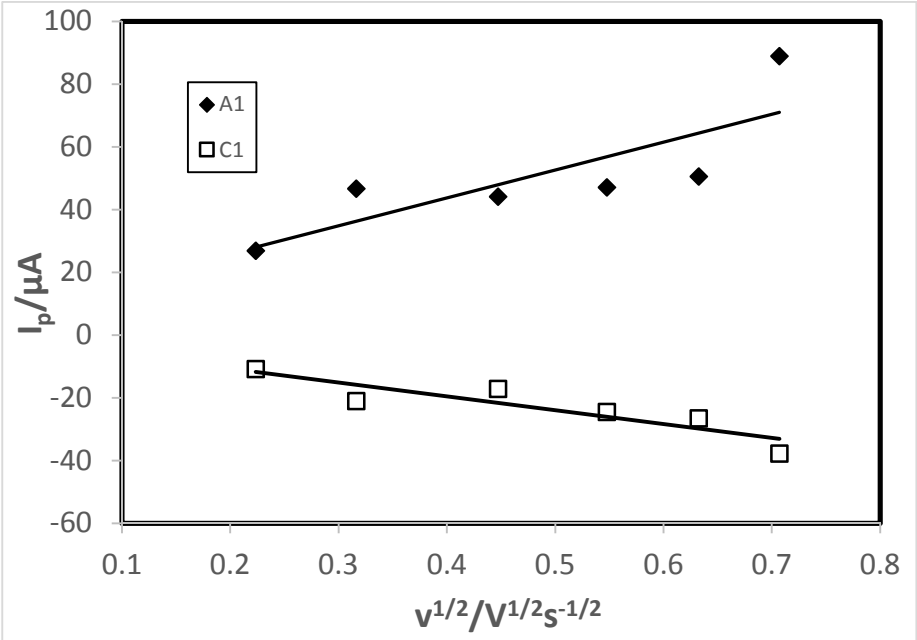

Fig. 4.104: Plots of peak current (I_p) versus square root of scan rate ($v^{1/2}$) of 2mM Hydroquinone in buffer solution (pH 3) of GC electrode (1st cycle)

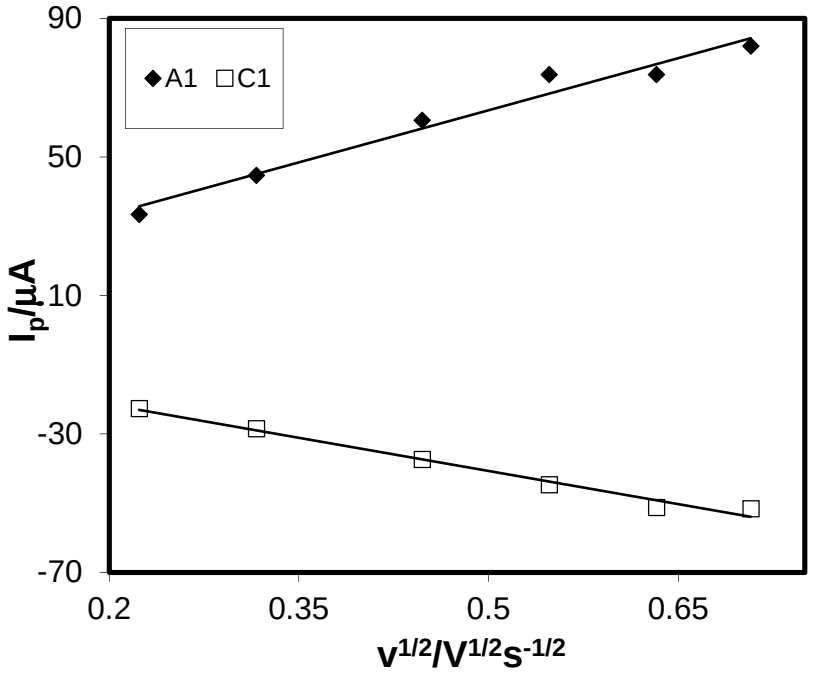

Fig. 4.105: Plots of peak current (I_p) versus square root of scan rate ($v^{1/2}$) of 2mM Hydroquinone in buffer solution (pH 5) of GC electrode (1st cycle)

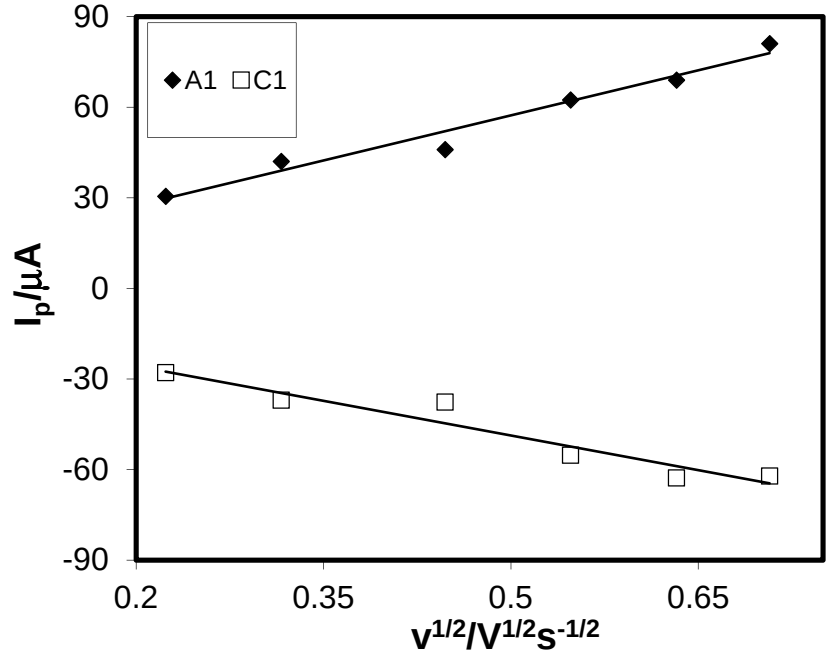

Fig. 4.106: Plots of peak current (I_p) versus square root of scan rate ($v^{1/2}$) of 2mM Hydroquinone in buffer solution (pH 7) of GC electrode (1st cycle)

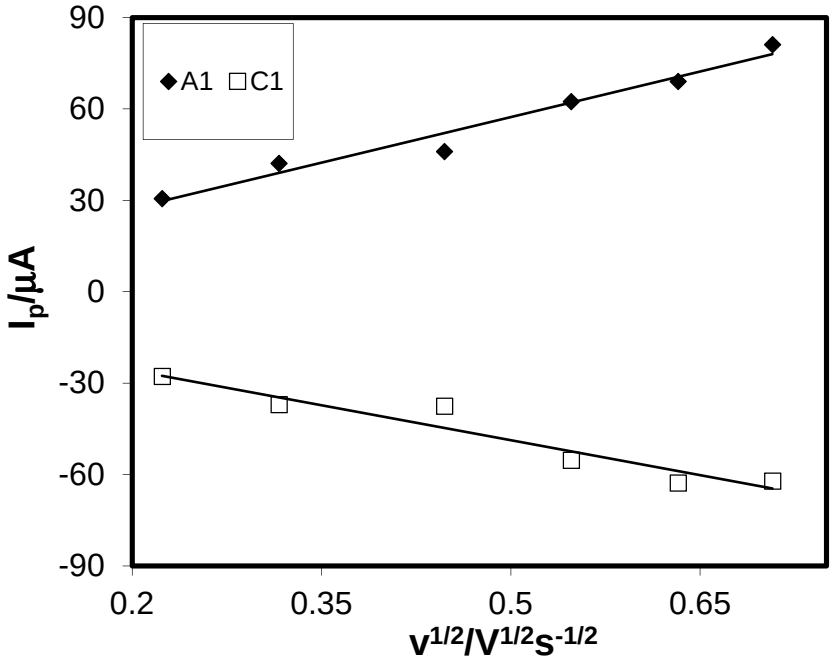

Fig. 4.107: Plots of peak current (I_p) versus square root of scan rate ($v^{1/2}$) of 2mM Hydroquinone in buffer solution (pH 9) of GC electrode (1st cycle)

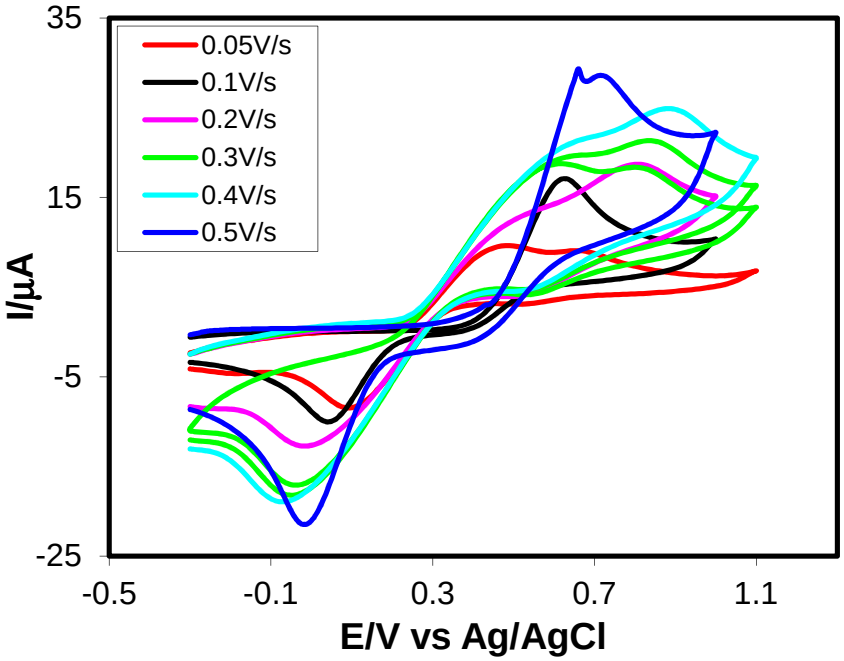

Fig. 4.108: Cyclic voltammogram of 2mM Hydroquinone in buffer solution (pH 3) of Au electrode at different scan rate (1st cycle)

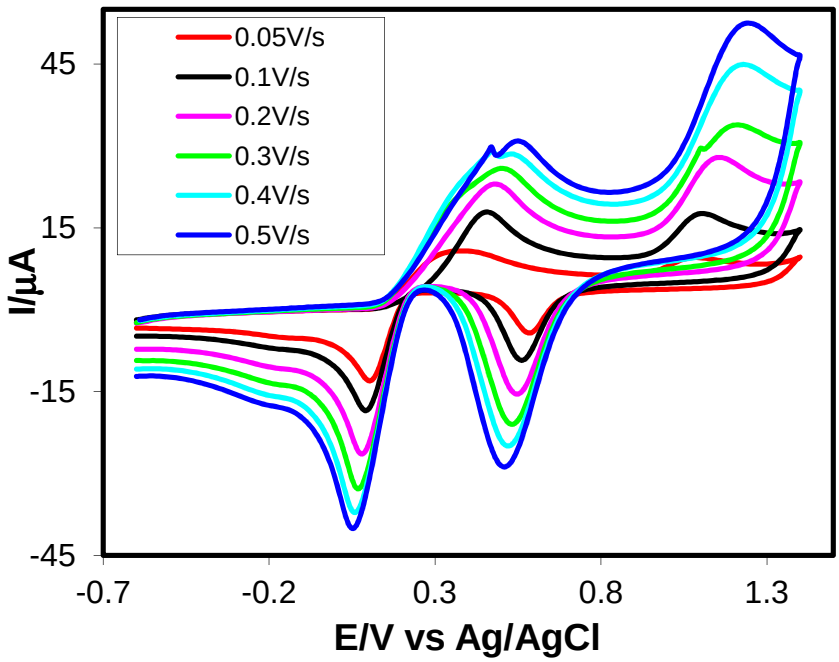

Fig. 4.109: Cyclic voltammogram of 2mM Hydroquinone in buffer solution (pH 5) of Au electrode at different scan rate (1st cycle)

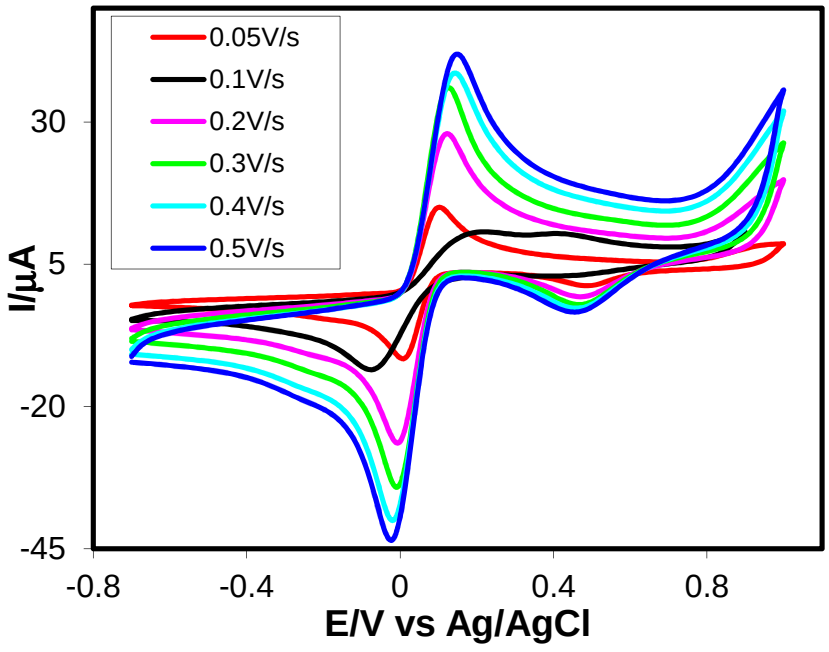

Fig. 4.110: Cyclic voltammogram of 2mM Hydroquinone in buffer solution (pH 7) of Au electrode at different scan rate (1st cycle)

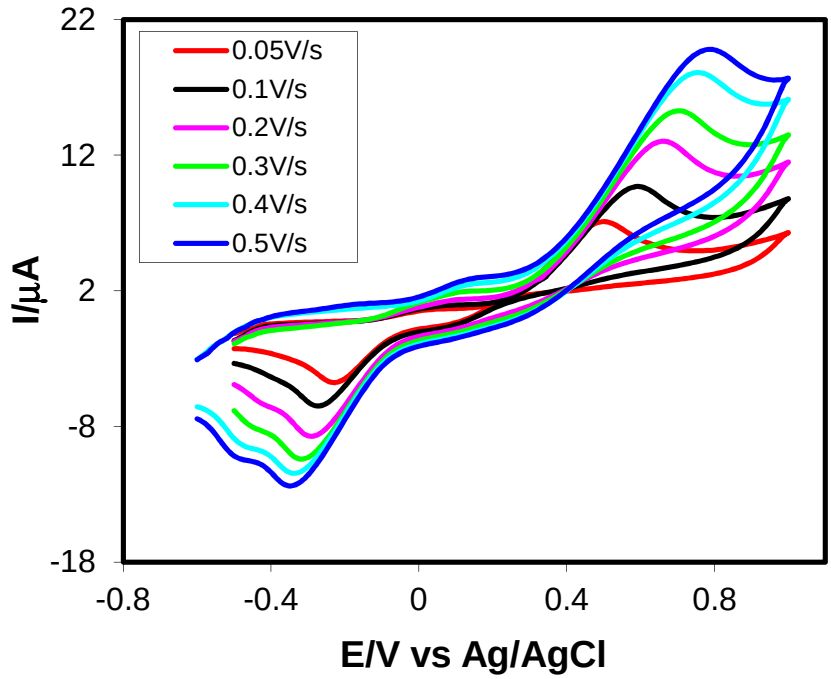

Fig. 4.111: Cyclic voltammogram of 2mM Hydroquinone in buffer solution (pH 9) of Au electrode at different scan rate (1st cycle)

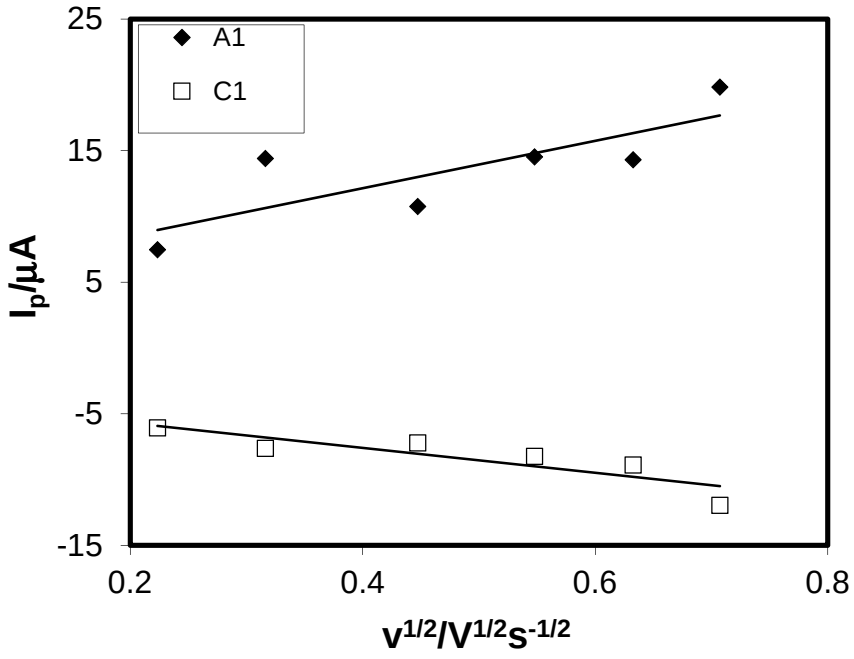

Fig. 4.112: Plots of peak current (I_p) versus square root of scan rate ($v^{1/2}$) of 2mM Hydroquinone in buffer solution (pH 3) of Au electrode (1st cycle)

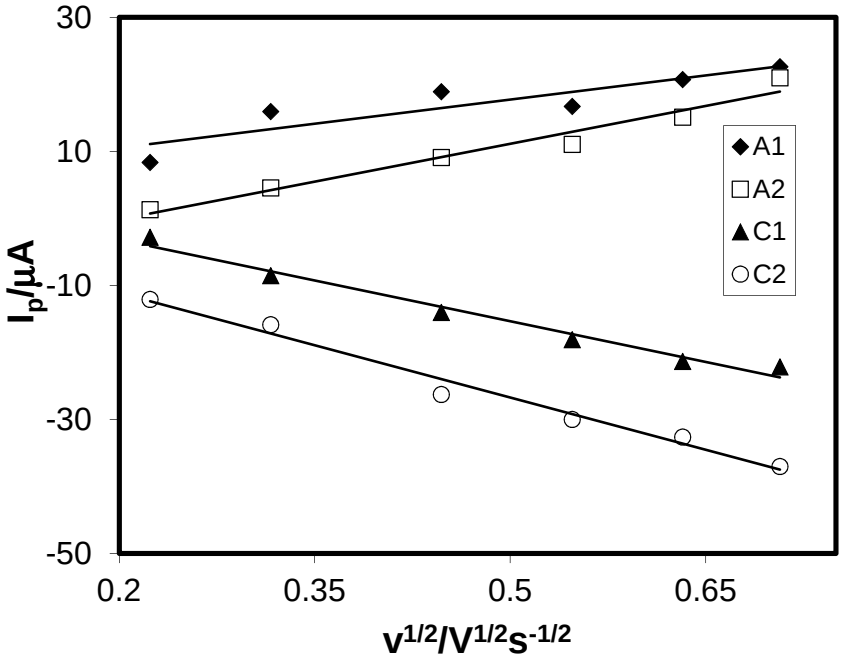

Fig. 4.113: Plots of peak current (I_p) versus square root of scan rate ($v^{1/2}$) of 2mM Hydroquinone in buffer solution (pH 5) of Au electrode (1st cycle)

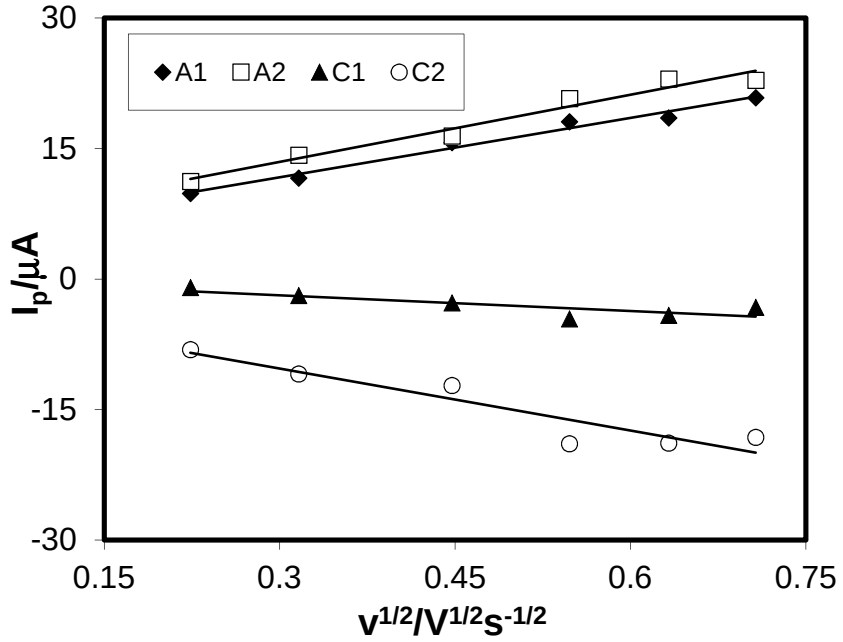

Fig. 4.114: Plots of peak current (I_p) versus square root of scan rate ($v^{1/2}$) of 2mM Hydroquinone in buffer solution (pH 7) of Au electrode (1st cycle)

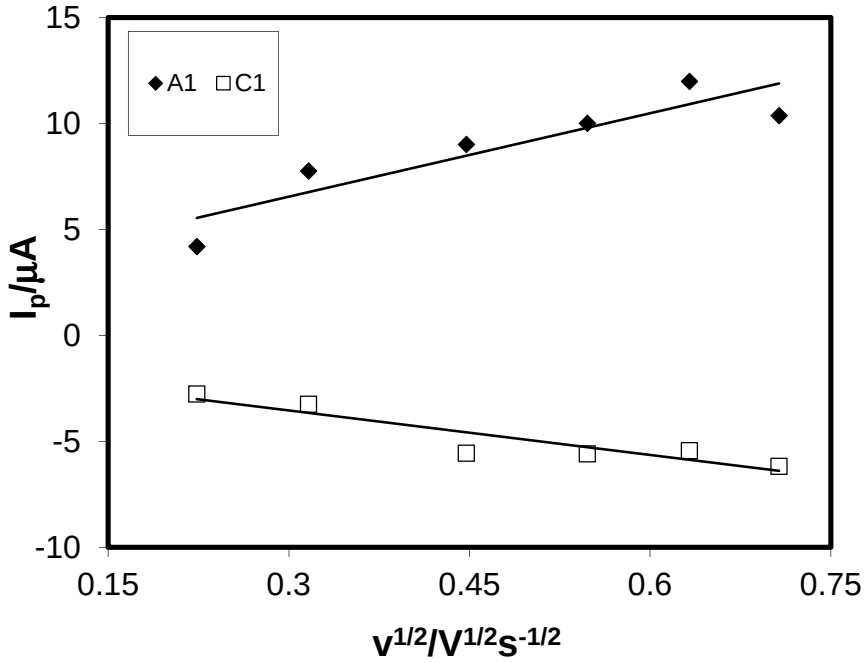

Fig. 4.115: Plots of peak current (I_p) versus square root of scan rate ($v^{1/2}$) of 2mM Hydroquinone in buffer solution (pH 9) of Au electrode (1st cycle)

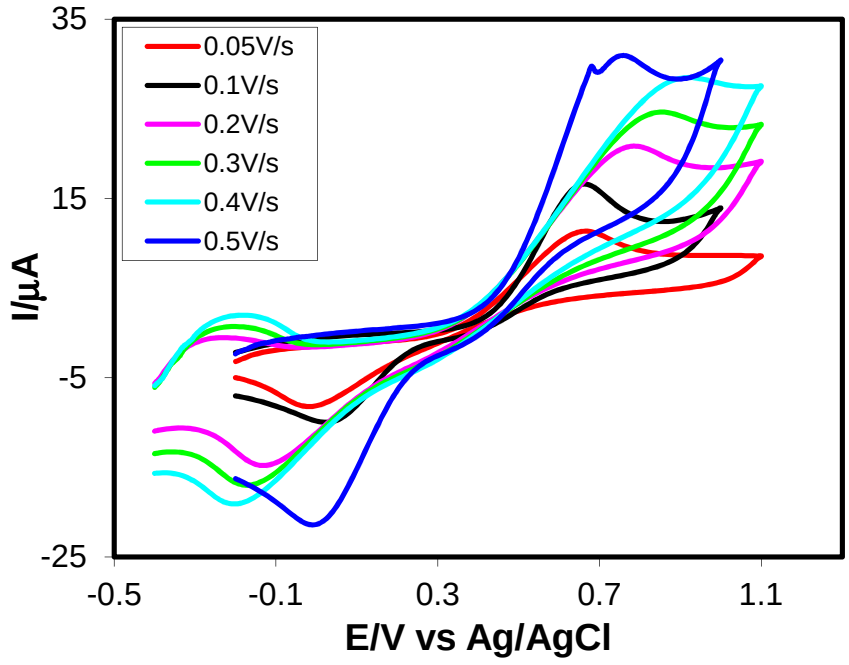

Fig. 4.116: Cyclic voltammogram of 2mM Hydroquinone in buffer solution (pH 3) of Pt electrode at different scan rate (1st cycle)

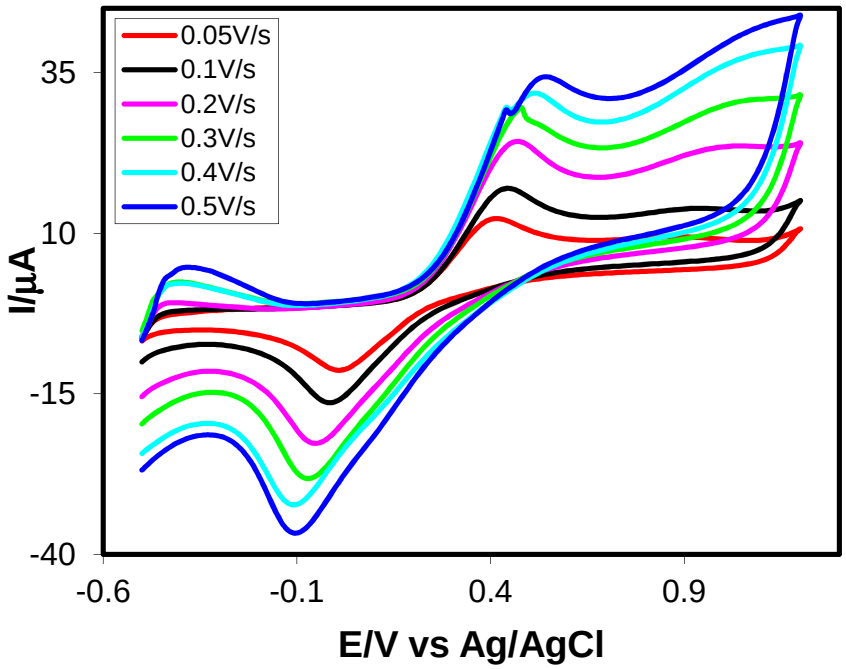

Fig. 4.117: Cyclic voltammogram of 2mM Hydroquinone in buffer solution (pH 5) of Pt electrode at different scan rate (1st cycle)

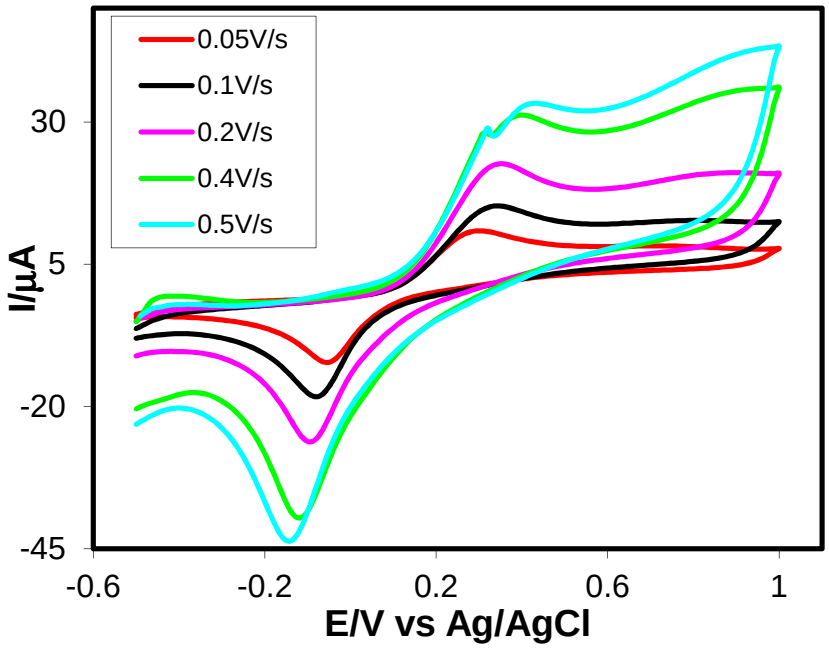

Fig. 4.118: Cyclic voltammogram of 2mM Hydroquinone in buffer solution (pH 7) of Pt electrode at different scan rate (1st cycle)

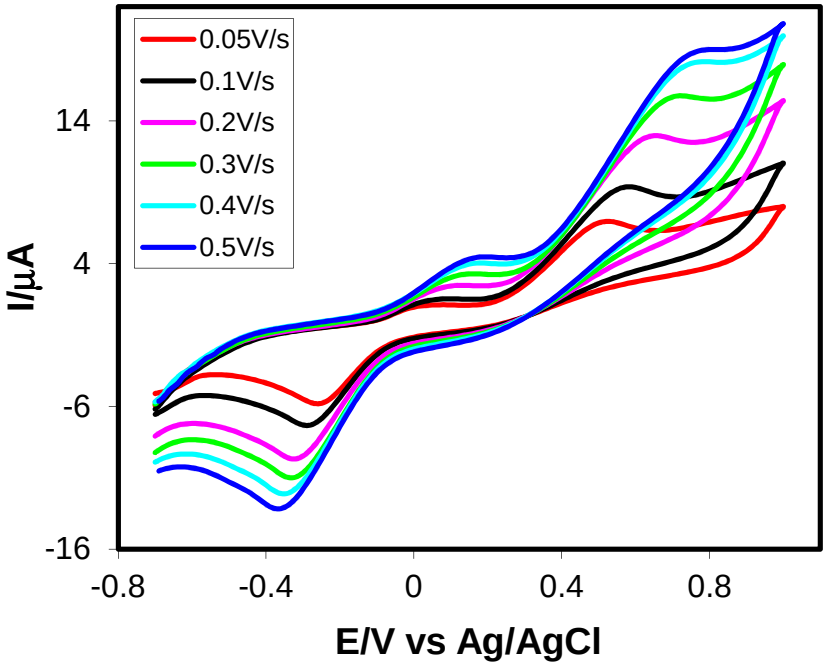

Fig. 4.119: Cyclic voltammogram of 2mM Hydroquinone in buffer solution (pH 9) of Pt electrode at different scan rate (1st cycle)

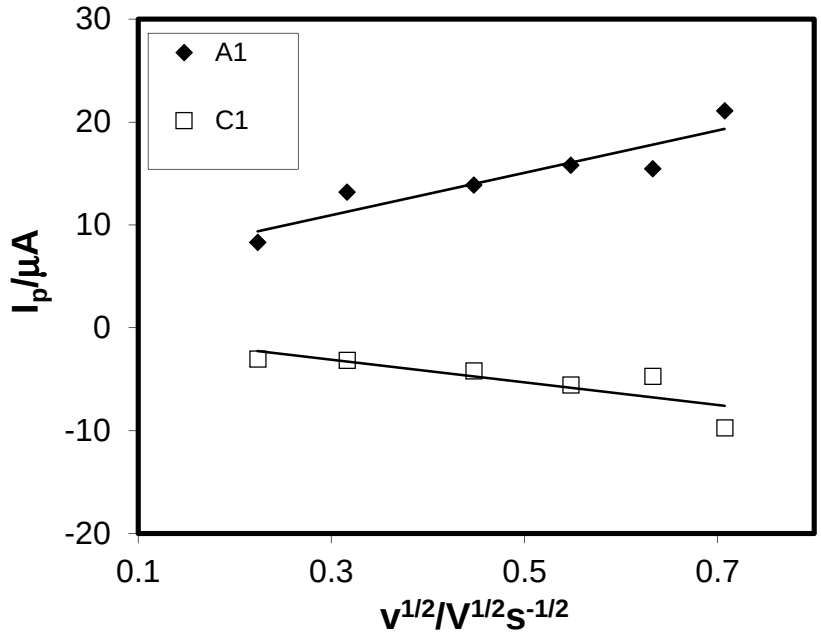

Fig. 4.120: Plots of peak current (I_p) versus square root of scan rate ($v^{1/2}$) of 2mM Hydroquinone in buffer solution (pH 3) of Pt electrode (1st cycle)

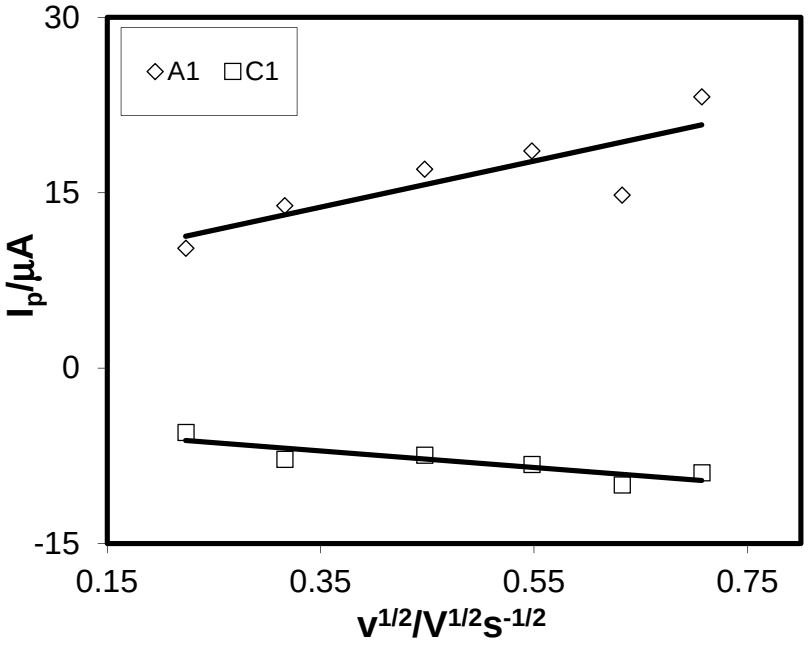

Fig. 4.121: Plots of peak current (I_p) versus square root of scan rate ($v^{1/2}$) of 2mM Hydroquinone in buffer solution (pH 5) of Pt electrode (1st cycle)

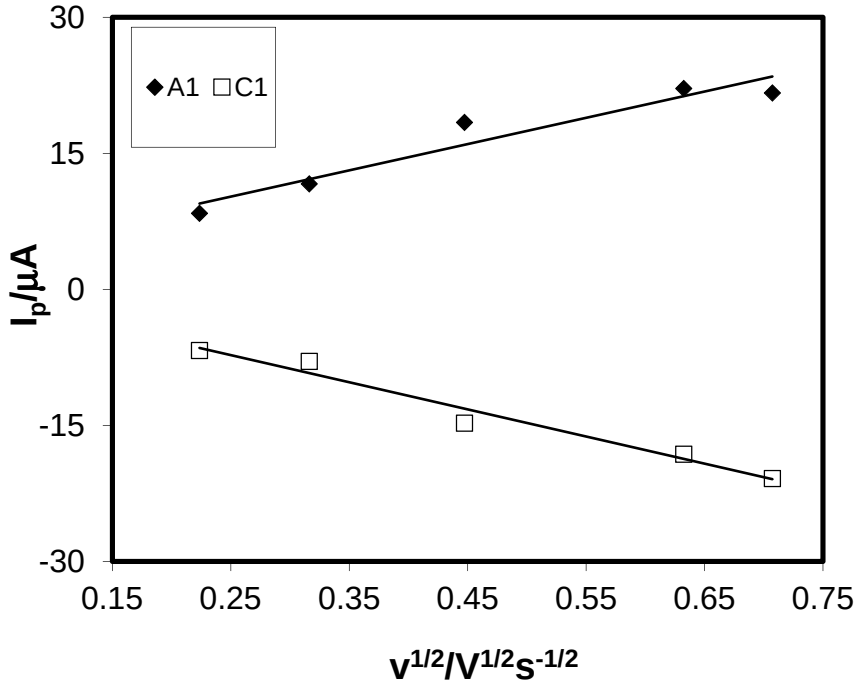

Fig. 4.122: Plots of peak current (I_p) versus square root of scan rate ($v^{1/2}$) of 2mM Hydroquinone in buffer solution (pH 7) of Pt electrode (1st cycle)

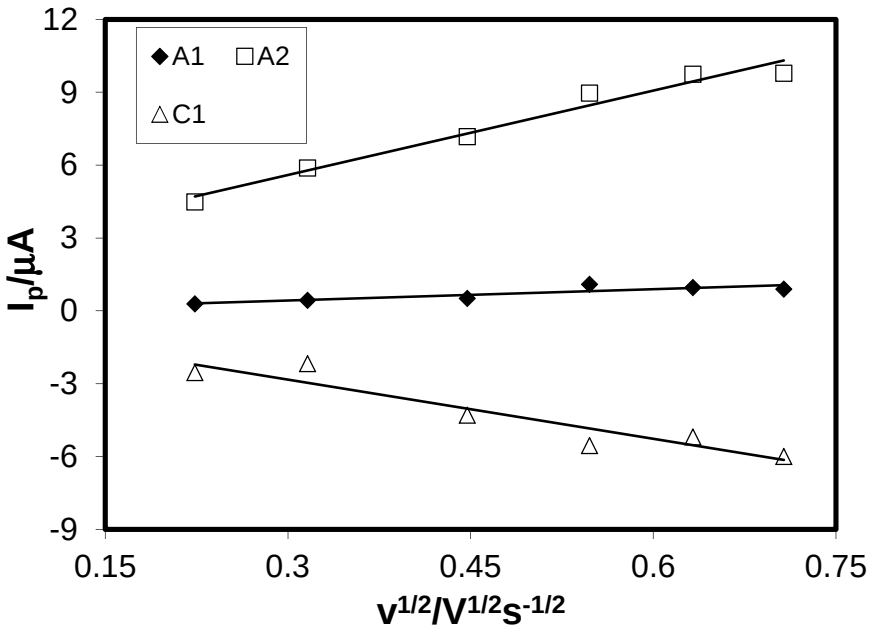

Fig. 4.123: Plots of peak current (I_p) versus square root of scan rate ($v^{1/2}$) of 2mM Hydroquinone in buffer solution (pH 9) of Pt electrode (1st cycle)

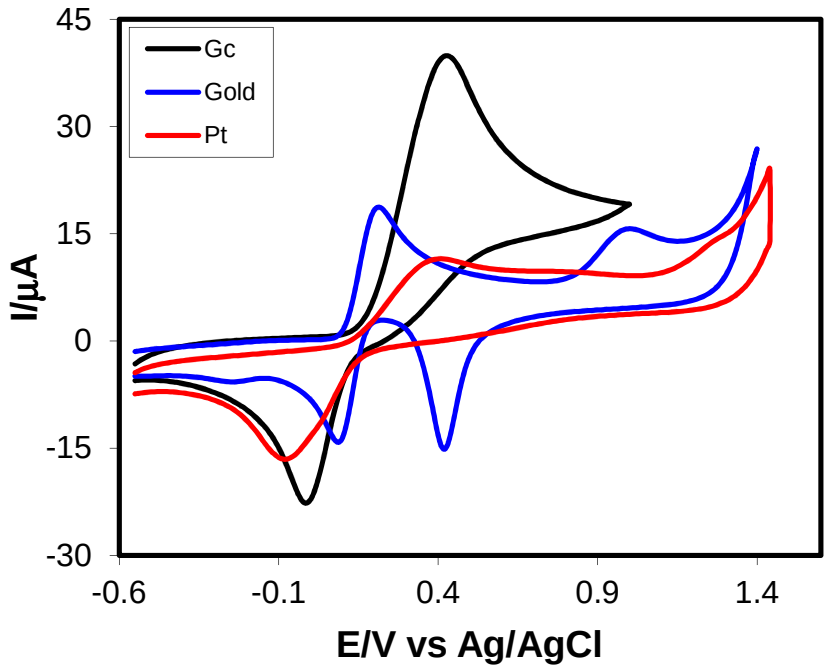

Fig. 4.124: Comparison of Cyclic voltammogram of 2mM Catechol of GC electrode (3.0mm), Au electrode (1.6mm) and Pt electrode (1.6mm) in buffer solution pH 7 at scan rate 0.1V/s (1st cycle)

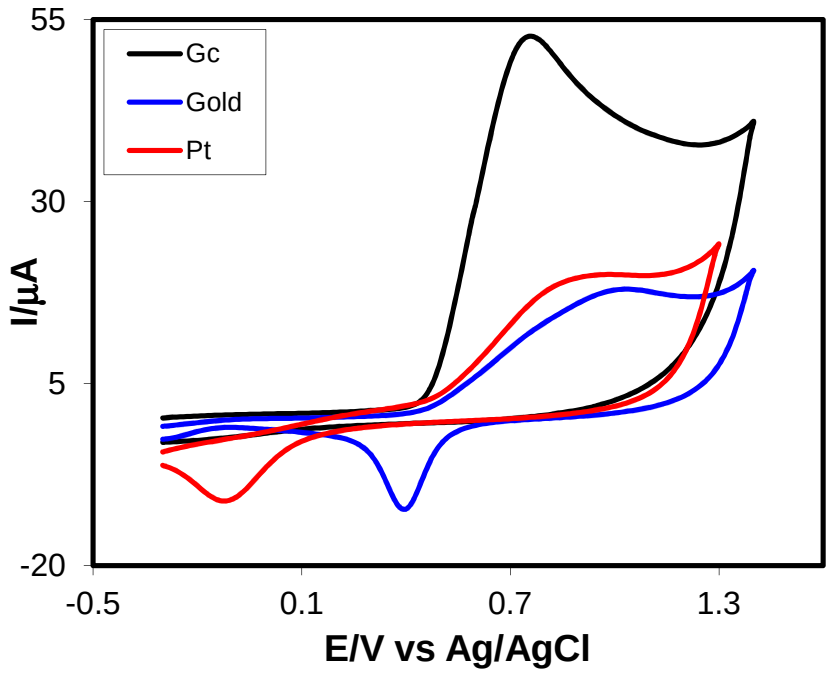

Fig. 4.125: Comparison of Cyclic voltammogram of 2mM Resorcinol of GC electrode (3.0mm), Au electrode (1.6mm) and Pt electrode (1.6mm) in buffer solution pH 7 at scan rate 0.1V/s (1st cycle)

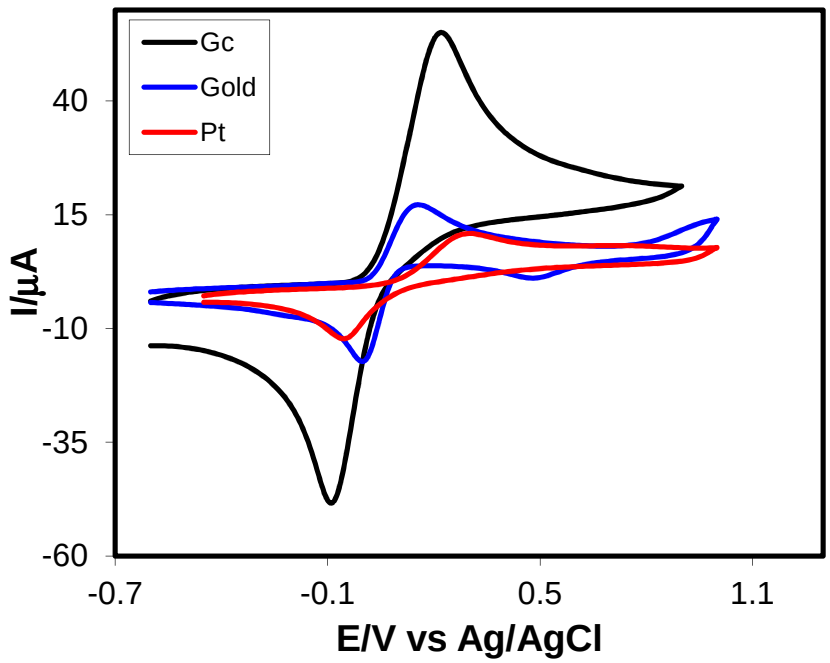

Fig. 4.126: Comparison of Cyclic voltammogram of 2mM Hydroquinone of GC electrode (3.0mm), Au electrode (1.6mm) and Pt electrode (1.6mm) in buffer solution pH 7 at scan rate 0.1V/s (1st cycle)

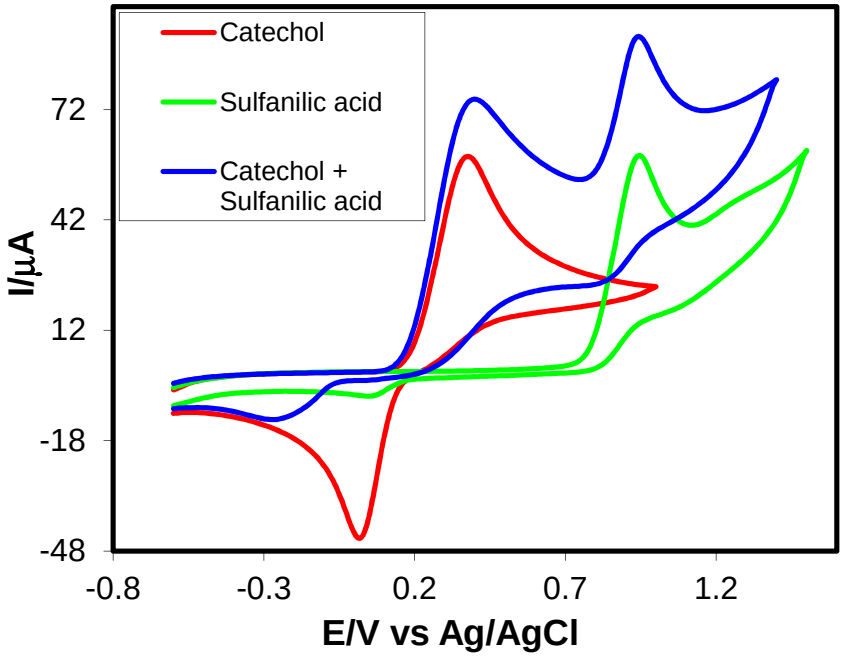

Fig. 4.127: Comparison of cyclic voltammogram of 2mM Catechol, 2mM Sulfanilic acid and 2mM Catechol + 2mM Sulfanilic acid in buffer solution (pH 7) of GC electrode at scan rate 0.1V/s (1st cycle)

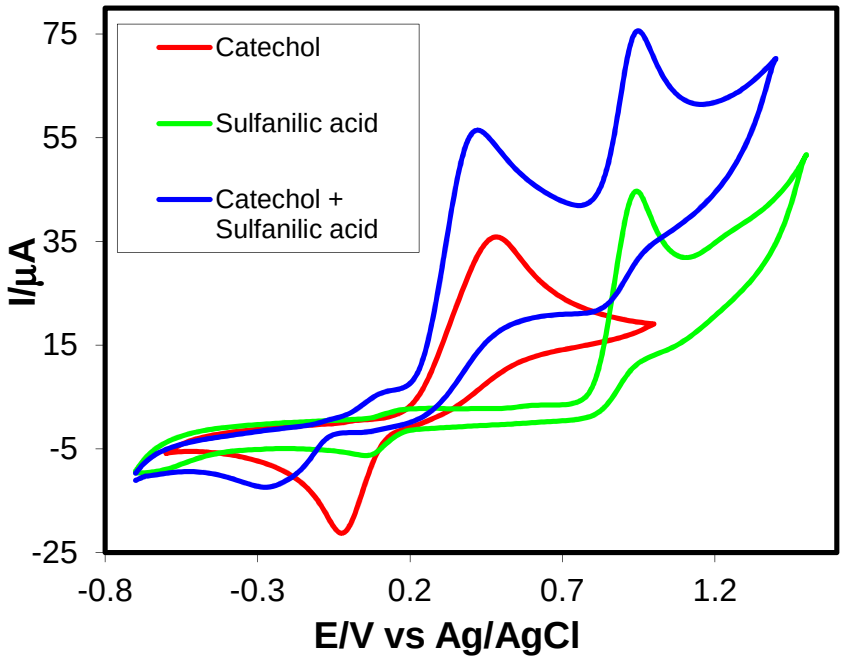

Fig. 4.128: Comparison of cyclic voltammogram of 2mM Catechol, 2mM Sulfanilic acid and 2mM Catechol + 2mM Sulfanilic acid in buffer solution (pH 7) of GC electrode at scan rate 0.1V/s (2nd cycle)

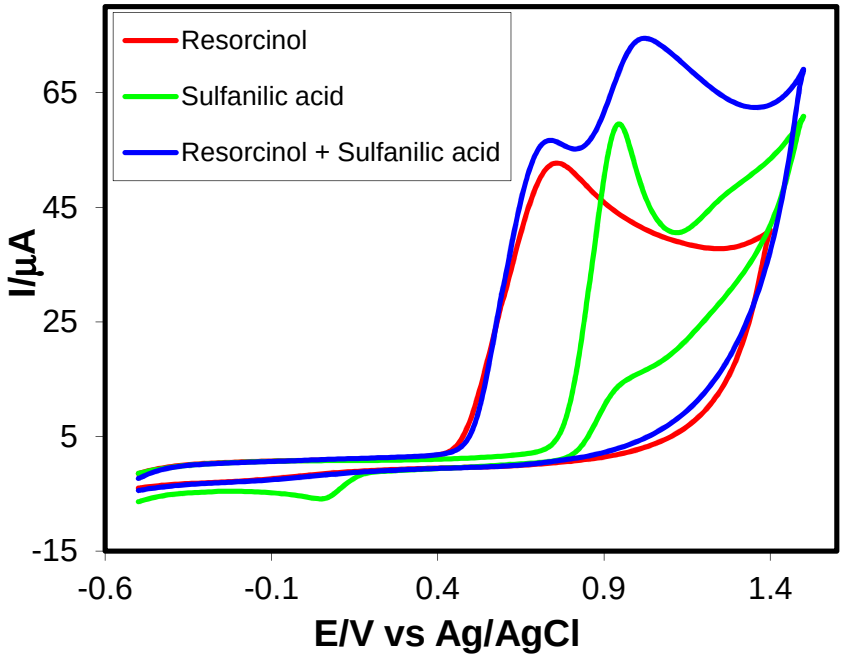

Fig. 4.129: Comparison of cyclic voltammogram of 2mM Resorcinol, 2mM Sulfanilic acid and 2mM Resorcinol + 2mM Sulfanilic acid in buffer solution (pH 7) of GC electrode at scan rate 0.1V/s (1st cycle)

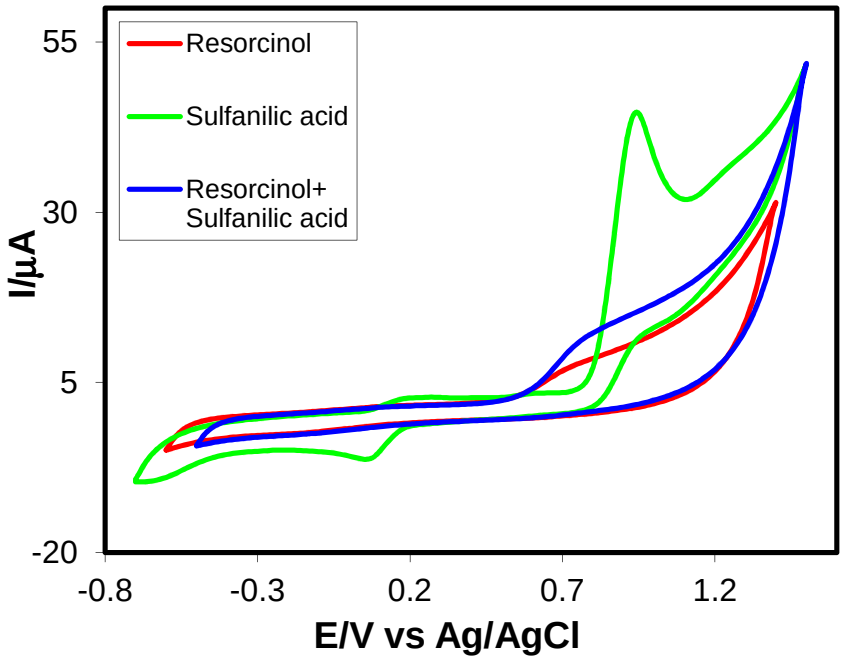

Fig. 4.130: Comparison of cyclic voltammogram of 2mM Resorcinol, 2mM Sulfanilic acid and 2mM Resorcinol + 2mM Sulfanilic acid in buffer solution (pH 7) of GC electrode at scan rate 0.1V/s (2nd cycle)

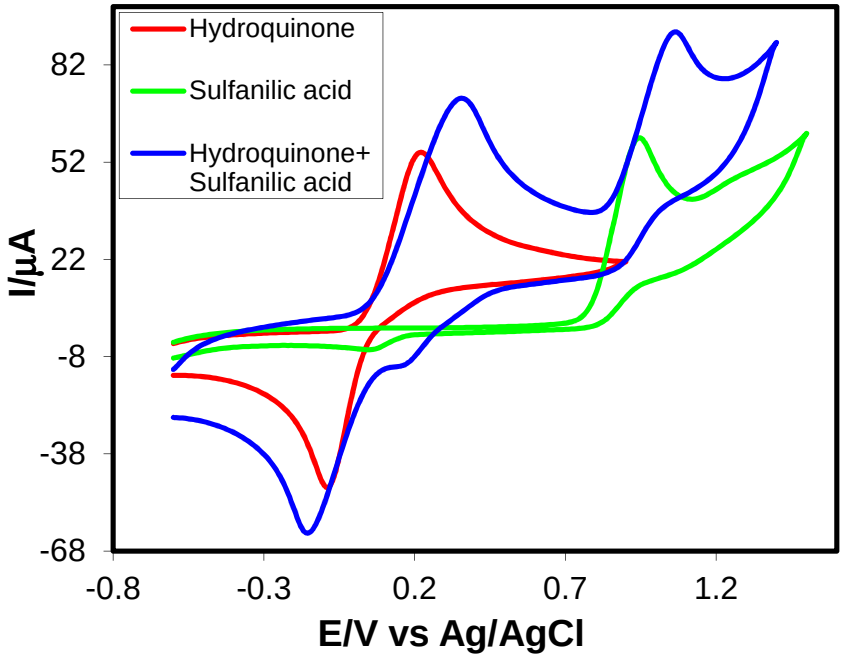

Fig. 4.131: Comparison of cyclic voltammogram of 2mM Hydroquinone, 2mM Sulfanilic acid and 2mM Hydroquinone + 2mM Sulfanilic acid in buffer solution (pH 7) of GC electrode at scan rate 0.1V/s (1st cycle)

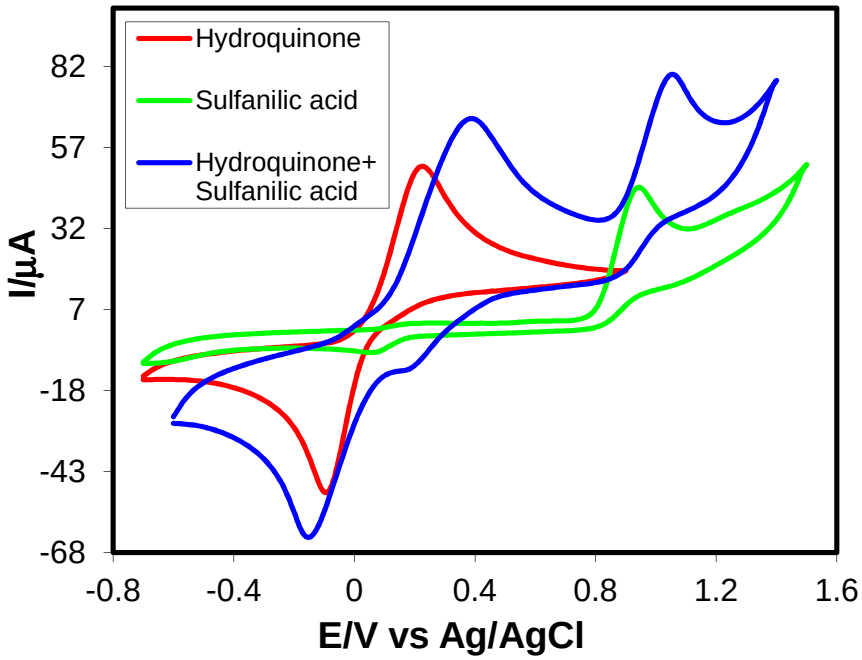

Fig. 4.132: Comparison of cyclic voltammogram of 2mM Hydroquinone, 2mM Sulfanilic acid and 2mM Hydroquinone + 2mM Sulfanilic acid in buffer solution (pH 7) of GC electrode at scan rate 0.1V/s (2nd cycle)

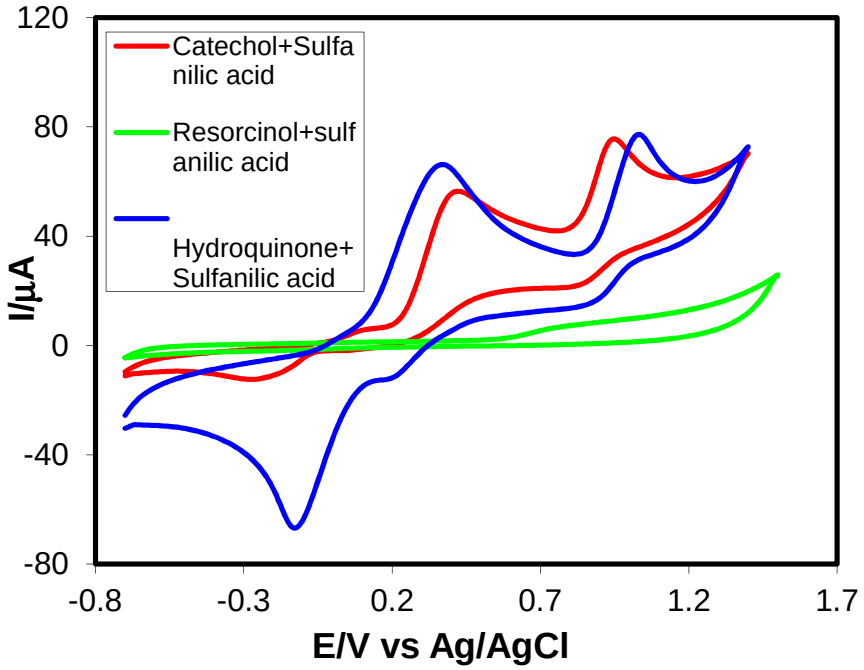

Fig. 4.133: Comparison of cyclic voltammogram of 2mM Catechol, 2mM Resorcinol and 2mM Hydroquinone with 2mM Sulfanilic acid in buffer solution (pH 7) of GC electrode at scan rate 0.1V/s (2nd cycle)

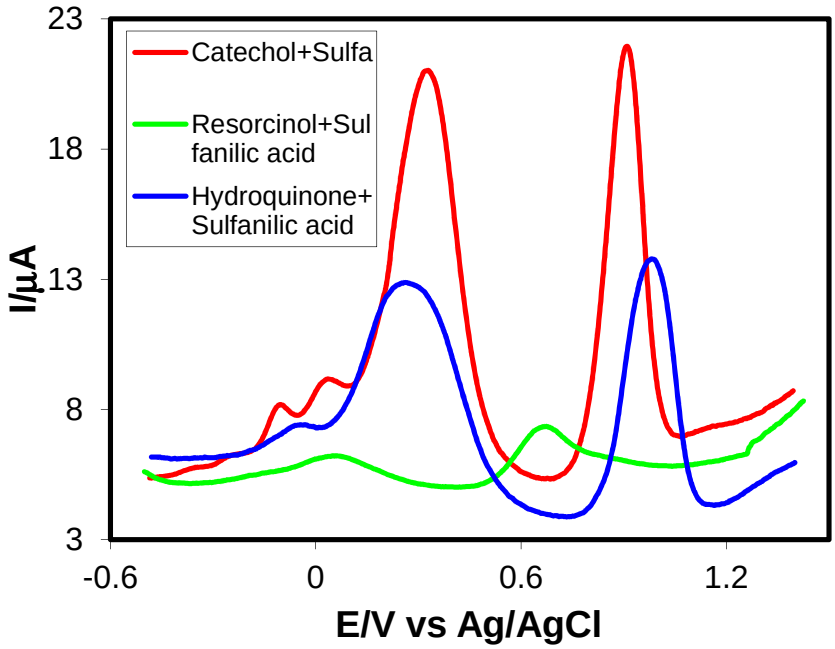

Fig. 4.134: Comparison of differential pulse voltammogram of 2mM Catechol, 2mM Resorcinol and 2mM Hydroquinone with 2mM Sulfanilic acid in buffer solution (pH 7) of GC electrode at scan rate 0.1V/s (2nd cycle)

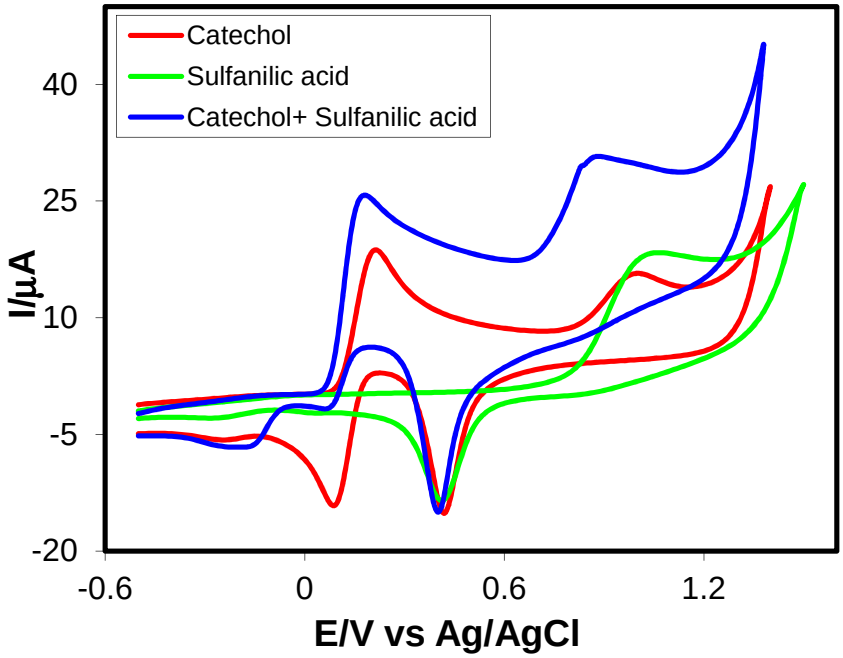

Fig. 4.135: Comparison of cyclic voltammogram of 2mM Catechol, 2mM Sulfanilic acid and 2mM Catechol with Sulfanilic acid in buffer solution (pH 7) of Au electrode at scan rate 0.1V/s (1st cycle)

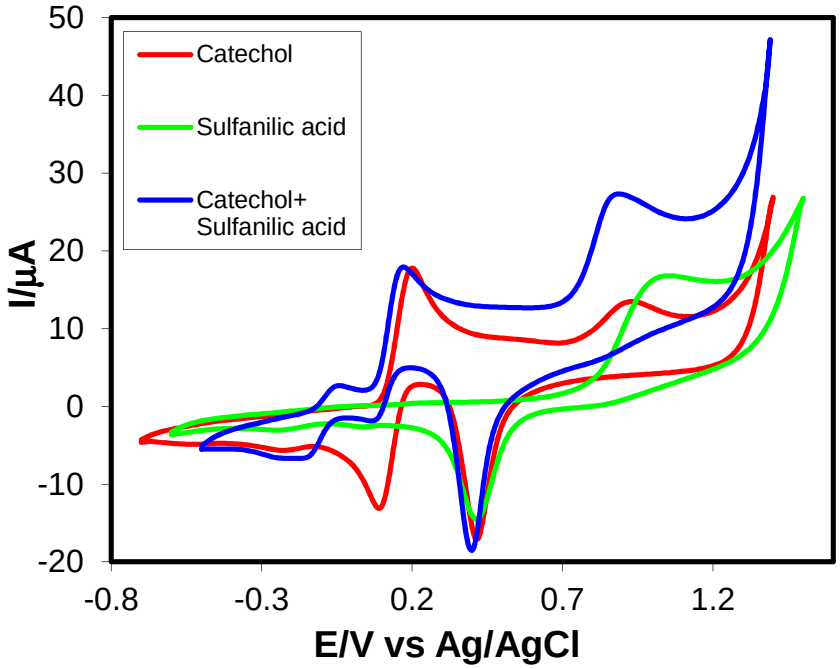

Fig. 4.136: Comparison of cyclic voltammogram of 2mM Catechol, 2mM Sulfanilic acid and 2mM Catechol with Sulfanilic acid in buffer solution (pH 7) of Au electrode at scan rate 0.1V/s (2nd cycle)

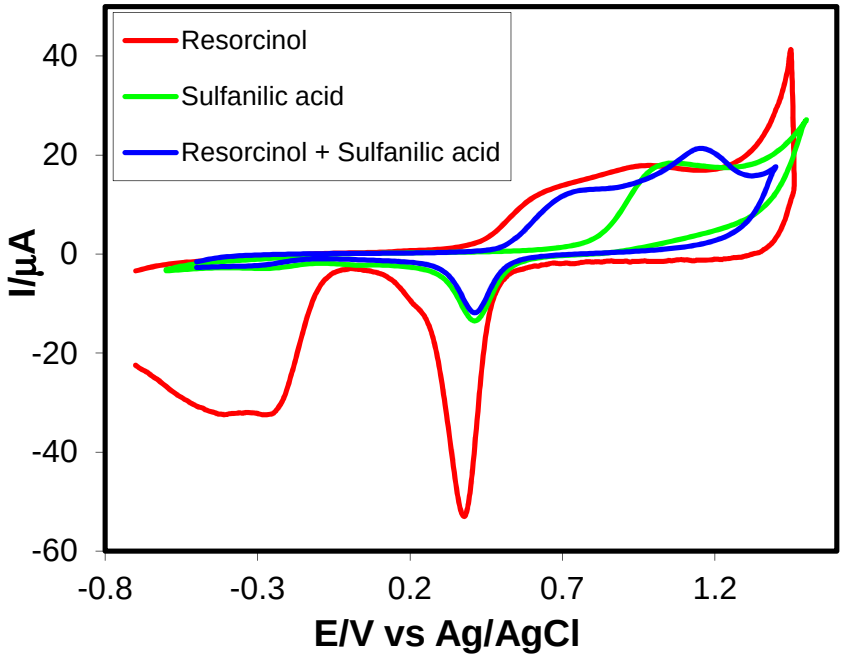

Fig. 4.137: Comparison of cyclic voltammogram of 2mM Resorcinol, 2mM Sulfanilic acid and 2mM Resorcinol with Sulfanilic acid in buffer solution (pH 7) of Au electrode at scan rate 0.1V/s (1st cycle)

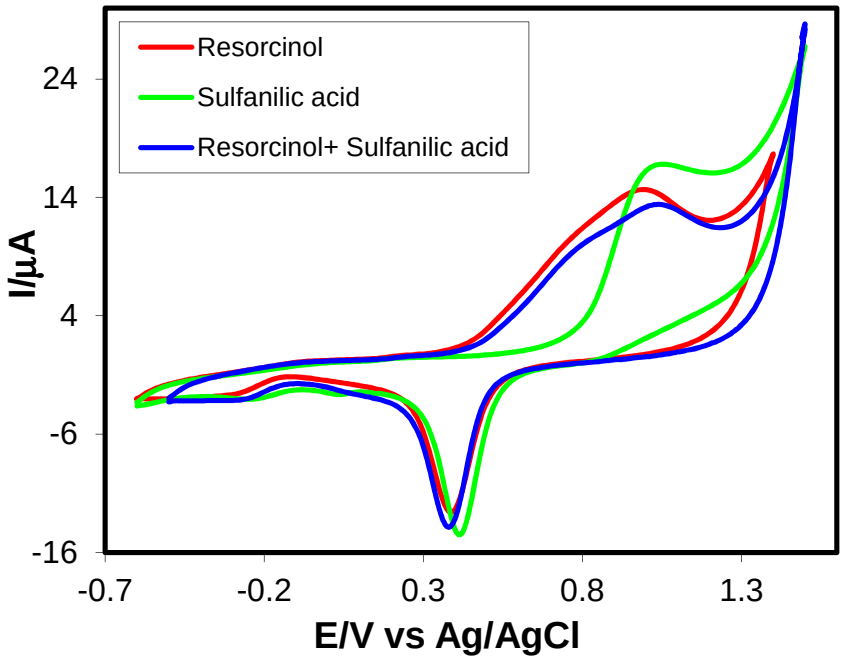

Fig. 4.138: Comparison of cyclic voltammogram of 2mM Resorcinol, 2mM Sulfanilic acid and 2mM Resorcinol with Sulfanilic acid in buffer solution (pH 7) of Au electrode at scan rate 0.1V/s (2nd cycle)

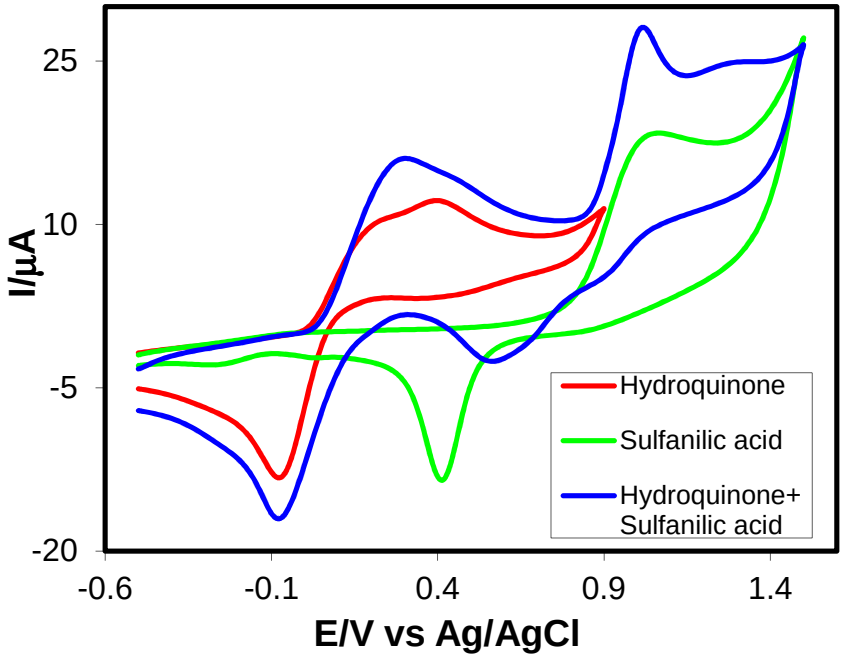

Fig. 4.139: Comparison of cyclic voltammogram of 2mM Hydroquinone, 2mM Sulfanilic acid and 2mM Hydroquinone with Sulfanilic acid in buffer solution (pH 7) of Au electrode at scan rate 0.1V/s (1st cycle)

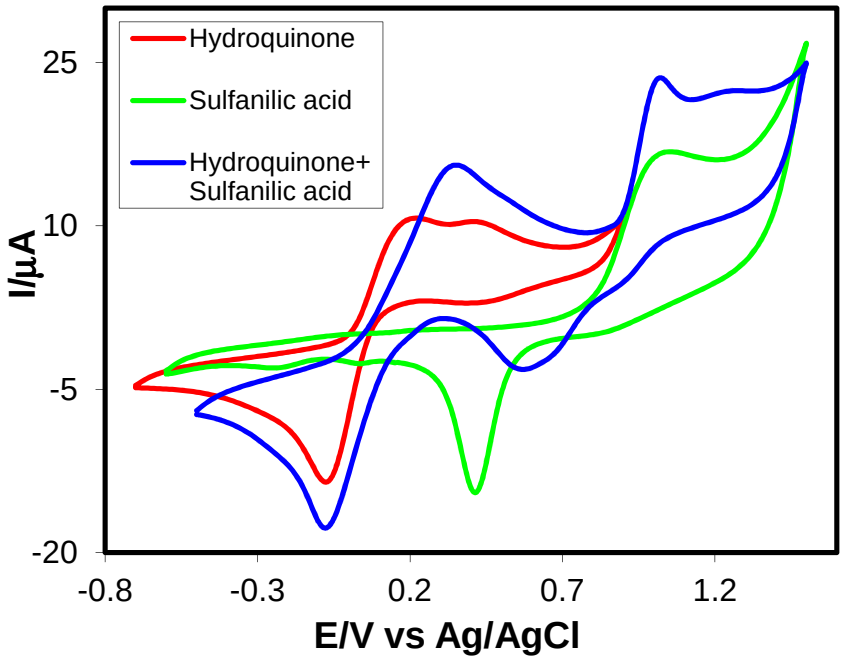

Fig. 4.140: Comparison of cyclic voltammogram of 2mM Hydroquinone, 2mM Sulfanilic acid and 2mM Hydroquinone with Sulfanilic acid in buffer solution (pH 7) of Au electrode at scan rate 0.1V/s (2nd cycle)

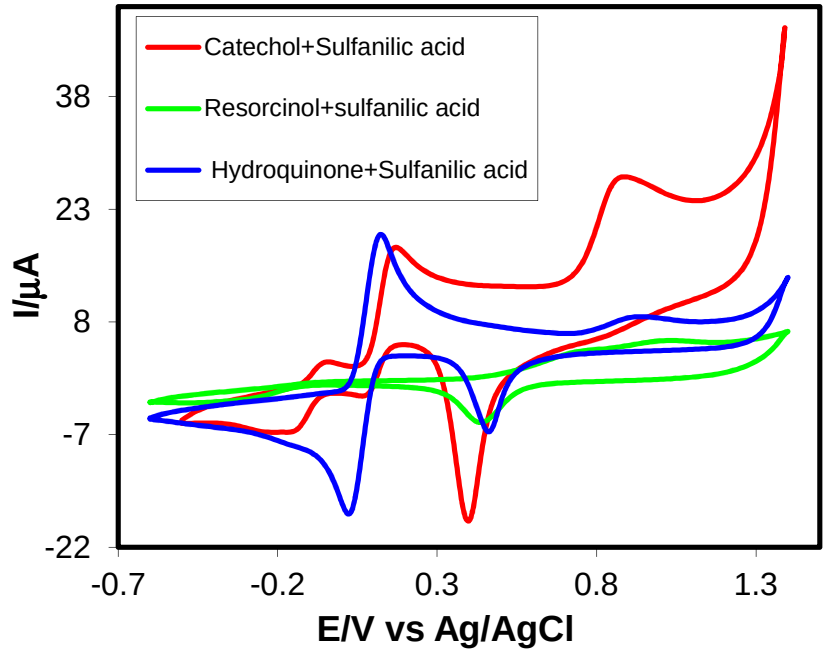

Fig. 4.141: Comparison of cyclic voltammogram of 2mM Catechol, 2mM Resorcinol and 2mM Hydroquinone with Sulfanilic acid in buffer solution (pH 7) of Au electrode at scan rate 0.1V/s (2nd cycle)

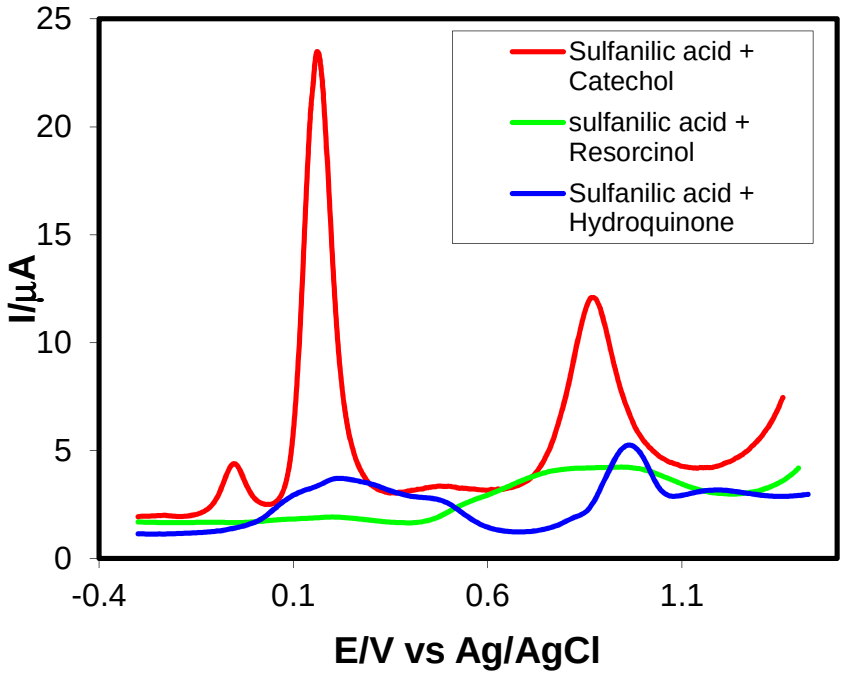

Fig. 4.142: Comparison of differential pulse voltammogram of 2mM Catechol, 2mM Resorcinol and 2mM Hydroquinone with 2mM Sulfanilic acid in buffer solution (pH 7) of Au electrode at scan rate 0.1V/s (2nd cycle)

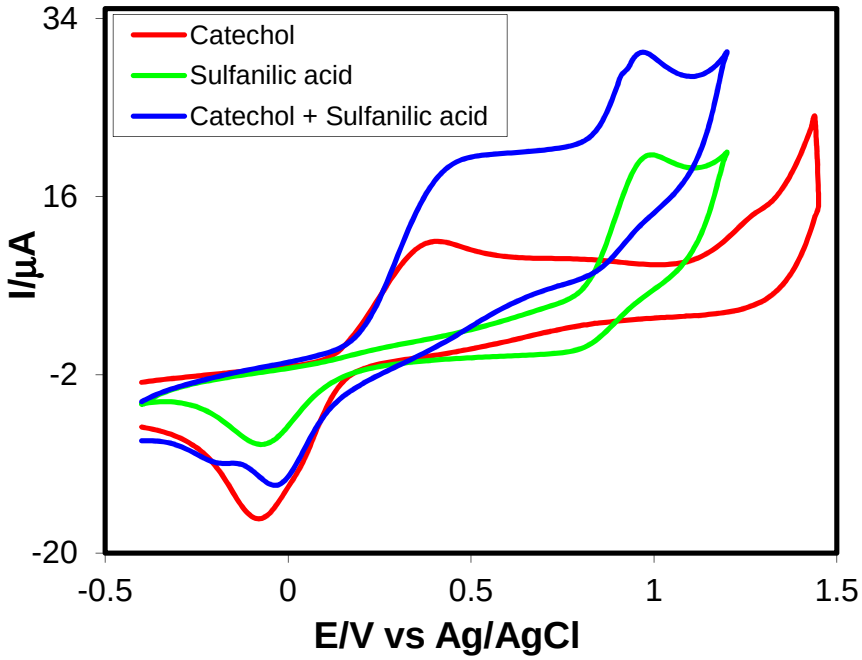

Fig. 4.143: Comparison of cyclic voltammogram of 2mM Catechol, 2mM Sulfanilic acid and 2mM Catechol with 2mM Sulfanilic acid in buffer solution (pH 7) of Pt electrode at scan rate 0.1V/s (1st cycle)

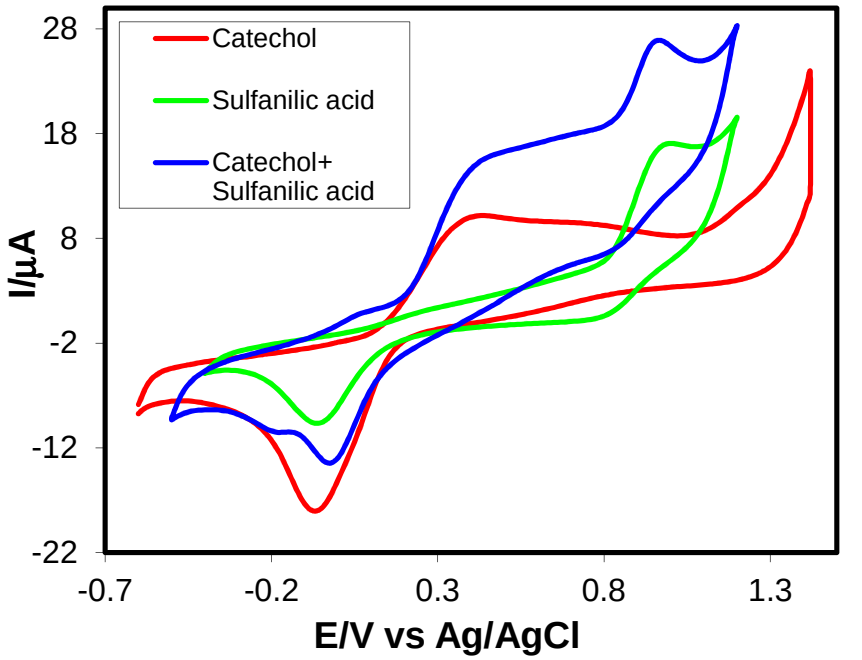

Fig. 4.144: Comparison of cyclic voltammogram of 2mM Catechol, 2mM Sulfanilic acid and 2mM Catechol with 2mM Sulfanilic acid in buffer solution (pH 7) of Pt electrode at scan rate 0.1V/s (2nd cycle)

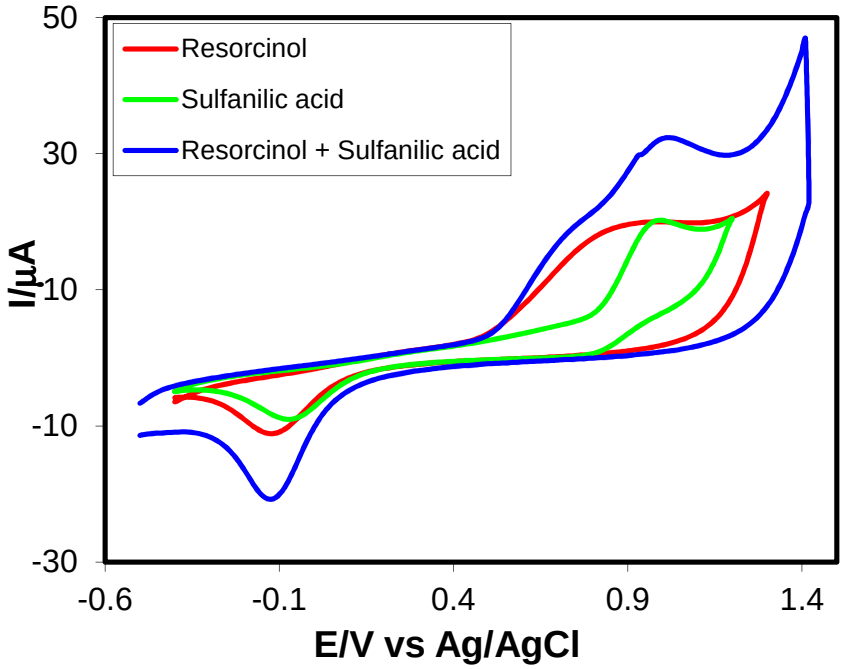

Fig. 4.145: Comparison of cyclic voltammogram of 2mM Resorcinol, 2mM Sulfanilic acid and 2mM Resorcinol with 2mM Sulfanilic acid in buffer solution (pH 7) of Pt electrode at scan rate 0.1V/s (1st cycle)

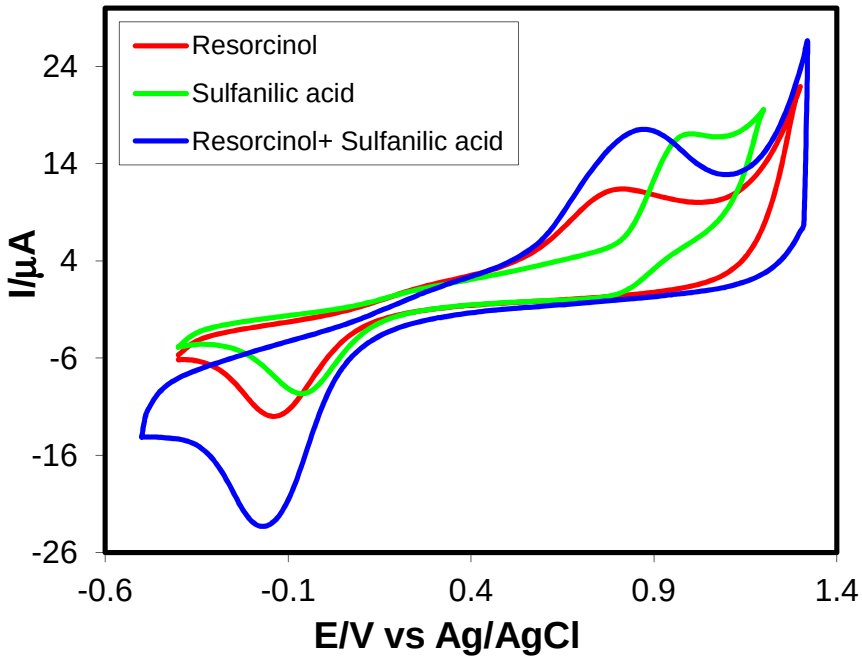

Fig. 4.146: Comparison of cyclic voltammogram of 2mM Resorcinol, 2mM Sulfanilic acid and 2mM Resorcinol with 2mM Sulfanilic acid in buffer solution (pH 7) of Pt electrode at scan rate 0.1V/s (2nd cycle)

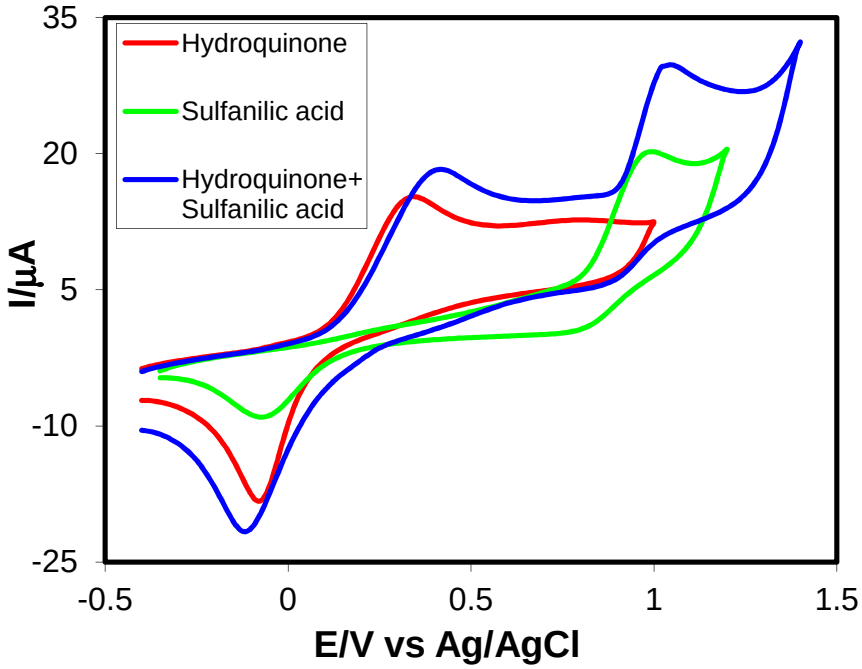

Fig. 4.147: Comparison of cyclic voltammogram of 2mM Hydroquinone, 2mM Sulfanilic acid and 2mM Hydroquinone with 2mM Sulfanilic acid in buffer solution (pH 7) of Pt electrode at scan rate 0.1V/s (1st cycle)

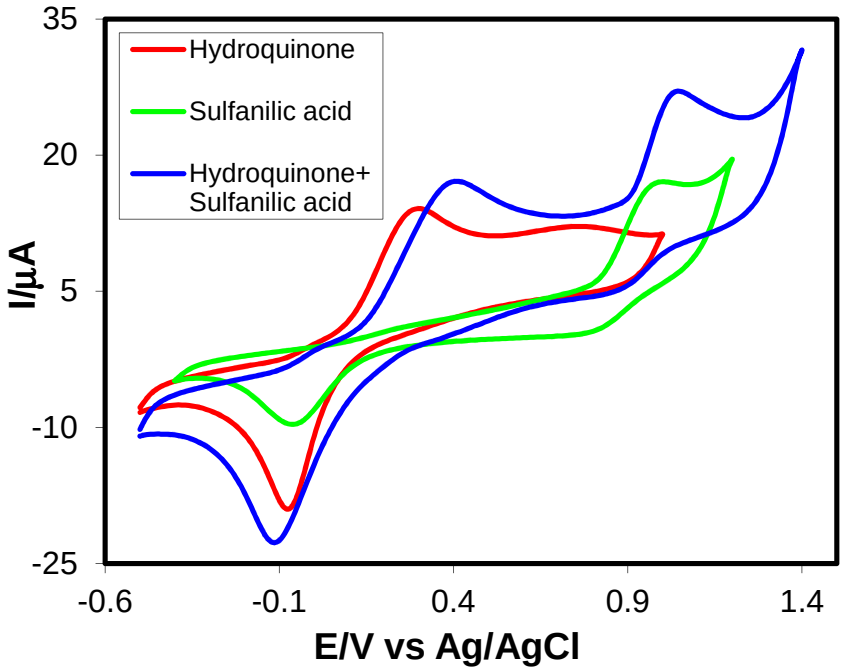

Fig. 4.148: Comparison of cyclic voltammogram of 2mM Hydroquinone, 2mM Sulfanilic acid and 2mM Hydroquinone with 2mM Sulfanilic acid in buffer solution (pH 7) of Pt electrode at scan rate 0.1V/s (2nd cycle)

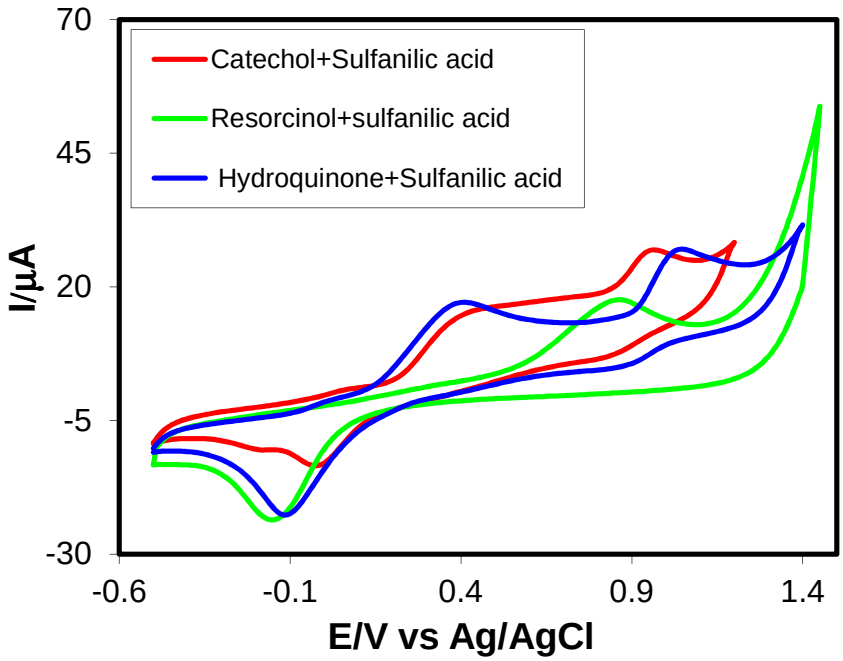

Fig. 4.149: Comparison of cyclic voltammogram of 2mM Catechol, 2mM Resorcinol and 2mM Hydroquinone with Sulfanilic acid in buffer solution (pH 7) of Pt electrode at scan rate 0.1V/s (2nd cycle)

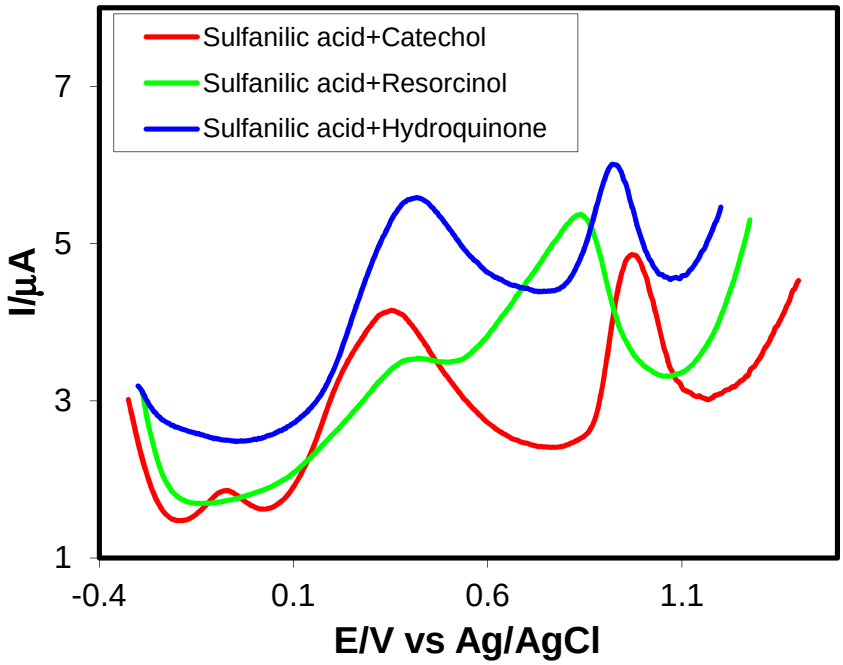

Fig. 4.150: Differential pulse voltammogram of 2mM Catechol, 2mM Resorcinol and 2mM Hydroquinone with 2mM Sulfanilic acid in buffer solution (pH 7) of Pt electrode at scan rate 0.1V/s (2nd cycle)

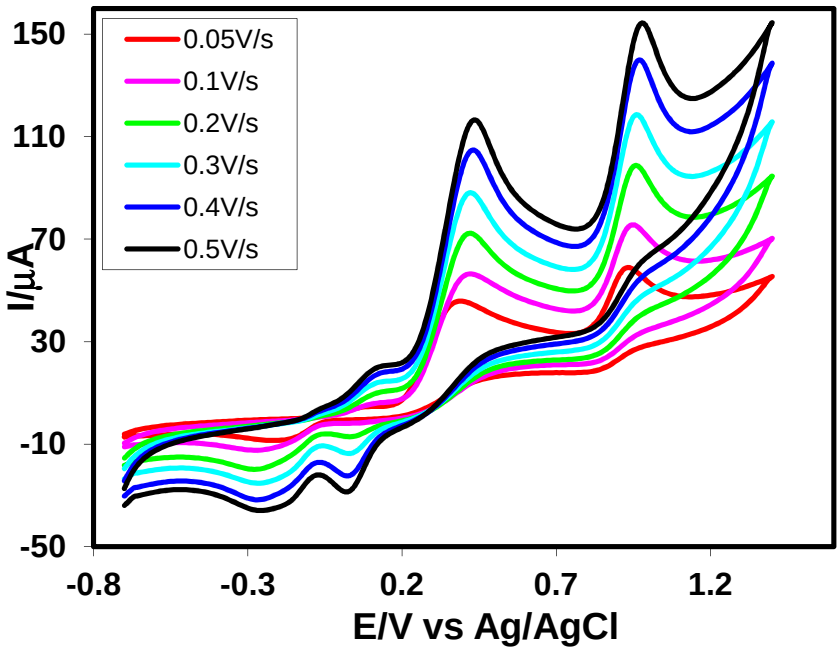

Fig. 4.151: Cyclic voltammogram of 2mM Catechol with 2mM Sulfanilic acid in buffer solution (pH 7) of GC electrode at different scan rate (2nd cycle)

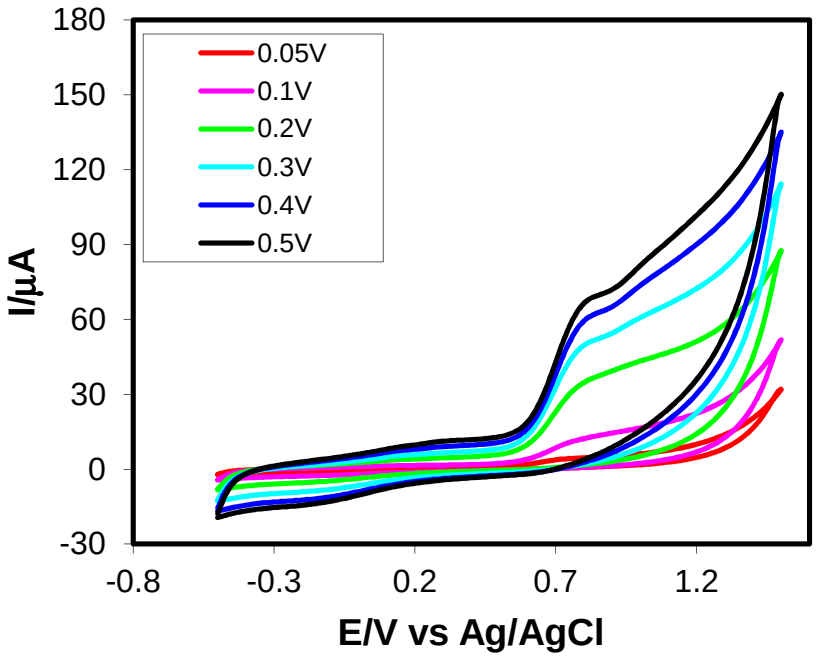

Fig. 4.152: Cyclic voltammogram of 2mM Resorcinol with 2mM Sulfanilic acid in buffer solution (pH 7) of GC electrode at different scan rate (2nd cycle)

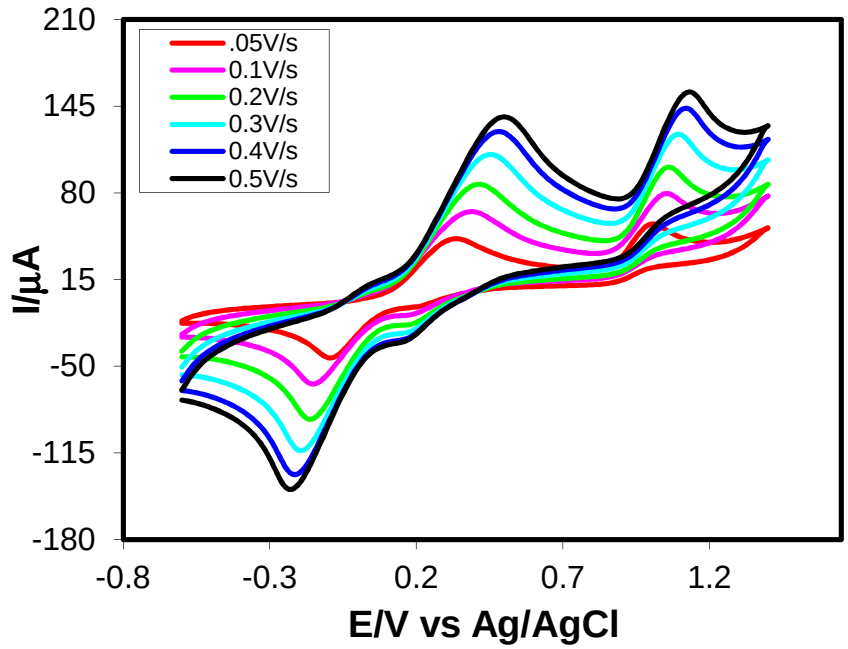

Fig. 4.153: Cyclic voltammogram of 2mM Hydroquinone with 2mM Sulfanilic acid in buffer solution (pH 7) of GC electrode at different scan rate (2nd cycle)

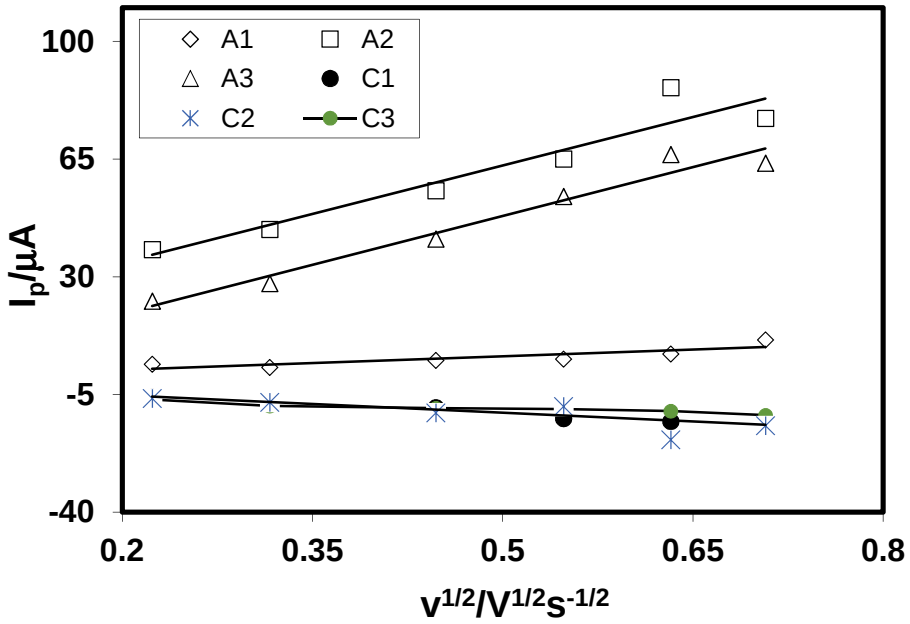

Fig. 4.154: Plots of peak current (I_p) versus square root of scan rate ($v^{1/2}$) of 2mM Catechol with 2mM Sulfanilic acid in buffer solution (pH 7) of GC electrode (2nd cycle)

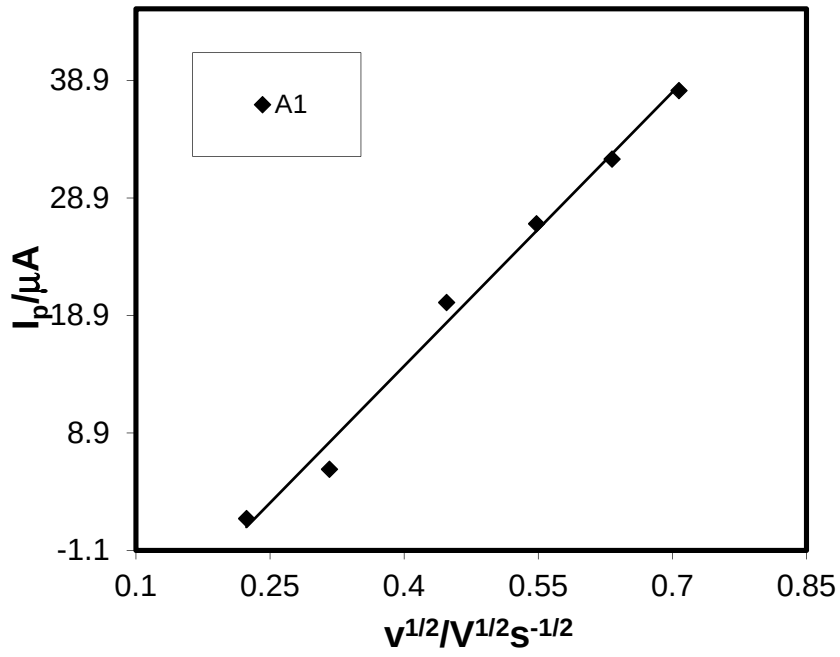

Fig. 4.155: Plots of peak current (I_p) versus square root of scan rate ($v^{1/2}$) of 2mM Resorcinol with 2mM Sulfanilic acid in buffer solution (pH 7) of GC electrode (2nd cycle)

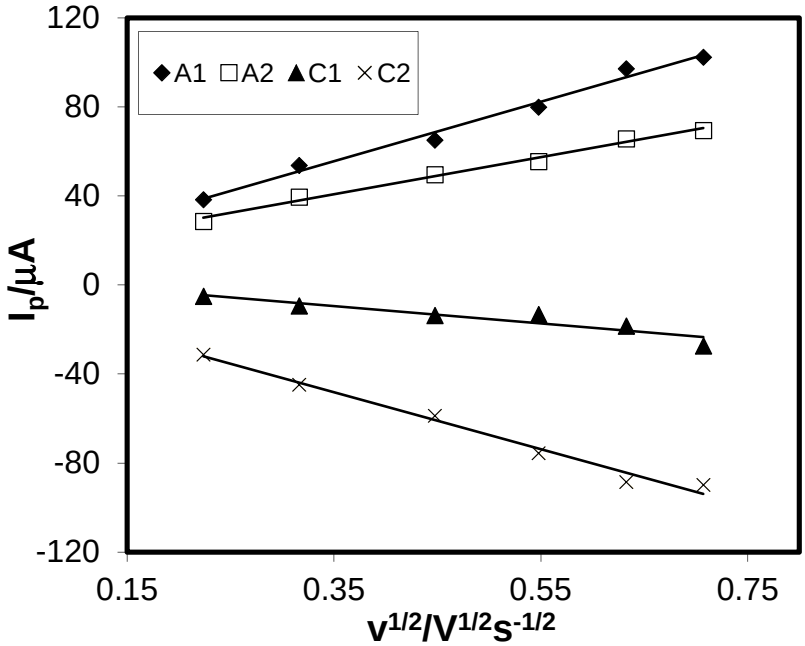

Fig. 4.156: Plots of peak current (I_p) versus square root of scan rate ($v^{1/2}$) of 2mM Hydroquinone with 2mM Sulfanilic acid in buffer solution (pH 7) of GC electrode (2nd cycle)

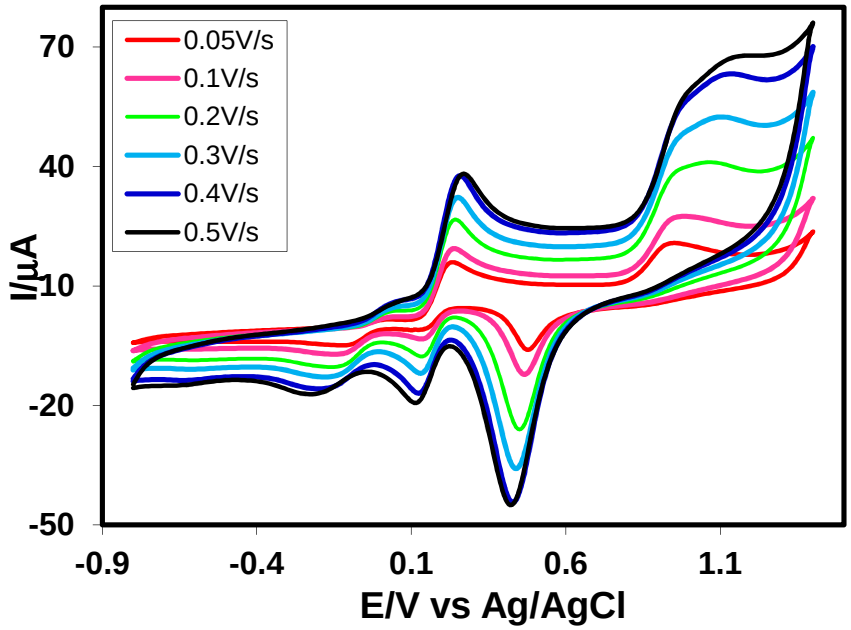

Fig. 4.157: Cyclic voltammogram of 2mM Catechol with 2mM Sulfanilic acid in buffer solution (pH 7) of Au electrode at different scan rate (2nd cycle)

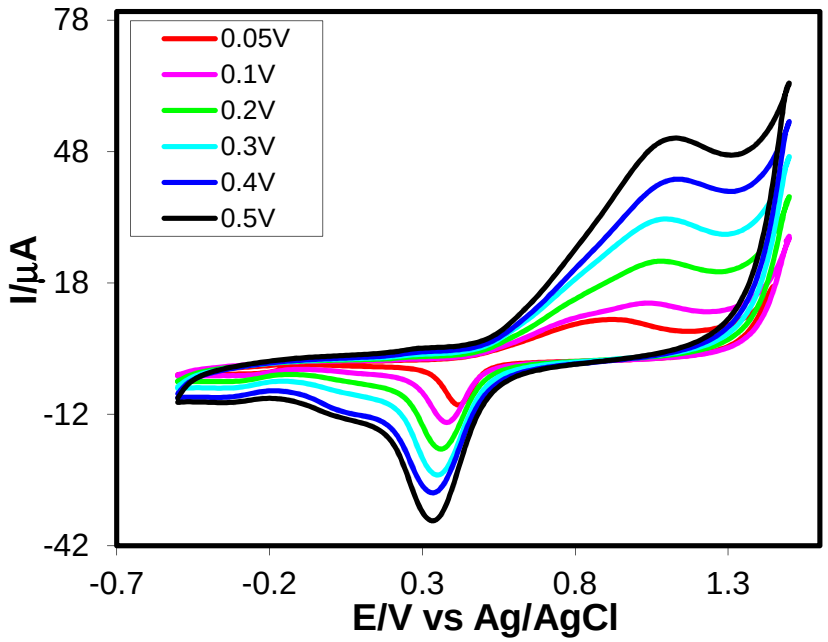

Fig. 4.158: Cyclic voltammogram of 2mM Resorcinol with 2mM Sulfanilic acid in buffer solution (pH 7) of Au electrode at different scan rate (2nd cycle)

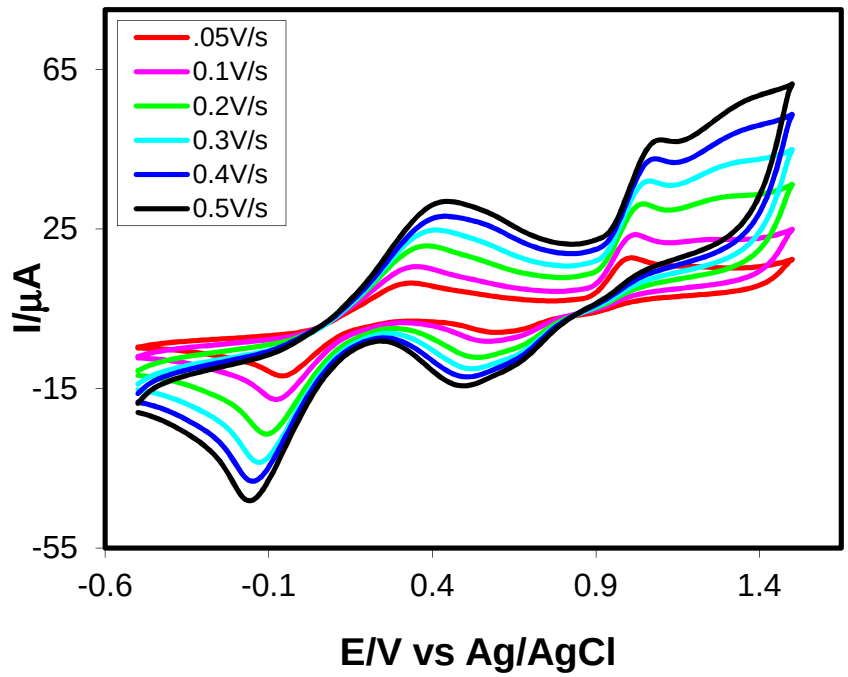

Fig. 4.159: Cyclic voltammogram of 2mM Hydroquinone with 2mM Sulfanilic acid in buffer solution (pH 7) of Au electrode at different scan rate (2nd cycle)

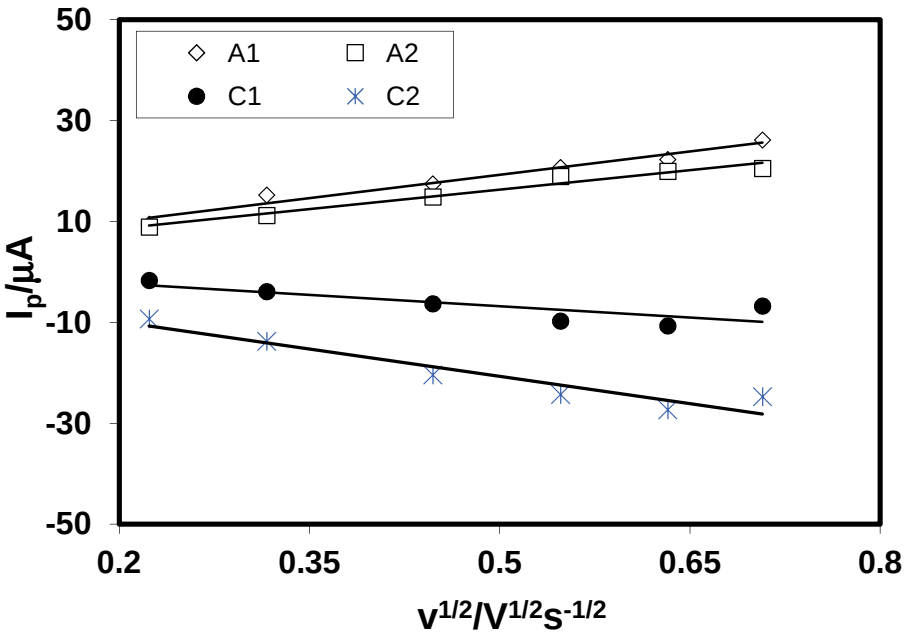

Fig. 4.160: Plots of peak current (I_p) versus square root of scan rate ($v^{1/2}$) of 2mM Catechol with 2mM Sulfanilic acid in buffer solution (pH 7) of Au electrode (2nd cycle)

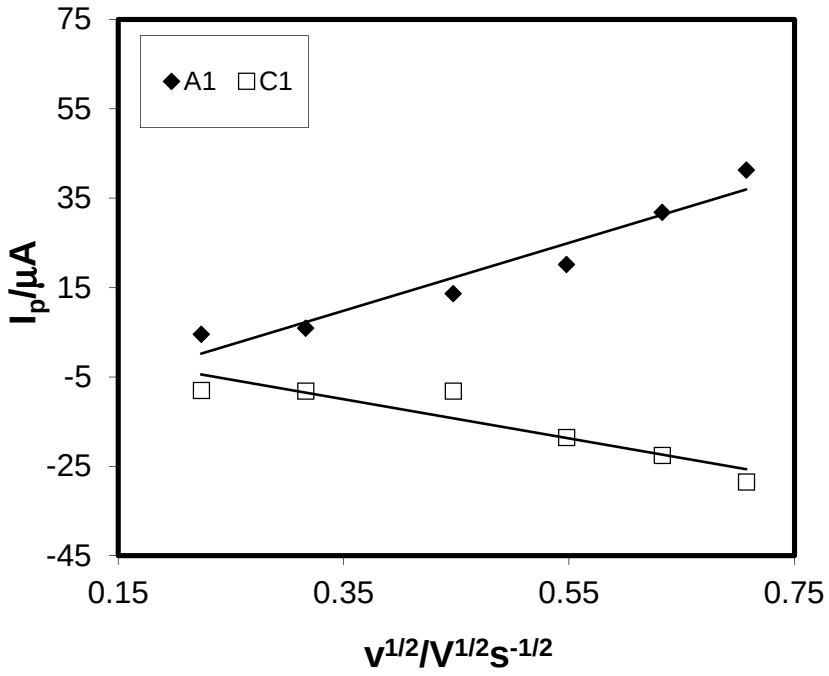

Fig. 4.161: Plots of peak current (I_p) versus square root of scan rate ($v^{1/2}$) of 2mM Resorcinol with 2mM Sulfanilic acid in buffer solution (pH 7) of Au electrode (2nd cycle)

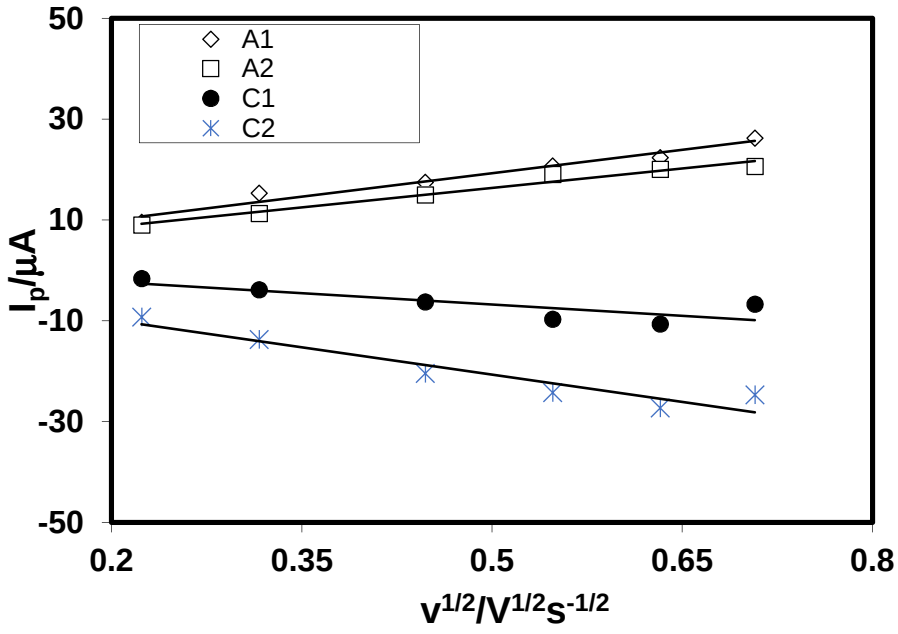

Fig. 4.162: Plots of peak current (I_p) versus square root of scan rate ($v^{1/2}$) of 2mM Hydroquinone with 2mM Sulfanilic acid in buffer solution (pH 7) of Au electrode (2nd cycle)

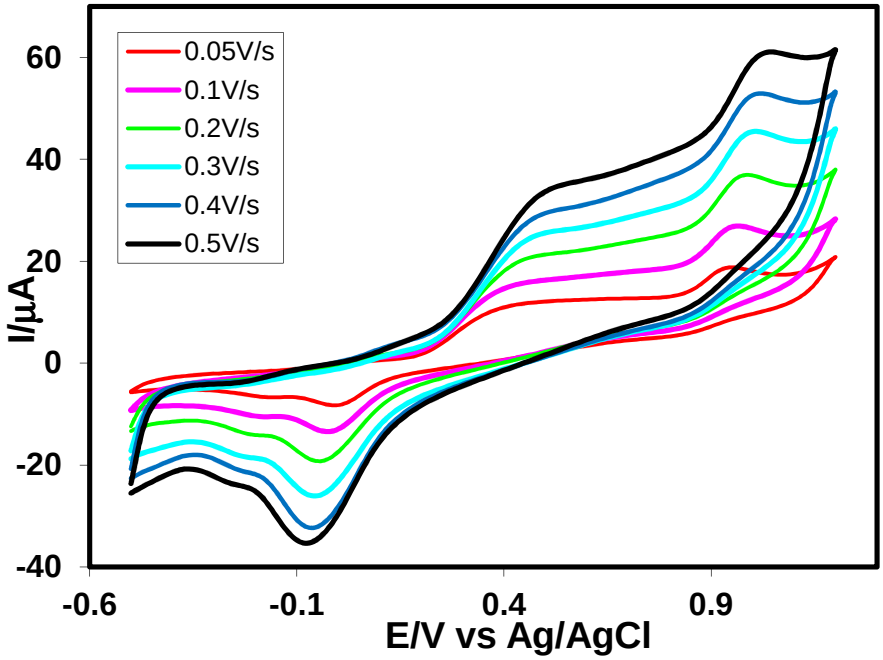

Fig. 4.163: Cyclic voltammogram of 2mM catechol with 2mM Sulfanilic acid in buffer solution (pH 7) of Pt electrode at different scan rate (2nd cycle)

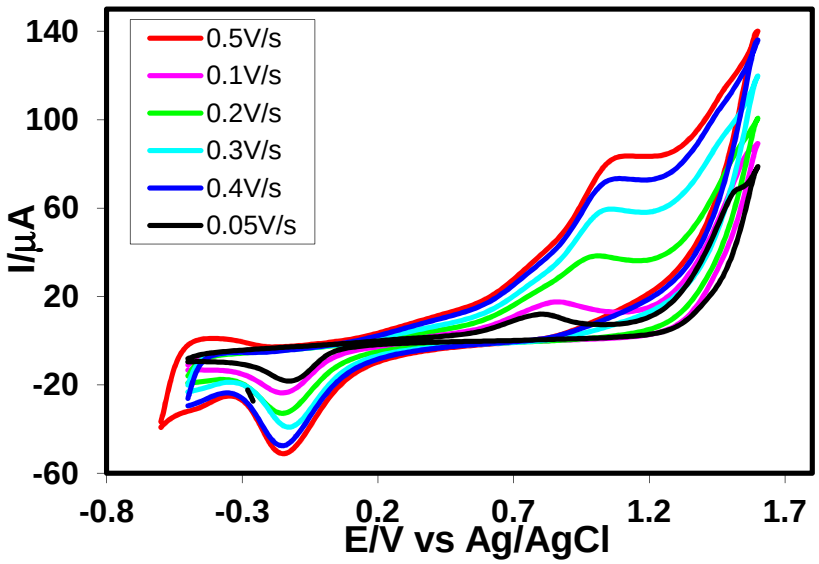

Fig. 4.164: Cyclic voltammogram of 2mM Resorcinol with 2mM Sulfanilic acid in buffer solution (pH 7) of Pt electrode at different scan rate (2nd cycle)

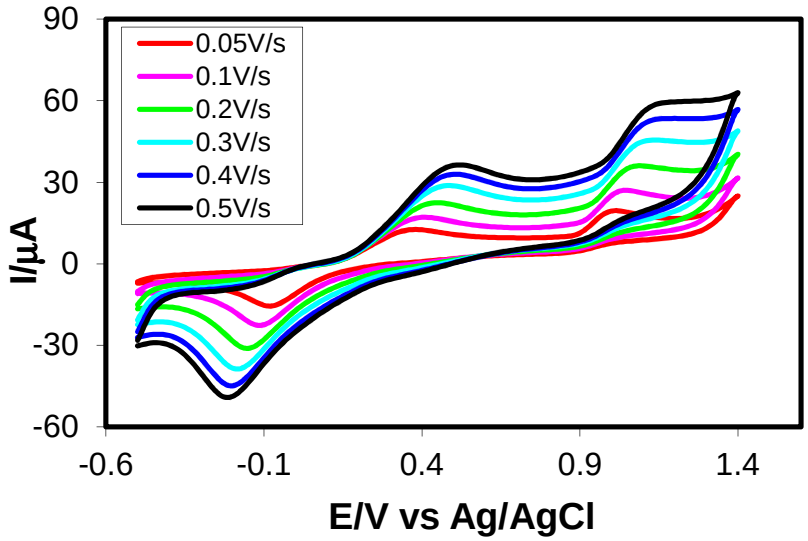

Fig. 4.165: Cyclic voltammogram of 2mM Hydroquinone with 2mM Sulfanilic acid in buffer solution (pH 7) of Pt electrode at different scan rate (2nd cycle)

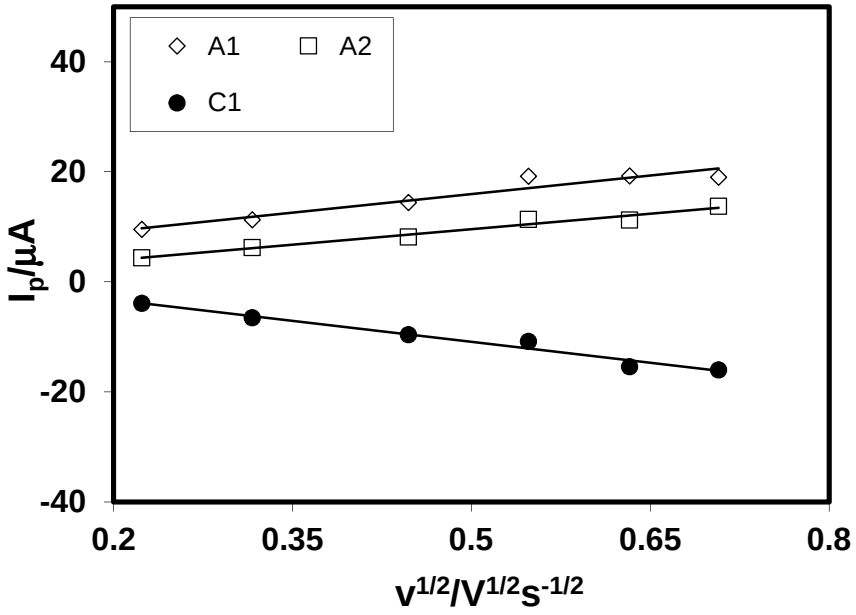

Fig. 4.166: Plots of peak current (I_p) versus square root of scan rate ($v^{1/2}$) of 2mM Catechol with 2mM Sulfanilic acid in buffer solution (pH 7) of Pt electrode (2nd cycle)

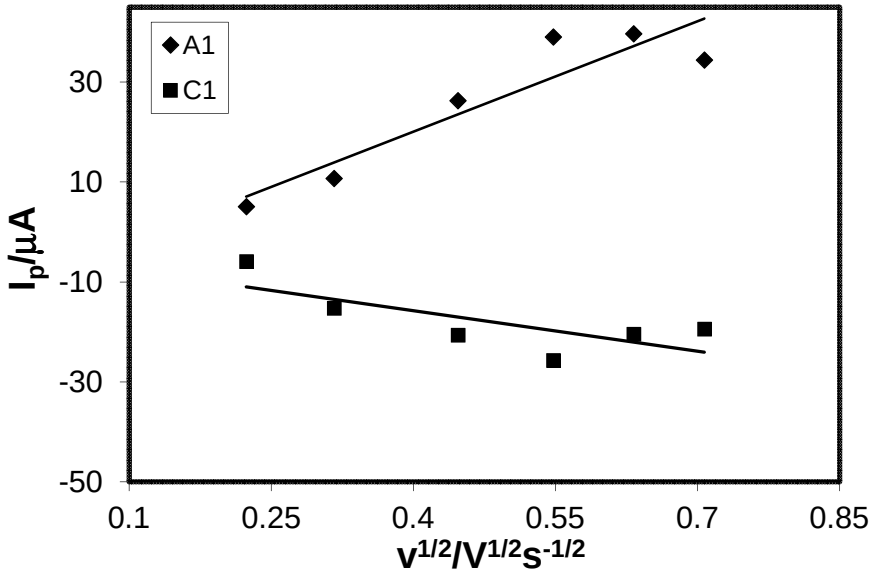

Fig. 4.167: Plots of peak current (I_p) versus square root of scan rate ($v^{1/2}$) of 2mM Resorcinol with 2mM Sulfanilic acid in buffer solution (pH 7) of Pt electrode (2nd cycle)

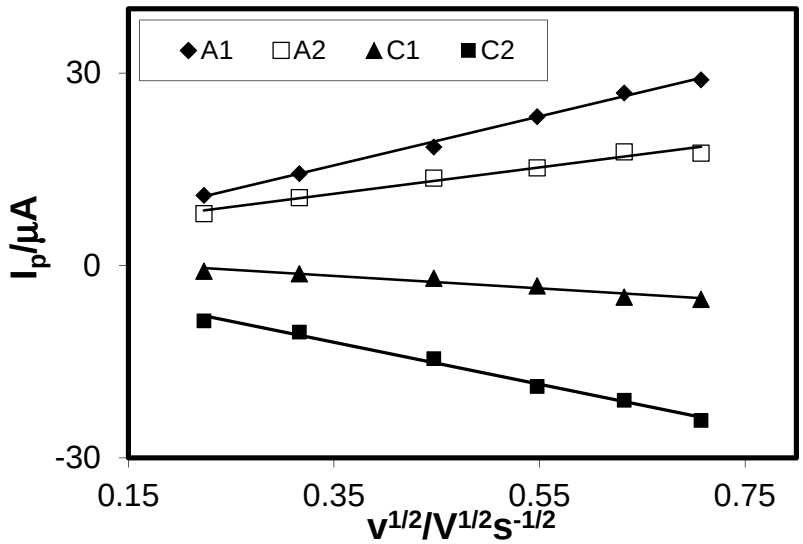

Fig. 4.168: Plots of peak current (I_p) versus square root of scan rate ($v^{1/2}$) of 2mM Hydroquinone with 2mM Sulfanilic acid in buffer solution (pH 7) of Pt electrode (2nd cycle)

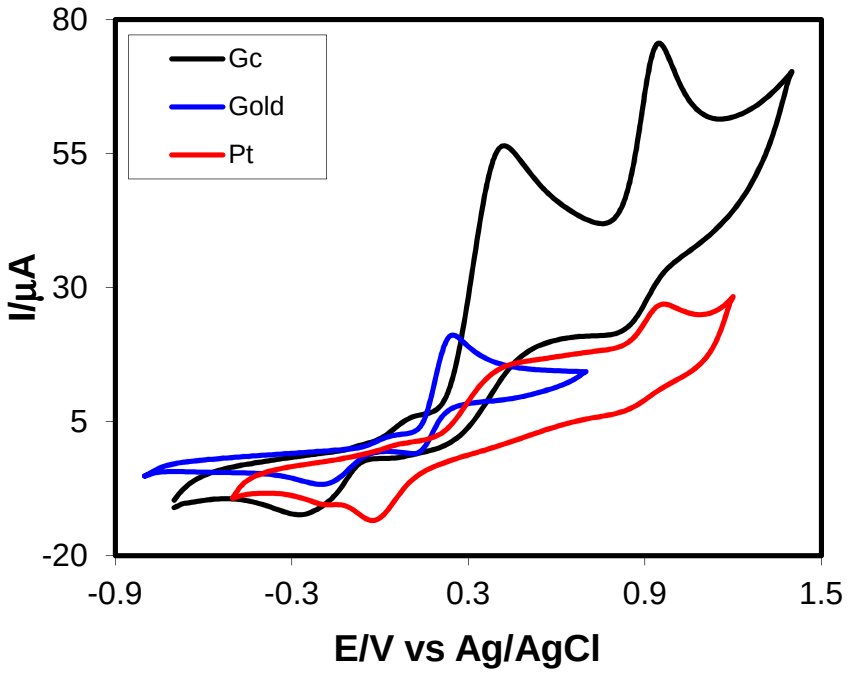

Fig. 4.169: Comparison of Cyclic voltammogram of 2mM Catechol with 2mM Sulfanilic acid of GC electrode (3.0mm), Au electrode (1.6mm) and Pt electrode (1.6mm) in buffer solution pH 7 at scan rate 0.1V/s (2nd cycle)

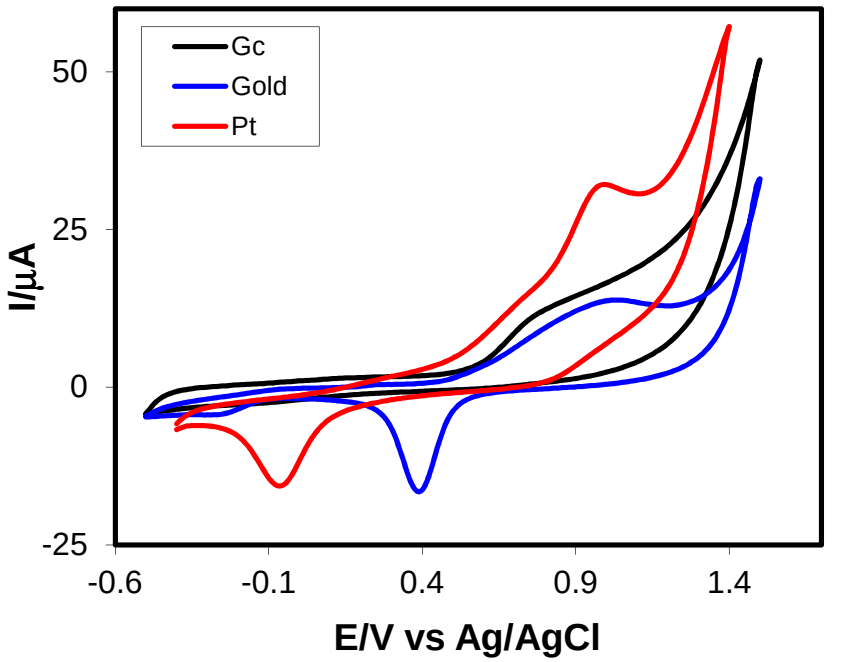

Fig. 4.170: Comparison of Cyclic voltammogram of 2mM Resorcinol with 2mM Sulfanilic acid of GC electrode (3.0mm), Au electrode (1.6mm) and Pt electrode (1.6mm) in buffer solution pH 7 at scan rate 0.1V/s (2nd cycle)

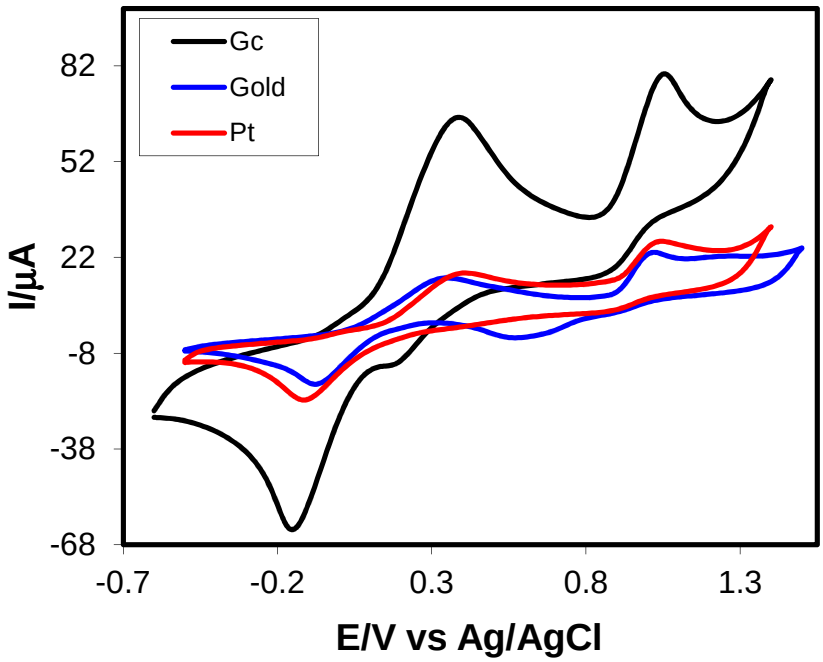

Fig. 4.171: Comparison of Cyclic voltammogram of 2mM Hydroquinone with 2mM Sulfanilic acid of GC electrode (3.0mm), Au electrode (1.6mm) and Pt electrode (1.6mm) in buffer solution pH 7 at scan rate 0.1V/s (2nd cycle)

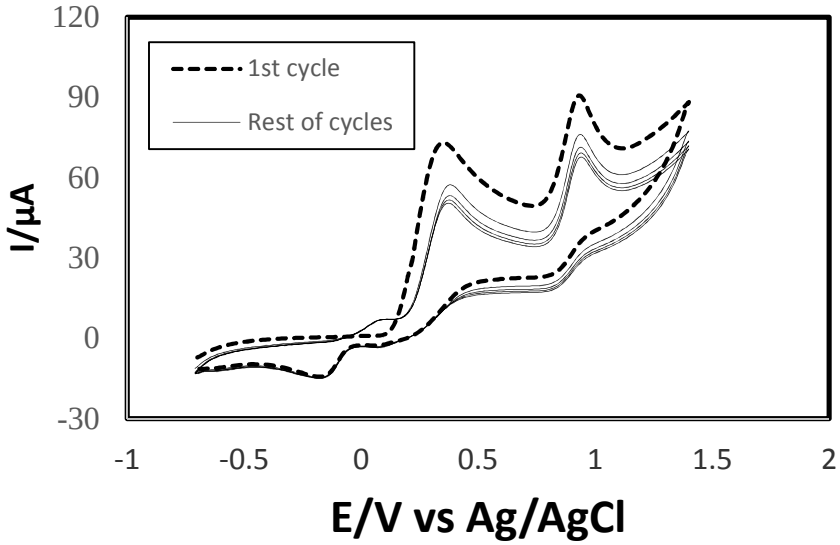

Fig: 4.172: Cyclic voltammogram of 2mM catechol with 2mM Sulfanilic acid in presence of buffer solution pH 7 (phosphate buffer) GC electrode at scan rate 0.1V/s (5 cycles)

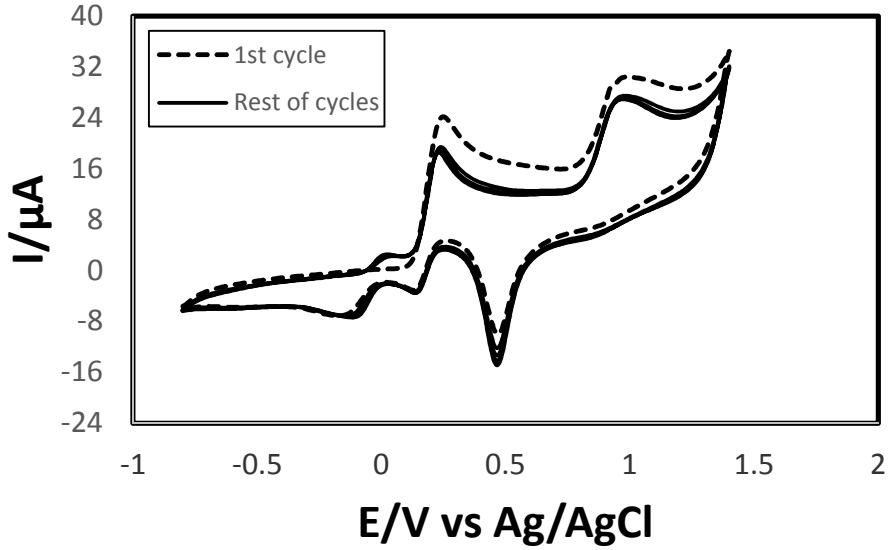

Fig: 4.173: Cyclic voltammogram of 2mM catechol with 2mM Sulfanilic acid in presence of buffer solution pH 7 (phosphate buffer) Au electrode at scan rate 0.1V/s (5 cycles)

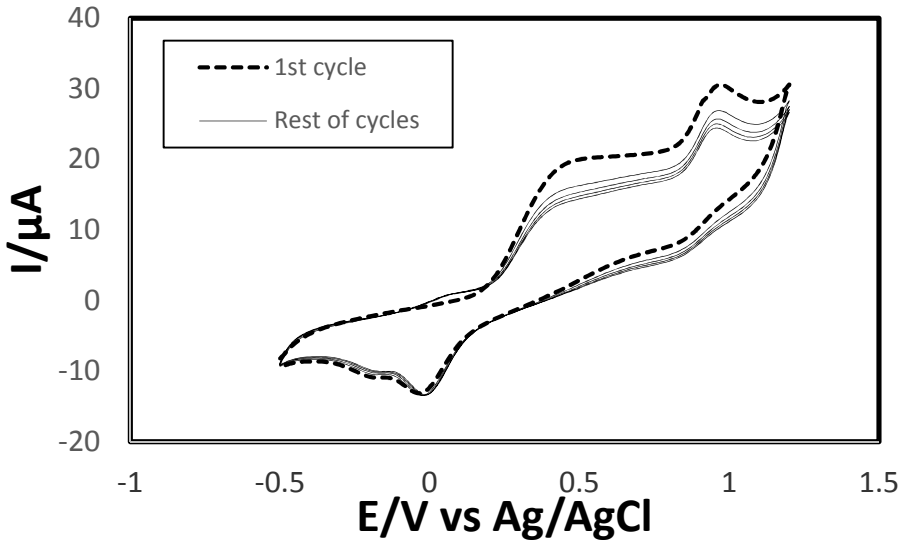

Fig: 4.174: Cyclic voltammogram of 2mM catechol with 2mM Sulfanilic acid in presence of buffer solution pH 7 (phosphate buffer) Pt electrode at scan rate 0.1V/s (5 cycles)

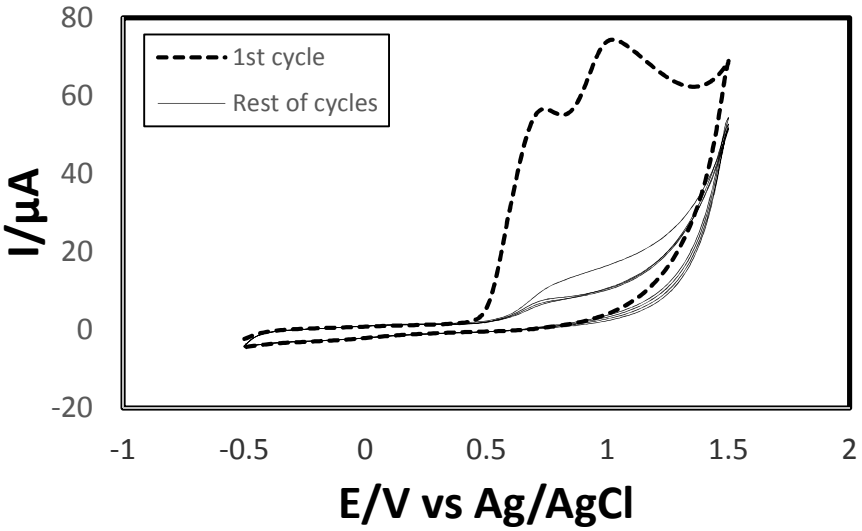

Fig: 4.175: Cyclic voltammogram of 2mM Resorcinol with 2mM Sulfanilic acid in presence of buffer solution pH 7 (phosphate buffer) GC electrode at scan rate 0.1V/s (5 cycles)

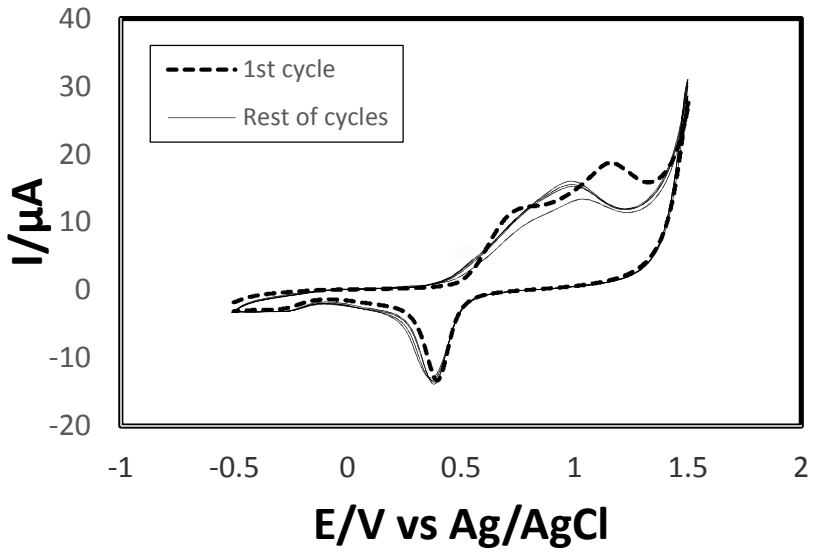

Fig: 4.176: Cyclic voltammogram of 2mM Resorcinol with 2mM Sulfanilic acid in presence of buffer solution pH 7 (phosphate buffer) Au electrode at scan rate 0.1V/s (5 cycles)

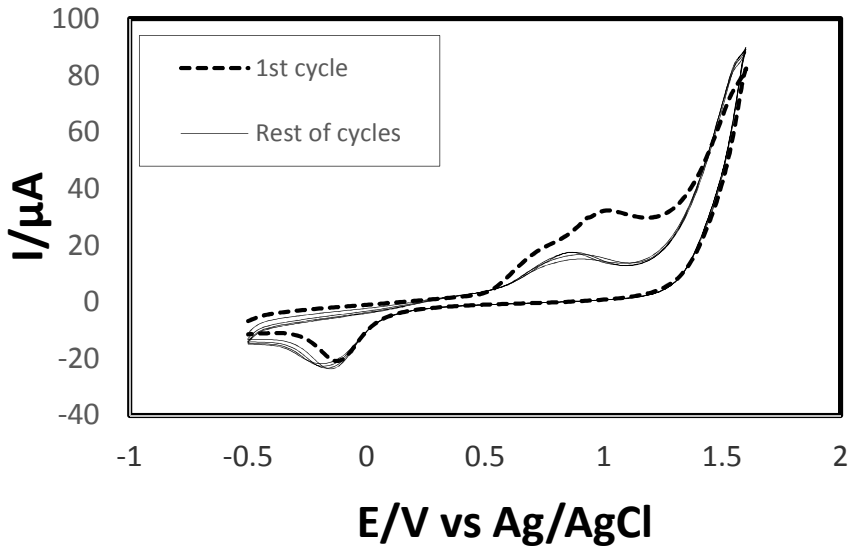

Fig: 4.177: Cyclic voltammogram of 2mM Resorcinol with 2mM Sulfanilic acid in presence of buffer solution pH 7 (phosphate buffer) Pt electrode at scan rate 0.1V/s (5 cycles)

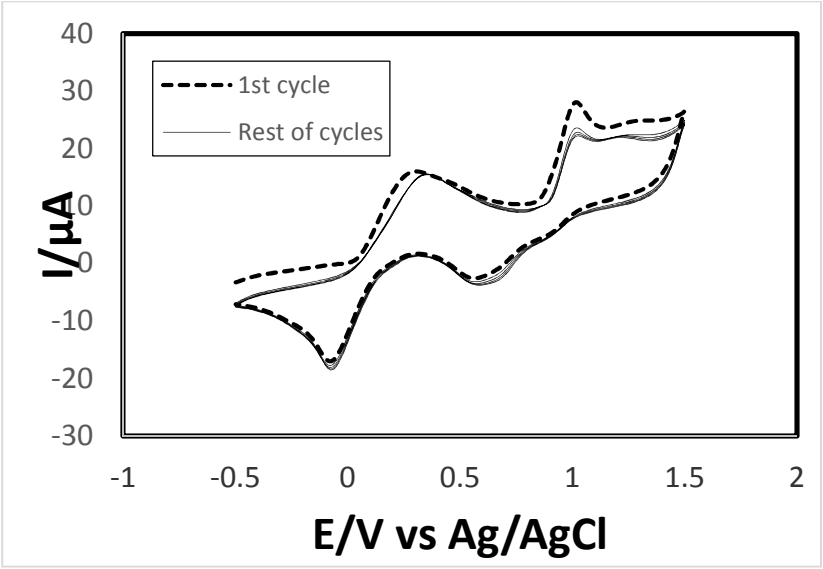

Fig: 4.178: Cyclic voltammogram of 2mM Hydroquinone with 2mM Sulfanilic acid in presence of buffer solution pH 7 (phosphate buffer) GC electrode at scan rate 0.1V/s (5 cycles)

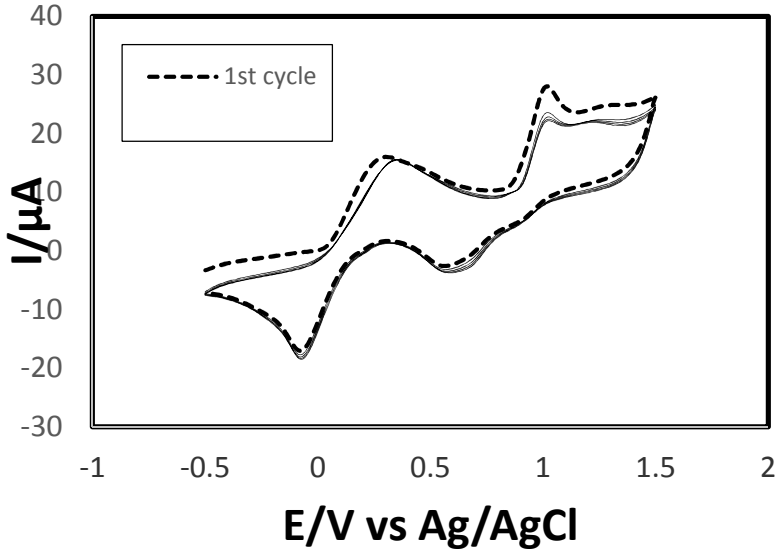

Fig: 4.179: Cyclic voltammogram of 2mM Hydroquinone with 2mM Sulfanilic acid in presence of buffer solution pH 7 (phosphate buffer) Au electrode at scan rate 0.1V/s (5 cycles)

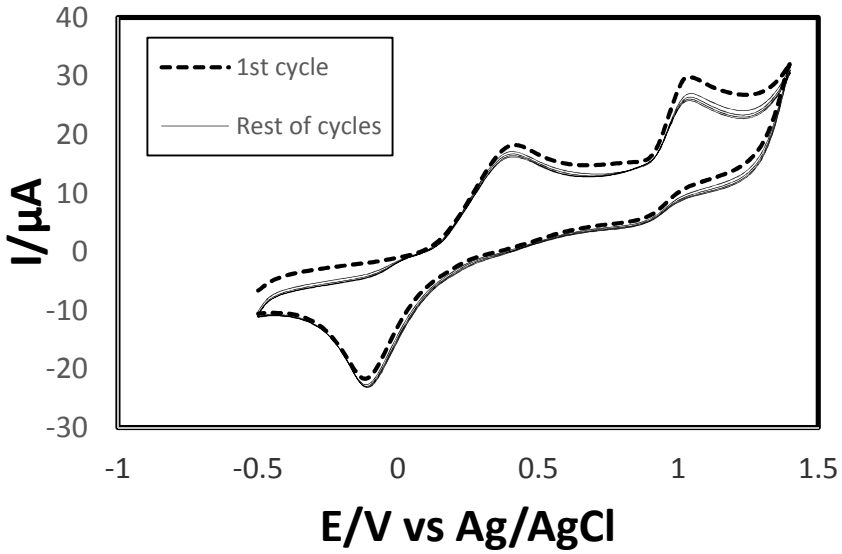

Fig: 4.180: Cyclic voltammogram of 2mM Hydroquinone with 2mM Sulfanilic acid in presence of buffer solution pH 7 (phosphate buffer) Pt electrode at scan rate 0.1V/s (5 cycles)

Conclusion

The redox interaction of` the isomers of dihydroxybenzene have been studied by using cyclic voltammetry (CV) and differential pulse voltammetry (DPV) technique. The study has been carried out at different electrodes in different pH, KCl media, at various scan rates and various concentrations.

Both catechol and hydroquinone provided two anodic and two cathodic peaks in KCl media. But catechol and hydroquinone show one pair of redox peaks in buffer solution of pH 7 at GC and Pt electrode. At Au electrode, catechol and hydroquinone show two pairs of redox peaks at different pH. Resorcinol shows irreversible anodic peak at GC electrode but it shows quasi-reversible voltammogram in Pt and Au electrodes in all electrolytic media. The interaction energy of hydroquinone, catechol and resorcinol in KCl media are 38.60J, 37.63J and 0.0J respectively. This result suggests that the redox interactions of hydroquinone and catechol are higher in KCl media than acetate and phosphate buffer solution. Also the redox interactions of hydroquinone and catechol are higher in Au electrode than the Gc and Pt electrodes. This also suggests that the redox interaction of hydroquinone is higher than catechol and catechol is higher than resorcinol. The redox interactions of the dihydroxybenzene isomers are media dependent.

For all the systems, the peak current ratios have been found to be greater than unity. The electrode reaction of dihydroxybenzene isomers in presence of Sulfanilic acid has been studied by cyclic voltammetry and differential pulse voltammetry. Voltammetric appearance reflected that sulfanilic acid has been formed adduct with catechol and hydroquinone. But no reaction has been occurred between sulfanilic acid and resorcinol. This result suggest that redox interaction at para and ortho-position is higher than meta-position which is consistent with the common sense of organic chemistry concept- a substation reaction at a meta-position is unfavorable to that at a para or ortho –position.

REFERENCES

1. Kim, D. H, Britt, R. D, Klein, M.P. and Sauger, K., 1990, J. Am. Chem. Soc., Vol. 112, p. 9389.

2. Bard, A. J., 1971, Pure Appl. Chem., Vol. 25, p. 379.

3. Demadis, K. D, Hartshorn, C. M. and Meyer, T. J., 2001, Chem. Rev., Vol. 101, p. 2655.

4. Barlow, S. and O'Hare, D., 1997, Chem. Rev., Vol. 97 p. 637.

5. Barriere, F. and Geiger, W. E., 2006, J. Am. Chem. Soc., Vol. 128, p. 3980

6. Motin Md. Abdul, 2007, "Electroactive arylamines with multi step electron transfer reaction", PhD thesis, Fukui University, Japan.

7. Creutz, C. and Taube, H., 1969, J. Am. Chem. Soc., Vol. 91, p 3988

8. D. Richardson and H. Taube, 1981, Inorg. Chem., Chap.20, p. 1278.

9. Kramer, J. A. and Hendrickson, D. N., 1980, Inorg. Chem., Vol. 19, p. 3330.

10. N. S. Hush Prog., 1967, Inorg. Chem., 8, p. 391.

11. Richardson, D. E. and Taube, H., 1984, Coord. Chem. Rev., Vol. 60, p. 107.

12. Ammar F. and Saveant, J.M., 1973, J. Electroanal. Chem., Vol. 47, p. 215.

13. Saji, T., Pasch, N. F., Webber, S. E. and Bard, A. J., 1978, J. Phys. Chem., Vol. 82, p. 1101.

14. Flanagan, J. B., Margel, S., Bard, A. J. and Anson, F. C., 1978, J. Am. Chem. Soc., Vol. 100, p. 4248

15. Creutz, C. and Taube, H., 1969, J. Am. Chem. Soc., Vol. 91, p. 3988

16. Abruna, H. D., 1988, Coord. Chem. Rev., Vol. 86, p. 135.

17. Roth, H. D., 1986, Tetrahedron, Vol. 42, p. 6097.

18. Lambert, C. and Noell, G., 2002, J. Chem. Soc. Perkin Trans., Vol. 2 p. 2039.

19. Aoki, K. and Chen, J., 1995, J. Electroanal. Chem., Vol. 380, p. 35.

20. Aoki, K., Chen, J. Nishihara, H. and Hirao, T., 1996, J. Electroanal. Chem., Vol. 416, p. 151.

21. Pe´rez, I., Liu, S.-G., Martı´n N. and Echegoyen, L., 2000, J. Org. Chem., Vol. 65, pp. 3796-3803.

22. Wienk, M.M. and Janssen, R.A.J., 1997, J. Am. Chem. Soc., Vol. 119, p. 4492.

23. B.A. Barner, 2004, "Catechol" in Encyclopedia of Reagents for Organic Synthesis Wiley & Sons, New York, (Ed: L. Paquette)

24. Fahlbusch, K.G. Hammerschmidt, F. J. and Panten, J., 2005, "Horst SurburgFlavors and Fragrances" in Ullmann`s Encyclopediaof Industrial Chemistry, Wiley- VCH.

25. Fiegel, H., Voges, H. W., Hamamoto, T., Umemura, S. and Lwata, T., 2002, "Phenol Derivatives" in Ullmann`s Encyclopedia of Industrial Chemistry, Wiley- VCH.

26. S. Auerbach, Paul**.** Wilderness Medicine. Philadelphia, PA: Mosby, Inc., an affiliate of Elsevier Inc., 2007. ISBN: 978-0-323-03228-5

27. United Nations Environment Programme World Health Organization**.** Hydroquinone: Health and Safety Guide No. 101. IPCS International Programme on ChemicalSafety. [Online] 1996.

28. Nishiumi, T., Chimoto, Y., Hagiwara, Y., Higuchi, M. and Yamamoto K., 2004, Macromolecules, Vol. 37, pp. 2661-2664.

29. Wurster, C., 1879, Chem. Ber., Vol. 12, p. 522 and 2071; Wurster, C., Sendner, R., 1879, Chem. Ber., Vol. 12, p. 1803; Wurster, C. and Schobig, E., 1879, Chem. Ber., Vol. 12, p. 1807.

30. Weitz, E., 1928, Electrochem, Vol. 34, p. 538.

31. Weissman, S.I., Townsend, J., Paul, D.E., Park, G.E., 1953, J. Chem. Phys., Vol. 21, p. 2227.

32. Coropceanu, V., Gruhn, N. E., Barlow, S., Lambert, C., Durivage, J. C., Bill, T. G., Noll, G., Marder, S. R. and Bre´das, J.-L., 2004, J. Am. Chem. Soc., Vol. 126, pp. 2727-2731.

33. Chiu, K. Y., Su, T.-H., Huang, C. W., Liou, G.-S. and Cheng, S.-H., 2005, J. Electroana. Chem., Vol. 578, pp. 283–287.

34. Nelsen, S. F., Ismagilov, R. F. and Powell, D. R., 1996, J. Am. Chem. Soc., Vol. 118, pp. 6313-6314.

35. C. Creutz, 1983, In Progress in Inorganic Chemistry, Lippard, S. J., Ed. Wiley and Sons: New York, Vol. 30, p. 1.

36. Richardson, D. E. and Taube, H., 1984, Coord. Chem. Rev., Vol. 60, p. 107.

37. Ward, M. D., 1995, Chem. Soc. Rev., p. 121.

38. Chen, P. and Meyer, T. J., 1998, Chem. Rev., Vol. 98 p. 1439.

39. Barlow, S. and Marder, S. R., 2000, Chem. Commun., 1555.

40. Astruc, D., 1997, Acc. Chem. Res., Vol. 30, p. 383.

41. R. J. Crutchley, 1994, Adv. Inorg. Chem., Vol. 33, p. 273.

42. Paul, F. and Lapinte, C., 1998, Coord. Chem. Rev., Vol. 178, p. 431.

43. Crutchley, R. J., 2001, Coord. Chem. Rev., Vol. 25, pp. 219-221.

44. Al-Noami, M., Yap, G. P. A. and Crutchley, R. J., 2004, Inorg. Chem., Vol. 43, p. 1770.

45. Nelsen, S. F., 2000, Chem. Eur. J.,Vol. 6, p. 581.

46. Lambert, C. and Noell, G., 2002, J. Chem. Soc., Perkin Trans., 2Vol. p. 2039.

47. Lindeman, S. V, Rosokha, S. V, Sun, D. and Kochi, J. K., 2002, J. Am. Chem. Soc., Vol. 124, p. 843.

48. Motin, M.A. Nishiumi, T., and Aoki K, 2007, J. of Electroanal. Chem., Vol. 601, pp 139–147.

49. http://en.wikipedia.org/wiki/Catechol.

50. Briggs, D.E.G., 1999, "Molecular taphonomy of animal and plant cuticles selective preservation and diagenesis". Philosophical Transactions of the Royal Society B: Biological Sciences, Vol. 7, p. 354.

51. S. Auerbach, Paul**.** *Wilderness Medicine*. Philadelphia, PA : Mosby, Inc., an affiliate of Elsevier Inc., 2007. ISBN: 978-0-323-03228-5

52. http://www.inchem.org/documents/hsg/hsg/hsg101.htm#SectionNumber:2.5

53. C.M.A. Brett and A.M.O. Brett, 1993, Electrochemistry Principles, Methods and Applications, Oxford University Press.

54. Nematollahi, D. and Goodarzi, H., 2001, Iran Journal of Electroanalytical Chemistry, Vol. 510, p. 108.

55. Nematollahi, D. and Goodarzi, H., 1997, Iran Journal of Science and Technology, Vol. 21, p. 121.

56. Nematollahi, D. and Forooghi, Z., 2002, Tetrahedron Letters, Vol. 58, p. 4949.

57. Shahrokhian, S. and Hamzehloei, A., 2003, Electrochemistry Communications, Vol. 5, p. 706.

58. Grujic, Z., Tabakovic, I. and Trkovnic, M., 1976, Tetrahedron Letters, Vol. 52, p. 4823.

59. Tabakovic, I., Grujic, Z. and Bejtovic, Z., 1983, Journal of Heterocyclic Chemistry, Vol. 20, p. 635.

60. Golabi, S.M, Nourmohammadi, F. and Saadnia, A., 2002, Journal of Electroanalytical Chemistry, Vol. 529, p. 12.

61. Fotouhi, L., Kiani, S.T., Nematollahi, D. and Heravi, M.M., 2007, Journal of Electroanalytical Chemistry, Vol. 10, p. 1002.

62. M. E. Hossain, 2014, "Electrochemical sensor simultaneous detection and estimation of environmental toxic pollutants", M.Phil Thesis, KUET.

63. D.A. Skoog, F.J. Holler and T.A. Nieman, 2007, "Principles of Instrumental Analysis", Thomson Brooks/ Cole, 6th Ed., pp. 349-351.

64. P.T. Kissinger and W.R. Heineman, 1996, Laboratory Techniques in Electroanalytical Chemistry, Marcel Dekker, Inc.

65. C.M.A. Brett and A.M.O. Brett, 1998, Electroanalysis, Oxford University Press.

68. Shahrokhian, S. and Hamzehloei, A., 2003, Electrochemistry Communications, Vol. 5, p. 706.

67. Jr. D.K. Gosser, 1993, "Cyclic Voltammetry (Simulation and analysis of reaction mechanisms)", Wiley-VCH, Inc.
.

68. F.M. Hawkridgein, P.T. Kissinger and W.R.(Eds.) Heieman, 1996, "Laboratory Techniques in Electroanalytical chemistry", Marcel Dekker Inc., New York. 2nd Ed.

69. Armada, P.G, Losada, J. and Perez, S.V., 1996, "Cation analysis scheme by differential pulse polarography", Vol. 73, pp. 544-546.

70. Coropceanu, V., Malagoli, M., Andre´, J. M. and Bre´das, J. L., 2002, J. Am. Chem. Soc., Vol. 124, pp. 10519-10530. (b) Coropceanu, V., Gruhn, N. E., Barlow, S., Lambert, C., Durivage, J. C., Bill, T. G., Noll, G., Marder, S. R. and Bre´das, J.-L., 2004, J. Am. Chem., Soc. Vol. 126, pp. 2727-2731.

71. Thibodeau, P.A. and Paquette, B., 1999, Free Radical Biology & Medicine, Vol. 27, p. 1367.

72. Md. Alim Uddin, 2015, "Electrochemical Study of Catechol in Presence of Sulfanilic acid and Diethylamine at Different pH, M.Sc thesis, KUET.

73. Stum, D.I. and Suslov, S.N., 1979, Bio. Zika, Vol. 21, p. 40.

74. Khalafi, L., Rafiee, M., Shahbak, M., et al., 2013, Journal of Chemistry, Vol. 1, pp. 1-5.

75. Belenky, P., Bogan, K.L. and Brenner, C., 2007, Trends in Biochemical Sciences, Vol. 32, p.
76. Md. Hafizur Rahman, 2016, “Voltammetric Studies of Paracetamol with Some Functional Amines at Different pH Media”, M.Sc thesis, KUET.